Doctoral Dissertation
Doctoral Program in Energy Engineering (38th Cycle)

Switched Reluctance Motor Designed for Circular Economy in Transportation Electrification

Salvatore Mafrici
* * * * * *

Supervisors
Prof. A. Tenconi, Supervisor
Prof. L. Settineri, Co-Supervisor
Prof. G.A. Blengini, Co-Supervisor

Politecnico di Torino
April 10, 2026

I hereby declare that, the contents and organisation of this dissertation constitute my own original work and does not compromise in any way the rights of third parties, including those relating to the security of personal data.

…….....

Salvatore Mafrici

Turin, April 10, 2026

Summary

The propulsion systems are conventionally conceived for a linear business model, which considers phases from the material extraction to the product disposal and are usually optimized for the use phase. Circular Economy is one of the main research areas in recent years, driven by increasing attention to sustainability. Another significant topic over the past decades is the decarbonization of the transportation sector due to its high impact on global carbon dioxide emissions and global warming. These two fields of research have been addressed by coupling technological aspects with methodological ones, aiming to rethink an industrial product featuring circular design.

This thesis focuses on developing a Design for Circular Economy methodology and applying it to a rare earth-free electric motor, specifically a Switched Reluctance Machine designed for automotive applications, aiming to improve its environmental and economic impact. To the best knowledge of the author, the applied methodology resulted in a patented design, never presented on the market nor reported in literature.

The first portion of the thesis delves into design techniques and phases to be included in a conventional design process for an industrial product. In this process, product environmental impacts are considered from the initial development phase, implementing design features that enable circular loops (Durability, Maintenance, Reuse, Refurbish, Remanufacturing, Recycle, etc.) throughout the product lifecycle. This part of the research is dedicated to implementing a framework for identifying potential CS and related design approaches to be adopted. The process concluded with the selection of three promising strategies, respectively oriented to increase durability and the possibility of remanufacturing. The last strategy was presented in two versions, each characterized by different degrees of component substitution.

Design features, framed at a theoretical level, were then transferred into the real design of the electric motor, allowing both higher durability and complete disassembly of subparts, making motor remanufacturing possible. The developed novel concept, compared with traditional design, allows complete motor recovery at the end of life without damaging reusable parts, replacing the most critical parts like bearings and winding.

The aforementioned solutions were compared from an environmental and economic standpoint using specifically developed tools. Environmental burdens were calculated using the Life Cycle Assessment methodology with a cradle-to-grave approach.

For this analysis, a model was developed including all life cycle stages from material acquisition to end of life, simulating defined circular paths, including the recycling process. The model was also used to gain a better understanding of how electric motors affect the environment, providing guidelines on subcomponents and cycle phases' influence on overall environmental impacts, investigating the effect of geographical boundaries and vehicle applications. The same model was used to assess the baseline Switched Reluctance Machine, comparing it with a Permanent Magnet Synchronous Machine, which represents the mainstream topology for the transportation sector. Furthermore, the analysis was enriched by evaluating the improvement of an Ecodesign strategy applied to the magnet-free use case, through the virtual substitution of copper with aluminium within the stator winding. Additionally, the material flow and circularity of the identified strategies were evaluated through a Material Circularity Indicator, adapted to account for different recirculation paths, complementing the Life Cycle Assessment findings on narrower boundaries.

The economic evaluation focused mainly on motor manufacturing costs, directly impacted by CS. Other factors affecting cost, not included in the boundaries of this research, may be considered in future studies.

Acknowledgment

I thank Dumarey Automotive Italia S.p.A. for funding this Industrial Ph.D. and granting permission to publish the material in this thesis. Their trust made this project possible.

I sincerely thank my former supervisor, Ken, for supporting this research and believing in its potential. I am also grateful to my Advance Engineering colleagues, Cesare and Vincenzo, for developing the electric motor that enabled applying the Design for Circular Economy approach, Fabio for providing key input through the cost model and Paolo for the valuable discussions we shared in our everyday work.

I am grateful to Politecnico di Torino for accepting my Industrial Ph.D. candidature and for the support of its professors. In particular, I thank my supervisor, Prof. A. Tenconi, for his guidance on electric motor topics and valuable advice in preparing papers and this thesis.

I would like to thank my parents for teaching me to believe in myself, encouraging me to pursue my dreams without setting limits. I am also grateful to my sister, whose perseverance and respect for principles have always made her a role model and an exemplary researcher in my eyes.

My heartfelt thanks go to Ilaria for giving me the confidence to embark on this journey, always believing in my abilities and supporting me with her daily love, an essential strength to overcome difficulties. Finally, I thank Blue who, despite being only four years old, has brightened the darkest moments with her radiant joy.

The presence of these people has made the path less harsh and winding, a journey that demanded great resilience and allowed me to mature personally and professionally.

Dedicated to my family,
in hope that this path
may serve as a source of
inspiration for them

Contents

List of Tables

List of Figures

Chapter 1

Introduction

1.1 Context and outlook

The three post-2015 agendas, which include the Paris Agreement [1], the 2030 United Nations Agenda for Sustainable Development [2], and the Sendai Framework for Disaster Risk Reduction, together provide the foundation for a sustainable, low-carbon and resilient development in the face of climate change [3]. The first, adopted by 196 Parties at the UN Climate Change Conference (COP21) in Paris, is a legally binding international treaty on climate change. Its overarching goal is to hold "the increase in the global average temperature to well below 2°C above pre-industrial levels" and pursue efforts "to limit the temperature increase to 1.5°C above pre-industrial levels." Greenhouse gas (GHG) emissions must peak as soon as possible to limit global warming as climate change has become one of the greatest challenges facing humanity due to the high increase of CO_2 emission. The second, with its 17 Sustainable Development Goals (SDGs) represents a plan of action for people, planet, and prosperity. This plan is indeed touching the social, economic and environmental dimensions of sustainable development. The two agendas are coherent and their connections are described in the analyses [4], [5].

Concerning GHG, they globally increased in the last 30 years from 34 billion tons in 1990 to 52 billion tons in 2022 [6]. The referenced article presents various breakdowns of GHG emissions by sector and geographic region, supported by historical data. Figure 1.1a, offers an elaboration based on the article's data, illustrating percentage influence of the key sectors on the global GHG emissions in 2022. It is clearly shown that the largest contributors are electricity and heat production, followed by the transport sector, which accounts for 16% of the overall emissions. Figure 1.1b focuses on GHG emissions, measured in tonnes of CO_2 equivalent, within the European Union, highlighting a descending trend over the analysed period.

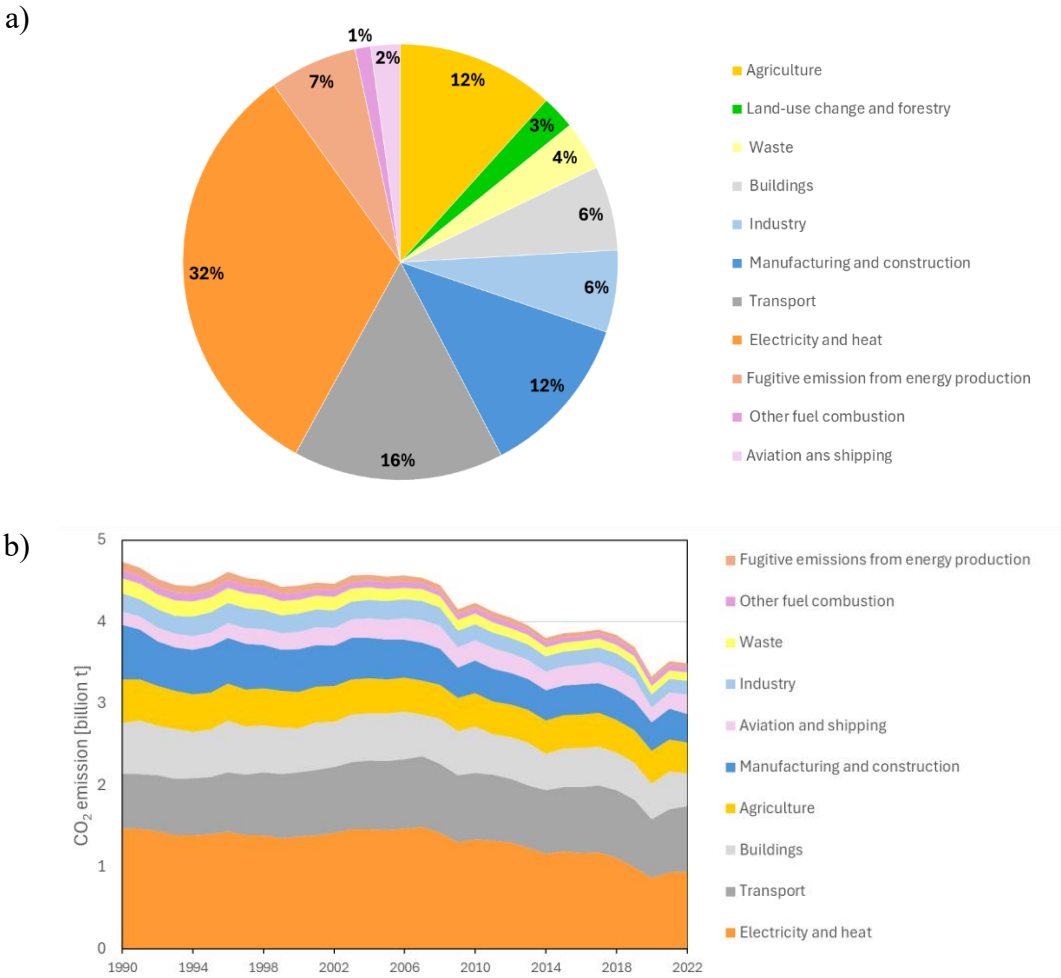

Figure 1.1 a) Key sectors percentage influence on Global GHG emission in 2022; b) European Union CO_2 emission breakdown by sector from 1990 to 2022

However, even in this case transport sector remains the second largest contributor to the overall emissions and shows an ascending trend, with a 21% increase. A similar analysis, including projections over a 35-years horizon up to 2050, is provided by European Commission [7] and illustrated in Figure 1.2. In July 2025, the European Commission proposed a GHG emission reduction target of 90% by 2040 compared to 1990 levels, with the ultimate goal of achieving net-zero emissions by 2050. Given the trend observed, achieving the 2040 target will demand a reduction of about 82% both of the transport sector and of the overall emissions, relative to 2022 levels, according to the S2 scenario described in [8] and coherent with the Net GHG emissions curve represented in Figure 1.2.

Within this context, the transport sector is undergoing a significant transformation, driven by the urgent need to reduce carbon emissions and transition towards sustainable energy sources. Electric vehicles (EVs) are at the forefront of this transition, with the intent to offer a cleaner alternative to traditional internal combustion engine vehicles, thanks to their superiority in terms of GHG emission [9]. The EVs market will see a strong increase with annual sales projected to reach 45 million units in 2030 and close to 65 million in

2035, based on stated policies scenario reported in the global EV outlook 2024 [10].

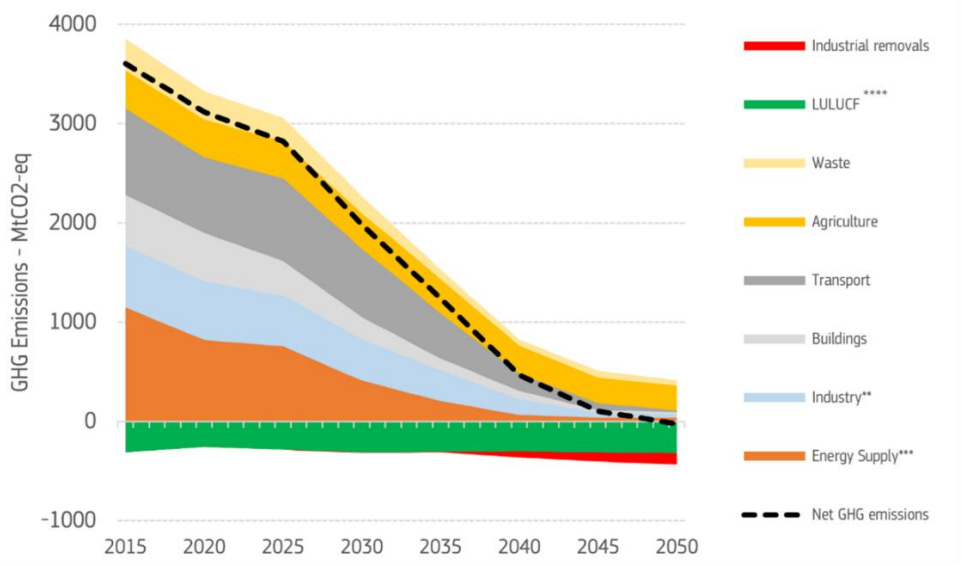

*Source: PRIMES, GAINS, GLOBIOM
**Excluding non BECCS industrial removals
***Including Bioenergy with carbon capture and storage (BECCS)
**** LULUCF: Land Use, Land-Use Change and Forestry

Figure 1.2 GHG emissions projection from 2015 to 2050, provided by EU commission, with a breakdown by sector [7]

An analysis conducted by Dumarey Automotive Italia, based on internal data, confirms the previously cited forecast for global EV sales by 2030. It also highlights that hybrid vehicles are expected to hold a significant market share, with approximately 30 million units projected to be sold, as shown in Figure 1.3. The exponential growth of EVs adoption will drive an expansion of the market for electric motors (EMs), as each EV is equipped with at least one EM that converts electrical energy into mechanical energy.

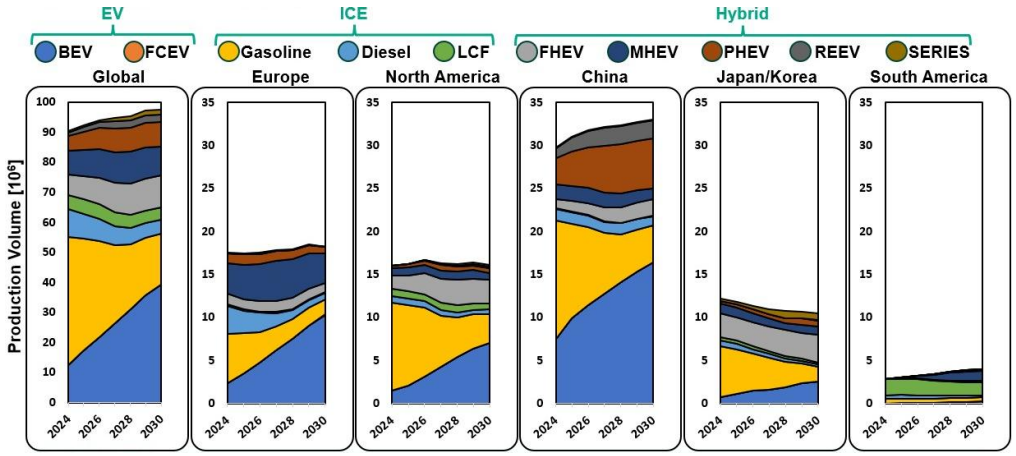

Figure 1.3 Passenger car and commercial vehicles market forecast in different regions and global, broken down into diverse propulsion unit typologies (Dumarey Automotive Italia internal data)

With respect to the above-mentioned background, EMs sustainability both in terms of cost and environmental impact, plays a crucial role in the transition towards electrification. Indeed, according to [11] EMs in 2020 consumed about 53% of the European Union end-use electricity consumption and if no measures would have been taken since 2009, the electricity consumption of motors would have increased from 1192 TWh in 2010 to 1378 TWh in 2020 and 1449 TWh in 2030. However, the implementation of policies leading to an average motor's efficiency improvement, resulted in a saving of 52 TWh in 2020 that is projected to reach 106 TWh in 2030. Same report highlights that in terms of GHG emissions, the EM sector will be characterized by a reduction of 11 Mt CO_2 eq. per year in 2030, in the same policy scenario, with respect to a scenario without any regulation for efficiency improvement. Specifically, focusing on the EVs global market, in 2024 there was a consumption of 180 TWh that is forecasted to increase to 780 TWh in 2030, according to the stated policies scenario [12] , while concerning GHG the market is forecasted to emit 380 Mt of CO_2 in 2035 [10].

This growth underscores the importance of developing efficient and sustainable electric motor technologies to support the expanding EVs market. The increasing demand for EMs highlights the criticality of certain raw materials, particularly Rare Earth (RE) elements such as neodymium and dysprosium, which are essential for manufacturing high-performance Permanent Magnets (PMs) used in EMs. According to [13] the projected global demand for EVs is expected to translate into an increased request of Neodymium-iron-boron (NdFeB) magnets to 114 kt in 2030 and 266 kt in 2050 from the 7 kt of the 2020. Even if extremely promising results in terms of environmental impact have been presented in [14], [15], for the magnet-to-magnet recycling in Hard Disk Drive, the recovery of magnets in Permanent Magnet Synchronous Machine (PMSM) is still a critical point, due to the difficulties associated to the separation process. From this perspective, the selection of a magnet free motor topology, represents an attractive solution both from an environmental and economic standpoint. Chapter 2 of this thesis describes the main criticalities associated with PMs adoption and explains the resulting choice of a RE free Switched Reluctance Motor (SRM) as case study for the application of the methodologies developed within this research work.

EMs could be deployed across a wide range of sectors responsible for high levels of emissions and, being part of the Battery Electric Vehicle (BEVs) propulsion unit, represent one of the most promising technologies in the decarbonization of the transport sector. These vehicles are characterized by zero emission during usage phase, nevertheless, the paradigm for which a technology is considered clean on the base of the emission produced during its usage phase should change taking into consideration the complete product life cycle and a whole set of categories influencing environmental impact, in addition to CO_2 emission. This background emphasizes, on one side, the convenience of the development of RE free machines and, on the other, the need for effective End-of-Life (EoL) management strategies and the development of a Circular Economy (CE) for EMs. CE is identified also as one of the main pillars in the European Commission's path towards climate neutrality [16], and it is gaining increasing

attention. Specifically for the electric machines, the concept of Design for Life Cycle Assessment (LCA) and Design for Disassembly are referenced in the 2020 roadmap of the Advance Propulsion Centre UK [17], which outlines as final goal for the EMs the implementation of a full CE, without adoption of RE. The JRC report [18] addresses circularity measures for critical raw materials and e-drive motors in vehicles, refining the European Union EoL vehicle regulation proposal (2023/0284/EC). It identifies as key measures, the mandatory labelling for PMs, recommending their recovery and the improvement of the disassembly process exploring also the repurposing of e-drive motors for industrial applications.

Both the electrification of the transport sector and circularity of material are identified as climate change mitigation options across various sectors. This is highlighted in Figure 1.4 which presents mitigation options for the transport and industry sectors, showing their synergies and trade-offs with the SDGs, along with associated confidence levels. The figure is extracted from [19] and the mitigation options relevant to the research discussed in this thesis are highlighted in yellow.

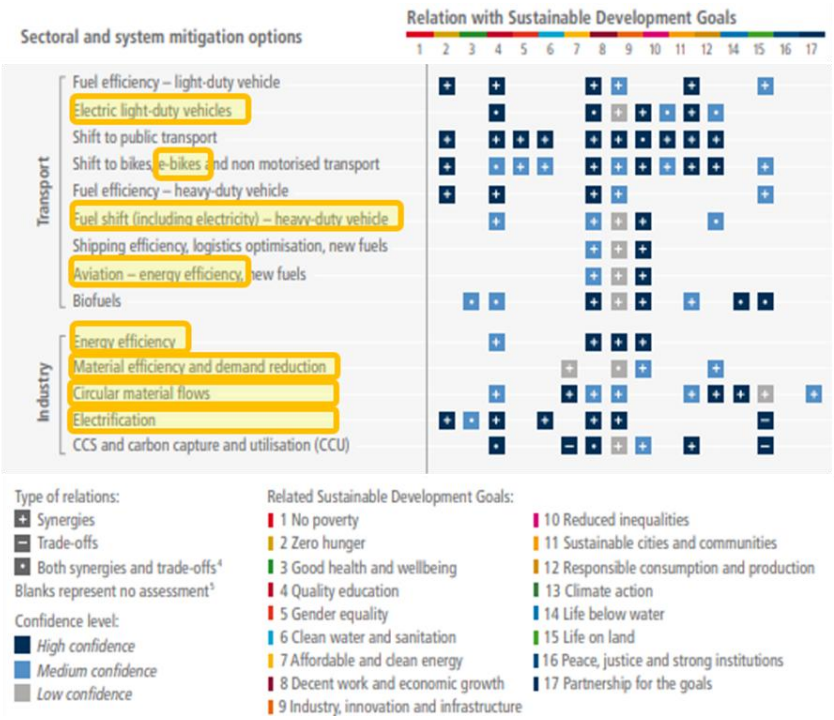

Figure 1.4 Mitigation options relationship with SDGs for the industry and transport sector, extracted from [19]

The increasing emphasis on the environmental sustainability of commercial products is driven both by government regulations aimed at reducing GHG emissions and by market strategies, where product sustainability is increasingly becoming a qualification for companies [20]. In the European context, several policies have been implemented in the transportation sector to address sectoral environmental impacts and support the transition to a low-carbon, CE [21]. Starting from July 2024 the European Union's Ecodesign for Sustainable Products Regulation (ESPR) [22] entered into force aiming to promote product circularity.

It introduces requirements to enhance durability, reuse, upgradeability and remanufacturing improvement as well as the increment of the recycled content, setting ambitious targets for the CE [23]. As illustrated in Figure 1.5 [24] the ESPR is part of a broader set of measures related to CE, confirming the presence of a legislative framework oriented towards sustainability. The package also includes the introduction of a Digital Product Passport (DPP), which, among other requirements, will incorporate LCA of products, based on a specific standard. EMs are included in the first ESPR working plan, with an indicative adoption of the Ecodesign requirements and Energy label in 2028.

Figure 1.5 Overview of initiative in the Circular Economy package

Several initiatives have been carried on by car makers automotive companies in the last years, confirming the above mentioned trend. The Future is neutral, subsidiary of the Renault Group, launched in 2024 remanufacturing activities of EMs, power electronics and batteries pursuing reconditioned BEVs business model [25]. Stellantis inaugurated in 2023 its first SUSTAINera Circular Economy Hub embracing the 4R strategy and starting up with engines, gearboxes, and high-voltage EVs batteries remanufacturing, vehicle reconditioning and dismantling [26]. Schaeffler presented in 2025 the first kit to replace Hyundai Ioniq EM's damaged bearings instead of substituting the complete motor [27]. Volvo launched in 2024 the first BEV with the battery passport [28].Toyota instead is publishing its 3R strategy (Reduce, Rebuilt and Reuse and Recycle) for automotive batteries, through which parts are both reused in automotive and non-automotive applications [29]. GM is introducing in EVs circular design principles as part of its climate risk mitigation strategy [30].

Most of the companies claim revenues associated with the mentioned strategies, confirming that CE is not only oriented to the environmental sustainability's branch.

1.2 Literature review

The literature review is structured into three main sections. It begins with a brief introduction to the CE concept, providing the foundational principles and context for the discussion. The second section focuses on circular design, describing the primary strategies and tools that are available in the existing literature to support circularity in product development. This part was explored to understand at general level how to approach the design for circular of a product. Finally, the review addresses Design for Circular Economy (DfCE) specifically within the EM field, exploring how circular principles can be applied to this sector and highlighting relevant approaches and practices. In this final section, particular attention is given to identifying gaps, challenges and future directions to bring advancements in the field of DfCE applied to electric traction systems. Literature review referred to electric motors or to the developed tools and methods is cited in the specific following Chapters.

1.2.1 CE concept

The concept of a CE cannot be attributable to a definite date or source [31], [32]. Indeed the CE concept has been shaped through different school of thoughts [31], [32], [33]. It is however well recognized that Ellen Mac Arthur Foundation (EMF) contributed to the diffusion of the concept, [34], [35] especially starting from 2012 when it was published a report on the potential economic benefit coming from a transition towards a circular economic model [31]. Although the concept is widely disseminated and numerous initiatives and implementations have been carried out, there is still no universally accepted definition of the CE, as described by [36], [37], where up to 221 definitions have been identified and analysed. Other sources, also argue about this ambiguity and provide their own definitions of CE [38]. However, the British Standard Institution (BSI), published the first standard on CE [39], presenting a coherent set of definitions. Among these, CE is defined as: “economy that is restorative and regenerative by design, and which aims to keep products, components and materials at their highest utility and value at all times, distinguishing between technical and biological cycles”.

CE is frequently associated with the sustainability concept, however [40] highlighted both the differences and commonalities between the two, ultimately suggesting that CE should be viewed as one of several strategies for promoting a sustainable system. Instead, [41] highlighted the positive influence of the CE indicators association with the sustainable development’s pillars on the economic growth. Specifically, from a design perspective, [34] highlights that Design for Sustainability (DfS) approaches can contribute to the implementation of CE solutions, that is conventionally referred to the most technically focused DfS approaches. This concept is practically pursed by [42], where CE inclusion in the design process is presented as a challenge to address sustainability.

1.2.2 Circular design and strategies

Within the CE context, the role of the design is commonly considered as crucial to enhance product circularity [43], [44], [45], and with regard to this, EMF conceives design as the mean to improve products and material circularity.

Circular design approaches and more in general DfS, have been addressed by many researchers with particular attention to the design enablers of circularity as reported in [35], [44], [46], [47], [48], [49]. It is worth to note that design techniques are defined differently across these sources, as circular approaches, objectives, strategies, methods or tools. In Table 1.1 is provided a summary of the design techniques enabling circularity, named as Circular Strategies (CS) in this thesis. These strategies are partially derived from the 44 design techniques mentioned in the referenced literature. The selection includes those strategies considered most relevant for industrial products, such as EMs, and condenses concepts with same intent but labelled differently by the various sources. The table reports also citations revisiting the sources mentioned and classified by topics in [44], [47]. The first provides a classification based on design approaches and related CS and tools, associating to each literature sources, while the second clusters 24 papers according to different circular objectives and related examples of design strategies.

Table 1.1 Summary of the design strategies relevant to enable CE model in an EM and related literature review

Design for	**Literature sources**
Durability	[50], [51]
Easy maintenance and repair	[35], [52]
Upgradability	[35], [52]
Disassembly and reassembly	[35], [53], [54], [55]
Reuse	[53], [55], [56], [57], [58], [59]
Remanufacturing	[35], [52], [55], [60], [61], [62], [63]
Refurbish	[35], [52], [64], [65]
Recycling	[66]

Design guides and framework

Since the final goal of the research is the design of a concept, part of the literature review focuses on the tools available in both peer-reviewed and non-peer-reviewed sources. Indeed, several design guides, of which some examples are reported below, are provided by institutions though their own websites.

The EMF provided a circular design guide, describing mindset, methods and examples of CE implementation [67], mainly providing a four step process going from the understanding to the release and passing through the definition and execution and related tools (Figure 1.6a). Some methodological circular design's guides following similar approach to the topic have been published. An example

is the Sustainability Guide [68] that provides a checklist for the designer, to verify if the circularity concept is embedded in the product design (Figure 1.6b). The Design school Kolding built a webpage, listing design approaches and concept, describing motivations, challenges and application example for each of them [69] (Figure 1.6c).

a)

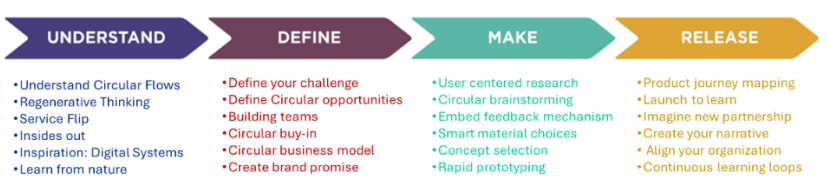

b)

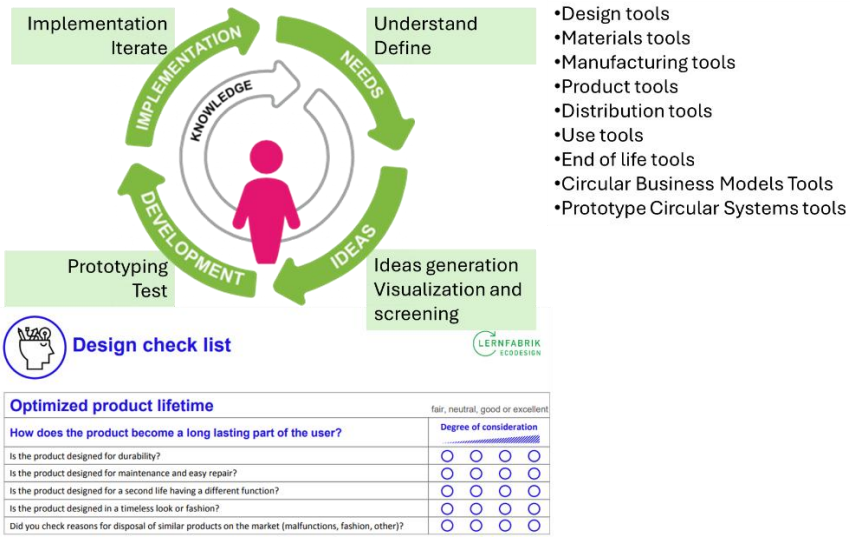

c)

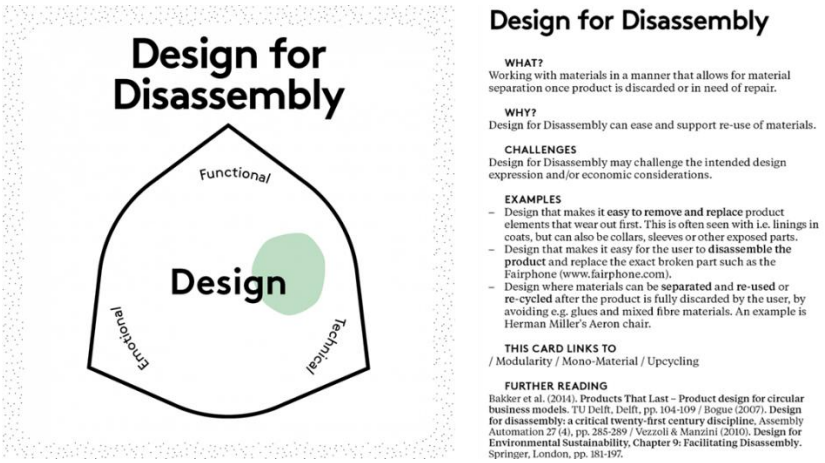

Figure 1.6 Examples of Circular Design guides

Another objective to which many researchers in this area worked, is related to the creation of frameworks for designers and decision makers approaching circular design. In Figure 1.7 are summarized some relevant examples. A framework coupling circular and design strategies, is presented in [48]. The accent is posed on the fact that product lifetime is related to obsolescence rather than failure and to the design for integrity, driving to resist (durability) obsolescence, postpone (maintenance/upgrade) obsolescence or reverse

(repair/refurbish/remanufacturing) obsolescence (Figure 1.7a). Instead, a framework that maps the design strategies against the circular business model and their value creation is outlined in [44] (Figure 1.7b). Another framework in which multiple levels of CS are linked to product life cycle phases and multiple lifecycles is proposed in [47] (Figure 1.7c). As evolution of the same framework the Circular Design Project [70] presents a detailed framework with multiple CS and case studies. Also, [35] provides a strategic framework (Figure 1.7d), based on concepts of slowing resource loops (extending utilization) and closing resource loops (connection with post-use and production). It couples product design strategies like design for product life extension with business model strategies such as extending product value.

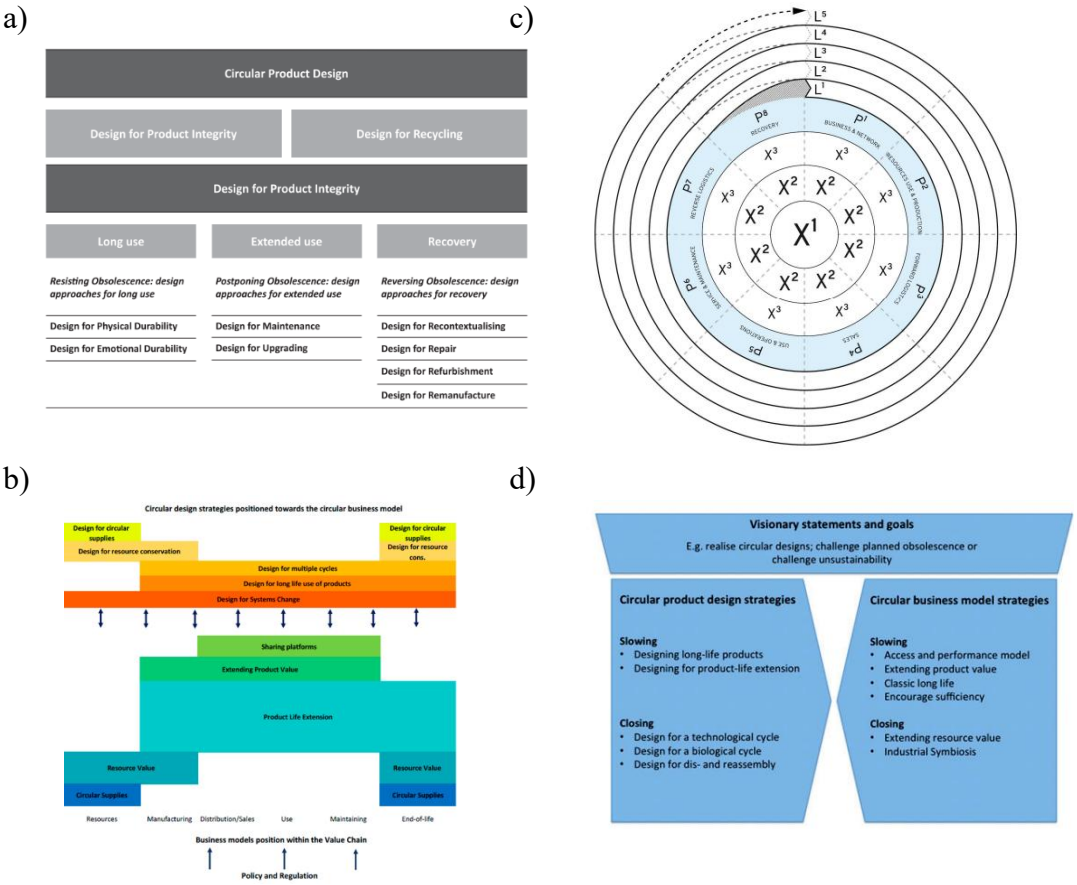

Figure 1.7 Examples of Circular Design frameworks

It is evident from the reported examples that both the guides and the frameworks provide a general path for designers approaching the DfCE discipline. Furthermore, [71] highlights that majority of the researchers in the field of DfS focused on theoretical approaches, while only few papers proposed practical applications. To effectively implement circular principles into product design, theoretical frameworks should be tailored to specific cases by designers who own detailed knowledge of the products to be developed. In this research, both guides and frameworks available in the literature, were analysed and with reference to

the second, a customized framework for this research has been developed and populated with design strategies, as described in detail in Chapter 3.

1.2.3 DfCE application to EM

Application of CE to the EMs field is an increasingly treated topic especially in the last years.

A systematic review that evaluates how CE strategies can be applied to EMs in automotive is provided by [72]. The paper introduces a framework for circularity based on the reuse, remanufacturing, upgrade, and recycling loops and analyses enabling technologies and research gaps. Referring to gaps and future directions, the paper highlights among other, the importance of the design for disassembly, recyclability, reuse and durability to improve sustainability. The selection of electric motor typologies alternative to PMs based machines, is another mentioned future trend, considered the high difficulty in the recovery at the EoL. It is also pointed out that the economical aspect of the CE, should be considered.

Another comprehensive review of CE strategies for EMs is offered in [73] that explores how Industry 4.0 technologies can enable these strategies. It combines a systematic literature review (2011–2021) with an industry survey of selected UK companies to understand landscape related to motor repair, remanufacturing, and recycling aiming to identify current practices, barriers, and opportunities for integrating CE principles. The paper mention necessity for a proper product disassembly to recover component, enabling remanufacturing. Between the identified challenges are reported, the absence of standardized methodology for selecting optimal EoL scenarios, the lack of automation in the operation related electric motor's CE, the lack of information on returned product condition and the economic uncertainty in the adoption of strategies for which cost evaluation should be executed.

The integration of the CE principles into electric traction motor design, is treated in [74], that proposes a formal design optimization framework. The research combines LCA and Techno-Economic Assessment (TEA), within a parametric design model, including a disassembly planning algorithm, to evaluate trade-offs between environmental performance, cost, and supply risk. The paper gives evidence about the positive effect of the CS integration on the overall life cycle and focuses on the necessity to transform design process, thinking the whole motor's life cycle since the early design stage.

A review of sustainable design and maintenance principles for modern EMs, emphasizing energy efficiency, eco-friendly materials, and CE strategies, is provided in [75]. While progress has been made in high-efficiency designs and material recovery, it is identified the importance of regulations to guide the development of more sustainable EMs. To achieve this, the inclusion of CE principles into design and manufacturing process could be crucial. Finally, it is recommended the adoption of standardized environmental impact assessment methods for a rigorous evaluation of the environmental impact.

An investigation on how lean principles can be applied to the remanufacturing of electric motors, is done in [76]. The paper provides a structured analysis of process steps, identifies key challenges, and proposes solutions grounded in lean production system. The study combines literature review with an industrial case study, focusing on traction and industrial motors and is mainly related to remanufacturing process rather than product design. Proper design of flexible handling equipment, involved in remanufacturing process, is highlighted as a challenge.

In [77], is instead provided a rigorous methodology of design for assembly and disassembly, oriented to product remanufacturing. The method is based on metrics like complexity and part accessibility, to evaluate the goodness of various solutions. It is highlighted also in this case how the inclusion of the evaluation at the early stage of the development is key to improve design.

The remanufacturing strategy of the company Ace Re-use Technology BV, is described in [78] and in particular two examples of durability oriented design of EMs are described.

The outlined context is the motivating background of the research activities described in this thesis, that addresses some of the challenges and potential future research underscored by the above-mentioned literature review. The practical implementation of a DfCE methodology into an EM was carried out, resulting in a novel design (patent pending) based on the author's knowledge, as well as the creation of a DfCE framework and models for the environmental and economic evaluation. These models include adaptations of the existing literature to provide customized tools for the treated case study.

1.3 Research objectives

The objective of the thesis is to develop and implement a DfCE methodology within Dumarey Automotive Italia. Specifically, a RE free SRM is adopted as a case study for the integration of this methodology into the conventional design process. The approach aims to identify and incorporate design features in a product enabling realization of CS. This practice leads to environmental and economic advantages and could be in principle applied transversally to any kind of industrial product. Figure 1.8, that is an elaboration of the technical cycle of the butterfly diagram [79], illustrates this concept, showing how the circular approach, in contrast with the linear one, seek to reintroduce products into the economic chain after use through multiple loops, maintaining their integrity and utility. These loops, ranging from maintenance to recycling, reflect different states of the product and correspond to varying levels of retained value. DfCE is one of the techniques within the broader DfS framework and considering it from the earliest stages of concept development, is key to achieve both environmental and economic impact through design.

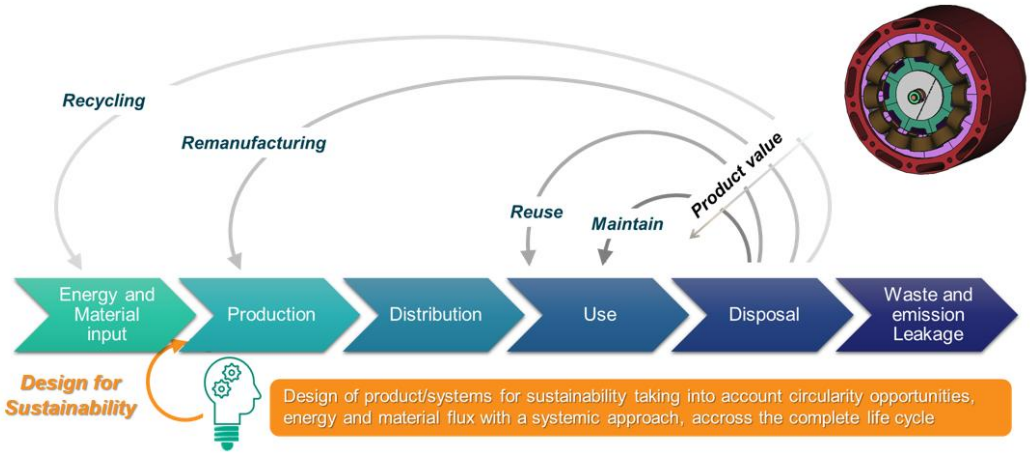

Figure 1.8 Schematic representation of the Design for Circular Economy concept and comparison of the linear and circular model

To achieve the final objective, the following main challenges must be addressed:

- Definition of a framework for the identification of CS and the associated design measures
- Implementation of the proposed design features in a SRM
- Development of tools for the evaluation of both environmental and economic impacts
- Balanced review of performance, environmental and economic analysis results

1.4 Thesis outline

This thesis outlines the following Chapters

Chapter 1 introduces the general background that led to the development of the research work. Specifically, the climate change context, the critical raw material issue and the relevant legislative framework are described. The attention is posed on the EVs market that represents the field of application of this work. The Chapter also includes a literature review focused on DfCE and its application to electric motor design.

Chapter 2 provides a general overview of the electric motor topologies, proposing a classification based on the adoption of RE elements. It then explains the motivation determining the selection of a magnet free SRM as the reference case study. Specifically, are treated criticalities associated with the RE, including the resource availability, the demand growth rate, the geopolitical dependency, the price and market volatility and the recycling difficulties. Additionally, it discusses

the cost-effectiveness and structural simplicity of SRMs compared to the most common topologies in the BEV market, namely PMSM and Induction Motor (IM). A benchmark review of RE-free motors introduced in recent years on the European market is also presented, along with insights into market responses to these emerging needs. Finally, the chapter describes the base architecture and performance of the SRM developed by Dumarey Automotive Italia, to which the circular design methodology is applied. A motor-vehicle matching analysis is included to demonstrate the suitability of the selected performance targets.

Chapter 3 describes how the DfCE methodology has been approached and implemented within the company's operational boundaries. In particular, the framework used to identify the CS and their associated design enablers is presented. Then the Ecodesign strategy and the CS, named as Extended Durability and Remanufacturing 1 and 2, are detailed. The first is achieved through a virtual substitution of copper windings with aluminium ones, the second through a proper selection of the component deemed critical for durability, while the third employs novel design features for the complete disassembly of the motor after usage.

Chapter 4 focuses on the development of a toolset for environmental and economic assessment. LCA model development into a three steps approach, is explained, detailing the input data constituting the inventory, main assumptions, calculation, boundaries and scope for each of the considered scenarios. Additionally, the Chapter describes the methodologies adopted to evaluate product circularity, complementing environmental impact and the cost model used for the economic assessment.

Chapter 5 reports the results of the environmental and economic evaluation. Regarding LCA results, a broad analysis is provided covering all the steps and scenarios evaluated. A more detailed analysis is then offered for the most influent impact categories identified for each case, clarifying the contributions of the life cycle phases, motor subsystems and design strategies. Results related to material circularity and cost are also presented, further supporting the research on circular design.

Finally, Chapter 6 concludes the work and suggests directions for future research aimed at reinforcing and expanding the implementation of the developed methodology.

Chapter 2

SRM selection

2.1 Electric Motor Topologies

This section describes the state-of-the-art electric motors topologies, within the field of alternating current (AC) machines. AC motors are considered in this work as they are widely recognized as the preferred solution, especially in the transportation field, specifically for their reliability, high speed capability, compact dimensions and efficiency, with respect to Direct Current (DC) motors [80], [81], [82], [83], [84],[85]. The aim of this description is to provide insights of the main differences between the machines' topologies and their preferred field of application, introducing to the selection of a SRM as object of the development, presented in the following sections. For detailed description on each motor topology, the interested readers can refer to relevant literature on this topic. Given the sustainability focus of this thesis, a classification of motor topologies based on the use of RE elements is proposed, as shown in Figure 2.1. In the figure a), are visible the three main families of AC motors, and in particular synchronous and reluctance motors are represented with orange and green boxes, while asynchronous with a yellow one. It is evident that the first two are both present in the magnet intensive and RE-free branches, while asynchronous motors are characterized by the absence of PMs. Figure b) instead provide a zoom on the RE-free machines, highlighting main pro and cons of each topology. Main functional difference between synchronous and asynchronous motors is that in the first the rotor runs at the same speed of the stator magnetic rotating field, called synchronous speed, while the second have a slip, with the rotor speed that is lower than the synchronous speed. Synchronous speed ω_s is defined according to equation 2.1 and is strictly related to current supply frequency f , provided by the inverter, and the number of poles p.

$$\omega_s = \frac{120 \cdot f[Hz]}{p} \tag{2.1}$$

Reluctance machines are also synchronous, even if their working principle is based on the magnetic reluctance variation concept and therefore are here described as a different family.

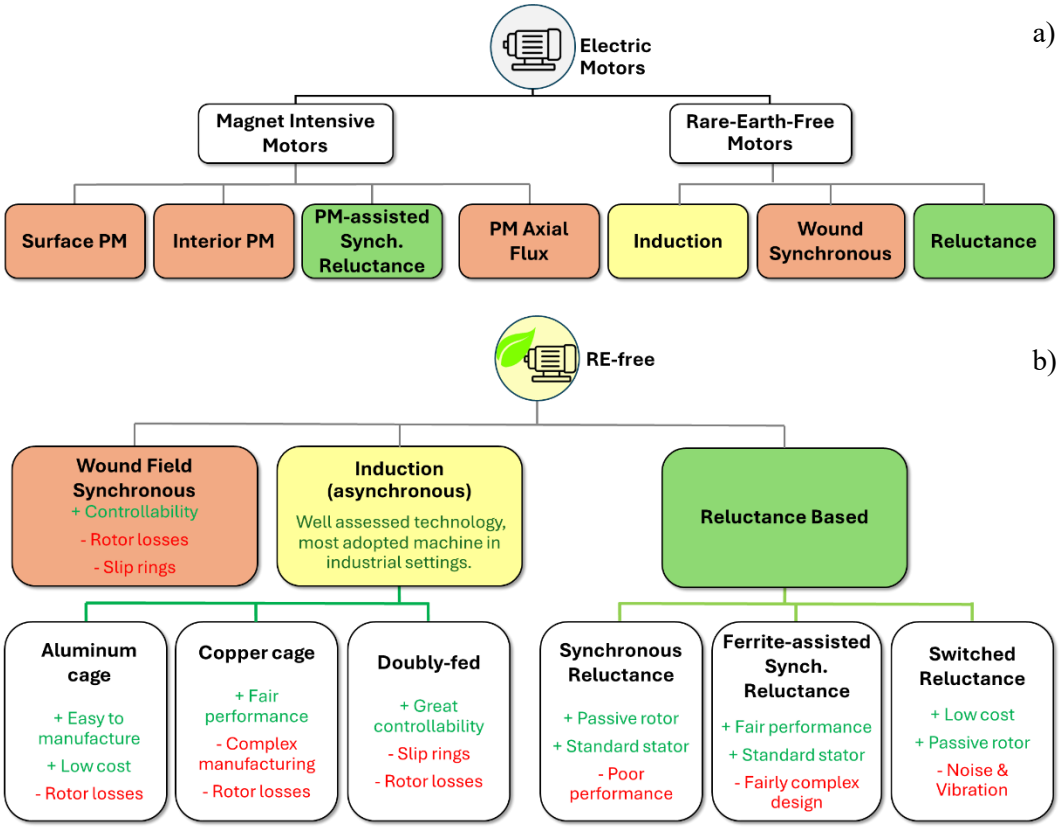

Figure 2.1 Classification of a) AC Electric Motors Topologies and b) RE-free machines with pro and cons

Magnet intensive motors represent the mainstream technology, especially referring to the electric passenger cars, as reported in section 2.2.1. This is mainly due to their typically higher efficiency, torque density, packageability and noise performances [80]. On the other side, the presence of the magnet is negative from a sustainability perspective, both in terms of cost and environmental impact. PM machines are part of the synchronous family, in which the various topologies differentiate each other on the base of the rotor structure as reported in Figure 2.2.

Permanent Magnet Synchronous Machine (PMSM)

The most common are the PMSM in which shaft torque is generated by the interaction between the magnetic field produced by the magnets and the rotating magnetic field produced by the stator through the current flow in the windings. PMSM can be furtherly classified based on the position of the magnets: if they are mounted on the rotor surface (Figure 2.2 a), they are called Surface Permanent Magnet Synchronous Machine (SPMSM), if they are embedded within the rotor

(Figure 2.2 b), they are referred to as Interior Permanent Magnet Synchronous Machine (IPMSM).

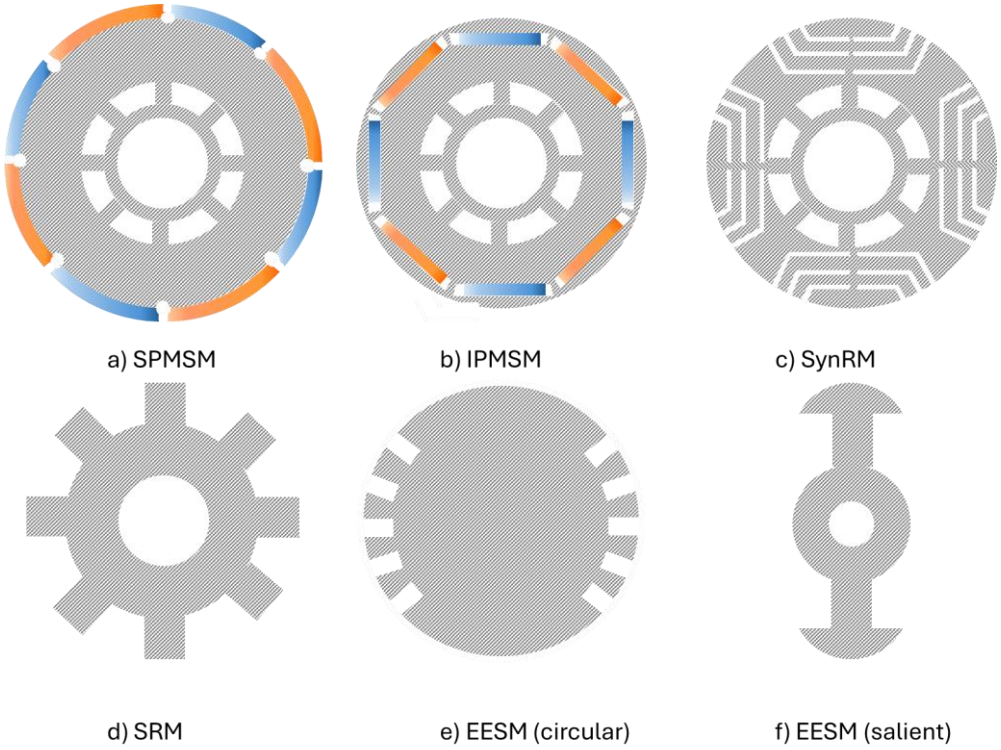

Figure 2.2 Synchronous motors rotor

SPMSM are characterized by a larger air gap and generally concentrated stator winding, while IPMSM have a reduced air gap and distributed stator winding in the majority of the cases. The losses on these machines are mainly on the stator portion both in copper and iron and on the rotor, particularly in the magnets. Concerning losses both analyses on high speed PM machines (operating above 20krpm), described in [86], [87], show that SPMSMs have lower losses than IPMSMs at rated condition. Meanwhile [88], [89], respectively highlight the higher efficiency of each topology at different speeds, within a range up to 12 krpm. The latest papers demonstrated also comparability of the two motors topology in terms of continuous power considering same size of the active parts. However, an important note is related to the difference in terms of overload capability that is good for the IPMSMs, whereas SPMSMs cannot exceed their continuous power rating regardless of the applied current overload. In [90] a qualitative comparative analysis of the two topologies is reported and here summarized. IPMSM machines are characterized by a better thermal management, thanks to the rotor's action as a barrier. Thermal shield provided by the rotor leads also to a lower demagnetization risk, comparing IPMSMs with SPMSMs. Another peculiar aspect of the IPMSMs is represented by the opportunity to control magnetic field strength optimizing efficiency over a wide speed range. The operation efficiency is also improved through the enhanced interaction between stator winding and PM magnetic field. The rotor design with

embedded PM is maintenance-free and is characterized by low windage noise and friction losses [80], making this design suitable for high speed application up to a certain speed. On the other side SPMSM design is simpler, however from the analysis reported in [86] SPMSM shows higher cost and comparable weight with respect to IPMSM. The direct interaction of PM with stator winding, leads to high torque value at low speed. Considering the main advantages and disadvantages reported, SPMSM machines are mainly adopted by wind turbines, means of the light mobility and robotics applications. IPMSM instead are widely adopted in passenger cars and more in general automotive sector, characterized by highly variable speed and load profile. One of the main reasons, is linked to the fact that torque is generated in the IPMSM by the permanent magnet and reluctance contributions. The latest is particularly effective in the extension of the operative speed range, concerning the ratio between maximum and base speed.

One of the cutting-edge motor technologies is represented by the Axial Flux Permanent Magnet (AFPM) motors. This family presents a geometrical variation to the radial flux motors and the concept could be in principle applied to all the other motor's topologies. In this thesis is referred to PMSM that is the mainstream solution in the automotive field. Its high performances concerning efficiency, power density and torque, makes this geometry particularly appreciated for high-end Original Equipment Manufacturers (OEMs) as stated in [91]. Main characteristic of this machine is that the magnetic flux is parallel to the axis of rotation instead of radial as it happens in the other topologies. AFPM motors are characterized by different architectures, basically defined by the number of stators and rotors. These motors are characterized by a compact "disc-shape" design instead of a "cylinder-shape" resulting in a reduced weight and axial length, compared to radial flux motors. The larger rotor radius contributes to the generation of higher torque. Also, the copper fill factor is much higher than in radial flux motors. The main disadvantages limiting the market adoption of this technology are related to manufacturing complexity and the cost of the materials used.

Reluctance Machines: Synchronous Reluctance Machines (SynRM) and Switched Reluctance Machine (SRM)

In the reluctance machines the torque is generated through the principle for which the rotor moves in a way to minimize reluctance once the current generates the magnetic field in the stator. Reluctance machines are basically split into Synchronous Reluctance Machines (SynRM) and Switched Reluctance Machine (SRM). In the first, reluctance is generated by the distinctive design of the rotor, which features electromagnetic steel flux carriers and air flux barriers. The purpose of this design is to facilitate the magnetic flux passage in one direction, preventing it perpendicularly.

SynRM (Figure 2.2 c) performances can be improved by the introduction of PMs in the rotor flux barriers coupling advantages typical of the magnets to reluctance topologies. This happens in the so-called Permanent Magnet-assisted

Synchronous Reluctance Machines (PMaSynRM). This topology is particularly suitable for passenger cars application thanks to the above-mentioned peculiar features of the PM motors. SynRM, however are fault tolerant and characterized by good robustness and efficiency [81], [83]. However, the rotor strength at high speed is a drawback and the introduction of the magnets for performance improvement, affects negatively the advantages associated to the reduced cost of this motor topology. A RE free alternative to the PMaSynRM is the ferrite-based PMaSynRM that employs ceramic material with lower magnetic strength in comparison to the conventional PMs. Also in this case, ceramic magnets are embedded in the rotor to enhance performance. SRMs (Figure 2.2 d) instead are characterized by a salient poles structure that tends to favour alignment of the rotor with the stator, following the principle of the minimum reluctance, allowing magnetic flux passage through stator and rotor poles and generating torque at the shaft. In contrast with the SynRM, the SRM is suitable for high-speed operation due to the single piece rotor structure [80]. However, this topology is characterized by a high torque ripple and by high acoustic noise due to large radial forces exerted on stator poles. SRM is characterized by concentrated winding around each stator tooth and in the base configuration, each pair of diametrically opposite coils, are connected in series, constituting one phase of the motor that is excited by unidirectional current. Main advantages of the SRM, explained in detail in the section 2.2, are related to simple construction leading to robustness and reduced cost, also due to the absence of RE. SRM are currently mainly adopted in industrial applications, home appliances and in aviation field, but thanks to their features are gaining interest in the field of Electric Vehicles (EVs) traction [81], [82], [92].

Externally Excited Synchronous Machine (EESynM)

Another RE free synchronous machine is the Externally Excited Synchronous Machine (EESynM). The rotor of this machine is wound with copper wire coils carrying DC current and producing a magnetomotive force (i.e., excitation field) rotating in synchronism with the rotor. The field current is fed to the rotor through slip-rings and brushes. The rotating stator magnetic field interacts with the rotor magnetic field originating synchronous rotation of the rotor itself. Two possible architectures are defined based on the rotor shape: the cylindrical rotor is isotropic and characterized by a constant air gap (Figure 2.2 e), while the salient pole rotor is anisotropic and features a variable air gap (Figure 2.2 f). The strengths of this topology are summarized in [91] and are mainly related to its good efficiency [93] and strong performance with the capability to deliver high torque over a wide speed range [94]. The features mentioned, coupled with low cost and proven design, have led to the increasingly frequent adoption of this topology in areas such as aerospace and traction [95]. Referring to the last point, in recent years, this topology has seen widespread adoption in EVs, as described in section 2.2.1, representing one of the most viable solutions in the race towards the RE removal from the motors.

Induction Machines (IM)

Asynchronous Machines, known as IM, are characterized by a rotor rotational speed lower than that of the magnetic flux generated in the stator winding. The speed difference induces currents in the rotor which generate a magnetic field of the rotor, interacting with the stator one and consequently originating torque. The stator structure of IMs is comparable with PMSMs. Main difference is in the rotor architecture that could be both with a squirrel cage or wound. Squirrel cage architecture features aluminium, or copper bars welded or casted to two circular rings at the extreme parts, creating a close circuit. The rotor wound architecture is characterized by the presence of the winding into the rotor slots similarly to the stator winding and the circuit is closed through slip rings to an external circuit (e.g. inverter). From a geometric standpoint, these machines feature small air gap and distributed stator winding, while from a performance perspective the absence of magnets leads to both a containment of the cost and to an improvement of the reliability [81], while the reduced torque ripple, leads to good Noise Vibration and Harshness (NVH) behaviour [80]. The rotor could be both with aluminium and copper cage. IMs have both stator (copper and steel) and rotor (copper or aluminium) losses. Aluminium cage type is characterized by lower cost and easier manufacturability with respect to copper cage one, that on the other side features higher performances. As highlighted in [85] the wound rotor type features high starting torque and low starting current, ability to withstand with frequent start and stop and a high-speed controllability. However, slip rings determine more maintenance, compared to the squirrel cage architecture. IM characteristics make this topology interesting for passenger car, wind turbines and home appliances.

Among the above-mentioned technologies, the SRM one has been selected for this research activity as it intrinsically oriented to both environmental and economic sustainability, mainly due to the absence of PMs. Even compared with other RE-free machines, its construction simplicity leads to a lower cost as explained in detail in the following section. Additionally, its robustness makes this motor inherently durable and therefore aligned with the CE concept. On the other side, as described, this topology presents drawbacks in particular referring to noise and vibration, posing a challenge in the development of the motor control system. This portion however is not developed in this thesis work that is mainly focused on the design for sustainability aspects.

2.2 Why SRM

In this section the main topics leading to the selection of a RE free machine and in particular of a SRM, are addressed. First, the main criticalities in NdFeB magnets supply are described with reference to:

- Resource availability
- Demand growth rate and market forecast
- Geographical concentration of production

- Price/Market volatility
- Recycling difficulties

In addition to all the critical aspects mentioned, there is growing attention to the environmental impact of the Rare Earth Elements (REEs). Specific analyses are described in Chapter 4 and 5 where their contribution as a subsystem within the motor's Life Cycle Assessment (LCA) is evaluated. Then an overview of the main technologies available on the EV market is provided followed by a brief qualitative comparison between motor topologies, particularly referring to cost and performances, leading to the selection of a SRM.

2.2.1 RE criticalities

REE group is constituted by fifteen elements with atomic number between 57 (lanthanum) and 71 (lutetium) on the periodic table of elements. While some REs are relatively abundant, obtaining them at usable purity, implies processing enormous amounts of raw ore at great expense, as they are spread over thin impurities. Figure 2.3 [96], [97] reports the abundance of the chemical elements in Earth's upper continental crust as a function of atomic number. It is visible that all of the REEs, except promethium, are more abundant on average in the Earth's crust than silver, gold, or platinum as mentioned in [98]. The eight elements in the upper left corner of the figure make up 98% of the Earth's crust: oxygen, silicon, aluminium, iron, magnesium, calcium, sodium and potassium. Copper is close to the threshold to be considered rare.

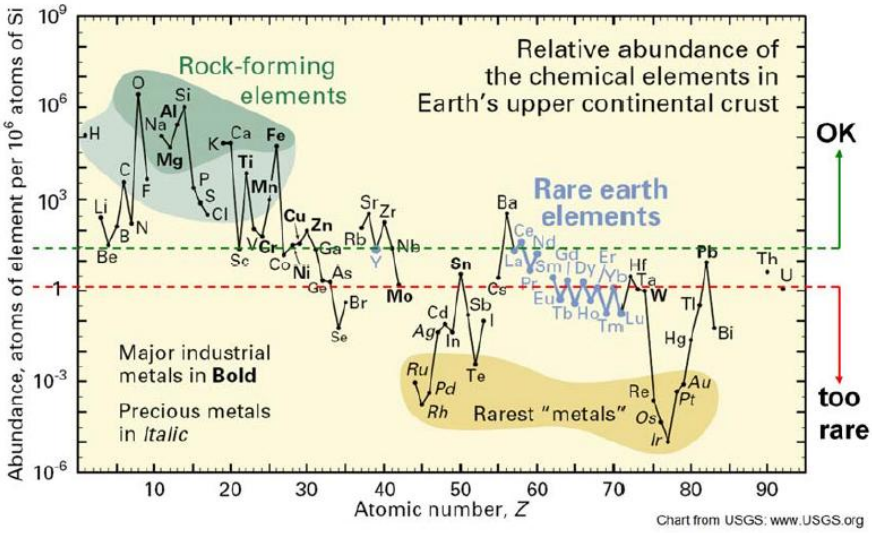

Figure 2.3 RE availability [96], [97]

However, due to the overall demand increase, RE intensive machines, that represent mainstream category in the transport sector, must face the resource availability issue, caused by the strong competition from other markets like wind turbines, defence and medical. Indeed, in the next decades, PM demand is predicted to heavily increase in transportation field but also in other relevant markets, where demand will be an order of magnitude higher like in the wind

turbines. Figure 2.4, published in [99], reports prediction for PM demand increase from 2020 to 2030 of respectively 5 times in automotive and 3 times in wind turbines European markets. However, an electric motor for EV traction may contain 1 to 2 kg of Nd-based PM, while wind generators use hundreds of kilograms per turbine.

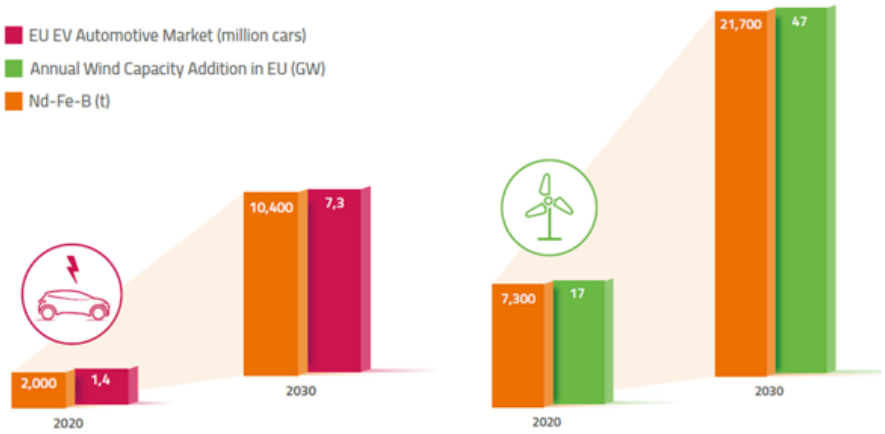

Figure 2.4 Nd-FeB demand in automotive and wind turbine application [99]

The analysis provided by IDTechEx, referred to the electric vehicle market, supports the above-mentioned PM demand and is even more optimistic in regard of the PM demand in EV market in the next decades. In particular, IDTechEx reported in [100] the motor topologies distribution in Figure 2.5 a) highlighting the fact that 85% of the market in 2023 is represented by PM based motors. In addition, in Figure 2.5 b) [101] it is highlighted the global Nd demand, which could outstrip the global supply, with demand projected to be 11 times higher in 2032 with respect to 2021.

a) b)

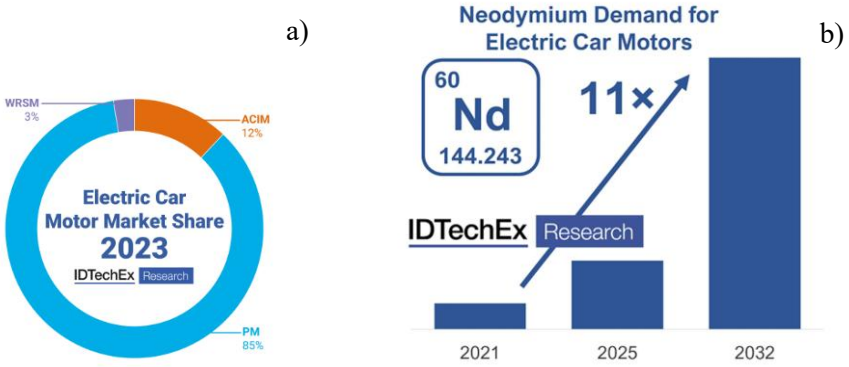

Figure 2.5 IDTechEx Market analysis for the different electric motor's topologies [100] b) Neodymium demand for EV motors [101]

In addition to the availability issue, REs present geopolitical concerns. Indeed, according to [13], China is dominating all the supply chain stages of the NdFeB magnets accounting for the 58% share of annual global rare earth mining in 2020 and for the 92% share of annual global magnet production. In Figure 2.6 the geographical distribution of the Nd-Fe-B magnets supply chain is represented, showing the relevant role of China particularly concerning the manufacturing

processes. This geographical supply limitation coupled with an increasing demand could lead to market instability, with extremely high increase in the magnet's prices or supply favour to local demand. This is reflected in a large prices fluctuation as it is visible analysing the price trend in the past decades. With particular reference to this point, in Figure 2.7, the price for neodymium and dysprosium from 2005 to 2024 is reported. The figure has been obtained merging absolute prices values reported in [102] and yearly percentage prices variation reported in [103]. In 2011 both neodymium and dysprosium prices grew up sharply, due to the fact that China decided to restrict the RE export, increasing taxation and significantly reducing the quota allocated for foreign markets [104]. An analysis of the RE prices trend is provided by [105], where relationships between prices and both economical activities and geopolitical risk are investigated. In the paper it is described how the supply chain crisis after COVID-19 epidemic period, and other occurrences lead to a new increase of the prices, from 2020 to 2022.

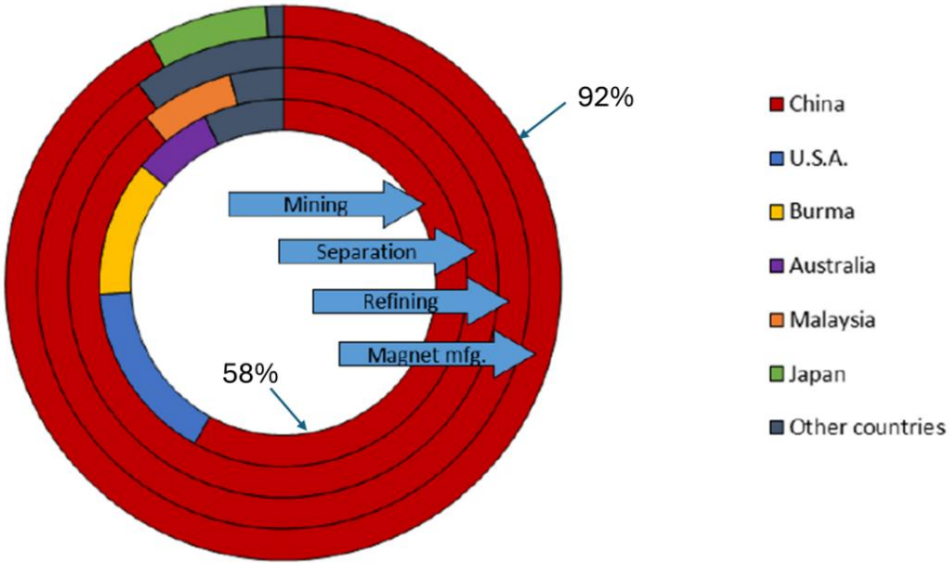

Figure 2.6 Geographical concentration for the Nd-FeB supply chain in 2019 [13]

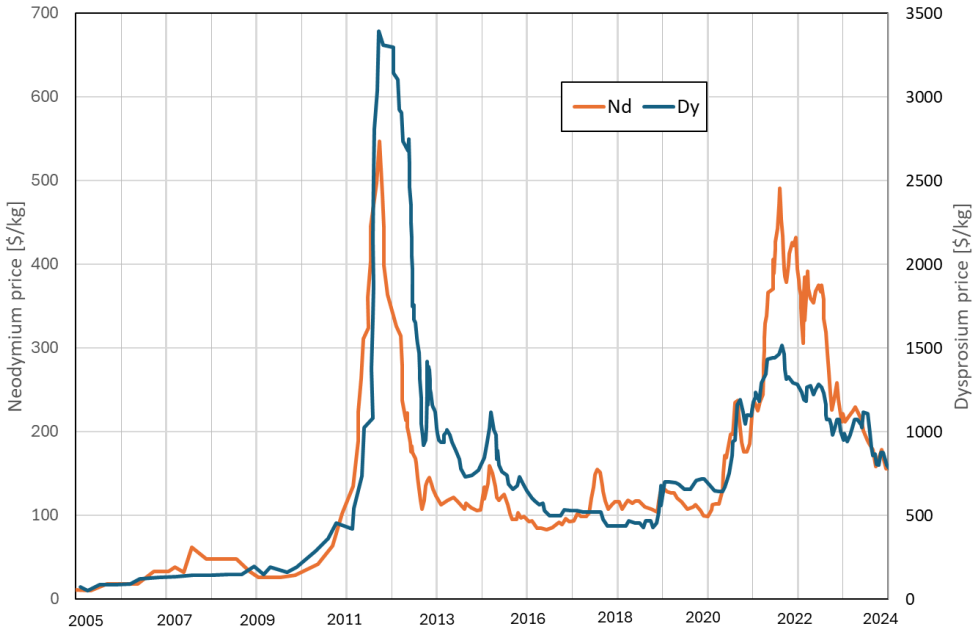

Figure 2.7 Neodymium and Dysprosium price historical variation

Recycling process is another critical aspect related to PM adopted in the motors. Looking at environmental impact advantage coming from the magnet recycling, extremely promising results are presented in [14], [15] where magnet-to-magnet recycling in Hard Disk Drive (HDD) is compared with magnet manufacturing process from virgin material. The analyses show a reduction of the environmental impact; however, the approach is still not mature for motors employed in transportation sector, that are mainly IPMSM, where magnets separation is a critical issue. Indeed, according to [106], electric motors are currently shredded after their disassembly from the vehicles. The shredding process causes the loss of the permanent magnets, that are currently not recovered. Some research initiatives are currently in place to develop high technology readiness level dismantling procedures and novel permanent magnet recycling processes to enhance the recoverability of REE, but they are not commercialized yet [107]. The paper reports difficulties of the magnets recycling process considering the metallurgical separation and refining processes as the main challenges. In the same paper Figure 2.8 reports the potential recycling supply ratio for neodymium and dysprosium calculated in [108] as a ratio between the Rare Earth Oxide (REO) collected at the End of life (EoL) of the product and the REO demand. Calculation reported is inherent to automotive industry, wind turbine, computer and HDD sectors. Results show that recycling potential both for neodymium and dysprosium are low compared to the global demand despite its forecasted step increase in the next years.

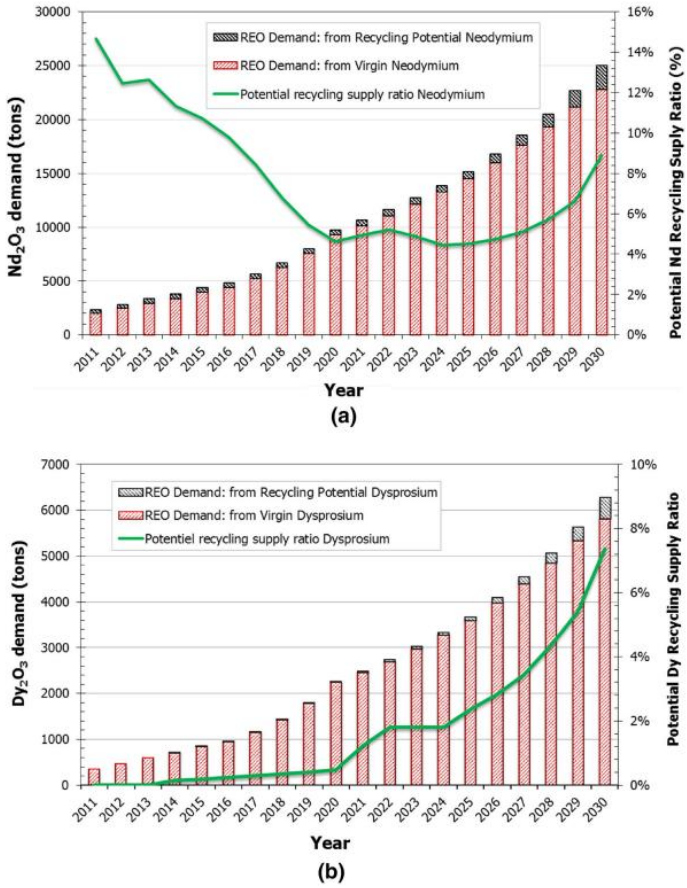

Figure 2.8 Predicted recycling potential for Neodymium a) and Dysprosium b) [108]

Automotive OEMs are therefore reacting to the described criticalities moving toward reducing their dependence from REs. The main actors in the production of rare-earth-free motors for passenger cars are introducing in the market both EESMs and IMs. On the first topology have been particularly active Valeo, ZF, Mahle, Renault, Vitesco, and BMW, while companies like Tesla and VW-Audi have mainly adopted the second topology. In Figure 2.9 main novelties introduced in the passenger car market in the recent years are reported. The boxes have same colours adopted in Figure 2.1, to identify the different topologies.

In 2021, Mahle introduced a magnet-free motor with an EESM, featuring an efficiency higher than 95% across all operating points. A distinctive feature of this machine is its innovative direct cooling system using a dielectric fluid, which is channelled through the hollow rotor and centrifuged outward toward the windings and stator [109].

Another motor manufacturer is ZF that in 2023 presented a system able to achieve high efficiency levels, close to 96%, with an average efficiency of 93% over the Worldwide Harmonized Test Cycle (WLTC) [110]. Considering vehicles manufacturers, Renault and BMW are main actors in the adoption of wound rotor machines. The first invested in this technology since the early versions of the Zoe in 2013, that was upgraded in 2018, reaching a power of 80kW [111].

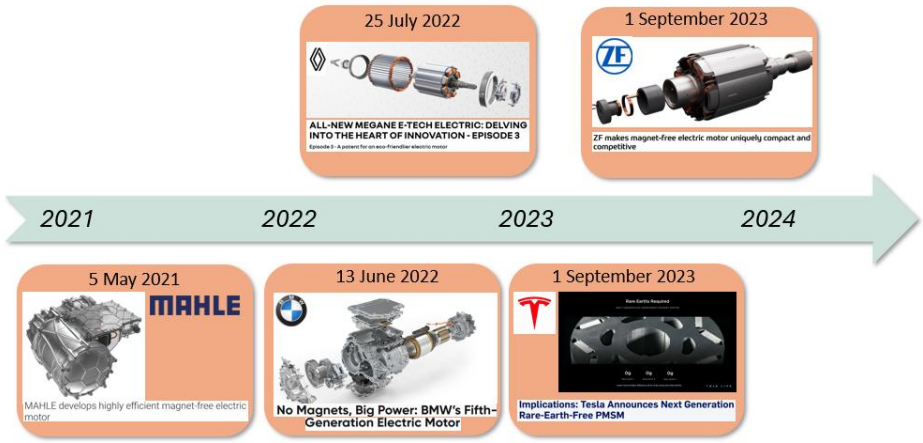

Figure 2.9 RE-free motors introduced in BEV market

In 2022 Renault presented the EESM for the Megane E-TECH Electric whose technology is used for the motors on the ZOE, Twingo Electric, Kangoo Electric, and Master Electric [112]. The second instead has recently introduced eAxles based on wound rotor synchronous motors (e.g., in the iX M60), clearly positioned in the premium segment. In fact, the iX M60 motor is based on a six-phase configuration powered by a dual inverter and is capable of delivering 360 kW of power up to a speed of 15,400 rpm. The motor, together with inverter and transmission are integrated into a single housing, ensuring compactness and high performance [113].

Among OEMs, Tesla must be mentioned as one of the pioneers in the development and adoption of IMs. In fact, such motors have been used for traction purposes since the early versions (e.g., the Roadster). More recently, Tesla has shifted to using permanent magnet motors, sometimes paired with one or more asynchronous motors with copper squirrel-cage rotors in a dual electric axle configuration. Tesla has recently adopted an eAxle composed of dual induction motors with aluminium cage rotors, in the TriMotor Cyberbeast version (two asynchronous motors on the rear axle and one permanent magnet synchronous motor on the front axle) [114]. More recently, the VW-Audi group has developed eAxles based on asynchronous motors with aluminium cage rotors, used in the e-tron (known since 2023 as the Q8 e-tron) [115]. In addition to the notable absence of rare earth magnets, despite the vehicle's premium segment, it is worth highlighting the adoption of an innovative liquid cooling system. Specifically, this system is based on a circuit that includes the inverter, the hollow motor shaft, and the water jacket integrated into the motor stator housing [116].

For what concern SRM specifically designed for passenger cars, the major examples are represented by Enedym and Advanced Electric Machines (AEM). Both the companies are university spin off, so highly oriented to the research activities. However, AEM has a manufacturing strategy at national level in UK and between its products portfolio, it features an aluminium winding rare earth free motor as described in section 3.3.1. In Table 2.1 the main features available

of the SRM developed by AEM [117] and McMaster University of which Enedym is a spin off [118], are reported.

Table 2.1 Main features for SRM benchmark

Parameter	AEM – HDSRM300	McMaster University
Peak power [kW]	295	60
Continuous power [kW]	98	-
Peak torque [Nm]	485	210
Continuous torque [Nm]	180	-
Max operating speed [rpm]	8400	13500

2.2.2 Topologies comparison

Considering the described context and PM criticalities, SRM could represent a viable technology as it is well known for its cost-effectiveness [119]. Indeed, SRM topology is constituted by an active electrical steel core, copper windings and a housing (generally aluminium-based). However, SRMs lower torque density, high torque ripple and acoustic noise have determined a preference of other technologies for road applications, while robustness (with proper mechanical design), that is another characteristic of the SRM [120], together with the cost advantages, make this technology suitable for off-road applications, less sensitive to the intrinsic SRMs drawbacks [121]. Furthermore, robustness could be crucial to enable physical durability in favour of product design for circular economy [48]. Considered the priority of the sustainability requirement both in terms of cost and environmental impact and given the competitiveness at performance level SRM has been chosen as a baseline for the DfCE research. In the next section are addressed specifically a cost comparison and a literature performance assessment, while environmental impacts are described in detail in Chapter 4 and 5.

Cost effectiveness

From an economic perspective, SRM are respectively 44% and 50% cheaper than a copper cage IM and a PMSM as reported in [119], where a cost comparison against the two most adopted topologies in passenger car is provided. In Figure 2.10 the concept is synthetized illustrating the main cost drivers leading to such a difference, elaborating and replotting data presented in [119], for the power density levels indicated in the paper itself. The material cost breakdown shows that the avoidance of magnets overcompensates the higher cost of copper both in IM and SRM. Despite magnets represent 5% of the overall motor mass, as reported in the same paper, they contribute to 40% of the overall manufacturing cost. Electrical steel core has comparable cost for the three topologies. SRM is then favourable both from a material cost standpoint, showing a potential cost saving of 25% and 34% compared to IM and PMSM and from an assembly and

testing cost perspective with potential cost saving of 72% and 75% over the other two topologies.

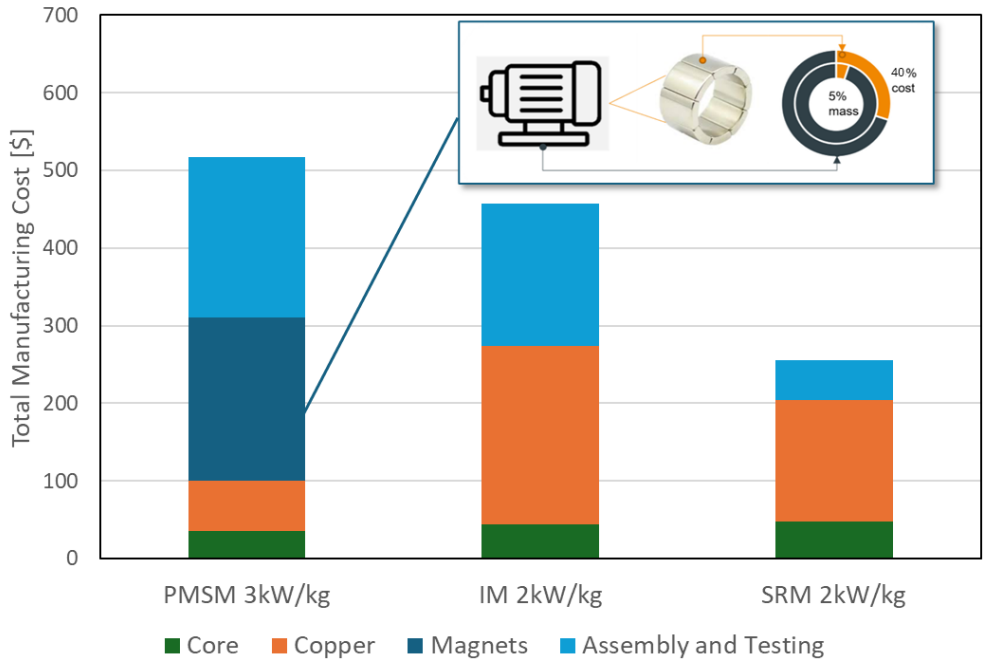

Figure 2.10 Cost comparison between PMSM, IM and SRM

Referring to cost, the potential indirect drawback of the SRM topology adoption, which requires a higher voltampere rating inverter, should be considered. Thus, the whole system including motor and inverter should be analysed in order to have a holistic technologies comparison. Inverter cost represents less than 40% of the overall system cost, based on latest power electronics and electrical machine roadmaps from the UK Advanced Propulsion Centre [17], [122] and complemented by UBS teardown studies [123], and in case of SRM drives could present both a penalty associated to the lower power factor [124],[125],[126] and a potential advantage due to the possible usage of a Miller converter, with respect to a conventional PMSM three-phase inverter, as described below in detail. Indeed, it can be stated that power converter's rating, in terms of components' current and voltage requirement (and thus cost), is influenced by the ratio between output shaft power vs. input rms voltampere [127]. At low speed, SRMs' power factor is comparable to induction machines, but lower than PMSMs [124], [127]. In [125] it is indicated that the converter's voltampere requirement for an SRM is greater than that of an AC machine, whilst [126] is another source, indicating SRMs potential factor and confirming the above mentioned references. It is to be noted here that, despite at base speed a PMSM can exploit at its best the power converter capabilities, by drawing only active power, this is not the case at high speed, where field-weakening requires the injection of d-axis (i.e., de-magnetizing) current. This leads to poor power factor, as the machine draws reactive power, and needs to be accounted for when sizing the power converter. This is not the case for SRMs, where rated power can be developed up-to 3-4 times the base speed, without the need for any field weakening. For the sake of

fairness, it is worth noting that whilst a three phase PMSM, for four quadrants operations, needs to be driven by at least a three-phase inverter (i.e., 6 switches and 6 diodes), a three phase SRM could be potentially driven by a Miller converter (i.e. 4 switches and 4 diodes), as shown in the Figure 2.11 Scheme of a Miller converter. This would bring to a considerable cost saving.

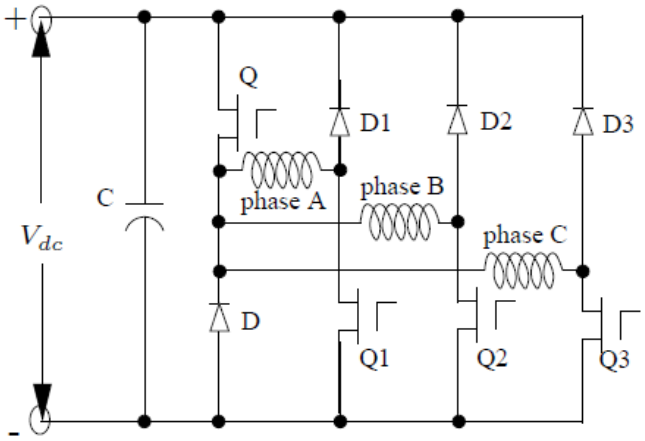

Figure 2.11 Scheme of a Miller converter

Performance competitivity

From a performance perspective SRM has been considered competitive with acceptable performance deterioration with respect to PMSMs. Electric motors topologies reviews summarized both with qualitative and quantitative analysis this aspect. According to the comparison performed in [81], where motors for EV are assessed in terms of power density, efficiency and reliability, SRMs have lower power density than PMSMs, but higher than IMs, while in terms of efficiency they are comparable to PMSMs and slightly higher than IMs. Another comparison, presented in [80], classifies SRMs as medium concerning size and performance, with lower evaluation respect to PMSM, but comparable to IM. In terms of efficiency SRMs are judged as the worst of the three, while they are at the top level referring to speed and reliability. An extensive comparison between all the relevant topologies for EV is reported in [91]. Here SRMs are evaluated at the maximum level in the production cost and torque density category. Also, in terms of efficiency, specific power and power factor are well considered, with values comparable to PMaSynRM. On the other side, same assessment highlights the SRMs low technology maturity, compared to the other topologies. The above mentioned reviews on performances have been complemented with a preliminary motor to vehicle matching analysis described in the next section.

2.3 Base Architecture and performances

The motor object of this research, in development in Dumarey Automotive Italia S.p.A., has been designed through in-house built tools and scripts, by

relying exclusively on open-source software. In this section its main data and performance are described to provide to the reader understanding of the product, to which the methodology described in the next chapters is applied. It is given a general description of the relevant literature on which the motor sizing is based, without describing in detail the developed toolset that is part of the Dumarey Automotive Italia S.p.A. Intellectual property (IP). The sizing of the motor has been performed by a Dumarey team of experts and is not object of this research, however the two activities run in parallel synergistically in a way to transfer DfCE methodology benefit to the motor design. The machine under consideration has been conceived for transportation sector, with particular focus on the LCV segment. In Table 2.2 the high-level requirements, adopted in the first design phase, are specifically reported leading to a set of consistent performance targets.

Table 2.2 Drive level requirement and constraints

Description	**Value**
DC link voltage [V]	600
Max peak current [A]	350
Base speed [rpm]	6000
Continuous power at *nb* [kW]	60
Peak power at *nb* [kW]	≥100
Overload time from steady state temperature 150°C [s]	≥ 60
Maximum speed [rpm]	18000
Continuous temp. rise [°C]	90
Peak temp. rise [°C]	120
Cooling method	Water jacket
Max coolant temperature [°C]	60
Max outer diameter [mm]	250
Max stack length [mm]	200
Slot fill factor	> 0.5

Main dimensions for stator and rotor cores, as well as the number of turns per phase necessary for producing the required airgap magnetic flux density and phase flux linkage, have been defined on the base of the classical methodologies reported in [125], [128], [129]. Then the design has been refined and validated through 2D FE simulations, by adopting the opensource software FEMM [130], given the strong non-linearity characterizing the magnetic circuit of SRMs. Main architectural data are reported in Table 2.3.

As reported in [131], a 3 phase, 12/8 configuration was selected by Dumarey specialists as it represents a fair compromise among:

- drive complexity and cost
- fundamental frequency and ensuing power losses both at machine and converter level

- acceptable (i.e., higher than two) harmonic orders for the stator modes of vibration [132], [133]

Table 2.3 Main architectural data

Description	**Value**
Stator/rotor poles	12/8
Phases	3
Turns per pole	10
Coils in series per phase	4
Single wire diameter [mm]	0.9
Equivalent conductor cross-section area [mm^2]	15.9
Stator outer diameter [mm]	246
Length to stator bore ratio	1.2
Minimum airgap thickness (aligned position) [mm]	0.8
Phase resistance at 150 °C [Ω]	0.0323
Overall Mass [kg]	67.8

A 2D cross section of the active portion for the SRM, object of this research, is reported in Figure 2.12

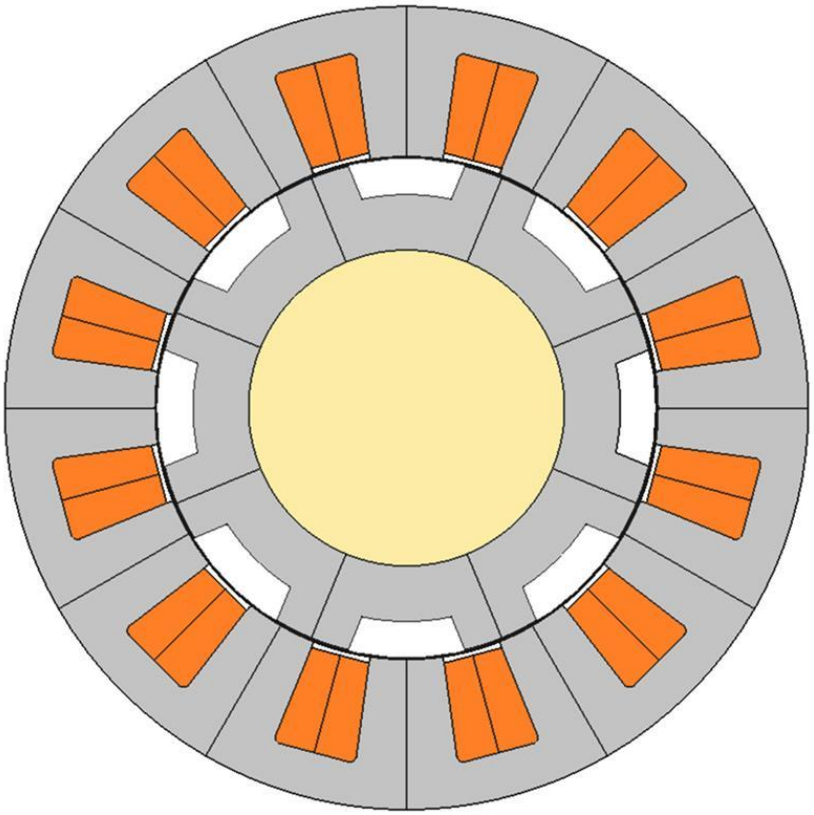

Figure 2.12 2D cross section of the active portion of the SRM object of the research

The goodness of the performance requirement has been verified through a motor to vehicle matching analysis. In particular, the motor has been virtually installed on a LCV available on the market and both acceleration reserve and motor capability to propel the vehicle at different speed and road gradient have been judged. In Table 2.4 are reported the vehicle and propulsion line data considered in the analysis. The vehicle chosen as exemplary reference of the LCV range is the Renault Kangoo Van Z.E, Medium Wheelbase, for which main data can be retrieved from [134].

Table 2.4 Characteristic data for vehicle – motor matching analysis

Symbol	**Parameter**	**Value**
m_1	Curb weight with driver [kg]	1752
m_2	Fully loaded weight [kg]	2230
f_r	Rolling resistance coefficient [-]	0.01
k_{gear}	Reducer ratio [-]	13.37
D_{tyre}	Wheel diameter [m]	0.6345
A	Frontal Area [m^2]	2.91
c_x	Aerodynamic drag coefficient [-]	0.3
η_{red}	Reducer efficiency [%]	97

However, data not available in the above-cited reference have been assumed or estimated following approaches provided in [135], where an extensive analysis of the BEV market is provided. For the rolling resistance coefficient, a mean value reported in the paper has been considered. The paper reports a classification of the rolling resistance coefficient on the base of the maximum vehicle speed, but in this case the average value was more conservative in the estimation of the resistant force. Concerning the estimation of the frontal area the approach provided in the same paper has been used, according to which the frontal area is the 86% of the product of vehicle width and height. An average aerodynamic drag coefficient, representative of a medium-large vehicle population has been extrapolated. Regarding reducer data, a transmission ratio closer as much as possible to the ideal ratio has been defined, while a reducer average efficiency of 97% has been considered.

For the calculation of the torque required an ad-hoc model was developed to take into account the longitudinal dynamics of the vehicles under study, according to conventional well-known literature. The model is also the base for the calculation of the energy adsorbed in the LCA use phase as described more in detail in chapter 4. Equation from 2.2 to 2.3 are used for the calculation of the required motor torque and speed to drive the vehicle at a defined speed. For this purpose, the reference vehicle has been considered fully loaded, in order to verify performances of the motor in the worst condition.

$$T_{mot} = \frac{P_{mot}}{n_{mot}\frac{\pi}{30}} = \frac{\frac{P_{Wheel}}{\eta_{red}}}{n_{mot}\frac{\pi}{30}} \quad (2.2)$$

$$n_{mot} = \frac{60 \cdot k_{gear} \cdot V}{\pi \cdot D_{tyre}} \quad (2.3)$$

Where:

n_{mot}: motor angular speed expressed in rpm, T_{mot}: Motor torque; P_{mot}: Motor power; P_{Wheel}: Wheel power; V: vehicle speed

Power required at wheel is function of vehicle speed, characteristic and road slope. In particular, the force resistant to the motion of the vehicle is the sum of the forces requested to oppose respectively the rolling resistance caused by the deformability of tires and road, the aerodynamic resistance and the road gradient.

$$P_{Wheel} = V \cdot \left(F_{rolling} + F_{aero} + F_{gradient}\right) \quad (2.4)$$

$$F_{rolling} = m_2 f_r g \quad (2.5)$$

$$F_{aero} = \frac{1}{2} c_x A \rho_{air} V^2 \quad (2.6)$$

$$F_{gradient} = m_2 g \sin\alpha \quad (2.7)$$

Where:

ρ_{air}: air density assumed as 1,225 kg/m3; g: gravitational force; α: road inclination angle calculated for gradient from 0 to 50%.

In Figure 2.13 both the continuous and peak motor characteristic torque curves are reported and compared with torque requested to the motor output at different road slope in a representative vehicle speed range (dash curves). Three areas have been identified, respectively below the continuous torque curve (green), between the continuous and peak torque curve (yellow) and above the peak torque curve (red). It is visible that the torque provided continuously by the motor is sufficient to drive the fully loaded vehicle till a 20% gradient, at vehicle speed up to 54km/h. Increasing the slope the motor is able to move the vehicle for a shorter time, reaching peak torque, at a road gradient up to 35% till base motor speed. It has to be noted that the effective traction capability of the tyres, which is influenced among others by the tyres characteristics, the road conditions and the weight distribution, has not been considered here. This comparison gives confirmation that the motor requirements, from a performance point of view are correct, considering the installation on a typical LCV.

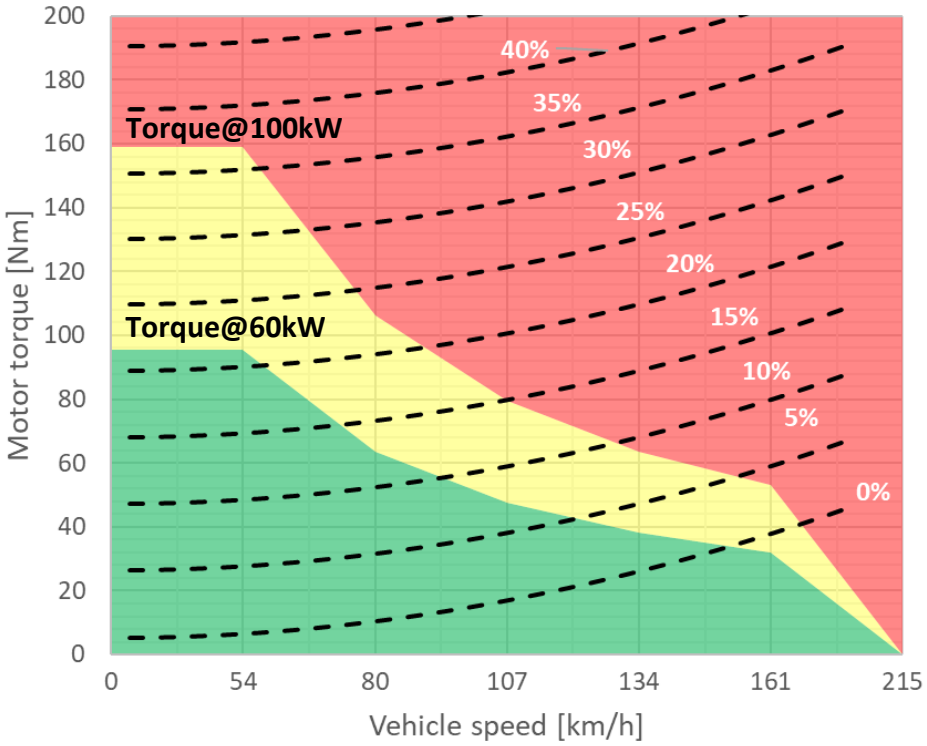

Figure 2.13 Motor – Vehicle Matching

Similar investigation has been performed calculating the acceleration reserve defined as the difference between the maximum traction force at wheel (F_{tr}), and the force required to drive the vehicle, known also as road load (F_{res}), both normalized by vehicle mass. This calculation has been performed according to equation from 2.8 to 2.10 without considering road slope resistance and assuming curb weight of the vehicle and a driver mass.

$$\alpha_r = \frac{F_{tr}}{m_1} - \frac{F_{res}}{m_1} \tag{2.8}$$

$$F_{tr} = \frac{T_{mot} \cdot k_{gear} \cdot \eta_{red}}{\frac{D_{tyre}}{2}} \tag{2.9}$$

$$F_{res} = F_{rolling} + F_{aero} \tag{2.10}$$

In Figure 2.14 are reported the normalized maximum traction force, and roadload and the acceleration reserve.

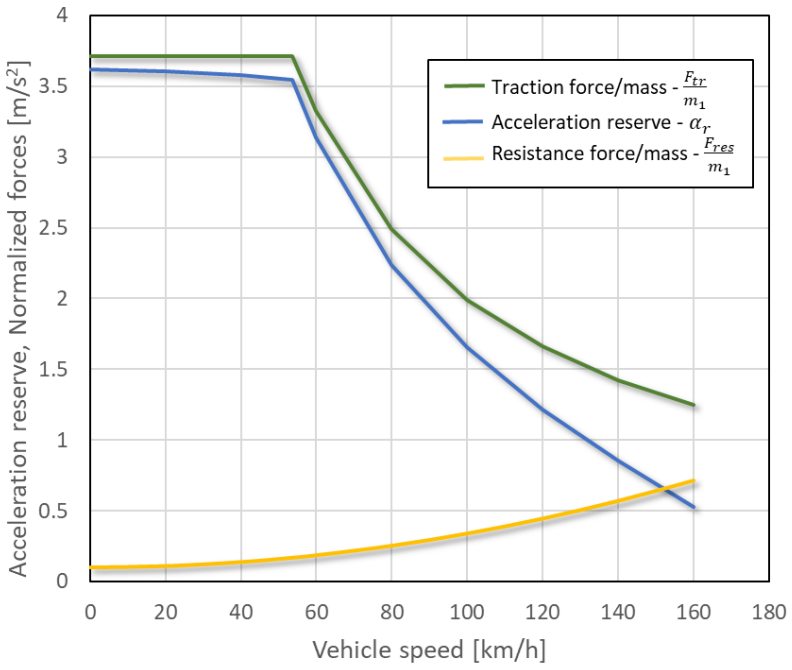

Figure 2.14 Acceleration reserve, maximum normalized traction force and normalized required force against vehicle speed

Values calculated are aligned with benchmark data reported in [135]. Indeed, the medium-large EV population, that is comparable in terms of performances and mass to the case study here proposed, is characterized by normalized traction force between 3.5 and 6 in the speed range between 0 and base speed. Also estimated roadload is comparable with the same evaluated database.

Chapter 3

Design for Circular Economy Methodology

3.1 Design for Circular Economy approach

CE model for electric motor is a cutting-edge research topic as highlighted in the literature review [73], that indicates also the recycle as predominant field of investigation, rather than reuse and remanufacturing. However, more than half of the papers related to remanufacturing are dedicated to product design, even if they are oriented towards efficient resource usage. A design for assembly and disassembly methodology, applied to the electric motor case study, is described in [77], focusing on the disassembly operation process and its criticalities. In this paper is not considered the opportunity to disassemble critical parts from the assembly. An example of remanufacturing of electric motor is represented by the company Ace Re-use Technology, that however is focused on the replacement of bearings with higher quality counterpart, to increase durability, as reported in [78].

This research, on the other hand, focuses on a systemic approach to product design for sustainability improvement, incorporating CE principles into the design itself. In this chapter, the selected design methodology, its integration into the conventional design flow, the identified design strategies, and the associated implemented features are described. Tackling this topic, the first question was related to which level of design to concentrate the work on, starting from the baseline design described in Chapter 2. As detailed in [34] many Design for Sustainability methodologies have been adopted and have evolved in the last decades. In short, methodologies are classified based on two main aspects. On one side, it is considered the evolution from a technology innovation perspective towards a socio-technical perspective, with user practices and behaviours playing a fundamental role. On the other side, it is considered the enlargement of the

boundaries from the firm's perimeter to wider socio-economic system. Additionally, methodologies are characterized by a different scope concerning the environmental, social, and economic sustainability branches. This work focuses on the product space, exploring methodologies like Ecodesign and Emotionally Durable Design, integrating CE principles into product design. The design activities concentrate mainly on technical innovation and are conducted within the boundaries of a company, without involving external actors. Regarding sustainability directions, the research is currently oriented towards environmental and economic aspects. The intent of this research is to integrate the CE concept within the conventional Design process, building tools to support decision-making at product design level.

Product design conventionally follows a route starting from requirements setting to analysis results through iterative loops. To improve product sustainability, some additional phases need to be considered from the beginning of this process. The Figure 3.1 shows the novel steps, reported in the green boxes, introduced into the traditional workflow summarized with the white boxes.

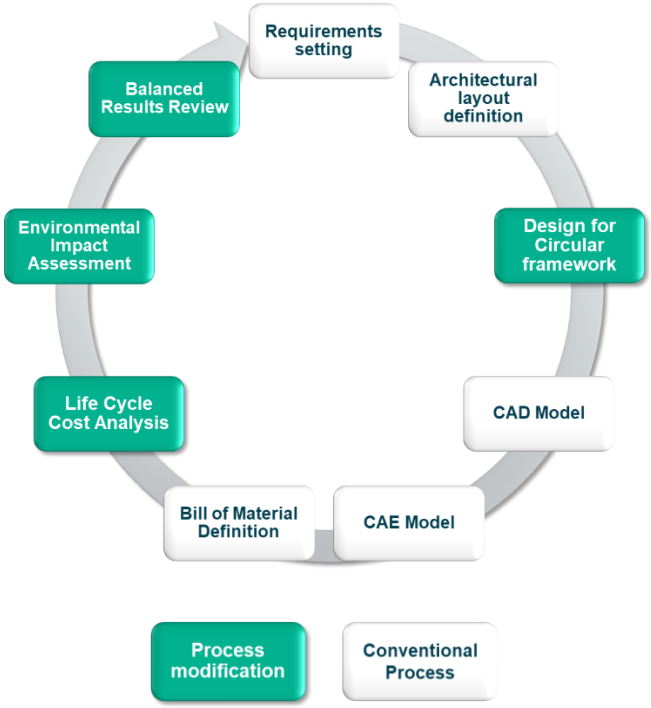

Figure 3.1 Design for Circular process developed, highlighting conventional (white boxes) and novel (green boxes) steps

Main process modifications are summarized as follows:

1. The first step is the introduction of a framework through which the CS for the reintroduction of the motor into its cycle and the initial design proposals to implement them are defined, as described in detail in section 3.1.1.

2. The design features enabling product circularity have to be introduced in the CAD model through the conventional approach. The design modifications are described in detail in sections 3.3.1 to 3.3.3.
3. The conventional cost estimation approach should evolve to consider a life cycle approach. However, in the activities covered by this research, only manufacturing costs are considered. The implemented cost model is described in detail in a dedicated section in Chapter 4.
4. Another step is the calculation of environmental impacts through life cycle analysis (LCA). Detailed modelling activities and the considered scenarios are reported in Chapter 4.
5. The last step is the evaluation of both environmental and economic impacts, as well as classic Key Performance Indicators (KPIs) such as performance and duration, which are evaluated in a traditional workflow.

3.1.1 Design for Circular Economy Framework

In this section, the DfCE framework built and adopted within the research activity is described. It was developed for the purpose of this research, but it is also usable for the design of other products conceived for a CE from the beginning of their development. The adoption of such a structure is key to considering all the opportunities available and reachable through proper design features from the earliest phases. The established framework includes both design for circular concepts described in [48] and design for life cycle, specifically Ecodesign, providing guidelines in terms of design configuration to achieve the highest level of sustainability. Ecodesign was considered in the developed framework as it provides a comprehensive approach to the entire product life cycle, facilitating the integration of the CE principles into design [34].

However, the DfCE methodology seeks to enhance the maintenance and reintroduction of a product into its lifecycle. This is achieved through various CS, which are briefly outlined in this paragraph. These strategies focus on optimizing the product's design, extending its life, and facilitating its recovery.

Figure 3.2 illustrates Ecodesign and circular design strategies, divided into durability, extended use, and recovery. These are further broken down into life cycle stages, durability paths, and circular loops, as shown in the graph slices. For each of these slices, design approaches have been identified to reach the final goal. The contents present in the baseline design are reported in black. Strategies selected and evaluated within this research are highlighted in dark blue, while opportunities still not implemented or evaluated from an environmental and economic standpoint are reported in light blue, as they are considered out of the perimeter for this work.

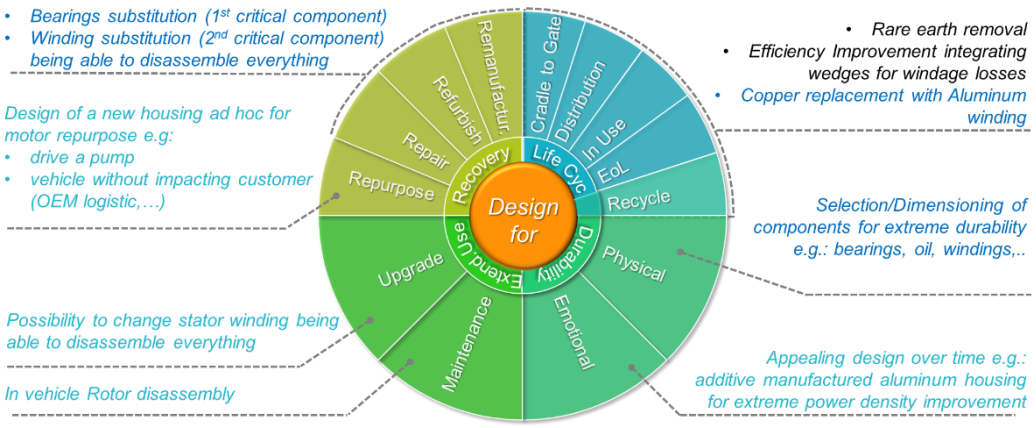

Figure 3.2 Design for Circular economy Framework developed for the identification of the design strategies and definition of the related design features

- **Design for Life Cycle** With reference to the life cycle portion, the phases from material extraction to motor production, summarized as Cradle to Gate (C2G), the distribution, the use phase, and the End of Life (EoL) are included. The selection of a RE free machine implicitly aims to improve the environmental and economic impact of the C2G, distribution, and EoL phases, as described in Chapter 2. Additionally, the baseline SRM design is oriented towards efficiency improvement through the adoption of rotor wedges, which are able to reduce the windage losses by about 1kW at high speed, according to in-house calculations (patent pending). Furthermore, stranded windings are adopted to minimize AC losses due to skin and proximity effects. Within this research, the potential to improve the sustainability of the motor through Ecodesign has been further exploited, with the evaluation of a virtual configuration adopting aluminium stator winding, as described in detail in section 3.3.1.

- **Design for Durability**. The possibility of design for durability has been explored by considering both physical and emotional aspects. The product physical advancement can be achieved through the adoption of technical solutions oriented towards robustness, while emotional durability enhancement can be achieved by following strategies that enable the product to maintain a durable appeal for customers throughout its lifespan. Both the strategies, however, could increase the complexity and the cost to the product. Regarding physical durability, the initial step involves analysing the most critical components of an electric motor. In this context, various sources identify the bearings and the stator winding as the most reliability-critical elements. According to [136] a failure breakdown for Totally Enclosed Fan Cooled (TEFC) motors shows that bearings are responsible for 69% of the failures, while stator winding account for

21%. ABB, in its guide to prevent failure of the industrial motors, states that bearings and stator winding respectively account for 51% and 16% of total motor failures [137]. It is important to note that the aforementioned surveys typically focus on industrial, mains-fed motors, where the windings are generally not exposed to extrinsic stress (i.e., partial discharge inception). However, when examining converter-fed machines, such as those used in transportation, the incidence of winding failures may increase compared to that of bearings. In this regard, different pathways in the motor design could be pursued, such as using higher load capacity bearings, higher thermal class windings, and properly designing cooling and lubrication circuits, as described in more detail in the section 3.3.2. Regarding the emotional aspect, both an extraordinary performance increase and an unconventional technological approach could represent ways to increase customer awareness about owning a long-lasting product. In this respect, an example is the adoption of techniques like Design for Additive Manufacturing (AM) to significantly improve the power to weight ratio and efficiency of the motor [138]. This is however true for solid piece rotor, not characterized as the laminated rotor, by layer thickness conventionally lower than minimum printable features [139]. AM could enable the creation of unique rotor designs that improve weight and efficiency, offering environmental benefits during the use phase of the product lifecycle. In particular, employing AM makes it possible to create hollow features, rotor blades, and honeycomb structures, which positively impact windage losses and reduce torque ripple, especially relevant in SRM, as reported in [140]. Another opportunity offered by AM is the ability to create coil cross-sections that maximize the slot fill ratio and customize windings for weight and volume advantages, resulting in a positive environmental impact during the use phase of the product lifecycle. Additionally, AM enables the creation of custom-shaped windings which can embed cooling channels, allowing for a direct heat extraction and leading to extreme current densities as highlighted in [141], [142]. Finally, AM could enable the creation of unique cooling channel designs in the aluminium housing, enhancing both thermal exchange (performance and durability) and lightweight design. Such a design improves weight and, in principle, efficiency leading to environmental benefits during the use phase. This could impact durability by improving both physical durability (better temperature distribution) and emotional durability, providing an opportunity for advertising the product. For example, the company Equipmake presented its electric motor as the most power-dense Permanent Magnet motor in the world [143]. This pathway, however, has not been pursued at the moment, as it is considered not aligned with the SRM selection, which is highly cost oriented.

- **Design for Extended Use**. Moving to the other framework slices, both for the extended use and recovery fields, the design approach focused on developing a product capable of full disassembly. This allows for both an easy maintenance and replacement of parts as needed (e.g., regular maintenance, repair after failure, or upgrades to favour market permanence) and facilitate the selected business strategy (refurbishing, remanufacturing, or repurposing). The above-mentioned approach is described in detail in the section 3.3.3.

- **Design for Recovery**. In the field of Recovery, another opportunity lies in the Repurposing CS. This approach evaluates the potential for giving a motor a second life in a different market or application, which may involve a less demanding use phase. This strategy can be implemented by designing a custom housing that allows for flexible adaptation to various applications. As mentioned, both the application and market can change in this second life. For instance, the motor could be repurposed to drive a pump with lower power requirements or reduced dynamic demands. Another possibility is installing the motor in a vehicle with different usage patterns and operating environments, such as a forklift. However, the repurposing strategy is not addressed by this research, due to the necessity of knowing in advance the scope of potential repurposes.

- **Design for Recycle.** It is the final circular loop, as it focuses solely on preserving the material value of a product. In the framework, recycling is depicted after the EoL stage, as it is more commonly applied than other CS. Additionally, recycling of SRM is advantageous because the product has a 99% recyclable Bill of Materials (BOM), making it a lower priority for this research. Moreover, the ease of disassembling the entire motor is advantageous for materials recycling. Consequently, the LCA model and results presented in Chapters 4 and 5 incorporate recycling in all the CS evaluated, including the baseline scenario. In fact, the recycling phase is considered the default EoL option, following the linear model.

3.2 Design strategies

This paragraph describes the Design Strategies considered within the PhD research, which were already identified through the DfCE framework described in paragraph 3.1.1. In particular, four strategies are presented that aim to increase product sustainability by improving life cycle phases, extending the life cycle, and reintroducing the product into its life cycle.

The aforementioned strategies and the associated design features are summarized in Figure 3.3. As mentioned, recycle phase is considered the final stage in all the identified configurations, including the baseline one, in addition to

the linear model (production, use, and disposal), to which all the others are compared. Indeed, it is possible to recycle majority of the material even if the motor is conceived for a linear model. This concept applies even more to the SRM case, which is characterized by the absence of PMs. Unlike in the typical PMSM for automotive field, permanent magnets cannot be recycled with a magnet-to-magnet approach. Hence, in the results section, the impact of recycling will be evaluated for all the considered strategies, not representing a characteristic difference between them. The first strategy is represented by an Ecodesign configuration, where the baseline copper winding has been replaced with aluminium winding. In this case, in addition to the environmental impact, KPIs have been compared with the baseline to verify the acceptability of the technical solution. Regarding CS, the intent is to focus on increasing the lifetime or substituting only the components considered critical from an aging perspective while maintaining the rest of the motor. Stator winding and front bearing are the sole parts of the studied motor to be considered critical, from a durability stand point, as described in section 3.3.2. This approach reduces the environmental and economic impact linked to C2G phases. Following this path, three CS have been exploited and are defined as Extended Durability, Remanufacturing 1, and Remanufacturing 2, respectively, according to the different degrees of new parts adoption in the second life cycle. In the figure, components required for Ecodesign, remanufacture options and extended durability, which are identical to the baseline, are reported in black, while new contents considered in each configuration, as well as for a second life cycle, are reported in green. The Ecodesign configuration, as mentioned, is identical to the baseline except for the aluminium winding. In the Extended Durability configuration, the motor is equipped with a higher load capacity front bearing (considered critical after one life cycle in the baseline design) and a higher thermal class winding, doubling the life of the motor. This strategy is ideal for material maintenance in the life cycle and energy expenditure; however, it could present challenges from a business perspective in certain applications. Regarding Remanufacturing 1, it is characterized by starting hardware comparable to the conventional design in terms of bearings and windings. In this strategy, bearing and winding will be replaced at the end of the first life cycle with equivalent counterparts, making the realization of a second life cycle possible. Remanufacturing 2, on the other hand, features a higher thermal class winding, which doubles the life of the winding itself and results in only the front bearing needing replacement at the end of the first life cycle. It is worth mentioning that this is valid only if the machine is designed with thermal stress as the winding's prevailing aging factor.

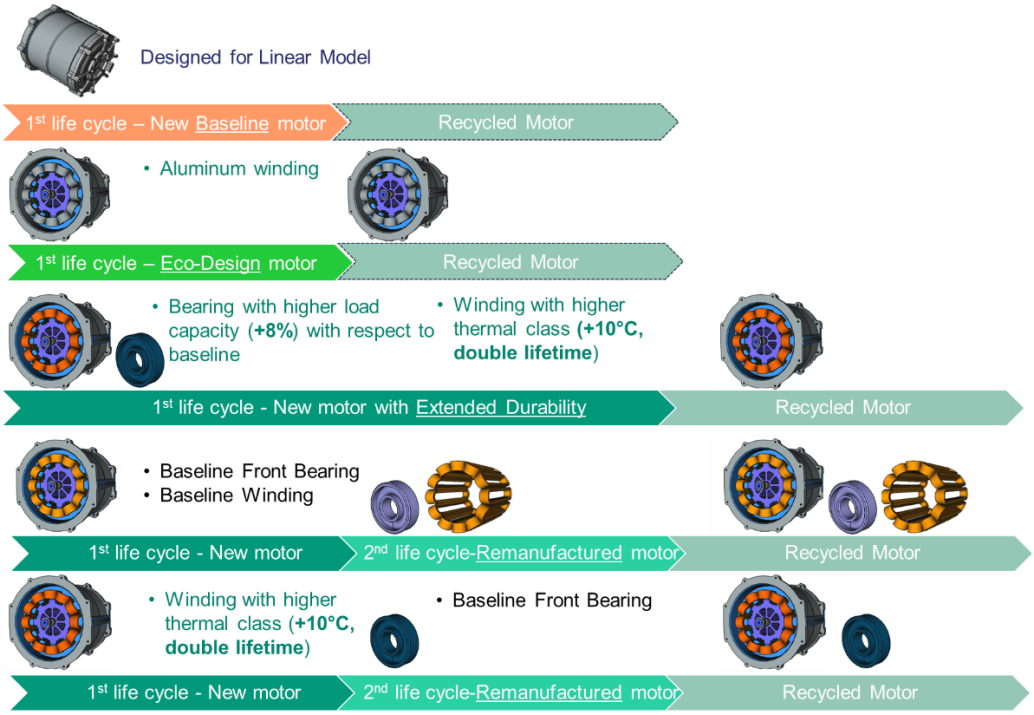

Figure 3.3 Design Strategies (Ecodesign, extended durability, remanufacturing 1 and 2) implemented and evaluated against baseline within the research activities

3.3 Design features

In this section are described design features and approaches implemented to allow realization of the described design strategies. Indeed, in the following paragraph are reported both the design activities oriented to life cycle optimization, and those related to the improvement of the product for what concerns its maintenance and reintroduction in the economy chain. The baseline motor to which the design features are applied is the one described in Chapter 2.

3.3.1 Design for life cycle (Ecodesign): aluminium winding

Ecodesign of electric motors, and more in general of vehicles, is historically associated with efficiency improvement. Nowadays, however, design strategies for life cycle and for CE are becoming topics of high interest as stated in [73], [106]. Asynchronous motors with different efficiency levels, due to material change, have been studied evaluating trade-offs between various life cycle stages in [144]. Within this piece of research, the implementation of an Ecodesign strategy has been realized through the change of the stator winding material from conventional copper to aluminium. The novel configuration is considered appealing for its high cost-effectiveness and is evaluated, taking into account not only the materials' change effect, but also the different efficiency influence on environmental impact. For all these considerations, aluminium winding together with RE free machines is currently representing a cutting-edge topic, as noticeable from the increasing number of research works. In particular, the company

Advanced Electric Machine (AEM), that along with Enedym represents a significant reference for SRM development, has patented a compressed coil technology capable of delivering up to a 30% increase in motor power density, allowing the replacement of copper with recyclable aluminium windings in their next-generation motor designed for passenger cars and showed in Figure 3.4 [145]. Indeed, a compression of the coils after a pre-winding eliminates fill gaps and air pockets increasing slot fill rates with respect to conventional technology.

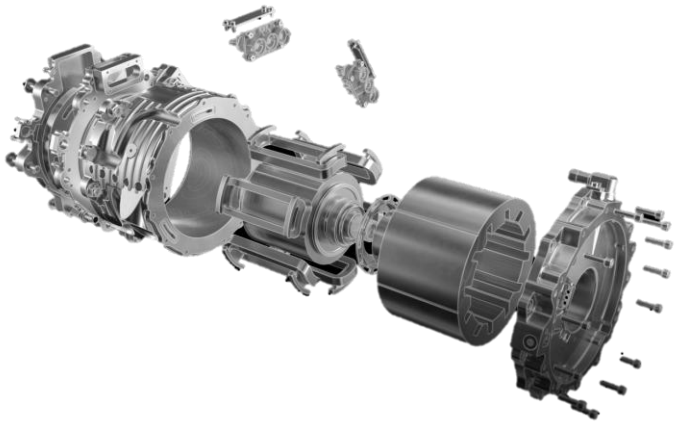

Figure 3.4 SSRD rare earth free motor with aluminium winding from AEM [145]

Another example of RE, copper free motor is the SynRM developed by the Alumotor-UK consortium [146]. The intent, in alignment with the strategy behind the development of the SRM object of this research, is always to offer a low cost, sustainable and robust machine for LCV and Off-Highway market. Figure 3.5 shows the main components of the motor, that in its highest power version, will be equipped with ferrites permanent magnets.

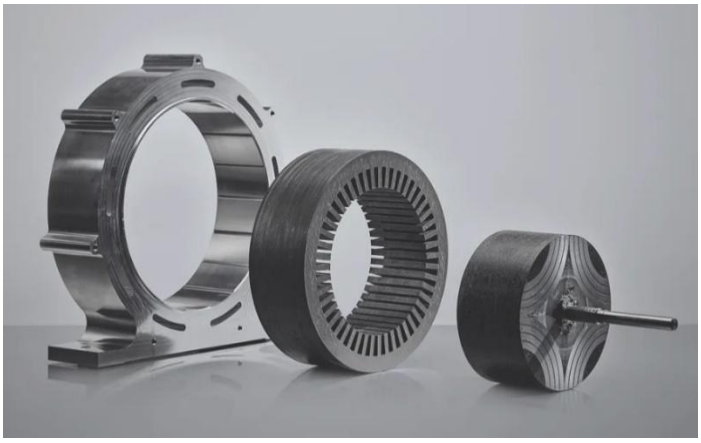

Figure 3.5 Alumotor rare earth copper free from UK-Alumotor [146]

Additionally, there are many studies comparing copper winding with aluminum winding even if on PMSM. In particular [147] provides a thermal comparison, showing loss and weight reduction in some circumstances when adopting aluminium, while [148] presents an assessment of the compressed

aluminium winding compared to a conventional distributed copper winding, demonstrating the comparability of electrical loading between the configurations. A similar investigation is presented in [149], where however lower output performance for the aluminium configuration has been shown. Regarding hairpin winding, a performance comparison between aluminium and copper configurations is shown in [150]. In this case, the aluminium configuration shows higher losses at peak torque but competitive performance under power conditions.

The aluminium winding machine considered, described in detail in [131], is a "virtually re-wound copper machine" featuring identical magnetic structure of the baseline one (including winding layout, wire cross section, insulation class). In particular, the architectural features reported in Table 2.3 are applicable also to the aluminium winding configuration, with the exception of the overall motor mass, that is influenced by the different material density, as described in detail in this chapter. The investigation approach here described is finalized to assess winding material change through evaluation of performance achieved in the new configuration with respect to the conventional one. A detailed comparison, based on a multidisciplinary approach, is described in the mentioned paper and is just briefly reported in this section. The performance assessment reported in this section is the result of analyses executed through in-house (i.e., Dumarey Automotive Italia), custom-developed tools and scripts, by relying exclusively open-source software. The Figure 3.6 a, b and c below report the continuous rms current for the two machines, and the corresponding continuous torque and power vs. speed capability respectively in the speed range. Aluminium winding SRM, confirms the achievement of the requirement set for the base copper machine and mentioned at section 2.3. However, it has to be mentioned that the new configuration leads to both lower maximum power and torque, compared to copper winding SRM. It is important to mention that the aluminium version leads to a decrease in the overload time margin from 60 to 20 seconds, reaching earlier the critical temperature threshold of 180°C as represented in Figure 3.7. The figure shows the time for which the peak power can be delivered before exceeding a hot-spot temperature rise of 30°C, considering starting from a steady-state temperature of 150°C. Lower performances of the aluminium winding SRM configuration are associated both to winding material change and to the fact that the structure of the machine is identical in the two configurations, including cooling circuit architecture and the winding fill factor. Concerning the first, a temperature limit is reached earlier in the aluminium winding SRM case than in the copper winding case, however, the performance reduction is considered acceptable as other products on the market are featuring similar behaviour. Indeed, Toyota Prius 2010 motor tested by Oakridge National Laboratory [151] is maintaining peak power of 60kW for 18s before reaching a stator temperature of 150°C while Ioniq 5N achieves an extra power for a 10s interval [152]. These values are also aligned with the targets for 2020 selected by the US DOE, which are 55kW peak power for 18 seconds [153].

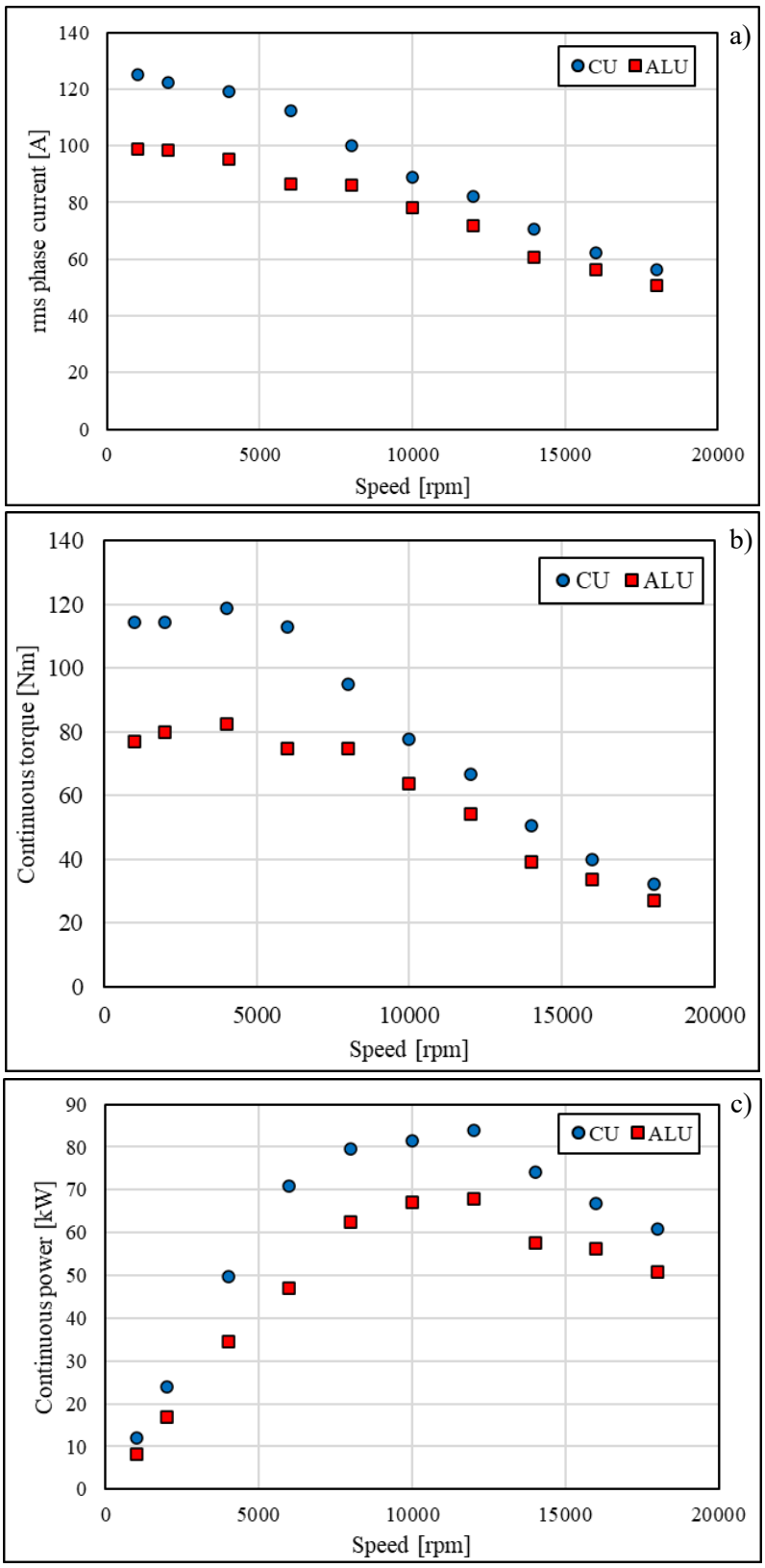

Figure 3.6 Copper vs Aluminium: winding performances against motor speed a) rms phase current, b) continuous torque, c) continuous power

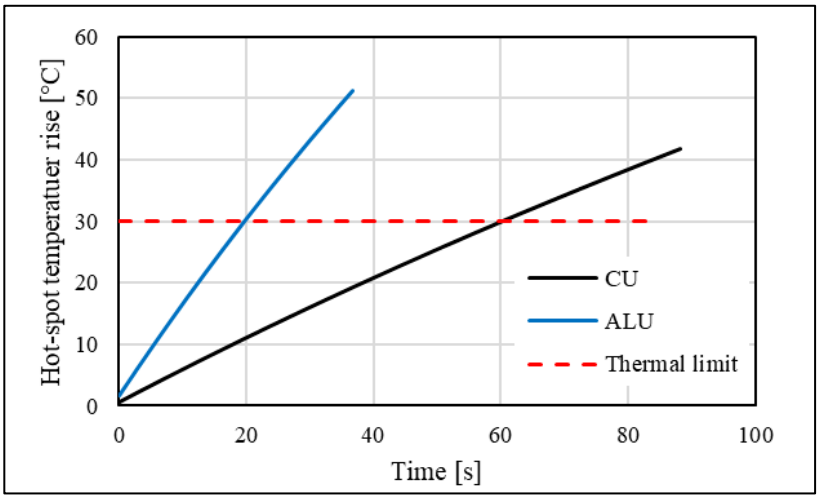

Figure 3.7 Copper vs Aluminium: temperature rise

As known, the electrical resistivity of aluminium is 60% higher than that of copper, while the mass density of aluminium is about 30% that of copper, leading to higher peak power density and to lower peak efficiency at a given electrical loading. Current density is different consistently with the different resistivity and in particular the copper winding SRM can withstand 20% higher continuous current density, up-to base speed (6 krpm). The current density withstand-ability difference between the two machines tends to decrease at higher speeds (i.e., within the range 6 to 18krpm), as in this operating range core losses tend to prevail over Joule losses. Difference in efficiency is key to determine behaviour of the two configurations from an energy consumption perspective, however in the LCA the utilization of the different machines within a specific application is also considered. Figure 3.8 shows the steady-state efficiency comparison between the two machines configurations at maximum continuous performances, while Figure 3.9 illustrates the efficiency map of the aluminium winding SRM, its cycle operative point and the copper winding SRM envelope.

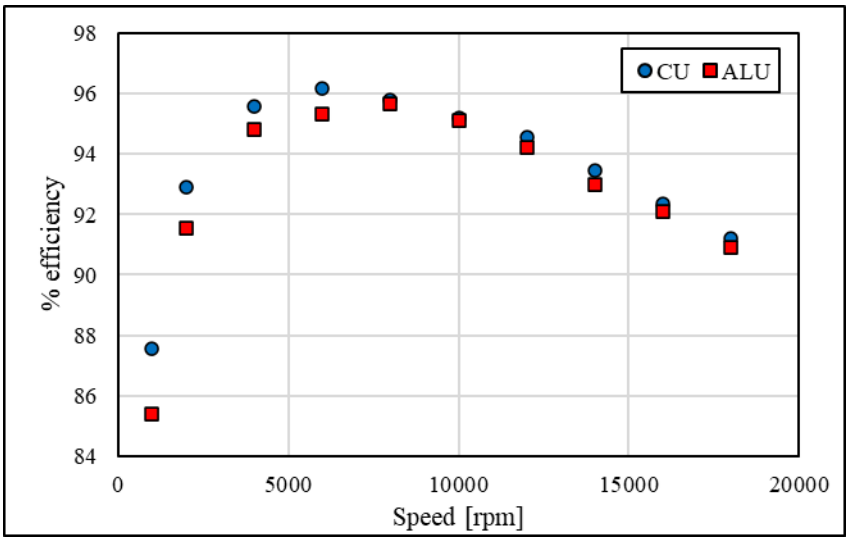

Figure 3.8 Copper vs Aluminium: efficiency

The life cycle energy calculation methodology, dependant also from application and used for the definition of the cycle operative points, is described in detail in section 4.2.1 and it's here just mentioned. It is possible to note that the machine's torque capability exceeds the application requirement, implying a wide margin for mass/volume reduction, and cycle efficiency increment. However, it is also noticeable the torque-speed envelope reduction at higher speed, with respect to copper winding SRM envelope, due to the aluminium's lower thermal limit. The above-mentioned derating for speeds higher than the base motor speed, leads to lower losses in the aluminium winding SRM in the operating cycle points. This is mainly due to a better combination of winding resistance (i.e., turns per phase) and control strategy to limit thermal overload in the mid-high-speed region. Aluminium winding SRM is virtually running the considered driving cycle at higher torque level than copper SRM with respect to their own maximum capabilities, working at favourable efficiency. This is reflected in lower energy losses with respect to both the analysed PMSM and copper winding SRM with a value of 25 [Wh/km], as described in the section 4.2.3. The substitution of copper winding with aluminium affects all phases of the life cycle. This is due to the differences in raw resources extraction, manufacturing process, efficiency during the use phase, and recycling process. Also, the different winding mass, reduced from 7.8kg of the copper configuration to 2.1kg of the aluminium configuration, impacts the use phase. Concerning the manufacturing stage, due to lack of data related to the aluminium wiring process in the background dataset, for the purpose of this research, it has been conservatively assumed to not modify the copper's winding wire manufacturing process as it was considered more energy intense with respect to aluminium counterpart, due to the higher melting temperature of copper.

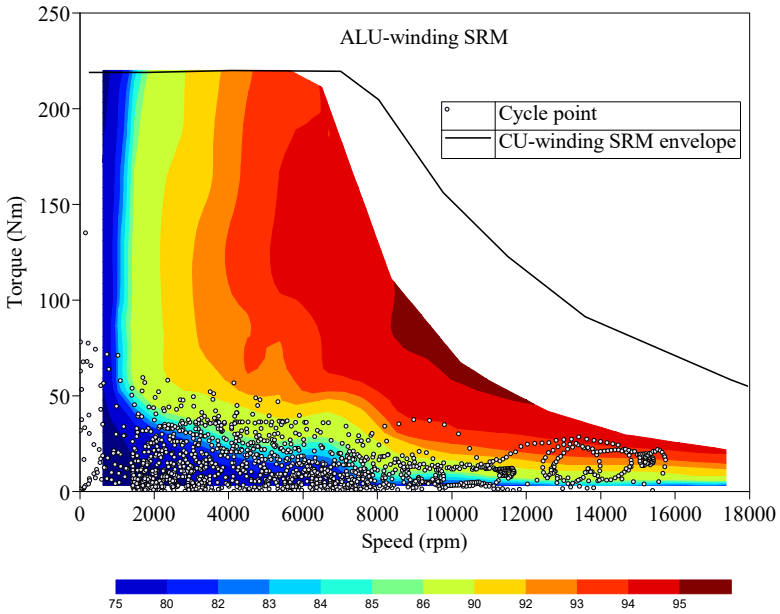

Figure 3.9 Efficiency map of the SRM with Aluminium windings compared with the copper winding SRM envelope and operating point of the WLTC

In Table 3.1 are summarized the most significative differences between copper winding SRM and aluminium winding SRM configurations.

Table 3.1 Main differences between copper and aluminium winding configuration

Parameter	**Copper winding**	**Aluminium winding**
Winding mass [kg]	7.8	2.1
Power density [W/kg]	1.5	1.6
Winding material cost [$/kg]	57.8	5.25
Overload time margin [s]	60	20

From a noise and vibration perspective, the aluminium winding configuration has slightly better performance as summarized in Figure 3.10 where are reported the forcing frequency harmonics related rotational speed and stator resonance frequencies for circumferential mode 4, that is the first circumferential mode to be excited (apart from mode 0 or "breathing mode") in the considered SRM. Indeed, it is visible that aluminium winding configuration is characterized by a higher modes' excitation compared to the copper winding configuration.

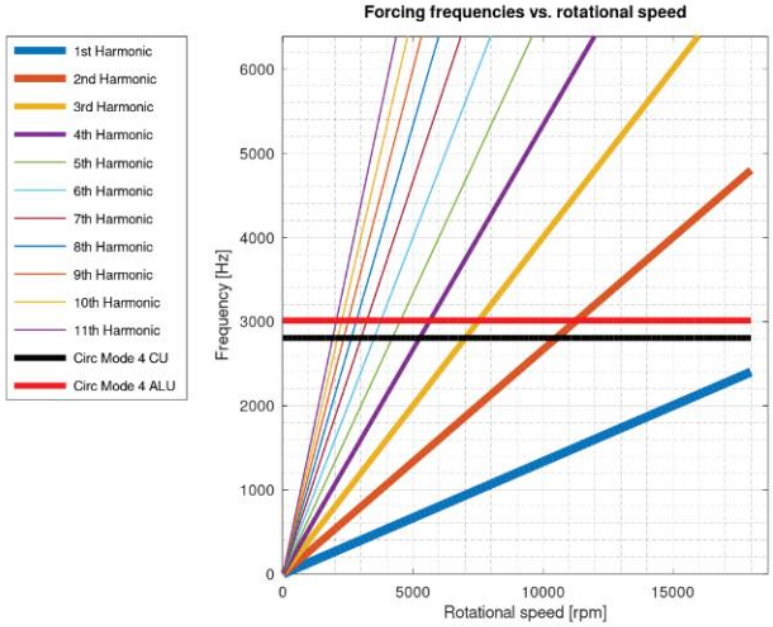

Figure 3.10 Copper vs Aluminium frequency: forcing frequency harmonics against rotational speed and stator resonance frequencies for circumferential mode 4

The stator's cylindrical vibration modes are analytically evaluated using cylindrical shell theory [154], modelling the stator yoke as an infinitely long hollow cylinder. Stator teeth and windings are assumed to contribute only as added mass, without providing stiffness. The natural frequencies of the stator structure follow equation (3.1), where $circ$ represents the circumferential mode order, M_y the yoke mass and $M_{t\&w}$ the lumped mass of teeth and windings. The corresponding stiffness term K_{y-circ}, is derived Donnel-Mushtari theory [132].

$$f_{n-circ} = \frac{1}{2\pi}\sqrt{\frac{K_{y-circ}}{M_y + M_{t\&w}}} \tag{3.1}$$

The usage of aluminium winding represents a further mean for lowering cost of a machine that is intrinsically cheaper than other technologies as demonstrated in [119] where the total cost of the SRM is respectively 50% and 44% lower compared to a PMSM and to an IM.

3.3.2 Design for Durability: bearings and winding sizing

Design for Durability is oriented to extend the life of the product, increasing consistently the use phase in comparison to the conventional configuration. In order to achieve this objective, this research focused on the sizing of the identified most critical components. All the parts of the baseline SRM were considered to be durable for twice the duration compared to the conventional lifetime with the exception of the front bearing and the stator winding.

Concerning bearings, the baseline motor is equipped with two deep groove ball bearings respectively mounted on the front and rear side. Alternative bearing types have been discarded due to the increased integration complexity. Bearings for the various configurations have been sized according to the conventional SKF life estimation approach thoroughly described in [155], applied to a selected application through an in-house developed tool. Bearings life under variable operating condition at 90% reliability is rated using:

$$L_{10m} = \left(\sum_{i=1}^{n} \frac{U_i}{L_{10m\_i}}\right)^{-1} \tag{3.2}$$

Where U_i and L_{10m_i} are respectively the life cycle fraction and the SKF rating lives under variable conditions calculated for fractions of 1 second for the WLTC, assumed as representative of the motor usage in real life. The life rating instead has been calculated assuming the life modification factor that takes into account lubrication conditions, the load level in relation to the bearing fatigue load limit and the contamination level, according to the following equations:

$$L_{10m\_i} = a_1 a_{SKF\_i} L_{10\_i} = a_1 a_{SKF\_i} \left(\frac{C}{P_i}\right)^p \tag{3.3}$$

Where C is basic dynamic load rating, P the equivalent dynamic bearing load, p is the exponent of the life equation, assumed equal to 3 for ball bearings, while a_1, assumed equal to 1, and a_{SKF} are respectively the life adjustment factor for reliability and the life modification factor. Being the bearings, loaded with simultaneously acting radial load F_R and axial load F_A, the equivalent dynamic bearing load P is obtained from the general equation:

$$P_i = X_i F_{R\_i} + Y_i F_{A\_i} \tag{3.4}$$

Where X and Y are respectively the radial and axial load factor for the bearings, determined from tabulated values, for each cycle interval as function of axial force Fa and of the bearings static load C_0 and calculation factor f_0, according with the relationship:

$$X_i, Y_i = f\left(f_0 \frac{F_{A\_i}}{C_0}\right) \tag{3.5}$$

Radial and axial loads F_{R_i} and F_{A_i}, are dependant from the vehicle application, transmission and motor architecture described in Chapter 2. The life modification factor has been also determined from tabulated values for each interval of the considered operative cycle, on the base of the above-mentioned influencing factor according to following equations:

$$a_{SKF} = f\left(k_i, \eta_c \frac{P_U}{P_i}\right) \tag{3.6}$$

$$k_i = \frac{\upsilon}{\upsilon_{1\_i}} \tag{3.7}$$

Where lubrication condition k is instantaneously evaluated on the base of the of the actual operating viscosity selected υ and of rated viscosity υ_1, function of the mean bearing diameter and rotational speed. The contamination factor η_c has been assumed equal to 0.6 as representative of normal cleanliness condition for the considered application, while the fatigue load P_U is tabulated for each bearing.

Specific parameters required for the described calculation cannot be disclosed as they are considered Dumarey Automotive Italia's industrial property. However, they are listed in Table 3.2 in normalized form for the front bearings selected to build the Baseline, the Remanufacturing and the Extended Durability configurations. Rear bearings are not reported as they are not critical and so identical in all the adopted Design Strategies. Additionally, dynamic load on bearings and lubrication conditions are reported in Figure 3.11 and Figure 3.12. It is visible that a front bearing with a higher load capacity and same key dimensions has been selected for the Extended Durability strategy to double the lifetime of the baseline.

Table 3.2 Bearings main specifications and life rating

Symbol	Description	Baseline, Remanufacturing 1,2	Extended Durability
d	Internal diameter [mm]	d_F	d_F
D	External diameter [mm]	D_F	D_F
C	Dynamic load [kN]	C	1,08 C
C_0	Static load [kN]	C_0	1,15 C_0
P_U	Fatigue load limit [kN]	P_U	1,13 P_U
V_{limit}	Limiting speed [rpm]	V_{limit}	V_{limit}
f_0	Calculation factor	f_0	f_0
υ	Operating viscosity [mm^2/s]	υ	υ
L_{10m}	SKF rating life [km]	L_{10m}	~2 L_{10m}

Load calculation on both front and rear bearing provide clear explanation of why the front bearing is more critical in this application; indeed, the dynamic load on the front side is six times higher with respect to rear one.

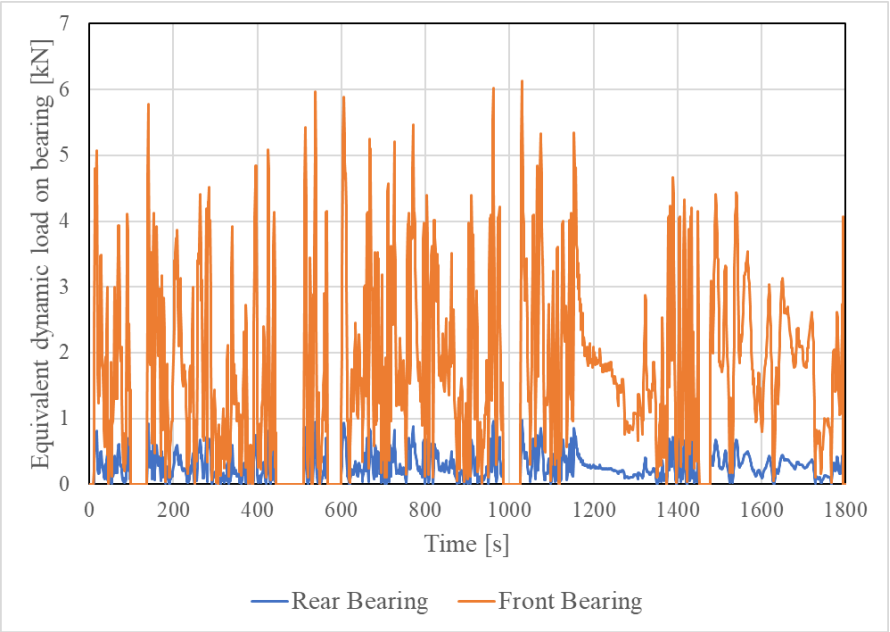

Figure 3.11 Copper vs Aluminium frequency Dynamic load on motor's front (orange) and rear (blue) bearings calculated along WLTC

The Figure 3.12 shows the viscosity ratio that is an index of lubrication condition; in particular during active parts of the cycle, the front bearing is involved for almost 82% of the time by boundary lubrication ($0.1 < k < 4$) and for the rest by fully lubricated film ($k > 4$) while the rear bearing is instead always in boundary lubrication.

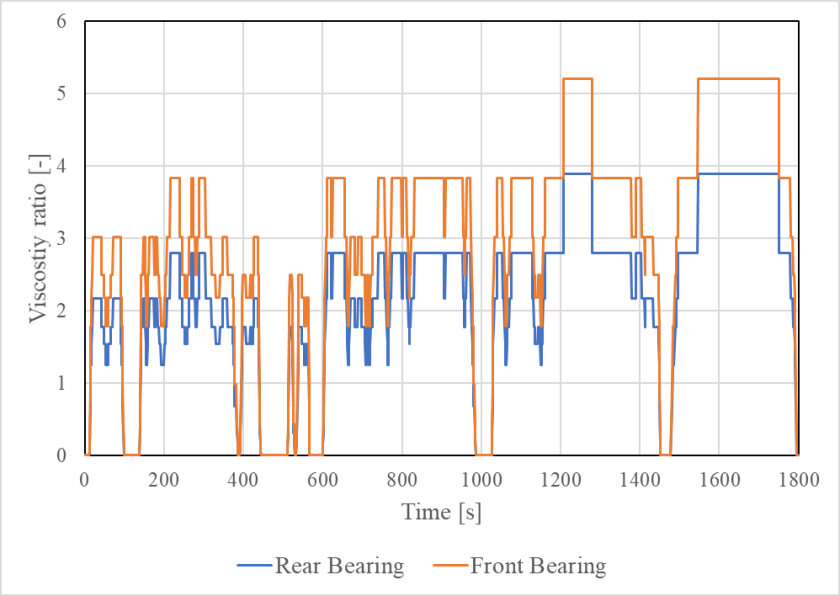

Figure 3.12 Viscosity ratio on front (orange) and rear (blue) bearings calculated along WLTC

Regarding the winding, the baseline motor is equipped with a winding that can meet performance and thermal requirements, specifically being able to withstand a critical peak temperature of 180°C. Indeed, in the baseline configuration, a stator winding with polyesterimide insulation has been adopted. This insulation is characterized by a wire material Temperature Index of 195°C at 20,000 hours, according to IEC 60172. To achieve the durability target set by the Extended Durability strategy, a higher thermal class winding has been selected for this configuration. Specifically, a copper winding with a Temperature Index of 212°C has been chosen. This winding is characterized by a Theic-modified polyesterimide, enhanced with polyamide-imide. The new material results in a 20°C higher temperature class as reported in Table 3.3 with respect to the baseline winding.

Table 3.3 Winding main specifications and life rating

Description	Baseline, Remanufacturing 1	Extended Durability, Remanufacturing 2
Insulation Material	Polyesterimide	Theic-modified polyesterimide with polyamidimide
Temperature Index [°C]	195	212
Thermal Class [°C]	180	200
Insulation Class	H	H+

A 10°C higher thermal limit would lead to a double lifetime (L_{Bp}), as summarized in the Figure 3.13 and calculated according to the thermal model described by following equation:

$$L_{Bp} = 20000\ exp\left[-R_{Bp}\left(\frac{1}{\theta_{\_Bp}} - \frac{1}{\theta}\right)\right] \tag{3.8}$$

Where R_{Bp} is one of the characteristic parameters of the insulating material, which are functions of the reaction's activation energy, $\theta_{\_Bp}$ is the thermal class at a specific Weibull cumulative distribution function percentile of the time to failure, while θ is the operative constant temperature. Relevant data for the calculation are reported in the Table 3.4 and are relying on experimental Arrhenius curves described in [156] and obtained adopting Weibull probability distribution. For this research have been considered data referred to the 10th percentile resulting in more severe reliability than higher percentiles.

Table 3.4 Input data for the lifetime estimation

Symbol	Description	Value
R_{Bp}	Characteristic parameter [K]	16028
$\theta_{\_Bp}$	Time to failure thermal class [°C]	195.8
θ	Operative temperature [°C]	<180
L_{Bp}	Estimated Lifetime [h]	40-0.8 10^6

In the figure are reported characteristic curve for lifetime and operative temperature respectively for the baseline configuration, for the extended durability configuration and a hypothetical 10°C higher curve. The higher thermal class winding curves are rigidly translated to show a duplication of the lifetime for 10°C higher temperature interval in a temperature range representative of the considered application. The estimated lifetime values are also represented on the three curves at an operative temperature of 180°C, showing increment from about 65854h of the L_{Bp} Baseline to of the L_{Bp} +10°C 146290h and to 337173h L_{Bp}+20°C.

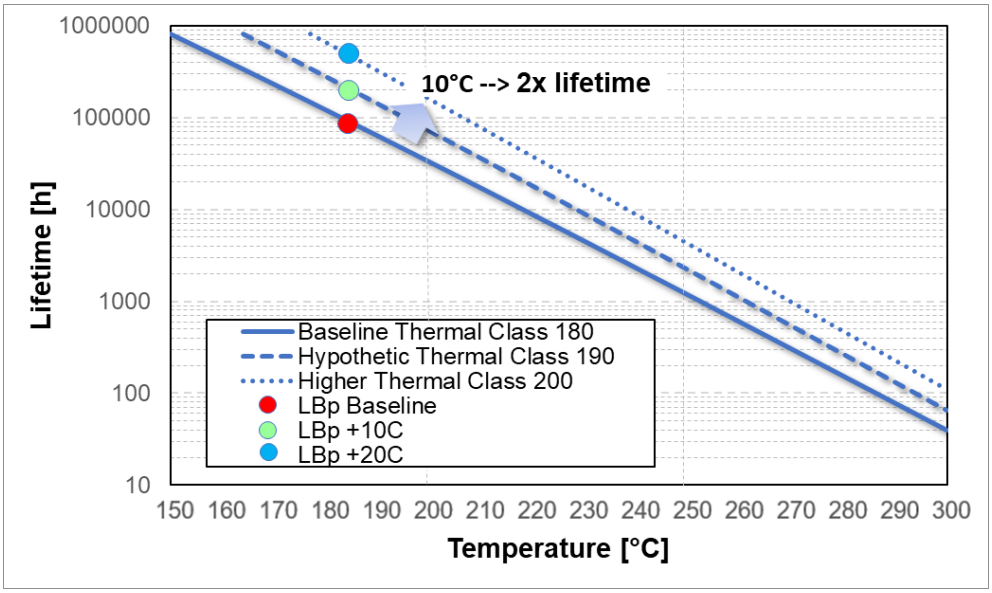

Figure 3.13 Thermal endurance curves for different thermal class at an operative temperature of 180°C

Here it is worth mentioning again that the reported thermal endurance curves refer to the 10th percentile of failure time. This is why they do not intercept the 20,000 hours ordinate at their specific L_{Bp}, as one would expect in a 'conventional' Arrhenius plot. The above design choice allows to partially compensate for:

- the generally lower thermal life of the insulation system as a whole (i.e., wire enamel and impregnation resin/varnish) with respect to the life of the enameled wire on its own and

- for the 'geometrical size factor' as defined in [157], namely the lower thermal life of a full winding, with respect to a small-size specimen. Indeed, thermal endurance curves provided by magnet wire manufacturers are extrapolated through accelerated lifetime tests on non-impregnated twisted pairs, by taking the mean time to failure among multiple specimens as failure point, thus leading to an overestimation of the real thermal life of a full winding.

Front bearing and windings selected for extended durability strategy, have been evaluated from a cost perspective in order to consider also potential drawbacks of these selection and results of this analysis are described in Chapter 5. Instead, from an environmental impact point of view the components have not been considered directly influent due to the fact that from a material and mass perspective, the introduced changes can be considered negligible. In contrast with the Ecodesign strategy, in this case a performance assessment has not been performed as the components introduced are supposed to not influence this aspect.

3.3.3 Design for Circular: housing design for disassembly

This section describes the main architectural features of the SRM, with particular reference to the design features that enable the Remanufacturing Strategies. The motor is conceived for full disassembly as mentioned in the section 3.1.1 and this represents a novelty to the best of author's knowledge. Indeed, from benchmark analysis and internal teardown, many state-of-the-art motors have been investigated and in all the cases it was not possible to disassemble all the motor's components without damaging or cutting other parts. In particular, it could be stated that the critical point from a disassembly perspective is represented by combination of stator and inner housing that are conventionally characterized by a press fit mounting. In the Figure 3.14 (a, b, c, d) are reported some examples of torndown motors coming from published (a, b) [158], [159] or from internal analysis of motors available on the market (c, d).

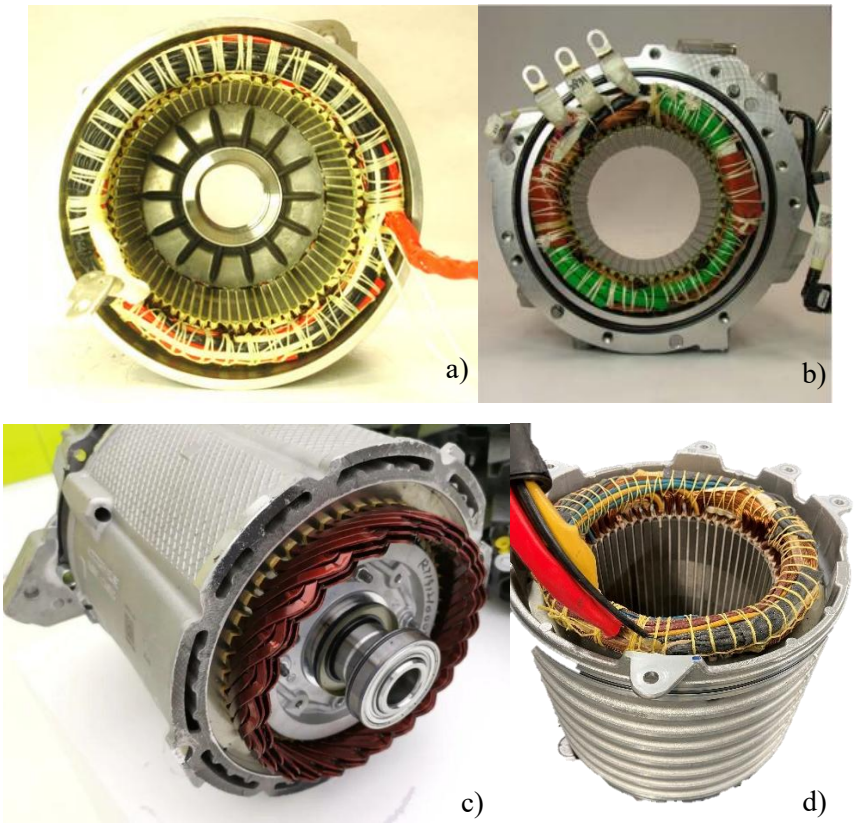

Figure 3.14 Stator-Inner housing mounting from Benchmark analysis for different motor's topologies and winding configurations

Figure 3.14 a and b are referred to two PMSM with round wire winding, while in c is reported a PMSM with hair pin winding and in d an IM, showing that stator assembly into inner housing is independent from motor topology or winding adopted technology. Normally, these components are recovered using either common extractors that cause permanent deformations or by cutting the external housing, thus preventing the possibility of their reconditioning and subsequent reuse. Therefore, this issue does not allow for the adoption of a CE model for this type of machinery.

With reference to Figure 3.15, that shows an exploded view of the SRM with its components, it can be stated that, by just unscrewing it, the rear cover can be easily removed, as is conventionally verifiable in the majority of motors available on the market. However, the step forward compared to the conventional approach is represented by the possibility to dismount the shaft with the rotor and both front and rear bearings, which are usually press-fit onto the housing and successively the stator, which is press-fit in the aluminium housing, without damaging the housing, the stator, or bearings themselves. The front bearing's outer ring may be installed with interference into the housing as well. The interference mounting between components with housing is respectively between 0 and 300µm for the stator and 0 and 50µm for the front bearing.

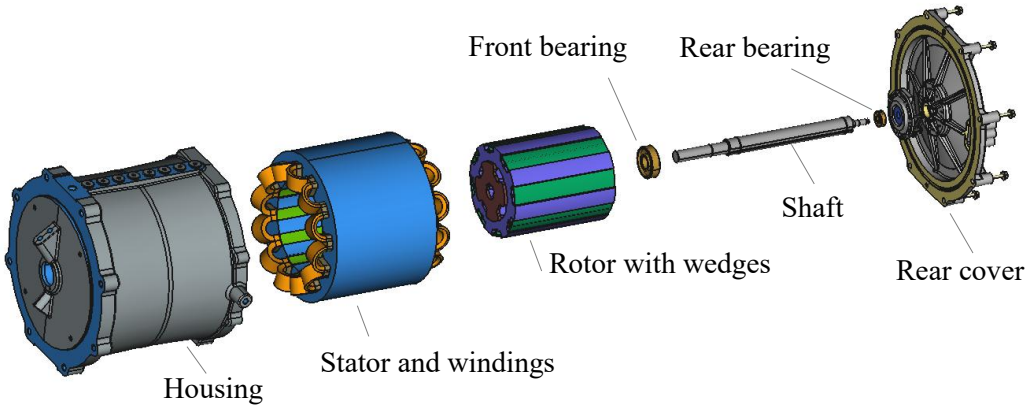

Figure 3.15 SRM exploded view, representing full disassembly potential

Concerning the new design, main enabling features are represented in Figure 3.16 where are respectively reported an axonometric view from the front side (a), a frontal view (b) and a simplified scheme of the motor in a transversal section (c). In the presented design, as showed in Figure 3.16 a and b , threaded holes (numbered 1 and 2 in the figure) in the front cover are circumferentially placed with the intent to insert screws to push away the stator and the front bearing, which would otherwise be impossible to remove. Additionally, the aluminium housing featuring a fully integrated water jacket, highlighted with number 3 in the Figure 3.16 c, is inherently designed for the CE because it enables reuse without concerns about sealings, leakages, or distortions, which are typical of multi-piece housings. Furthermore, the disassembly strategy envisions the possibility of introducing warm oil into the coolant circuit to expand the housing, facilitating stator extraction during teardown operation.

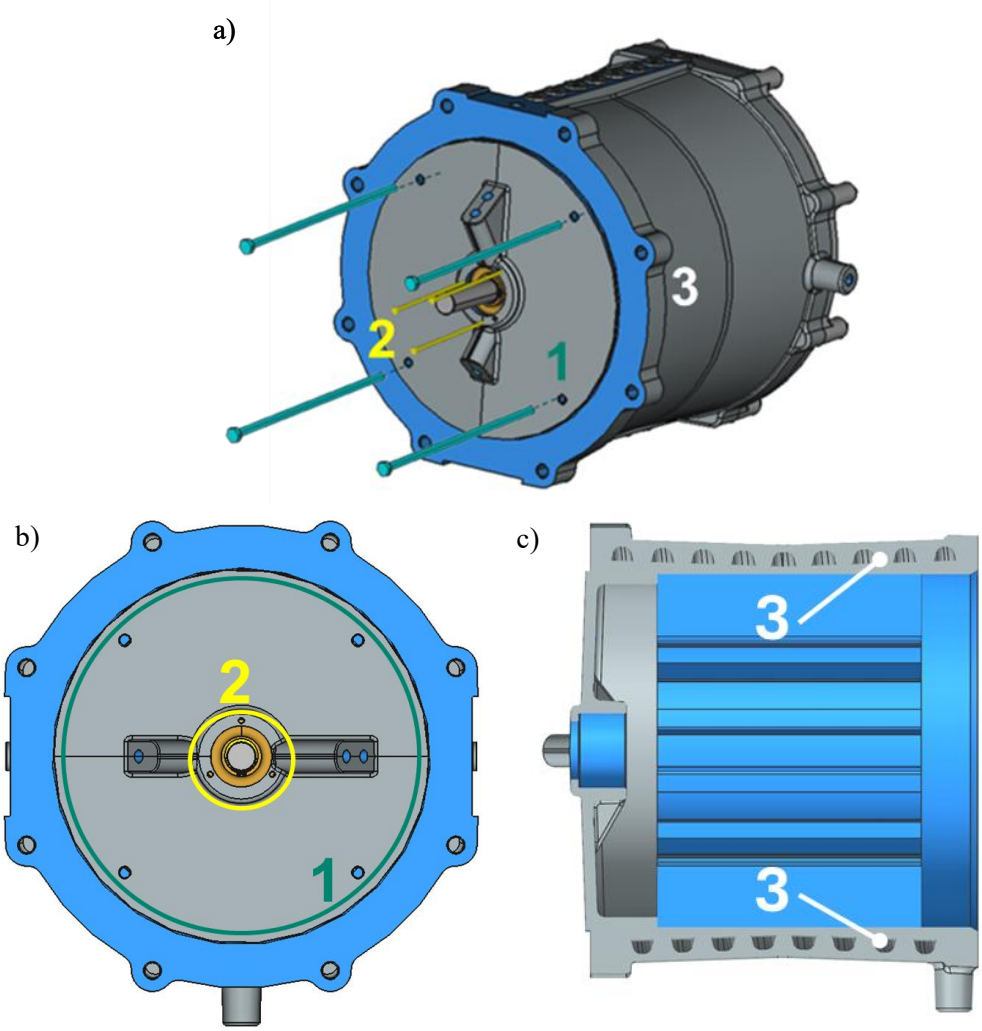

Figure 3.16 SRM CAD views a) axonometric, b) frontal, c) transversal section, highlighting specific features introduced (Patent Pending)

Such a design (patent pending) makes it possible to realize the Remanufacturing Strategies described in the previous section, through substitution at the end of the first life cycle of the critical components. In Remanufacturing 1 case it is possible to replace both winding and front bearing, while in Remanufacturing 2, is possible to substitute just front bearing. The latest features higher performance windings following the selection guidelines described at the extended durability section 3.3.2.

Chapter 4

Toolset for the environmental and economic impact evaluation

4.1 Modelling approach

This chapter describes the methodology adopted for the evaluation of the motor environmental and economic impacts. Specifically, the models used for the LCA study (Section 4.2), the material circularity evaluation (Section 4.3), and the cost estimation (Section 4.4) are presented in detail. The toolset presented in the chapter is based on both literature models and analytical framework and data from Dumarey Automotive Italia. All the models have been adapted and refined to fulfil the objectives of this research, addressing also the research question related to the development of tools to support decision making at both managerial and strategic levels as described in [34]. The tools developed within this research relate to both the economic and environmental dimensions, as reported in the same paper, which describes design for sustainability methodologies, acting at product level. Therefore, although the main objective of this research is to evaluate environmental impact of the proposed electric motor design and the resulting CS, an economic evaluation has also been performed, tackling two of the three pillars of the sustainability. These tools are integrated into the DfCE process depicted in Figure 3.1. To offer a comprehensive view of the product's environmental sustainability, LCA has been used in conjunction with a circularity indicator. Indeed, the first provides a comprehensive assessment of environmental impacts, including factors such as energy consumption, greenhouse gas emissions, and resource depletion, accounting for the resources extracted from ecosphere to supply all the activities of the product lifecycle, in contrast with the second, that, on the other hand, is more narrowly focused on material flows and circularity [160]. Part of the contents presented in this chapter have already been published by the author in the papers [161], [162], [163].

4.2 LCA model

Despite the growing attention to product's sustainability and resulting need to assess environmental impact, there are relatively few life cycle investigations in the literature specifically focused on electric motors. These components are often treated as subsystems within broader vehicle LCA studies. At the time of the modelling activities reported in this thesis, and to the best of the author's knowledge, 17 papers have been published on the topic [106], [144], [164], [165], [166], [167], [168], [169], [170], [171], [172], [173], [174], [175], [176], [177], [178]. Among these, 9 papers are focused on electric motors for transportation sector. All these works focus on the environmental impact comparison, between motor topologies, sizes, or end-of-life disposal. Motor architecture comparison includes PMSM, PMaSynRM, IM, SynRM and EEsynM. This portion of the literature review was conducted considering "LCA", "life cycle assessment" and "electric motor" as research keywords. In [171], different motor technologies (i.e., PMSM, ferrite-based PMSM, ferrite-based PMaSynRM and SynRM) are compared in terms of performance, weight and carbon footprint adopting a cradle-to-grave approach. In [172], a cradle-to-use LCA of six different subcases is performed, varying both technologies (i.e., Nd(Dy)FeB PMSM, SmCo PMSM, Sr-ferrite PMaSynRM) and production and use countries (i.e., Sweden, USA). In [173], four different electric motors are compared (i.e., IM, PMSM, EEsynM and SynRM) in terms of mass and GHG emissions adopting a cradle-to-gate approach. In [174], [175] a scalable life cycle inventory model for designing and manufacturing of PMSMs is developed. In [176], three examples of CE loops (reclaim, recycle and reuse) for an electric motor and inverter are evaluated in terms of carbon footprint. In [177], [178] the environmental impacts of the magnet production for a PMSM compared with a SynRM are evaluated adopting a cradle-to-gate approach. In [106], the environmental impact of a high speed PMSM and the environmental saving associated to Ecodesign strategies are evaluated. Regarding SRMs, only one LCA study [168] was found in the literature and not referred to transportation field, with specific reference to passenger car. Indeed, the magnet free solution is compared with two IMs representative of the low power range (1.5kW). Results indicate the SRM's lower environmental impact across all analysed categories and a lower life cycle cost, primarily due to the lower energy demand during the use phase. This review highlighted the need to integrate the existing models for the purpose of the treated research. In particular, the following aspects are distinctive in the LCA study here compared to those available in the literature:

- consistent evaluation of the factors influencing environmental impact of electric motor
- assessment of a SRM specifically designed for transportation sector
- integration of alternative CS (remanufacturing, recycle) into the model, as opposed to conventional motor disposal at the EoL phase

- consideration of the aluminium winding effect, including the impact of different material choices across all cycle phases

These aspects are addressed, through a three-step incremental analysis path, in which both the system boundaries and motor architecture evolve. Table 4.1 summarizes the three steps covered in this research, detailing the motor architecture, the LCA phases evaluated for each scenario and the sections where the boundaries of each step are described.

Table 4.1 LCA studies

Steps	**Motor Architecture**	**Approach**
Geographical & Application Scenarios (4.2.2)	PMSM	Cradle to Use
Ecodesign (4.2.3)	PMSM, SRM copper, SRM aluminium	Cradle to Grave
Circular Strategies (4.2.4)	SRM copper	Cradle to grave with circular loops

The LCA methodology applied in this study follows the international standards [179], [180]. It is articulated thorough four phases, that are respectively the goal and scope definition, the Life Cycle Inventory (LCI), the Life Cycle Impact Assessment (LCIA) and the results interpretation. The latter two are described in detail in Chapter 5, which is dedicated to the analysis of the results. All the LCA steps are based on Ecoinvent v3.8 [181], which was used as background database while the LCA model was carried out using the LCA software SimaPro [182]. This section of the thesis aims to provide a comprehensive summary of the LCA activities conducted during the Ph.D. research. Accordingly, it focuses extensively on the LCA relevant aspects across all the investigated scenarios, without detailing all the model elements that are available in the cited literature. Additionally, to avoid repetition in the description of the investigations conducted, all common aspects related to the modelling approach and data used in the three mentioned steps, are reported in a general LCI section (4.2.1). Instead, specific descriptions of the goals and scope, system boundaries, assumptions and data used for all the case studies are provided respectively in Section 4.2.2 for the geographic and application scenarios, in Section 4.2.3 for the comparison between PMSM and both SRM machines with copper and aluminium winding, and in Section 4.2.4 for the CS portion. The functional unit (FU) is defined as one kilometre (km) driven along the entire lifespan of the vehicle (i.e., 200,000 km), in accordance with [172] and is considered identical for the three investigated steps. Although the SRM is conceived for the LCV market, the LCA investigations described in the following sections have been applied to passenger car market, mainly due to data availability and because this does not negatively affect the main objective related to the methodology development.

4.2.1 General LCI

LCA includes compiling the so-called Life Cycle Inventories (LCIs) of the environmentally relevant flows (i.e., direct emissions in air, water, and/or soil, material and energy input/output flows, and waste flows) related to all processes involved in the production, use, and EoL of a product and, based on these, quantifying the associated life cycle burdens [183]. The LCA model of the electric motor built through three investigations steps within this research, is composed of four main stages called cradle-to-gate (C2G), use, transport and EoL.

Cradle to Gate

Regarding the C2G portion (i.e., raw material acquisition, preprocessing and motor assembly), the approach presented in [172] was followed. In this approach, the main LCI data source for the processes involved in material extraction and preprocessing is the Ecoinvent 3.8 database. For some processes related to both motor and magnet material preprocessing, as well as for the manufacturing phase, data on energy consumption, ancillary materials, waste and emissions were retrieved from the LCI reported in [175]. For this reason, all the processes are not explained in detail in this document but are briefly summarized in Figure 4.1, which is an adaptation of the model already presented in [172] and adopted in this research activity. The colors used for each phase are consistent with those in the results chart shown in Chapter 5 and support the understanding of each operation included in the motor breakdown of environmental impact results. The figure outlines the operations required for the motor manufacturing, the material preprocessing phase and the main materials required as input for the model. Boxes with mixed colors (blue and pink) represent operations necessary for the manufacturing of both the stator and the rotor. The influence of each component is evaluated according to the legend: stator (blue), winding (yellow), rotor (pink), shaft (grey), permanent magnets (orange), housing (green), and fasteners, which are included in the assembly and painting operations (black). However, all details related to the LCI built within this work, are reported in the Appendix A.2 in order to provide useful information for LCA practitioners aiming to build a model on electric motors. To avoid repetitions, the Baseline motor BOMs, is provided in the next section, while all the others, which determine the material input for the model, are summarized trough pie charts, highlighting material composition, in the following sections for each of the considered case studies. The selected material inputs are, as far as possible, comparable to those used in the reference model adopted for this investigation. This choice is coherent with the BOM of the SRM considered in the research, with exception of PM, and also allows for a fair comparison of the results with the reference model. This comparison is reported in the supplementary material of the paper [161].

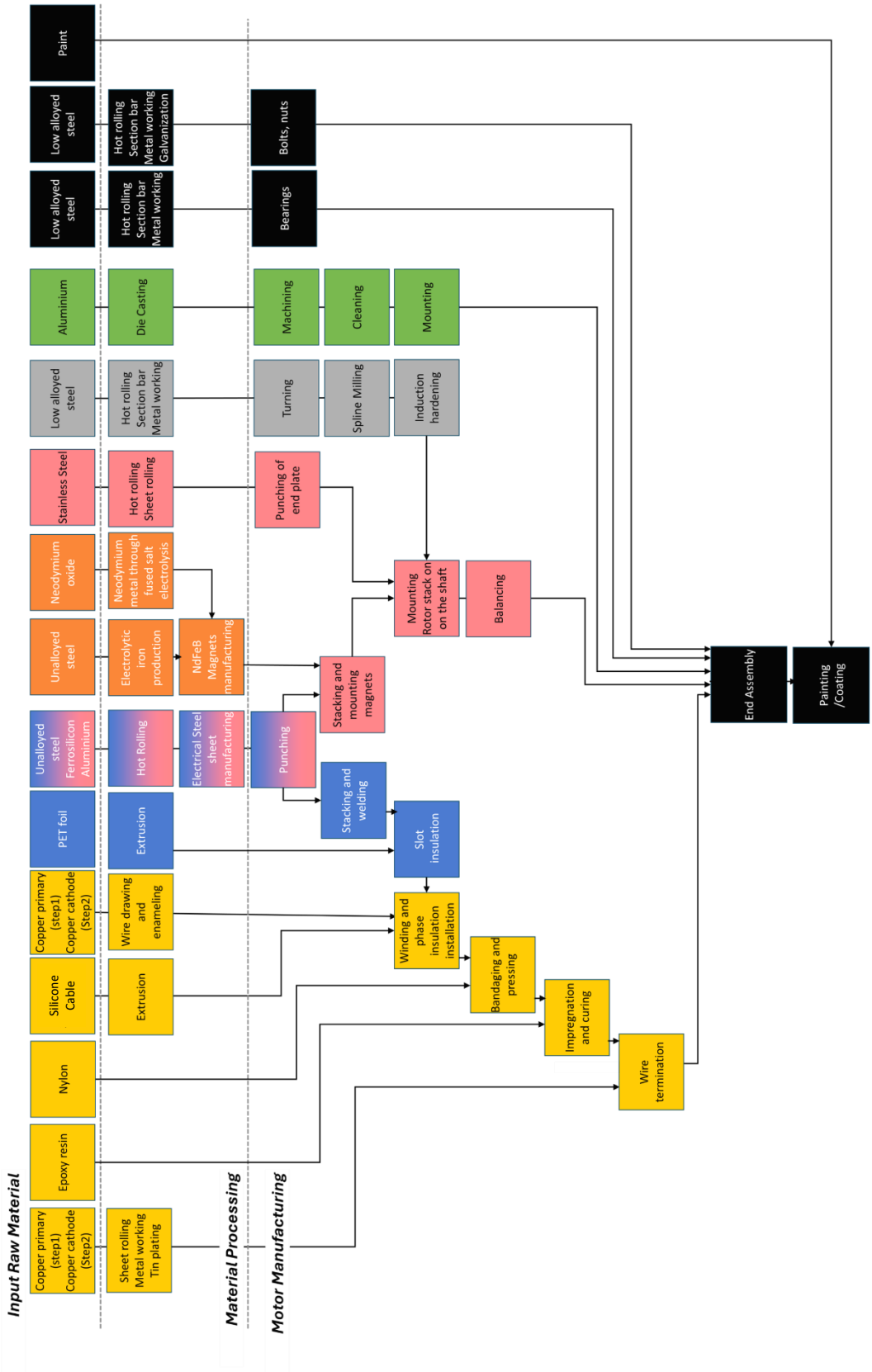

Figure 4.1 LCA model: C2G processes for the specific components

Use phase

The use phase covers both the Well-to-Tank (WTT) and the Tank-to-Wheel (TTW) stages. In other words, it comprises all the life cycle stages from energy

resource extraction to energy conversion within the vehicle. The use phase varies according to the mechanical energy demand of a specific type of vehicle, including its propulsion system and driving cycle. The model already described in Chapter 2 has been integrated and used to take into account the longitudinal dynamics of the vehicles under study. It is fed with vehicle and propulsion unit characteristics, as well as speed profiles. By means of dynamics equations, the energy required during the use phase for each vehicle under study is determined. Each vehicle is defined by its mass *m*, frontal area *A*, aerodynamic drag c_x, and rolling resistance *fr* coefficients, while the powertrain is characterized by the efficiencies of the various components η and gear ratio *kgear*. Regarding speed profiles, the WLTC is used as the reference driving cycle for evaluating the energy demand for motion. Energy requirement calculated over the cycle is then extrapolated over the entire lifespan distance of 200000km, in accordance with the FU. In compliance with [106], [172], not all the energy required by the vehicle is allocated to the electric motor. Instead, only the energy associated with the electric motor's conversion losses and its mass-related effects on WLTC are considered. The energy allocated to the electric motor, $E_{due\ to\ EM}$, is determined based on [172] as the difference between the net energy provided by the battery, including motor losses and motor mass, $E_{net\ with\ EM}$, and excluding them, $E_{net\ without\ EM}$ as reported in equation 4.1. The net energy provided by the battery over the driving cycle is determined subtracting the energy recovered through regenerative braking E_{rec} from the energy required to drive the vehicle, E_{req}. These correspond respectively to the energy at the wheels during braking, $E_{wheel(BR)}$ and during acceleration $E_{wheel(p)}$, increased by the powertrain losses during braking $E_{losses_{PT(BR)}}$ and acceleration $E_{losses_{PT(P)}}$ (equation 4.2). The powertrain includes a battery, an inverter, the motor and a reducer. The energy required to drive the vehicle, E_{req}, is determined by dividing the energy at the wheels during acceleration, $E_{wheel(p)}$, by the powertrain efficiencies. The energy recovered through regenerative braking, E_{rec}, is determined by multiplying the energy at the wheels during braking, $E_{wheel(BR)}$, by the powertrain efficiencies. Based on [184], the energy available at wheels is defined in the equation 4.3 as the time integral over the WLTC cycle of the power at wheels, which is the product of the vehicle speed and the force, required to overcome inertia, aerodynamic drag and rolling resistance. The first term related to inertia is of a conservative type (positive during acceleration and negative during braking with same absolute value) and in a battery electric vehicle is equal to zero, assuming that 100% of the energy due to inertia braking is recovered. The second and third terms are instead always resistant to motion and are therefore not recoverable during braking. The resistant force is dependant from the above-mentioned vehicle characteristic data and has been already treated in Chapter 2. For what concerns efficiencies of the driveline, fixed values have been assumed for all the components except the electric motor, for which an efficiency map, function of motor speed and torque has been used. The motor speed, and consequently the motor torque required as input for the efficiency calculation in the specific

operative points, are determined according to equations 2.2 and 2.3 where the motor power is calculated as described in equation 4.4, respectively for the braking and acceleration phases.

$$E_{due\ to\ EM} = E_{net\ with\ EM} - E_{net\ without\ EM} \tag{4.1}$$

Where:

$E_{due\ to\ EM}$: energy allocated to the electric motor; $E_{net\ with\ EM}$: net energy including the motor; $E_{net\ without\ EM}$: net energy excluding the motor.

$$\begin{aligned} E_{net} &= E_{req} - E_{rec} \\ &= E_{wheel(p)} + E_{losses_{PT(P)}} - E_{wheel(BR)} \\ &+ E_{losses_{PT(BR)}} \\ &= {E_{wheel(P)}}/{\eta_{batt}\eta_{inv}\eta_{mot}\eta_{red}} \\ &- E_{wheel(BR)}(\eta_{batt}\eta_{inv}\eta_{mot}\eta_{red}) \end{aligned} \tag{4.2}$$

Where:

η_{batt}: battery efficiency; η_{inv}: inverter efficiency; η_{mot}: electric motor efficiency; η_{red}: transmission efficiency; E_{net}: net energy; E_{req}: energy required to drive the vehicle; E_{rec}: energy recovered through regenerative braking; $E_{wheel(p)}$: wheel energy over acceleration phase *;* $E_{losses_{PT(P)}}$: powertrain energy losses over acceleration phase*;* $E_{wheel(BR)}$: wheel energy over braking phase*;* $E_{losses_{PT(BR)}}$*:* Powertrain energy losses over braking phase.

$$\begin{aligned} E_{wheel} &= E_{inertia+} + E_{aero} + E_{rolling} = \\ &= \int_0^{cycle} P_{inertia}dt + \int_0^{cycle} P_{aero}dt \\ &+ \int_0^{cycle} P_{rolling}dt = \\ &= \int_0^{cycle} VF_{inertia}dt + \int_0^{cycle} VF_{aero}dt \\ &+ \int_0^{cycle} VF_{rolling}dt = \end{aligned} \tag{4.3}$$

$$= m\int_0^{cycle} V\frac{dV}{dt}dt + \frac{1}{2}c_x A\rho_{air}\int_0^{cycle} V^3 dt$$

$$+ mf_r g\int_0^{cycle} Vdt$$

$$P_{mot} = \begin{cases} P_{wheel}\eta_{red}, & P_{wheel} < 0 \\ \dfrac{P_{wheel}}{\eta_{red}}, & P_{wheel} \geq 0 \end{cases} \quad (4.4)$$

Where:

E_{wheel}: wheel energy over cycle; $E_{inertia}, P_{inertia}, F_{inertia}$: energy, power, force request to oppose inertia resistance; $E_{aero}, P_{aero}, F_{aero}$: energy, power, force request to oppose aerodynamic resistance; $E_{rolling}, P_{rolling}, F_{rolling}$: energy, power, force request to oppose rolling resistance caused by the deformability of tires and road; $cycle$: WLTC cycle test duration;

In Table 4.2 are reported the fixed efficiencies values for the powertrain components, with the exception of the motor, assumed identical in all the LCA steps, following the approach explained in [172]. Coherently with the same approach, the losses over battery charging operations have been considered assuming an efficiency η_{charge} of the 94%.

Table 4.2 Efficiency of the propulsion unit components with exception of the motor

Symbol	Parameter	Data
η_{red}	Transmission efficiency [%]	97
η_{inv}	Inverter efficiency [%]	97
η_{batt}	Battery efficiency [%]	99

Figure 4.2 graphically illustrates the calculation of the various energy contributions over WLTC to determine the energy net.

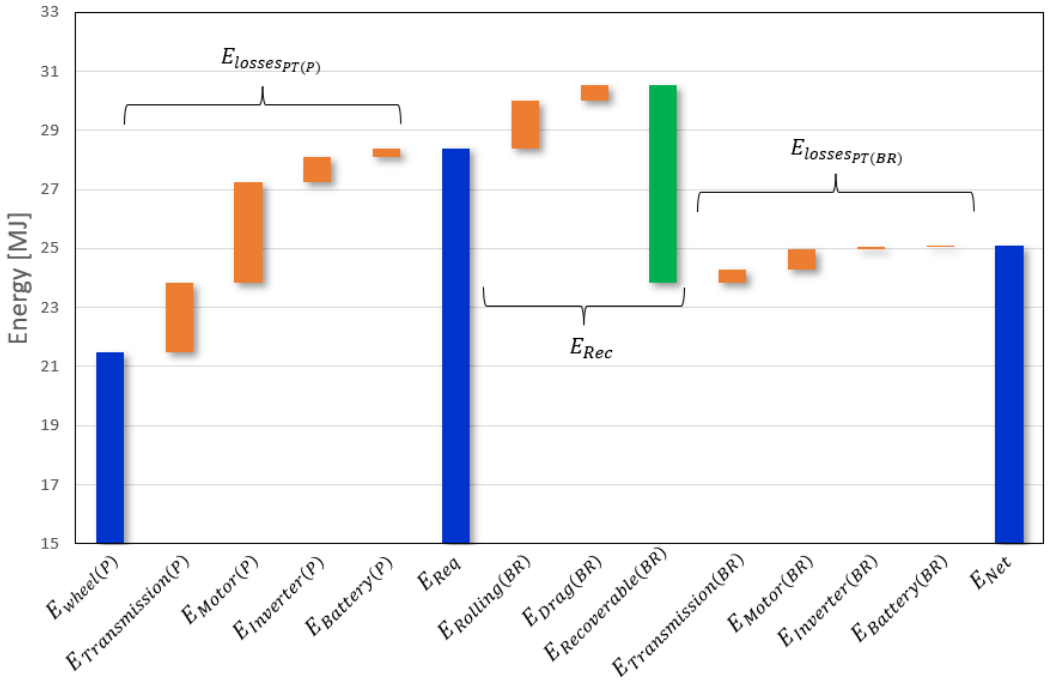

Figure 4.2 Energy contributions over WLTC

The figure shows energy losses (orange bars) and gains (green bars) respectively during the propulsion and braking phases, as previously described. The blue bars represent respectively the energy at the wheels, the energy required to overcome the propulsion phase and the net energy provided by the battery. The figure is representative of the installation of the SRM in a segment C application and provides a detailed breakdown of the losses in each propulsion unit subsystem. As above mentioned, an identical calculation is performed excluding the motor contribution, in order to estimate the energy value to be used as input in the LCA. The use phase energy values calculated according to the described model and input data are reported in the following sections for each of the considered case studies.

Transport

The transport phase follows the approach explained in [171], according to which all transportation happens within the boundaries of the country considered in the study. All the above, with the exception of magnets' transportation for the PMSM topology, which are modelled assuming the production in China and the shipment by boat to the country of usage, where they are subsequently assembled. This LCA stage encompasses operations occurring during the manufacturing, distribution, and EoL phases, with each phase treated differently across the various LCA steps. In the first LCA step, transport activities related to manufacturing were embedded within the C2G phase and are therefore not explicitly visible in the results. In contrast, the second and third steps introduce a dedicated transport cluster to make the environmental impact of these operations more transparent. These steps include activities associated with manufacturing, distribution, and EoL. However, the EoL phase is integrated into the recycling scenario models, and its environmental impact is accounted for within that portion of the life cycle. The specific approaches adopted for each scenario are detailed in the following sections, where transport distances and modes are described.

End of Life

As mentioned in Chapter 3, the recycling process is always considered part of the EoL phase, when the Cradle to Grave approach is adopted. The recycling description provided in this section is representative of all the cases studied.

Recycling is not often included within the system boundaries of electric motor LCA studies and a certain degree of uncertainty is noticeable in the literature [172]. However, given the product composition, characterized by nearly 99% of the overall mass being recyclable metals, the recycling process has been included, following the approach described in [164].

Accordingly, closed-loop recycling scenarios were defined for metals, assuming that material production is avoided at a certain point in the subsequent lifecycle. These recycling scenarios were developed retrieving benchmark data related to the energy required for the various processes from [185]. Table 4.3

presents the energy requirements, and material shares for recycling of steel, copper and aluminium. Process efficiencies have not been included in the recycling scenarios, as they were judged negligible for the results comparison.

Table 4.3 Recycling scenarios

Material	Energy [kWh/kg]	PMSM [%]	SRM copper [%]	SRM aluminium [%]
Steel	3.25	60.5	72.8	79.5
Copper	1.75	15.1	11.6	0
Aluminium	0.67	24.4	15.6	20.5

Figure 4.3 shows a comparison between the manufacturing processes adopted (orange), retrieved from [181] and the recycle scenarios (green) based on [185], considered in this study, respectively for steel (a), copper (b) and aluminium (c).

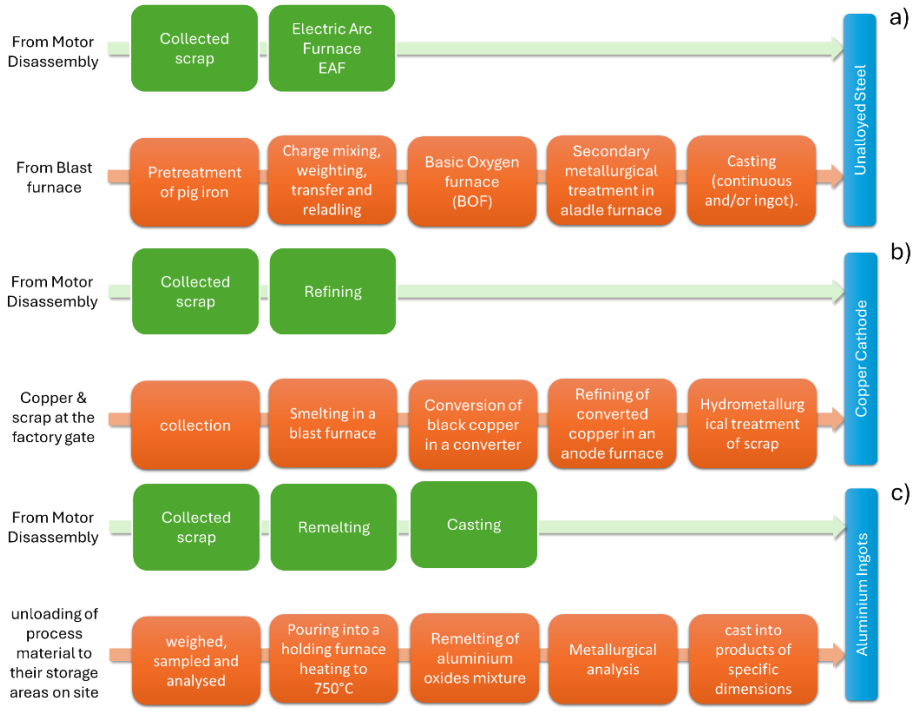

Figure 4.3 Manufacturing processes (dataset from Ecoinvent database) and recycle processes (energy requirements from the literature) for a) steel b) copper c) aluminium

Three different types of steel, as visible in Figure 4.1, are considered in the C2G phase. However, only one recycling scenario has been modelled, leading to the avoidance of primary unalloyed steel production due to both its higher presence within the motor BOM and its lower CO_2 emission during the production, compared to low alloyed and chromium steels. This approach is adopted, to avoid overestimating environmental benefits of the recycling phase in terms of CO_2 emission.

To support this point, Figure 4.4 shows a comparison of the CO_2 emissions associated with the production of 1 kg of steel for the three material types,

calculated using SimaPro, according to the Environmental Footprint (EF) 3.0 calculation method described in Chapter 5.

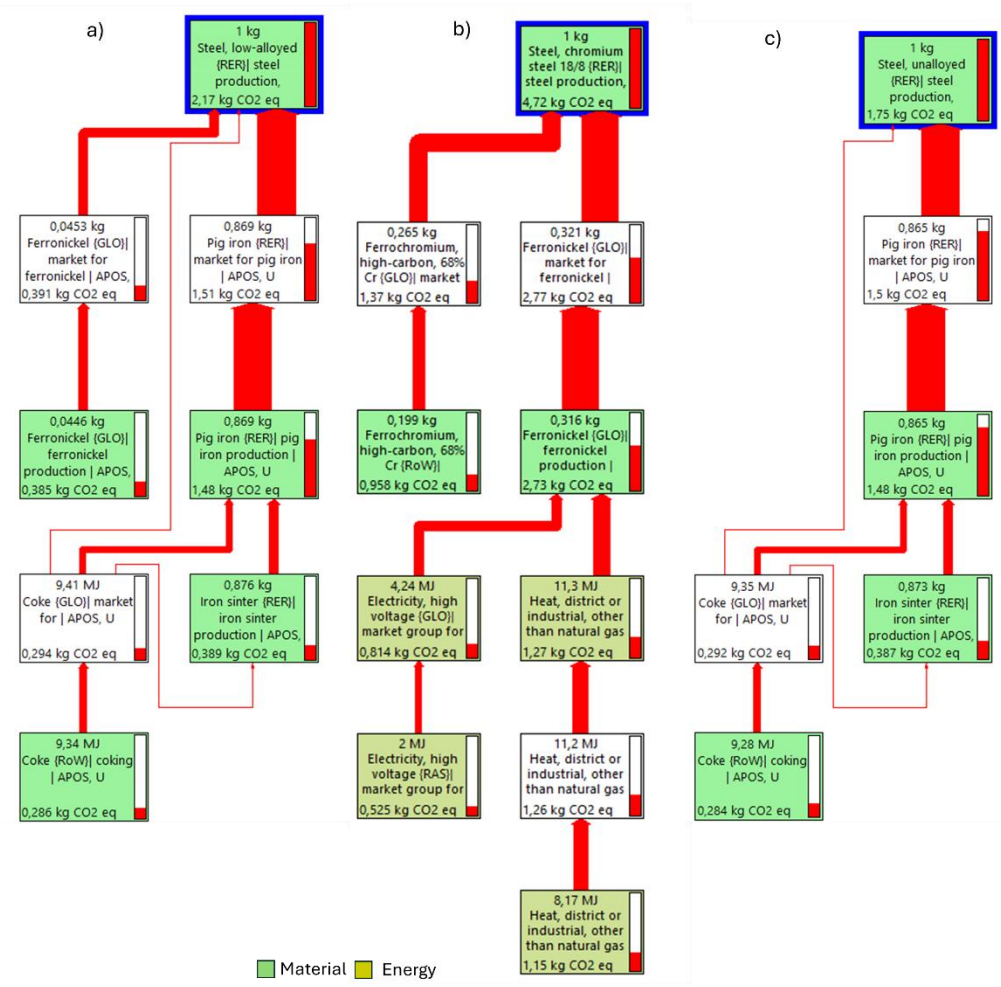

Figure 4.4 Steel manufacturing process and associated CO_2 emissions calculated through SimaPro, according to the EF3.0 methodology

The thickness of the arrows reflects the intensity of each process within the production chain, while the colours of the boxes highlight the different flows and in particular material and energy flows and unit flows (white boxes). It is evident that the production of unalloyed steel results in 1.75kg of CO_2 equivalent, compared to 2.17kg for low alloyed steel and 4.75kg for chromium steel. The unalloyed steel manufacturing process includes activities from the pretreatment of hot metal (pig iron) from the blast furnace to the casting. The recycling process accounts for the energy required to produce steel from collected scrap through electric arc furnaces (EAF). Referring to copper production a dataset has been considered, representing the production of copper cathodes from various type of scrap, with different copper content. The process begins with material collection and ends with the electrolytic refining of anodes, passing through smelting in a blast furnace, conversion of black copper in a converter and hydro metallurgical treatment of the scrap. The recycling process, accounts for the energy required to

convert copper scrap into copper cathode. Concerning to aluminium, the primary production of ingots has been considered starting from molten aluminium, obtained as the output of an electrolytic process. In contrast, the recycling process includes the energy required to produce aluminium ingots through the melting and casting of the scrap. Regarding magnets, for the reason described in Chapter 2, the developed LCA model, includes PM within the steel scrap scenario. Coating and insulation are not part of the recycling scenario as they were considered not influent for the purpose of this study, both due to their low presence and their comparable characteristics across the analysed motors.

4.2.2 Geographical and application scenario

Evaluating the environmental burdens associated with electric motors requires consideration of their complete life cycle, since substantial burdens can be generated not only in use, but also in their production and in energy supply chains. The distribution of these burdens varies significantly depending on the powertrain architecture and the electricity production pathways. A balanced comparison therefore requires a consistent modelling framework across all life cycle stages of electric motors and boundary conditions appropriately reflecting realistic technological advancement. The activities outlined in this section are directly linked to the approach adopted for developing an LCA model aimed at providing OEMs and electric motor manufacturers with an assessment of the environmental impact of an electric motor. The investigation considers key influencing factors such as the countries of production and use, as well as the target vehicle applications. Specifically, a baseline PMSM has been selected and evaluated under two alternative scenarios: a geographical scenario and an application scenario. According to [186], during the LCA modelling of any system, the appropriateness of the used background processes must be evaluated in terms of geographical and technological representativeness.

The goal of this study is to provide a methodology for conducting LCAs of electric motors designed for passenger cars. The results of this study are supposed to answer the question, ‘‘What are the environmental burdens of travelling one kilometre with a certain electric motor manufactured in a specific country for a specific vehicle application, and where do they come from?’’. The scope of this analysis represents an attributional process-based cradle-to-use LCA, as shown in Figure 4.5. The figure also shows interaction between the adopted scenarios, described after in detail, and the system boundary. The system boundary includes the raw material acquisition and pre-processing, manufacturing, distribution, and use stages, grouped into two macro-phases. The first macro-phase is the C2G, and contributions are divided between electric motor (in orange) and magnets (in blue), while the second phase is related to use stage. The use stage follows the Well to Wheel (WTW) approach already described in section 4.2.1. As mentioned in section 4.2, the EoL phase is excluded from this first LCA investigation. Also in this figure, the colors used for each phase are consistent with those in the results chart shown in Chapter 5 supporting specifically the understanding of each

life cycle stage considered in the environmental impact results, within geographical and application scenarios.

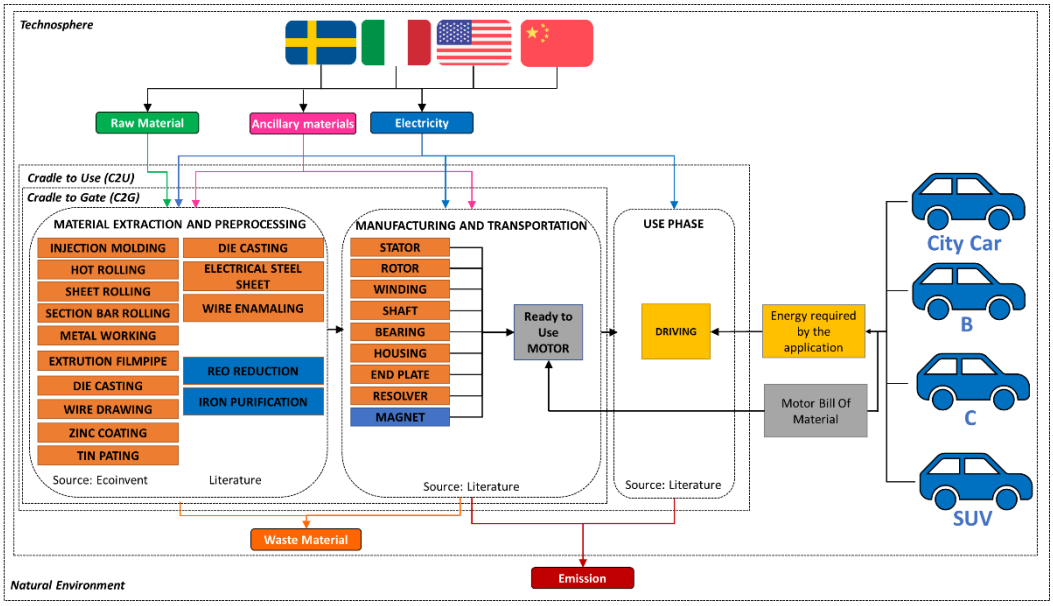

Figure 4.5 Step1 system boundary reporting lifecycle phases, data sources, considered geographical and application scenarios and their influence on the LCA phases.

Table 4.4 summarizes the scenarios considered, specifying the country of production and use, as well as the vehicle application in which the motor is virtually installed.

Table 4.4 Scenario setting

Scenario	Production and use locations	Vehicle application
Baseline	Italy Sweden	Segment C
Geographical	Italy US China	Segment C
Application	Italy	City car Segment B Segment C SUV

Baseline

The use case named Baseline has been developed to setup the model and provide initial indication of the environmental impact of the different motor components and life cycle phases. A PMSM topology was selected because, as described in Chapter 2, it is the most widely adopted in the transportation sector.

Moreover, the LCA model can be easily adapted to the SRM case, by simply removing the portion related to the environmental impact of the magnets.

The motor equipped in the 2013 Nissan Leaf was identified as the baseline motor. It was extensively analysed by the Oak Ridge National Laboratory, for the U.S. Department of Energy in 2013 and from the available reports both the BOM and the efficiency map were retrieved [159],[187], to perform the LCA. Specifically referring to the BOM, information on metal components were derived by the report from the Oakridge National Laboratory, while coating, insulation and fasteners were estimated using the scaling methodology presented in [174]. The detailed BOM for the baseline motor, including mass information by component, is provided in the Table 4.5.

Table 4.5 Baseline BOM

Component	**Value**	**Percentage wrt total mass**
Stator [kg]	15.1	26.25
Winding [kg]	5.6	9.74
Shaft [kg]	3.9	6.78
Magnet [kg]	1.7	2.96
Rotor [kg]	10.1	17.56
Housing [kg]	12	20.86
End Bells [kg]	7	12.17
Bearing [g]	559	0.97
Fasteners [g]	177	0.31
End plate [g]	580	1.01
PET foil [g]	166	0.29
Silicone cable insulation [g]	28	0.05
Silicone bond [g]	4	0.01
Nylon [g]	6	0.01
Epoxy resin [g]	321	0.56
Magnet fix resin [g]	70.1	0.12
Varnish [g]	205	0.36
Total [kg]	57.5	100.00

All vehicle data required to calculate energy consumption during the use phase have been derived from [188], [189], [190] and are the same as those used in the Segment C application considered in both the geographical and application scenarios (Table 4.7), and reported in application scenario paragraph. Due to the lack of specific data, the vehicle considered for the baseline analysis is not the original Nissan Leaf in which the motor was installed, but rather a representative model from the same vehicle segment.

Geographical scenario

The geographical scenario gives indications for OEMs and companies involved in the production and commercialization of electric vehicles and motors, providing hints related to geographical boundaries. It also highlights the influence of each life cycle phase across relevant environmental impact categories, leading to different conclusions depending on the country considered. To evaluate the effect of geographical boundaries, the baseline model was retrofitted to different production and usage countries. Four different countries (i.e., Sweden, Italy, USA, and China) were investigated in this scenario, varying the electricity mixes for production and use, as well as the transport distances for raw materials acquisition, and the raw materials, ancillaries and processes considered during the manufacturing stage. These variations affect the entire life cycle, including raw material acquisition and preprocessing, production, and use stages. Sweden was selected due to its green energy mix and high penetration of electric vehicles, ranking second in electric car sales share in 2022 [191]. Italy, on the other hand, was chosen as representative of an average European scenario for what concerns the share of fossil resources, despite the absence of nuclear sources in its electricity mix [192]. China and USA were considered because they are the two largest economies and two of the most influential and powerful countries in the world representing also the largest polluters. China has also a relevant role in the electric motor sector and, more in general, in electric vehicle industry accounting for half of the world's electric cars on its roads [191]. This is due to the REE availability on its territory and consequent technological leadership in manufacturing, as described in Chapter 2, with reference to the PM supply chain. In Figure 4.6 the electricity mixes of the four selected countries are represented considering the 2012-2022 timeframe according to [193].

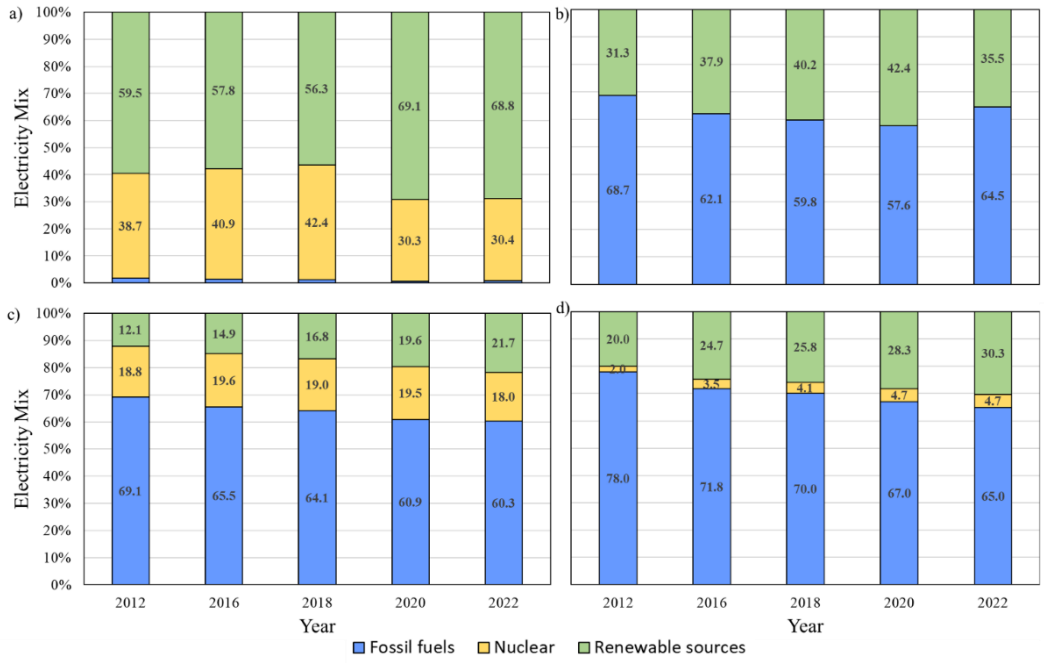

Figure 4.6 Country energy mix a) Sweden b) Italy c) USA d) China

The figure shows the trend in reducing fossil sources in favour of renewable sources over the last decade. The figure also highlights the differences between the countries, showing how Sweden is already independent from fossil sources with a contribution lower than 1%, while the other countries still rely on fossil sources for approximately 60 to 65% of their electricity production. China's energy mix is characterized by the greatest decrease reliance on fossil sources, resulting in a rapid expansion of the renewable energy sources implementation.

The different manufacturing processes adopted in the model for the geographical scenario, are not described in detail, for the sake of brevity, however in the LCIs provided in Appendix A.2, the baseline is reported as reference, related to Italy. Table 4.6 instead describes the approach used to evaluate transport operations during motor manufacturing within this LCA step. The same magnet manufacturing phase has been considered for all the countries, following approach detailed in [172] where, are accounted transports from Bayan Obo mine of Inner Mongolia to the magnet factory in the city of Baotou and to the port. Instead for magnet to assembly phase, were considered sea distances from Tianjin Binhai port to the respective countries of manufacturing and usage, retrieved from [194]. For China and USA has been considered an additional magnet to assembly transport by truck. Finally, the same distance, covered through truck, was considered for all the countries for the transport of all the components. Both motor and magnet manufacturing phase include material scrap, and the detailed tons-kilometre are reported in A.2 for the baseline.

Table 4.6 Transport boundaries

Parts	Distance	Route	Typology
Magnet manufacturing	1000 km	China	Train
Magnet to assembly	21000 km	China to Sweden	Ship
	17000 km	China to Italy	Ship
	10000 km	China to USA	Ship
	4000 km	USA, China	Truck
Motor Manufacturing	1000 km	Sweden, Italy, USA, China	Truck

Application scenario

This study aims at providing indications on the environmental impacts of electric motors varying vehicular application. Vehicle features and desired performance level, in fact, determine motor selection. After an extensive benchmark analysis of the European BEVs market based on publicly available data [188], [189], [190], four different vehicles, including the baseline one, known to mount PMSMs were chosen for this scenario and their environmental impacts were assessed. The four vehicles differ in terms of vehicle segment, specific road load and performance. Because both the use and manufacturing phases are

entailed by the vehicular application, a dedicated BOM of the electric motor was derived for each vehicle as a function of the power and torque level based on [175]. The rolling resistance coefficient is the only vehicle parameter not retrieved from the aforementioned reference. Instead, it was assumed based on the vehicle segment, as described in [135] and following the approach already outlined in Chapter 2 for modelling of the LCV for the vehicle-motor matching analysis with the SRM. Figure 4.7 shows the results of the benchmark analysis, distinguishing between two populations of vehicle, respectively equipped with one or two motors.

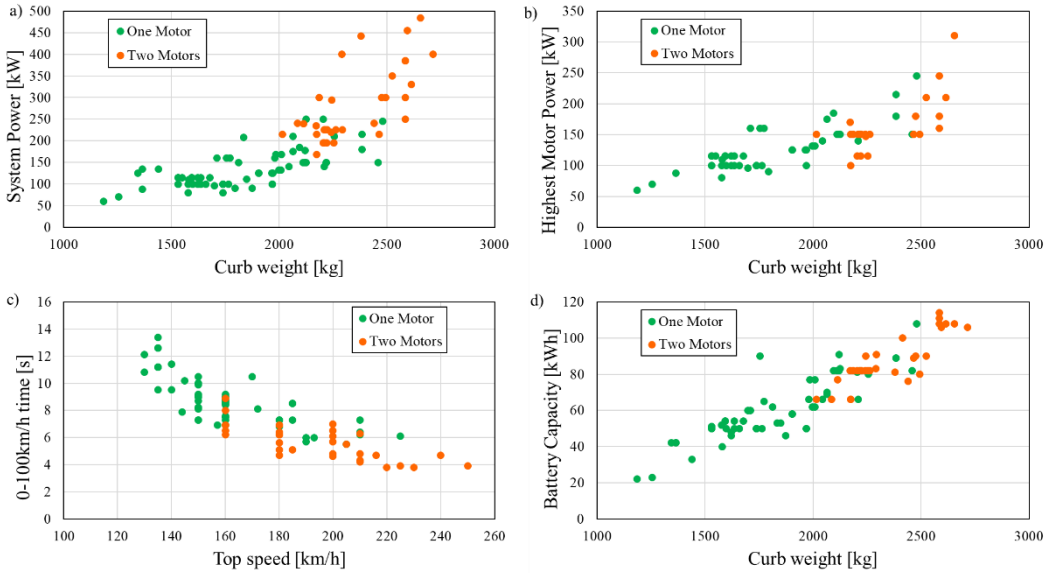

Figure 4.7 Electric motors sold in the European BEV market classified by a) system power as a function of the vehicle's curb weight, b) highest motor power as a function of the vehicle's curb weight, c) vehicle acceleration as a function of vehicle top speed d) battery capacity as a function of vehicle's curb weight.

Figure 4.7 a) illustrates the system power (i.e., equivalent to the motor power in the case of a single motor or to the sum of two motor powers in the case of two motor architectures) as a function of vehicle's curb weight. The vehicle's curb weight ranges from 1.2 to 2.7 tons, while system power spans from 60 to 484 kW. Notably, the single motor cluster (green dots) reaches its upper bounds at 2.5 tons and 245 kW suggesting that it may represent nearly the full spectrum of motor variants currently available on the market. Figure 4.7 b) shows the highest motor power (i.e., equivalent to the peak power in the case of a single motor architecture or to the highest peak power in the case of two motors architecture) as a function of vehicle's curb weight. The single motor cluster (green dots) has its highest values at 2.5 tons and 245 kW suggesting, also in this case, that it may be representative of almost all motor variants currently available on the market. For this reason, the single motor cluster was considered in this study, and four applications segments were identified: City car, Segment B, Segment C and Sport Utility Vehicle (SUV). Figure 4.7c) and Figure 4.7 d) show vehicle acceleration as a function of vehicle maximum speed and battery capacity as a function of the

vehicle weight. These figures confirm that, in terms of both maximum vehicle performance and available energy, the single motor cluster can be considered representative of the whole market. Data related to the selected vehicles and main parameters of their scaled motors are reported in the Table 4.7. The selected vehicles are characterized by different road load, which lead to a variation of electric motor operating points, as well as by different power and torque levels, resulting in different electric motor weights.

Table 4.7 Vehicle and motor data used in the application scenario

Parameter	**City car**	**Segment B**	**Segment C**	**Segment D**
Curb weight [kg]	1365	1530	1780	2125
Rolling resistance coefficient [-]	0.0065	0.00715	0.0084	0.0121
Reducer ratio [-]	9.59	9.3	8.19	12.98
Wheel diameter [m]	0.6099	0.6209	0.6319	0.7411
Frontal Area [m^2]	2.14	2.18	2.38	2.62
Aerodynamic drag coefficient [-]	0.311	0.29	0.28	0.28
System Power	87	100	160	150
System Torque	225	260	340	310
Homologated Power	43	57	90	70
Motor mass [kg]	41.5	47.2	64.5	59.7

The BOMs of the electric motors scaled according to the above-mentioned approach for each application, are represented in Figure 4.8. The figure provides a percentage distribution of the EM's material composition and exact mass of the parts expressed in kilograms.

Figure 4.9, instead illustrates the effects of both motor efficiency and motor weight on energy consumption during the WLTC, without charging losses. The Baseline motor efficiency map was applied across the four applications, assuming that efficiency differences within the considered performance ranges are negligible. Among the two factors, motor efficiency has the most significant impact on overall energy consumption, while motor weight plays a secondary role by influencing the operating point of the powertrain components. Although the same efficiency map is used for all applications, variations in transmission ratios and vehicle road loads determine an increase of the energy losses from city car to SUV. Additionally, the indirect effect of motor mass on the powertrain components becomes more pronounced as vehicle size increases from the smallest to the largest vehicle.

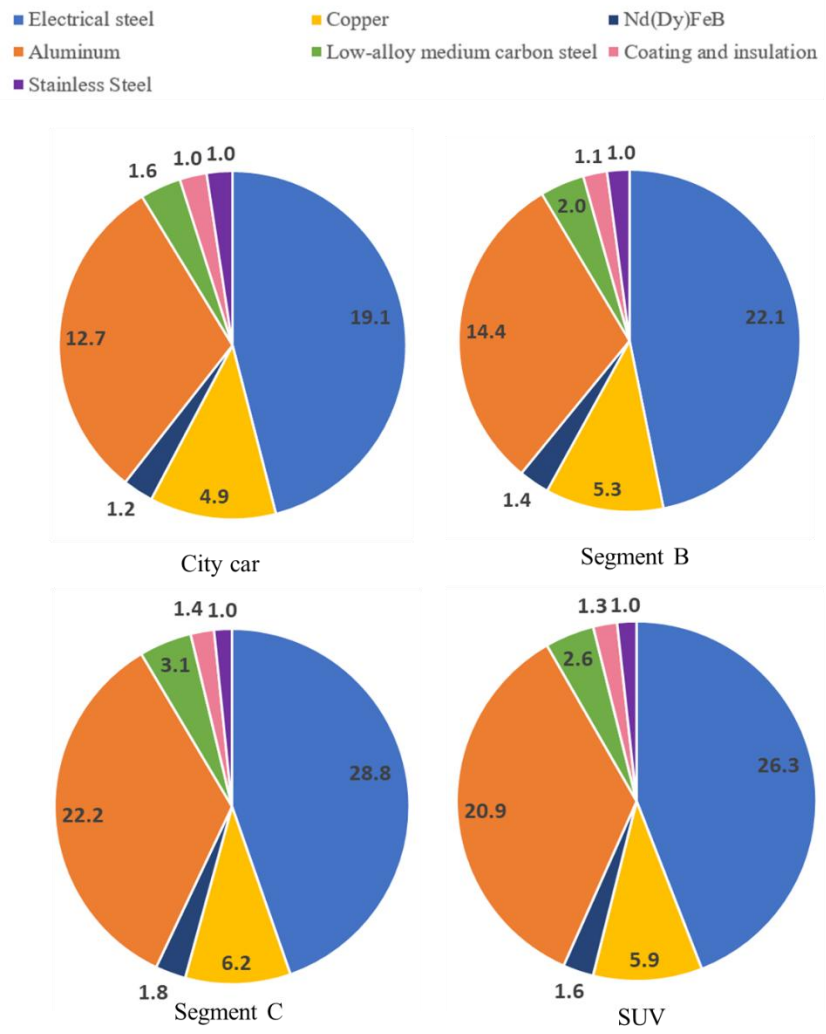

Figure 4.8 Selected applications' BOMs calculated with scaling methodology as function of maximum power and torque [175]

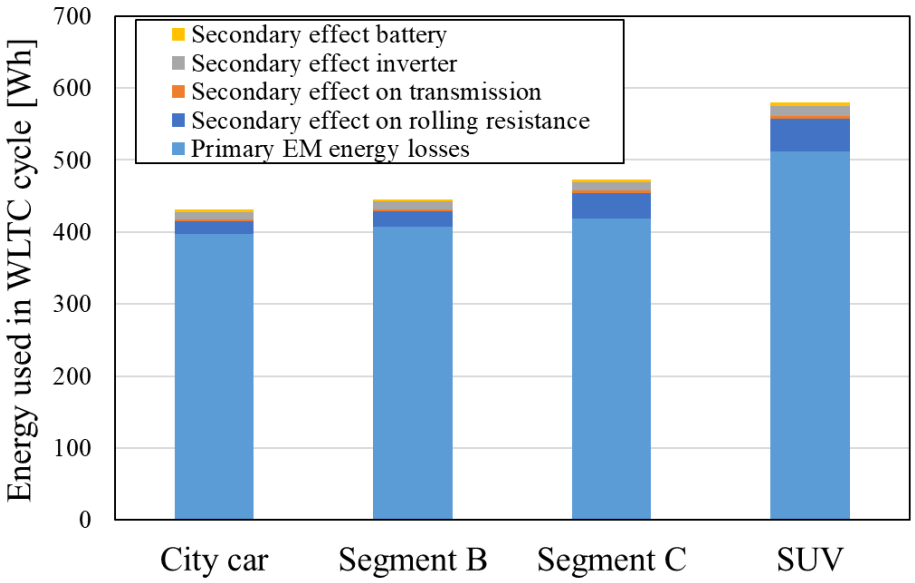

Figure 4.9 Energy used in the WLTC without charging losses, for the selected vehicles, considering weight of the scaled motors

4.2.3 PMSM vs copper and aluminium winding SRM

The goal of this study is to conduct a comparative LCA between a PMSM baseline and two SRM configurations, featuring respectively conventional copper winding and aluminium winding. The objective is to identify the specific environmental differences between these two motor technologies, understand the key drivers of environmental impact, and set the basis for future design improvements, of which aluminium winding configuration represents a first step towards Ecodesign strategies implementation. This study aims to answer the question "What is the environmental burden of travelling one kilometer with a magnet free SRM with respect to a PMSM, when both are manufactured in a specific country for a specific vehicle application, and where do these impacts originate?". The copper winding SRM is the object of the DfCE research, and its architecture and performance have already been described in the section 2.3. The aluminium winding variant, on the other hand, has been described in section 3.3.1. A state-of-the-art PMSM baseline used for comparison with the SRM configurations, as in the first step analysis, was selected through a benchmark study. The extensive benchmark analysis includes 200 BEVs available on the European market. From this dataset a subgroup of motors within a performance range, comparable with the use-case SRM, was identified, relying on published data [188], [189], [190]. A snapshot of vehicles featuring a single motor architecture, is shown in Figure 4.10, where both peak and homologated power (i.e., the power continuously available for 30 minutes) are plotted.

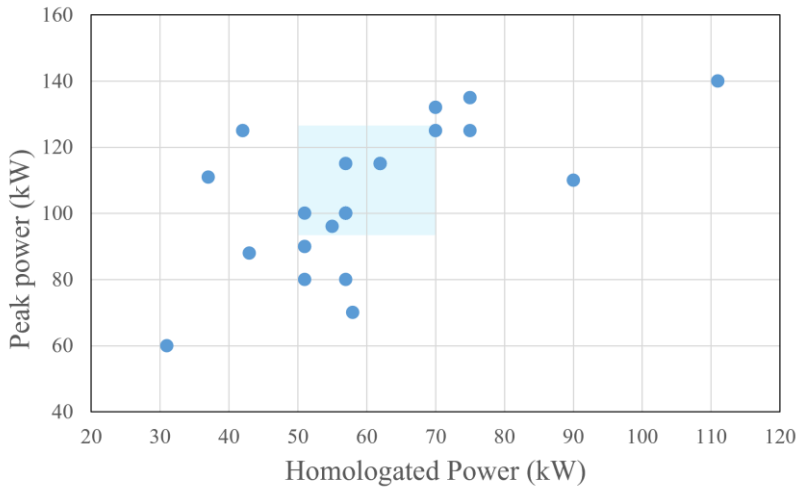

Figure 4.10 Peak Power as a function of homologated power from a benchmark analysis including 200 BEVs of the European market

These parameters were considered key drivers for the motor mass and consequently for the LCA. The figure also includes a highlighted range for both peak and homologated power, indicating suitable motor selections for the analysis. For the purpose of this study, the electric motor installed in the BMW i3 was selected as PMSM baseline due to its comparable performance with the SRM and the availability of detailed data. Indeed, this motor was extensively analysed

in terms of architecture and performances by Oak Ridge National Laboratory [158]. Some of the key performance and architecture parameters associated to PMSM baseline, copper and aluminium SRM motors are reported in the Table 4.8.

Table 4.8 Main motors parameters

Parameter	PMSM Baseline	SRM Copper-Aluminium winding
Peak power [kW]	125	100
Homologated power [kW]	75	60
Peak torque [Nm]	250	159
Base speed [rpm]	4500	6000
Maximum speed [rpm]	11400	18000
EM mass [kg]	48.4	67.8- 62.1
Power density [kW/kg]	2.6	1.5- 1.6
Stator/rotor poles [-]	12/12	12/8
Stator outer diameter [mm]	242	246
Length to stator bore ratio [-]	1.8	1.2
Coils in series per phase [-]	1	4
Single wire diameter [mm]	0.72	0.9
Winding configuration [-]	Distributed	Concentrated
Cooling method [-]	Water jacket	Water jacket

The evaluation of the environmental burdens has been performed with a cradle-to-grave approach encompassing all life cycle phases related to the electric motor, namely raw material acquisition, preprocessing, manufacturing, transport, use and end-of-life, as reported in Figure 4.11.

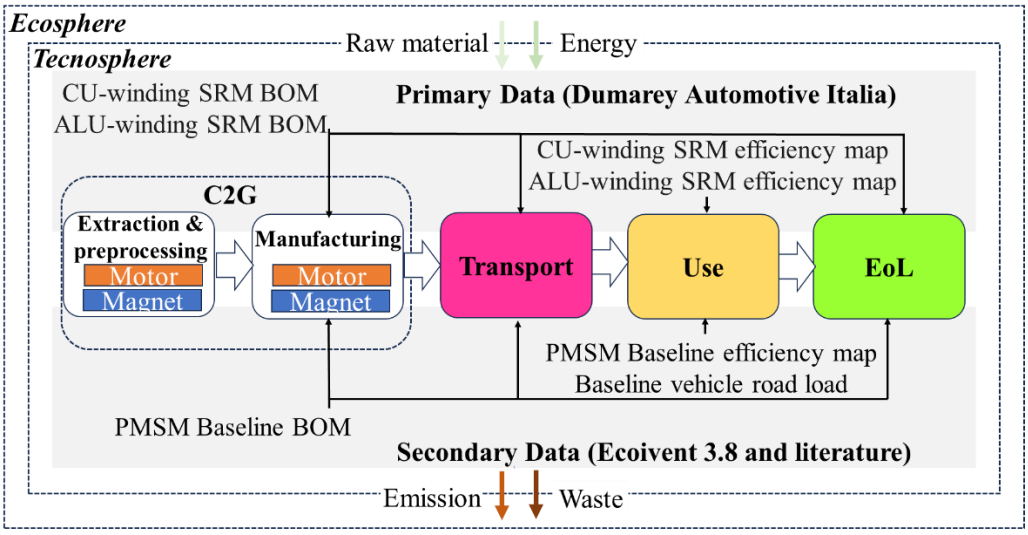

Figure 4.11 System boundary

Each phase is colour coded consistently with the results section to enhance readability. The figure also highlights the use of primary data, mainly related to SRM configurations, designed by Dumarey Automotive Italia S.p.A., and secondary data related to baseline PMSM and vehicle. These data sources are clearly marked at the respective stages of the life cycle where they are applied. The input data include the motor BOMs, the efficiency maps and the vehicle specifications relevant to the energy demand calculation. All remaining secondary data were sourced from the Ecoinvent v3.8 LCA database [181] and supporting literature. As in the first LCA step, the phases from material acquisition to motor manufacturing are grouped into one macro-phase called C2G including the two subgroups namely motor (accounting for all components of the motor without magnets) and magnets. The incremental main step with respect to the first one, as mentioned in Table 4.1, is the inclusion of the EoL phase, according to the approach already described in the general LCI section (4.2.1). Additionally transport phase is considered as stand-alone element, clearly highlighting its associated environmental impacts.

In the manufacturing phase electric motor BOMs were derived from different sources: for the PMSM, data were taken from literature based on a teardown analysis [158] while for both the copper and aluminium winding SRMs, primary design data were used, except for coating and insulation materials, which were assumed from literature sources [174]. As in the application scenario Figure 4.12, illustrates the percentage distribution of materials used, with corresponding mass values reported in kilograms for PMSM baseline, copper and aluminium winding SRMs. The absence of magnets in the SRMs is clearly visible. However, to compensate and ensure the desired performance, the SRM design features a larger active volume, resulting in an overall mass increase of approximately 20kg. The aluminium configuration is basically constituted by steel and aluminium.

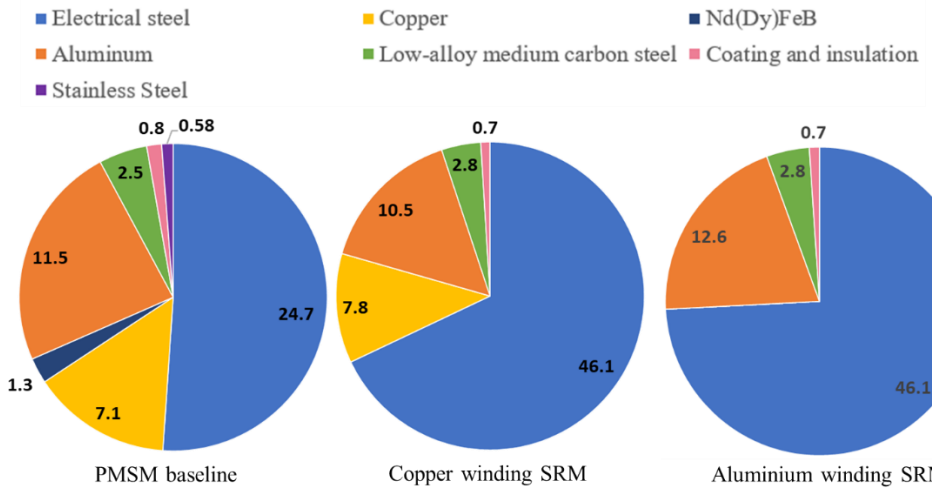

Figure 4.12 Material percentage distribution and mass values for the three considered motors within step2 LCA.

The data related to the vehicle and propulsion systems were sourced from literature and are detailed in the following section, which also describes the approach adopted for the virtual integration of the SRM configurations into the baseline vehicle. Italy was selected as the reference country for the analysis, based on the rationale provided in the geographic scenario section. Accordingly, the Italian electricity production mix, reflecting the 2018 technology shares, is used in the LCA, in line with the latest version of the Ecoinvent database. SRMs, are characterized by higher torque ripple than PMSMs, which can lead to increased vibration, noise, and potentially more frequent bearings maintenance operation if not properly sized from a mechanical standpoint, affecting use phase. However, bearings service life was not included in the life cycle assessment as its impact on both environmental and economic assessments was considered negligible, due to the fact that bearings account for a small fraction of the overall BOM. The transport phase includes operations occurring over manufacturing, distribution and EoL phases as reported in Table 4.9. Distances for the motor manufacturing, distribution and recycling are conservatively assumed close to the overall Italy length. Voices related to magnet manufacturing and magnet to assembly are just considered for the PMSM.

Table 4.9 Transportation boundaries

Parts	**Distance**	**Route**	**Typology**
Magnet manufacturing	1000 km	China	Train
Magnet to assembly	17000 km	China to Italy	Ship
Motor manufacturing	1000 km	Italy	Truck
Motor distribution	1000 km	Italy	Truck
Material recycling	1000 km	Italy	Truck

Vehicle and Propulsion unit

This section provides background information on the propulsion unit, comprising battery, inverter, motor and transmission and its virtual installation into the vehicle. It explains the methodology adopted and reports characteristic data, with the aim of establishing a reliable foundation for the environmental impact comparison. To meet the objective of the study, the SRM was virtually integrated into the baseline vehicle to enable a direct comparison between the two technologies within the same application, even considering the not optimal matching between SRM design and the selected vehicle. In this section related to the vehicle performances, SRM copper and aluminium winding configurations, are not distinguished as they have identical motor torque curve requirements (Figure 2.13). Main vehicle data and propulsion unit efficiencies used for calculation of the energy required are summarized in Table 4.10. Also in this case, vehicle data are published in [188], [189], [190], except for the rolling resistance coefficient assumed on the base of vehicle characteristic following [135].

However, for the SRM configurations, the transmission ratio (TR) was selected in a way to ensure that both vehicle performance is comparable to the reference vehicle and to guarantee a better usage of the motor efficiency map over the WLTC. Specifically, the reducer ratio has been increased to 16, allowing a better alignment between the vehicle's top speed and the motor's maximum speed.

Table 4.10 Reference vehicle main data

Symbol	Parameter	Data
m	Curb Weight [kg]	1345
fr	Rolling resistance coefficient [-]	0.00715
$kgear$	Reducer ratio [-]	9.665
D_{tyre}	Wheel diameter [m]	0.694
A	Frontal Area [m^2]	2.8
c_x	Aerodynamic drag coefficient [-]	0.29

The shift toward higher operating speeds not only improves efficiency map utilization but is also considered beneficial in mitigating the effects of torque ripple, which is inherently high in SRMs. Indeed, torque ripple is still present at high speeds, but its effect is 'damped' due to the higher rotational speed of moving parts. Following the formulation described in Chapter 2 (equation 2.8 to 2.10) the parameter referred to as "acceleration reserve" has been estimated. Figure 4.13 reports the acceleration reserves and required power curves of the baseline vehicle with PMSM and with SRM, for both with the baseline and the newly selected TR.

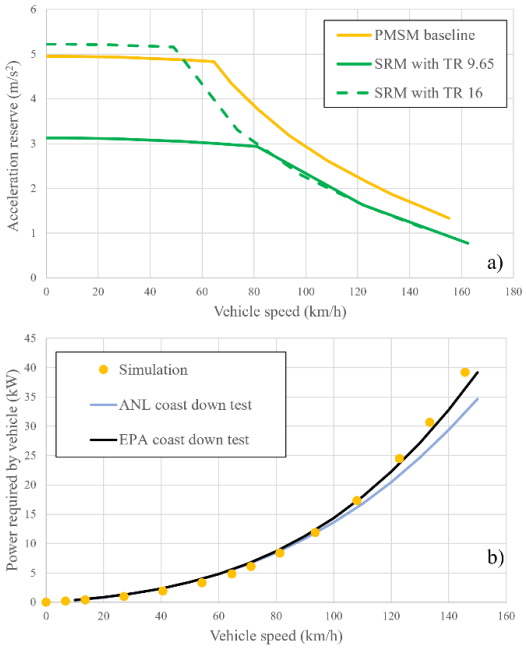

Figure 4.13 a) Acceleration reserve in relation to vehicle speed for reference vehicle and SRM with original and selected TR b) Reference vehicle required power calculated and measured in relation to vehicle

The shift of the SRM curve from a lower to a comparable acceleration reserve relative to the baseline PMSM is evident. The force required to propel the vehicle, known also as road load, was derived from vehicle data, as outlined in section 4.2.1 (Use Phase) to allow evaluation of indirect effect coming from the motor mass. Nevertheless, the curve obtained through simulation is compared against two different testing activities, executed at different times but using the same vehicle model, to demonstrate the robustness of the simulation results. This comparison is reported in Figure 4.13 b where the required power, simulated considering published vehicle data, is evaluated against experimental curves obtained from coast down target coefficients present in the literature available test reports from EPA and Argonne National Laboratory [195], [196]. A good correlation between data coming from simulation and testing can be observed. To determine the energy input for the LCA, the efficiency maps of the three motors were analysed. The baseline PMSM efficiency map was sourced from [158], while the SRMs maps result from in-house performed electromagnetic analyses, and represent the maximum electromagnetic torque-speed capability.

Figure 4.14 presents the efficiency maps of the two motor technologies, highlighting their respective performance characteristics and the associated WLTC operating points. It is noticeable that SRM has a broad torque-speed envelope. This, as already mentioned, indicates that the machine is not specifically targeted to the application at hand, demonstrating a considerable margin for improvement in terms of torque density and mean efficiency. It is also possible to appreciate the different position of the cycle operative points over the map, due to the TR. Concerning aluminium winding SRM variant, the efficiency map is already illustrated in Figure 3.9.

Figure 4.15, instead clearly illustrates the dominant influence of electric machine efficiency over the considered driving cycle, as described in the previous section for the application scenario. The specific energy loss values, calculated according to the assumptions described in the LCI and using the above-mentioned efficiency maps and vehicle data, are respectively 28 [Wh/km] for the PMSM, 32 [Wh/km] for the copper winding SRM and 25 [Wh/km] for the aluminium winding. A detailed explanation of the superior average efficiency of the vehicle with the aluminium-wound SRM over the WLTC is provided in Section 3.3.1.

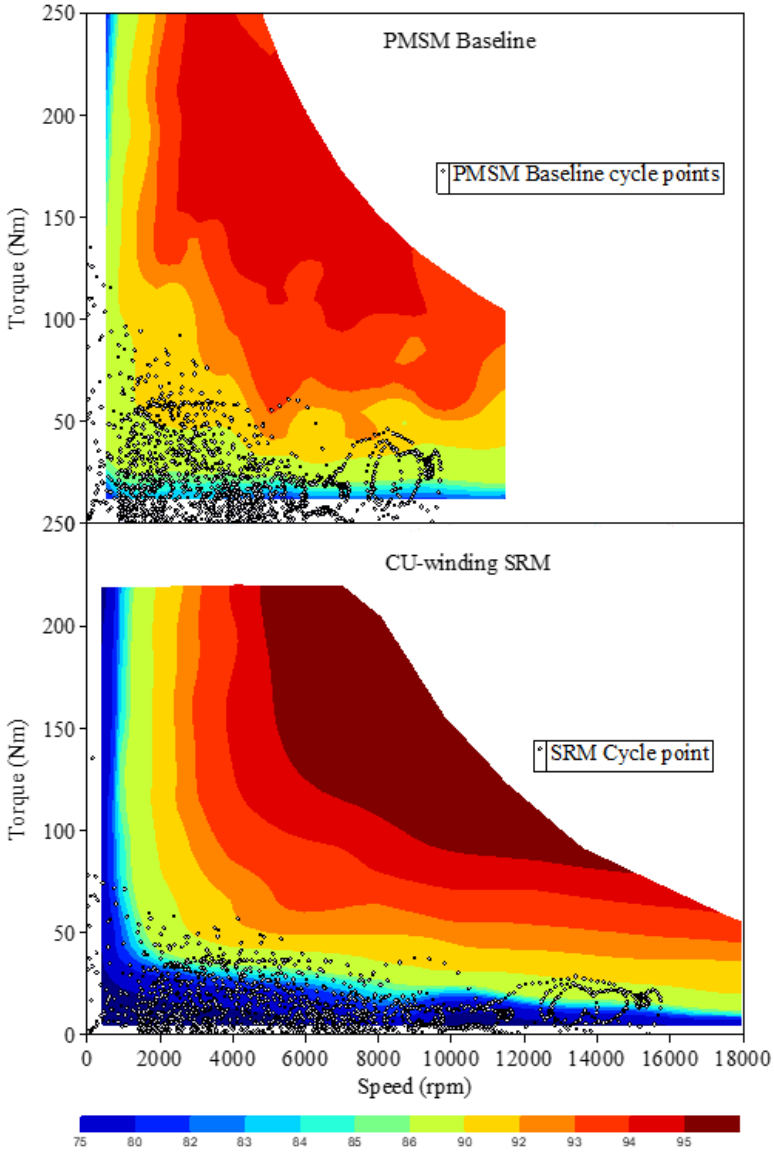

Figure 4.14 Efficiency maps of PMSM baseline and copper winding SRM and WLTC operating points

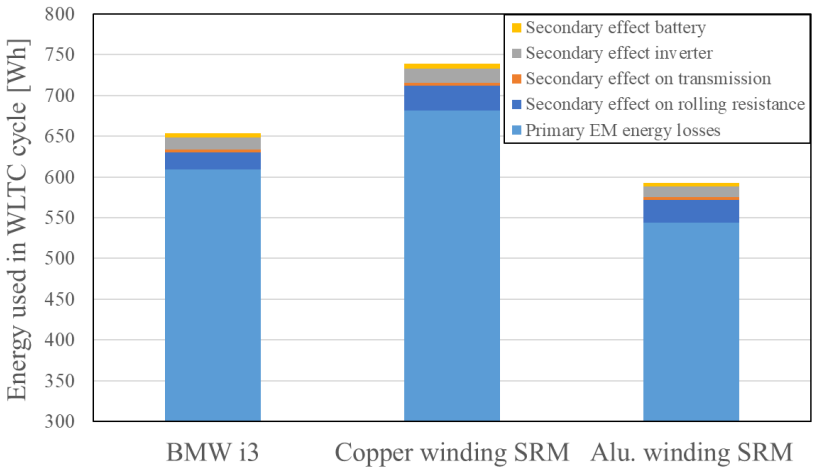

Figure 4.15 a) Energy used in the WLTC without charging losses, for the selected vehicle installing the three motors

4.2.4 Circular Strategies

The goal of this assessment is to provide a comparative LCA between a conventional linear model considered the baseline for this step and the CS described in detail in Chapter 3. This LCA study aims to answer the question "What is the environmental burden of travelling one kilometre with a magnet free SRM circulated in its economic chain with respect to a conventional usage, manufactured in a specific country for specific vehicle application, and where do these impacts originate?"

The benchmark for the LCA is the copper-wound SRM compared with the PMSM, as described in the previous section. Consistently with the methodology outlined in Section 4.2.3, the environmental impact assessment follows a cradle-to-grave approach, including electric motor related impact in all life cycle phases identically to the previous step investigation. Also, the country of production and usage and the application considered are those of the second LCA step. Also, from a modelling perspective this step present identical input with respect to step 2. however, the incremental step in this case is that the system boundaries include also the considered CS as illustrated in Figure 4.16 .

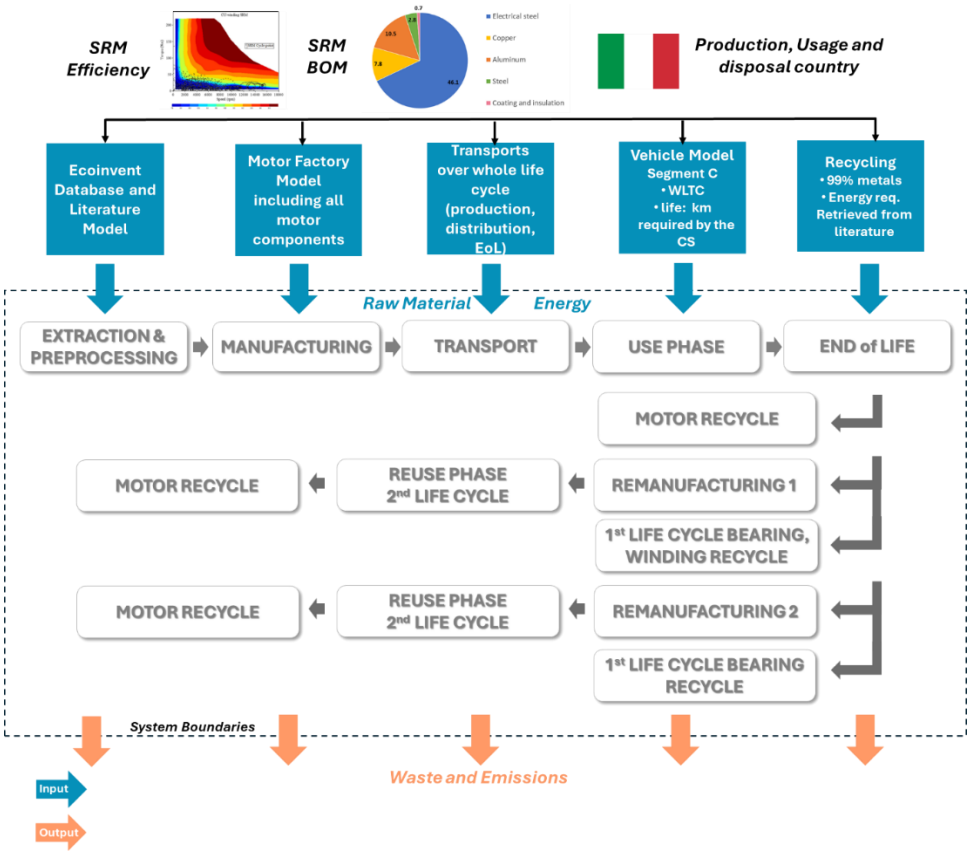

Figure 4.16 System boundary

This figure also details the sources of both primary and secondary data as well as the models and main assumptions adopted for the LCA activity. In the scheme above, additionally to the conventional life cycle, three distinct circular pathways, representing the EoL strategies are illustrated and called Recycle,

Remanufacturing 1 and Remanufacturing 2. The Extended Durability strategy is not represented in the figure because from a circularity perspective replicate a linear approach. The system boundaries considered for the treated CS, are reported in Table 4.11.

Table 4.11 CS boundaries

Cycle phases		**Baseline**	**Extended Durability**	**Remanufacturing**	
				1	**2**
Extraction and manufacturing number of components	Stator	1	1	1	1
	Winding	1	1	2	1
	Shaft	1	1	1	1
	Housing	1	1	1	1
	Rear Bearing	1	1	1	1
	Front Bearing	1	1	2	2
	Rotor	1	1	1	1
Number of Assembly	Motor	1	1	2	2
Transport	Motor	1	1	2	2
	Manufacturing, Distribution and EoL	1	1	2	2
Usage Phase	Assumed Life mileage [km]	200000	400000		
End of Life	Recycle after 1st cycle	Motor	Motor	Bearing and Winding	Bearing
	Recycle after 2nd cycle	-	-	Motor	Motor

The Table, outlines for both the baseline and the CS, the number of components to be manufactured, the total kilometres expected during the use phase and the materials designated for recycling when the motor approaches EoL, across the respective life cycles. It also includes the Extended Durability strategy. The key distinction introduced by the extended durability scenario respect to baseline is represented by assumed life mileage, which is double. In contrast, the two remanufacturing strategies consider the number of critical components, as defined in Chapter 3, to be equal to the number of remanufacturing cycles, as well as the assembly and transport operations. Noticeably, in both remanufacturing scenarios, the motor's operational life is doubled relative to the baseline, and recycling is performed at the end of each life cycle, both for the replaced critical components and the motor itself.

In Chapter 5 within the results section is shown the environmental impact of all the CS highlighting the effect of each life cycle phase. In this section are not considered operations for collection and disassembly of the system, both for the lack of data and because they were considered negligible for the overall evaluation. However, indication for potential future research, are described in the conclusion in Section 6.

4.3 Material Circularity evaluation and Material Flow Analysis

Among the various circularity indexes, the Material Circularity Indicator (MCI) is one of the most well-known, designed by the Ellen MacArthur Foundation in collaboration with Granta Design, aiming at measure the circularity at micro-level, focusing indeed, on product and company [197]. With reference to the implementation scale, the other levels are the meso, in which attention shifts to collaborative systems like eco-industrial parks and industrial symbiosis and the macro, where boundaries expands to geographic units such as cities, provinces, regions, or entire nations [33], [36]. MCI is a dimensionless indicator varying from 0 to 1, assessing how effectively a product or material maintains its value through successive cycles of use, reuse, and recycling. As shown in [160], MCI has a high level of alignment with the five CE requirements set out by [198] in comparison with other CE index-based method at micro level.The MCI incorporates several key factors such as the proportion of recycled content in a product, its potential for reuse or recycling at the end of its life, the efficiency of the recycling processes involved, and the overall product lifespan. The goal of the MCI is to offer a quantifiable indicator that supports designers in assessing and enhancing the circularity performance of their products and materials [197]. As for the LCA, also for the circularity assessment are required detailed data on material flows, product composition, and recycling processes. Integrating circularity metrics with LCA can help address some of the data limitations and provide a more holistic sustainability assessment. To the best of the author's knowledge, no studies in the existing literature have reported the application of a circularity indicator calculation to electric motors or propulsion systems. Circularity evaluation is often treated in conjunction with LCA investigation, especially for what concern results analysis, where it provides valuable insights into the environmental impact of a product. In particular [199] proposed a Multi Criteria Decision Analysis (MCDA) considering two material circularity based-indicators, MCI, Material Reutilization Source (MRS) in parallel with the evaluation of some categories of the LCA. The methodology was applied on eight beer pack with two different localizations (UK and India). Within the research described in [200] has been performed an evaluation of 4 different mixtures of asphalt with different reclaimed asphalt (RA) percentage through a developed composite parameter, that couples both LCA and MCI. The parameter incorporates specific design features of the product under evaluation and has therefore been tailored to meet the objectives of the study. The trade-offs between MCI and LCA have been explored in [201], where a Product Circularity Indicator (PCI) has been purposely developed to compare various design and usage strategies for washing machines from a sustainability perspective. A similar approach is adopted in [160] where the sustainability of various recycling and reuse strategies for tyres is assessed comparing LCA and MCI, with a proposed adaptation of the latter. Another adaptation of the MCI is proposed in [202] where

a trade-off analysis between circularity and LCA is applied to a case study involving three-layer plastic packaging, considering two end-of-life scenarios: incineration and closed-loop mechanical recycling. All the above studies have been reviewed in [203] which emphasizes the importance of complementing circularity assessments with LCA. The review highlights the communicative immediacy of circularity indicators and the necessity of LCA for delivering a holistic evaluation, particularly when selecting among alternative strategies. The above-mentioned conclusion is mainly based on findings from previous research, which often highlighted the fact that the LCA and MCI are not necessarily leading to aligned outcomes, especially when multiple impact categories are considered. Within this research, a circularity analysis has been performed to enrich LCA study, to provide evidence of the higher material circularity of the system, when adopting the proposed CS. To achieve this, the models presented in the cited literature [160], [197], [201], [202] were considered for the electric motor case study and applied to the CS configurations, with particular focus on two sub-cases: one considering a single life cycle, and the other incorporating two consecutive life cycles. In the following section are provided main formulation used. To complement the circularity analysis, a Material Flow Analysis (MFA) was also carried out, and results are reported in Chapter 5. This analysis leveraged LCI data, particularly regarding material and component production efficiencies, as well as the BOM. This analysis has been briefly treated as it is not the primary focus of the research. Its purpose is to support and reinforce MCI and LCA analyses, by highlighting the material paths, visualized through the adoption of Sankey diagrams.

4.3.1 MCI model adaptation

The adopted methodology is based on the model presented in [201], which was selected for its alignment with the objectives of this research to which has been slightly adapted. In particular, its advancement in comparison to the original MCI definition, concerning possibility to evaluate both feedstock and component manufacturing and to consider a product as a system composed by various components, are perfectly aligned with the electric motor case. The indicator defined in such a paper, is named Product Circularity Indicator (PCI), acting more at product level, rather than at material level. PCI is considered in this thesis and therefore, the formulation is just summarized, and not completely exploited, to avoid redundancy with the relevant referenced literature, which interested readers may consult directly. Table 4.12 summarizes the equations adopted to calculate all the parameters required for determining the circularity indicator in the various subcases. These equations are applicable to each material constituting the product and, in the electric motor case, to each subcomponent. Indeed, the PCI, applied to the electric motor, is then determined through equation 4.19, for each individual (i-th) material, using a mass-based weighting methodology [160], [201], [202].

Table 4.12 PCI calculation model equation

Parameter	Equation	
Virgin Material	$V = \frac{(1-F_U)M}{E_{cp}E_{fp}}(1-F_R)$	(4.5)
Waste Material	$W = W_{fp} + W_{cp} + W_U + W_{ms} + W_{rfp}$	(4.6)
Waste from feedstock production	$W_{fp} = \frac{(1-F_U)M}{E_{cp}E_{fp}}\left(1-E_{fp}\right)\left(1-C_{fp}\right)$	(4.7)
Waste from component production	$W_{cp} = \frac{(1-F_U)M}{E_{cp}} \cdot E_{fp}\left(1-E_{cp}\right)\left(1-C_{cp}\right)$	(4.8)
Uncollected waste	$W_U = M(1-C_R-C_U)$	(4.9)
Waste from material separation	$W_{ms} = M(1-E_{ms}) \cdot C_R$	(4.10)
Waste from feedstock recycle production	$W_{rfp} = ME_{ms}C_R\left(1-E_{rfp}\right)$	(4.11)
Recycled material used for feedstock production	$R_{IN} = F_R\frac{(1-F_U)M}{E_{cp}E_{fp}}$	(4.12)
Recycled material recovered	$R_{OUT} = \left(1-E_{fp}\right)C_{fp}\frac{(1-F_U)M}{E_{cp}E_{fp}} + E_{rfp}E_{ms}C_RM$	(4.13)
Net recycled material	$R = R_{IN} - R_{OUT}$	(4.14)
Net reused material	$C = M \cdot (F_U - C_U)$	(4.15)
Linear Flow Index	$LFI = \frac{V + W + \frac{1}{2}\lvert R\rvert + \frac{1}{2}\lvert C\rvert}{\frac{2M}{E_{cp}E_{fp}}}$	(4.16)
Utility Factor	$X = \frac{U}{U_D} = \frac{L}{L_D} \cdot \frac{I}{I_D}$	(4.17)
Product Circularity Indicator	$PCI = 1 - \frac{LFI}{X}$	(4.18)
Total Product Circularity Indicator	$PCI_{Total} = \frac{\sum_i M_i n_i PCI_i}{\sum_i M_i n_i}$	(4.19)

Where:

F_U: fraction of mass of product's feedstock from reused sources; F_R: fraction of mass of product's feedstock from recycled sources; M: mass of the material/components; E_{cp}: component production efficiency; E_{fp}: feedstock's production efficiency; C_{fp}: fraction of material losses recovered as scrap during feedstock production; C_{cp}: fraction of material losses recovered as scrap during component production; C_R: fraction of product at end of use collected for material recycling; C_U: fraction of product at end of use collected for reuse of component; E_{ms}: material separation process efficiency; E_{rfp}: feedstock production from recycled material efficiency; n: number of parts used.

The analysis was conducted for both single-cycle strategies (Baseline and Extended Durability) and for two-cycle strategies (Remanufacturing 1 and Remanufacturing 2). The system boundaries considered for the material circularity evaluation in the mentioned scenarios are illustrated in Figure 4.17. For both single and multi-cycle processes, the following assumptions and boundaries were applied:

- Feedstock and motor production efficiencies are aligned with the LCA model
- Feedstock recycling efficiency were sourced from literature and range between 90-100% depending on different material
- Scrap recovery from feedstock and component production is assumed to be 100% in all the cases
- Separation process was not considered, assuming it identical for all the configurations.
- In the single-cycle approach, reuse of material is not present.
- For both single and multi-cycle approaches, three recycling scenarios were evaluated (0%, 50% and 100% recycling) based on the assumption that 99% of the SRM is recyclable, coherently with LCA model
- In the Extended Durability strategy, the product lifetime was assumed to be twice that of the baseline
- In the Remanufacturing strategies, number of parts used, durability and reuse rate have been carefully selected for each component coherently with the different strategy

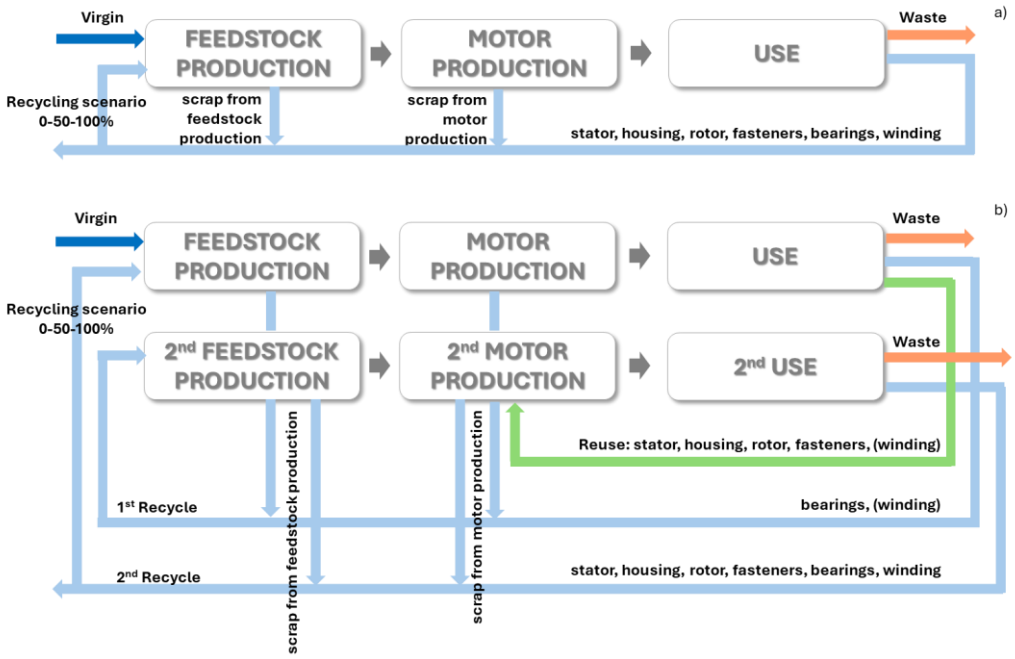

Figure 4.17 MCI System boundaries a) for one life cycle b) for two life cycles

In the proposed framework for the two-cycle case, all the output materials at the end of the first cycle are treated as input materials for the second cycle. Specifically, the fraction of product collected for reuse at end of the first use phase, is considered as reused feedstock mass in the second cycle. With reference to this, all the strategies applying reuse of parts are characterized by a complete reuse in the second life cycle, not exchanging outside the product boundaries, resulting in an exchange of reused parts as defined by equation 4.15 equal to 0 and representing the main difference with the approach presented in [201]. Similarly, the fraction of recycled material at the end of the first cycle is considered as recycled material mass for the second. Concerning recycling, depending on the different scenarios considered, product system can supply to a stock out of the boundaries or receive from it recycled material.

All the model input are reported in Table 4.13 and Table 4.14, enabling practitioners to replicate the analyses presented in this work, as for the LCA. Specifically, data related to the feedstock and component production efficiencies as well as their separation and fraction of material losses recovered as scrap during feedstock and component production used, are identical for all the CS and reported in the first table.

Table 4.13 PCI Efficiencies for feedstock and component production, material separation process and fraction

Component	**Material**	E_{fp}	E_{cp}	E_{rfp}	C_{fp}	C_{cp}	E_{ms}
Stator, Rotor	Electrical Steel	0.85	0.53	0.99	1	1	1
Winding	Copper	1	0.98	1	1	1	1
Shaft	Steel	1	0.8	0.99	1	1	1
Bearings	Steel	1	1	0.99	1	1	1
Fasteners	Steel	1	1	0.99	1	1	1
Housing	Aluminum	0.94	0.91	0.9	1	1	1
Coating	Plastic	1	1	-	0	0	-

Instead, number of parts used, utility factor, and fraction of components recycled or reused, vary according to the different CS and are reported in the second. Components mass is the same used in the LCA step2 and 3 for the copper wound SRM concept. In the baseline linear model, none of the components are reused and each is characterized by a utility factor of 1, representing the average market value. In the extended durability strategy, all components are assigned a utility factor of 2, indicating a doubling of their lifespan. Concerning remanufacturing strategies, the stator, rotor, housing, shaft, and fasteners are all reused at the end of the first cycle. This reuse is quantified as 0.5, calculated using Equation 4.20, where N is the number of times the components are reused. The winding, however, is reused only in the second remanufacturing cycle, while the bearing and coating are never reused, resulting in the use of two new parts over two use phases. All parts that are not reused are recycled at the end of the first use phase. At the end of the second use phase, all parts are assumed to be recyclable, with the exception of plastic components Finally, as previously mentioned, three

recycling scenarios have been considered: feedstock production entirely from virgin material (0% recycled), a mix of virgin and recycled material (50% recycled), and fully recycled material (100% recycled).

$$C_U = F_U = 1 - \frac{1}{N} \tag{4.20}$$

Table 4.14 Fraction of components recycled or reused as input for feedstock production and collected at the end of the cycle, number of parts used, utility factor

Component	CS	F_U	F_R	C_U	C_R	n	X
Stator, Rotor Shaft, Fasteners, Housing	Baseline	0	0,0.5,1	0	1	1	1
	Extended Durability	0		0	1	1	2
	Remanufacturing1	0.5		0.5	0.5	1	2
	Remanufacturing2	0.5		0.5	0.5	1	2
Winding	Baseline	0	0,0.5,1	0	1	1	1
	Extended Durability	0		0	1	1	2
	Remanufacturing1	0		0	1	2	1
	Remanufacturing2	0.5		0.5	0.5	1	2
Bearings	Baseline	0	0,0.5,1	0	1	2	1
	Extended Durability					1	2
	Remanufacturing1					2	1
	Remanufacturing2					2	1
Coating	Baseline	0	0,0.5,1	0	0	2	1
	Extended Durability					1	2
	Remanufacturing1					2	1
	Remanufacturing2					2	1

4.4 Cost Model

In line with the emerging paradigm of evaluating a product's entire life cycle, cost should also be treated with a holistic approach similarly to the approach already applied to environmental impacts, from raw material extraction to EoL. However, this study primarily focuses on motor manufacturing costs, including voices related to components production, assembly operation and testing. These cost elements are illustrated in Figure 4.18, which highlights the most significant differences between the considered CS. At the time this research was conducted, this portion of the life cycle was considered representative of the main cost related differences between the CS, given that the introduced design features do not affect motor efficiency and, consequently, have no impact on the use phase. However, certain aspects are influenced by the CS and potential directions for future research, particularly regarding economic evaluation, are outlined in the conclusion chapter. Also, the circular paths considered in this study share the same manufacturing phases, as previously described.

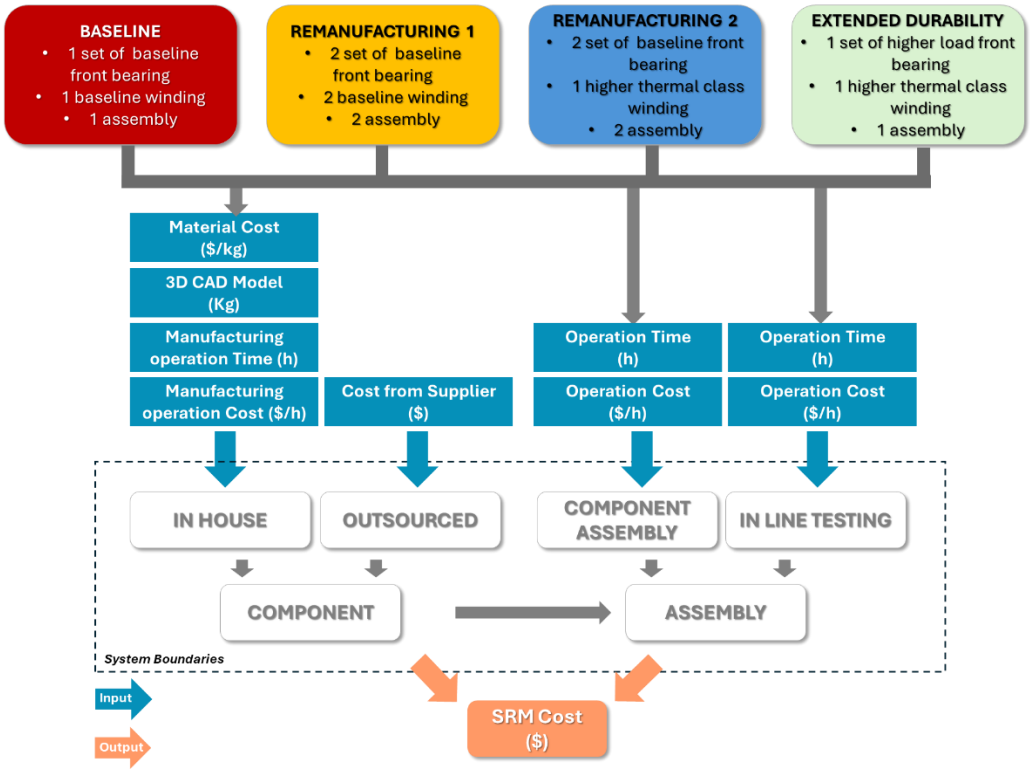

Figure 4.18 Cost Model boundaries

Furthermore, all the strategies analysed, face the same single cycle assembly cost, while the cost increments due to the specific critical components, described in Chapter 3, are respectively +191% for the higher load capacity bearing and +18% for the higher thermal class winding compared to the baseline components. In the diagram, the top row of boxes summarizes the cost-related differences among the various strategies: red for the Baseline, yellow for Remanufacturing 1, light blue for Remanufacturing 2, and green for the Extended Durability option. The blue boxes represent model inputs, while orange boxes refer to the output, that is the cost of one electrical machine produced. The white boxes represent the different phases of the motor manufacturing process: sub-components sourcing and final assembly. Concerning the components, both outsourcing and in house manufacturing strategies were considered and carefully selected. The cost of outsourced components is based on estimates from the selected supplier. In this study, being an initial concept evaluation, these costs were derived from Dumarey Automotive Italia's internal benchmarks or detailed calculations. For components manufactured in house, a detailed bottom-up cost analysis was always performed. This approach assumes a specific manufacturing process and calculates the final cost based on direct material expenses and manufacturing operation costs. A comparable approach is applied to both assembly and in line testing operations. Specifically, all the stations necessary to assemble components to obtain the finished motor have been included in the model. Both sub-components manufacturing and assembly operations account for the machine related costs (amortization plan, energy consumption, occupied space), labour cost, handling and transportation fees and production overheads costs. These voices associated to

manufacturing and assembly are influenced by several factors such as the electric motor topology, the manufacturing country, the level line automation and the degree of process optimization as discussed in [119].

Table 4.15, summarizes the main assumptions considered for the cost assessment, in addition to the BOM weight as already illustrated in Figure 4.12.

Table 4.15 Cost model input

Cost Description	**Considered assumption**
Supply Chain - Countries	Europe, Asia
Assembly Line - Country	Western Europe
Energy cost [$/kWh]	According to country specific databases, internal Dumarey Automotive Italia intelligence.
Labor cost[$/h]	According to country specific databases, internal Dumarey Automotive Italia intelligence.
Production Scenario - Volumes	30000 pieces 11 lots per year 7 years product lifecycle Dedicated line – 3 shifts

Data coming from Dumarey Automotive Italia's database and detailed cost model are considered confidential and, therefore, cannot be disclosed within this work. For the same reason, the economic results, described at Chapter 5, are shown in normalized way. However, the cost estimates for the CS, calculated through the above mentioned model, have been compared with those obtained using the simplified model described in [119], to provide consistency of the cost estimation. In the simplified model, cost of each motor's sub-assemblies C_i is obtained multiplying the mass of each system M_i by a fixed material cost density CD_i as expressed in equation (4.21).

$$C_i = M_i \cdot CD_i \tag{4.21}$$

Then the assembly and testing cost in the same paper is considered as a fraction k, ranging from 20% to 40% of the overall manufacturing cost, depending on the motor's topology and architecture. Finally, the overall manufacturing cost C_{mfg} is determined through the equations (4.22) and (4.23).

$$C_{mat} = \sum_i C_i \tag{4.22}$$

$$C_{mfg} = \frac{C_{mat}}{1-k} \tag{4.23}$$

Table 4.16 reports the supplementary data on component masses required to calculate motor manufacturing costs according to the simplified model.

Table 4.16 Simplified cost model input

Symbol	Parameter	Value
k	Assembly and testing cost fraction	0.2 - 0.4
CD_{el_steel}	Electrical steel cost density [$/kg]	1.25
CD_{copper}	Copper cost density [$/kg]	10
CD_{alu}	Aluminium cost density [$/kg]	3
CD_{steel}	Steel cost density [$/kg]	1.5

The simplified model, however, considers cost densities for the metal parts. Therefore, to enhance comparability with the Dumarey Automotive cost model, the overall perimeter has been reduced by excluding certain subsystems, as detailed in Chapter 5.

Chapter 5

Results of the environmental and economic impact assessment

5.1 Introduction

This chapter describes the environmental impact results of the LCA (Section 5.2) the material circularity evaluation (Section 5.3) and the cost assessment (Section 5.4). Some of the content reported in this chapter have already been published by the author in the papers [161], [162], [163]. All the assessments described in this thesis have been expanded compared to the cited literature, and some results differ slightly due to changes in model inputs aimed at harmonizing the various steps presented. However, no conceptual changes have been identified that would affect the conclusions or influence the motor's design recommendations.

5.2 Electric motor LCIA and results interpretation

LCA results are reported for the three steps described in Chapter 4. This section outlines, for each step, an assessment of all impact categories, a characterization of the life cycle stage impacts, and a selection of categories based on a weighting methodology. The interpretation of the results is conducted aiming to avoid repetition across the various steps and scenarios, considering that there are contact points between them. Therefore, a more detailed description of the processes affecting all impact categories is provided for the Step 1 baseline. The other scenarios within Step 1 and the subsequent steps are analysed using an incremental approach, focusing on a selected group of categories and in alignment with the defined goal and scope.

The LCIA was conducted through the most updated version of the Environmental Footprint (EF) method, in accordance with [204] and midpoint

impact categories were considered for the assessment. The EF method is recommended by the guidelines of the Product Environmental Footprint (PEF) methodology, developed by European commission [205]. The impact assessment method includes sixteen impact categories which are explained below to facilitate the interpretation of the results obtained across the three steps. Specifically, for each of the categories, a simplified description of their effect and relative emitters is provided, along with the category indicator as reported in [206] and the unit of measurement. Additionally, for the main emitters, a quantitative indication of their influence on the overall environmental impact is provided based on the Step 1 baseline LCIA, which is adopted here as the reference.

- **Climate Change**. GHG accumulated in the atmosphere, absorb heat and induce climate change. The most relevant gases are carbon dioxide (88%), methane (8%) and dinitrogen monoxide (1.5%). The indicator used is the Global Warming Potential (GWP) over a 100-year time horizon, which measures the relative warming impact of a unit mass of a greenhouse gas compared to carbon dioxide. Therefore, results are expressed in kilograms of CO_2 equivalent (kg CO_2 eq).

- **Ozone depletion**. The release of ozone-depleting substances causes damage the ozone layer, which protects the biosphere from harmful UV radiation. The most impactful substances are bromochlorodifluoromethane (64%), bromotrifluoromethane (21%) and bromomethane (5%). The indicator used is the Ozone Depletion Potential (ODP), which quantifies the destructive effects on the stratospheric ozone layer over a 100-year time horizon. The impact of all relevant substances is converted to the equivalent in kilograms of trichlorofluoromethane (CFC-11) and is therefore expressed in kg CFC-11 eq.

- **Ionizing radiation**. Ionizing radiation impacts human health, and the adopted indicator is the Ionizing Radiation Potentials, which quantifies the effect of ionizing radiation on the population in comparison to Uranium 235 and is expressed in kilobecquerels of U-235 equivalent (KBq U^{235} eq). The main sources of ionizing radiation generated by humanity, are related to nuclear power plant fuels, and their waste, nuclear weapons testing, and other uses of radioactive materials in scanning equipment like X-rays. The primary emissions are the Radon-222 (67%) and the Carbon-14 (32%).

- **Photochemical ozone formation**. Photochemical ozone is formed in the low-level atmosphere, by the effect of solar light on human emissions mainly coming from terrestrial transportation sector, as well as chemical, energy and manufacturing industries and agriculture sector. The indicator used is the Photochemical ozone creation potential

(POCP) that express the potential contribution to photochemical ozone formation in the troposphere. It is referred to the mass of non-methane volatile organic compounds (NMVOC) and expressed in kg NMVOC eq. The main contributing substances are nitrogen oxides (72%), NMVOC (13%) and sulphur dioxide (9%).

- **Particulate matter**. Particulate pollution characterized by different size is mainly emitted by combustion processes and industrial activities. These substances cause damage to human health and air quality. The category indicator is the disease incident due to kilograms of PM2.5 emitted that assess the respiratory health impacts from fine particles (PM2.5). The most impactful substances are particulate matter thinner than 2.5µm (56%), sulphur dioxide (27%) and particulate matter with size between 2.5µm and 10µm (9%).

- **Human toxicity, cancer and non-cancer**. The release of toxic chemicals into the environment through industrial processes, emissions from products containing harmful chemicals, emissions from vehicles, pesticides use in agriculture and landscaping and other sources can lead to human toxicity. The indicator for both carcinogenic and non-carcinogenic effect is the Comparative Toxic Unit for human (CTUh), which expresses the estimated increase in morbidity in the total human population per unit mass of a chemical emitted (cases per kilogramme). Main element impacting human toxicity cancer are the benzo (a)pyrene in air (33%), the chromium released to soil and air (40%) and the arsenic released into water (10%). Instead, main substances affecting human toxicity non cancer are the arsenic released into water and air (43%), the lead and mercury released into air (14% and 13% respectively) and the carbon monoxide into air (11%).

- **Acidification**. Acidifying substances are mainly emitted by combustion processes (especially with high sulphur amount) in transport, heating and electricity production, causing impacts on ecosystem. The Accumulated Exceedance (AE) indicator characterizes the change in critical load exceedance of the sensitive area in terrestrial and main freshwater ecosystems, to which acidifying substances deposit. The potential impact of these substances is converted to the equivalent of moles of hydron concentration and is expressed in mol H^+ eq. The main acidifying substances are sulphur dioxide (70%) and nitrogen oxides (26%).

- **Eutrophication freshwater, marine, and terrestrial.** Eutrophication is caused by emission of substances in the ecosystem by human activities, generating an overfertilization of soil, freshwater and marine ecosystems. In particular, a great amount of nutrients is generated,

resulting in a growth of plant and algae with a consequent oxygen reduction, that is negative for the ecosystem. The indicators for eutrophication freshwater and marine are respectively the Phosphorus and Nitrogen equivalents, which express the degree to which the emitted nutrients reach the freshwater and the marine end compartments. The corresponding units are kg P eq. and kg N eq. Concerning terrestrial eutrophication, the AE indicator characterizes the change in critical load exceedance of the sensitive area, where eutrophying substances are deposited. The main substances are the phosphate into water, accounting for the 99% of the freshwater impact, nitrogen oxides and nitrate, accounting for 86% and 12% of the marine and nitrogen oxides and ammonia representing the 90% and 10% of the terrestrial respectively.

- **Ecotoxicity freshwater**. This category refers to the toxic effect of substances emitted into freshwater ecosystems. The Comparative Toxic Unit for the ecosystem (CTUe) is the adopted indicator, which estimates the Potentially Affected Fraction of species (PAF) integrated over time and volume per unit mass of a chemical emitted. The main contributors to freshwater ecotoxicity are emissions from agricultural, mining and industrial activities. In the case considered, the most influential substance is aluminium, released into soil, water, and air, accounting for 88% of the overall impact.

- **Land Use**. This category refers to the soil quality loss and its indicator is the Soil Quality Index, which is based on four main ecosystem characteristics: biotic production, erosion resistance, groundwater regeneration, and mechanical filtration. It is expressed with the dimensionless unit Points (Pts). In the case considered, the main causes are forest occupation for intensive use (16%) and transformation and occupation for industrial areas, accounting for 10% and 7%, respectively. Additionally, numerous smaller contributions also play a role in determining the overall impact.

- **Water Use.** This category assesses water availability or scarcity in the considered regions. The indicator used is the User Deprived Potential, expressed in cubic meters of deprived water (m^3). The main causes are activities with a high-water footprint, such as cotton and beef production. In the case analysed, the most impactful elements are water use and water turbine operations, which account for 79% of the overall impact.

- **Resource use, fossil and mineral and metals**. The categories relate to the deprivation of fossil, mineral and metals resources used for the considered operations. The indicator used is the Abiotic Resource

Depletion (ADP-fossil or ADP ultimate reserve), expressed respectively in megajoules (MJ) for the fossil use and in kilograms of antimony equivalent (kg Sb eq.) for mineral and metal resource use. Antimony is used as the reference substance, due to its scarcity. The main contributors to fossil resource use are natural gas (50%), coal (20%), uranium (16%) and oil crude (12%). For mineral and metals resource use instead, the most impactful elements are tellurium (56%), copper (29%), gold (4%) and silver (3%).

5.2.1 Geographical and application scenarios

In this section, the LCA results related to the geographical and application scenarios described in previous Chapter are presented. The starting point is the baseline subcase, which is used to understand the influence of the life cycle phases on the overall environmental impact and the contribution deriving from the production of each component. Figure 5.1 shows the percentage influence of each life cycle phase across all impact categories considered within the EF calculation methodology. The colour scheme used, is consistent with that in Figure 4.5, where the system boundaries are defined. Specifically, the C2G phase is reported by distinguishing the effects of motor and magnet production from those of the use phase. The use phase is predominant in all considered categories, accounting for at least 50% of the total impact, except in the human toxicity carcinogenic and non-categories. Within the considered scenario, magnet manufacturing has the highest influence, reaching up to 10% of the total burden in the particulate matter category.

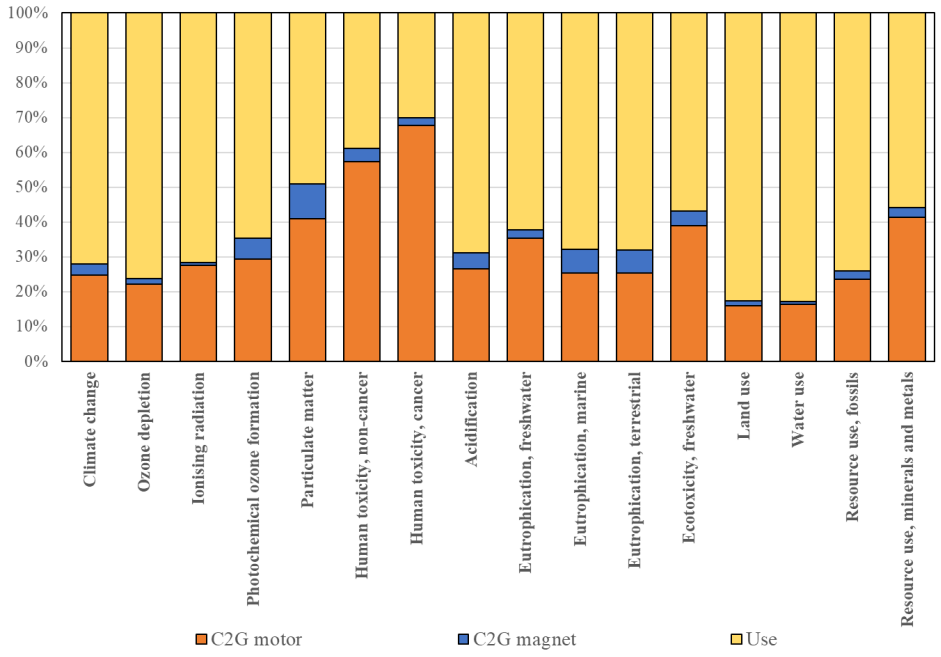

Figure 5.1 Percentage influence of the life cycle phases calculated with EF3.0 method for the baseline considered in the LCA step1

Table 5.1 summarizes the absolute values of the impact categories divided by cycle phases. Below a detailed description of the most influent processes for each impact category is provided, with the aim of improving the results interpretation across the LCA steps described in the following sections. Indeed, starting from this description, just the relevant differences for each of the investigated step is reported.

Table 5.1 LCA results for the categories included in the EF method for the baseline subcase, broken down into life cycle phases

Categories	**C2G motor**	**C2G magnet**	**Use**
Climate change [g CO_2 eq./km]	2.89	0.38	8.44
Ozone depletion [μg CFC-11 eq./km]	0.37	0.03	1.28
Ionising radiation [Bq U-235 eq./km]	0.46	0.01	1.18
Photochemical Ozone formation [mg MVOCeq./km]	8.95	1.81	19.70
Particulate matter [10^{-9} disease inc./km]	0.15	0.04	0.18
Human toxicity, non-cancer [10^{-9} CTUh/km]	0.13	0.01	0.09
Human toxicity, cancer [10^{-9} CTUh/km]	0.01	0.00	0.00
Acidification [10^{-6} mol H^+ eq/km]	16.24	2.83	42.12
Eutrophication, freshwater [mg Peq/km]	1.45	0.1	2.55
Eutrophication, marine [mg N eq/km]	2.51	0.67	6.69
Eutrophication, terrestrial [10^{-3} mol N eq/km]	0.03	0.01	0.07
Ecotoxicity, freshwater [CTUe/km]	0.11	0.012	0.16
Land use [Pt/km]	0.01	0.00	0.05
Water use [m^3 depriv./km]	0.00	0.00	0.01
Resource use, fossils [MJ/km]	0.04	0.004	0.13
Resource use, minerals and metals [mg Sbeq./km]	0.06	0.004	0.08

- Regarding the **Climate change** impact, the processes associated with high voltage electricity production from hard coal combustion and from natural gas both with and without heat and power co-generation, in conventional and combined cycle plants, represent the largest contribution, accounting for approximately 50% of the overall CO_2 equivalent emissions. Many other processes have a comparable, but low influence (below 3%). Referring to the sole manufacturing phase instead, relevant contributors are pig iron and aluminium production, that account for the 3.5% of the overall category impact, together with the electricity production processes. The environmental impact of electricity production is dependent on the specific energy mix adopted by each country, as explained in detail in the dedicated comparison.

- **Ozone depletion** impact is primarily linked to the processes involving the transportation of imported natural gas through pipelines from various countries, to produce electricity. These operations account for

approximately 63% of the total impact in this category. On-shore production of oil and natural gas contributes for the 14% of the overall impact, while the treatment of sewage sludge by anaerobic digestion for biogas production accounts for 4%. Natural gas transportation activities are also the major contributors within the manufacturing phase.

- **Ionizing radiation** is dominated by the treatment processes of the tailings from uranium milling, spent nuclear fuel and low-level radioactive waste, which respectively account for 62%, 12% and 10% of the overall radiation impact. The tailings from uranium milling originate from the uranium yellowcake production, which is part of the nuclear energy generation at French plant, also the source of the spent nuclear fuel. The energy produced is used to generate high voltage electricity, which is subsequently imported into Italy. The low-level radioactive waste instead, results from various uranium enrichment activities carried out in different countries. The manufacturing phase is characterized by the same distribution of contributions.

- Combustion processes involved in the electricity production from hard coal and oil, have the highest influence on both **Photochemical ozone formation** and on **Particulate matter**, contributing approximately 24% to the overall impact. However, in these categories, a series of other processes affect the overall impact, with relatively small and comparable influence. One of the major contributors to the photochemical ozone formation, representing the first one in the C2G phase, is the Coke coking process accounting for just 3%. For Particulate matter noticeable contributors include aluminium production (6%) and the operations and beneficiation of rare earth oxide concentrates form bastnaesite and monazite ores (3%), used to produce PM. These processes are the main contributors to the manufacturing portion, even if with a secondary effect compared to the electricity production from hard coal plant in China for coal mining.

- **Human toxicity**, as previously mentioned, are the sole categories in which the manufacturing phase is the most influent to the overall impact. Concerning the cancerogenic one, the main contributors are the coke coking process, representing the 20% of the total impact, followed by the activities related to the landfill treatment of EAF slag, red mud from bauxite digestion and copper slag that aggregated are reaching the 25% of the overall impact. Coke is used in the production of pig iron, which is employed in the manufacturing of unalloyed steel, while EAF slag originates from steel production, utilized both in the manufacturing phase, and in the construction of natural gas pipelines for electricity generation. The latter two processes are output of the aluminium and

copper processing chains. For non-carcinogenic effects, the impact is mainly driven by copper production and slag treatment. The latest accounts for 24% of the total impact, while primary copper production and the smelting of copper concentrate from sulphide ore to obtain copper cathodes contribute for an additional 19%. Primary aluminium production and the associated treatment of residual material follow with a 10% contribution.

- **Acidification** is mostly influenced by processes related to high voltage electricity production from hard coal and lignite combustion, as well as from oil-based heat and power co-generation. Together, these processes account for approximately 40% of the total impact in this category. Also in this category, many other contributors have a comparable, but low influence. In the manufacturing phase, the main contributors are the production of primary copper and aluminium, which together represent about 4% of the overall acidification impact.

- **Eutrophication of freshwater, marine and terrestrial** as shown in Figure 5.1, have similar distribution in terms of life cycle phases influence. Concerning the terrestrial and the marine eutrophication, the main contributors to nitrogen oxide emissions, are high voltage electricity production processes from hard coal and oil combustion, accounting for approximately 25% of the total impact for both categories. Other contributing processes have a relatively low influence, accounting for less than 5% of the overall impact. Freshwater Eutrophication instead, is primarily driven by phosphate emissions resulting from the landfill treatment of spoil generated during hard coal and lignite mining activities, which account for 68% of the total impact in this category. In addition to the processes already analysed, two other significant contributors to the overall environmental impact are the treatment of digester sludge through municipal incineration and the management of sulfidic tailings from copper mining operations, accounting for 12% and 8% respectively.

- The main contributors to **freshwater ecotoxicity** are blasting processes related to copper mine operations and to construction of opencast mine for hard coal mining and the treatment of sewage sludge by anaerobic digestion for biogas production employed in the high-voltage electricity production. They account for approximately 40% and 21% of the total impact, respectively. Other contributing processes have a relatively minor influence, each accounting for less than 5% of the total impact.

- **Land and water use** impact categories are characterized by a predominancy of the use phase, which accounts for approximately 82% of the total impact. For Land use, the main contributors are the

installation of open ground photovoltaic systems, used for low voltage electricity production (24%), and the production of woodchip used in cogeneration plants (19%). For Water use, the primary driver is high voltage electricity production through hydroelectric plants, and oil which together account for 60% of the total impact. Additionally, the anaerobic digestion treatment of sewage sludge for biogas contributes 20%. The manufacturing phase shows a similar distribution of contributing processes.

- Regarding **fossil resource use**, the main contributors are the production of natural gas (40%), uranium yellowcake (6%), and hard coal (5%), all involved in the high-voltage electricity generation chain. These processes also significantly contribute to the manufacturing phase. Many other processes have a comparable, but low influence (below 4%).

- The **metals and minerals resource use** category is also mainly influenced by the use phase, as the main driver is the copper adoption in the infrastructure of the electricity distribution network, that however assumes importance also in the manufacturing phase for the configurations with copper winding. Indeed, the main contributing processes are the copper mine operation and beneficiation accounting for 85% of the overall impact category.

An environmental impact analysis was conducted excluding the use phase, with the aim of identifying the most impactful components and suggesting priorities for environmental design interventions. Furthermore, considering the ongoing shift in the energy mix towards renewable sources, the manufacturing phase is expected to become increasingly relevant in the overall environmental burden in the coming years. For these reasons, the motor analysis was also carried out using a C2G boundary, with results broken down by subsystem, as shown in Figure 5.2. Each bar represents the impact deriving from material extraction, preprocessing, manufacturing, and assembly required for the final component production. The blue bars indicate the stator contribution, the yellow bars represent the windings contribution, the pink bars correspond to the rotor contribution, the grey bars represent the shaft contribution, the orange bars represent the magnet contribution, the green bars represent the housing contribution, and the black bars reflect the final assembly and painting, including the bearings contribution. The windings (yellow bars) resulted in the highest contribution in almost all the categories except for particulate matter, human toxicity cancer and ionizing radiation. In the categories where windings are the dominant contributor, they account for approximately 30-60% of the total impact, and up to 82% in the mineral and metal resource use category, primarily due to copper extraction and preprocessing. The second major contributor to the environmental impacts is the housing (green bars) which ranges between 10 and

50% across all categories, except for mineral and metal resource use. This is mainly due to the extraction and preprocessing of aluminium, as well as the manufacturing of aluminium components. The stator (blue bars) and rotor (pink bars), constituted by electrical steel, contribute between 5% and 20% in all categories with exception of mineral and metal resource use, where electrical steel extraction, preprocessing and manufacturing have a negligible influence. Permanent magnets (orange bars) account for approximately 20% of the overall impact in eutrophication marine, terrestrial and particulate matter, where they represent the second highest contributor after the housing. In the other categories, permanent magnets contribute between 3% and 16%. Lastly, results related to final assembly and painting, including contribution from bearings (black bars) are below 3% in all categories, except for land use where the contribution reaches the 8%.

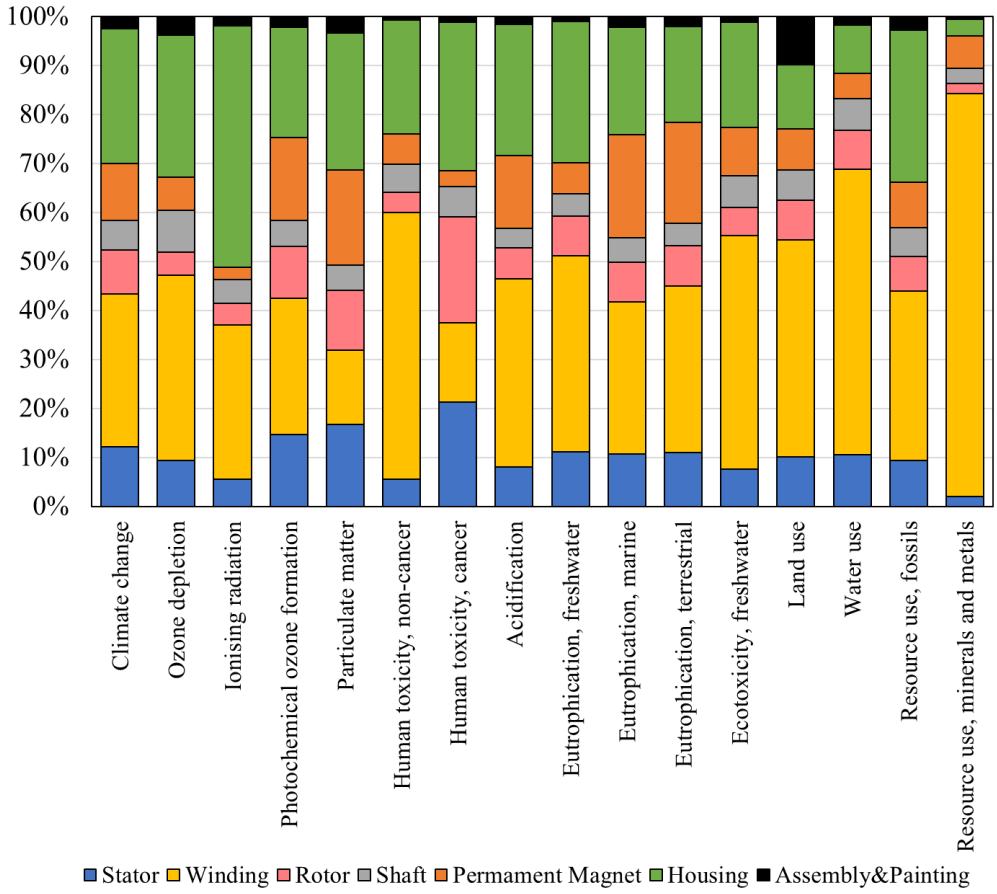

Figure 5.2 Percentage influence of the C2G phase broken down into subsystems, calculated with EF3.0 method, for the baseline considered in the LCA step1 phase

Geographical scenario

The geographical scenario analysis aims at evaluating the effect of the region where an electric motor is produced and used on its environmental impacts. A direct correlation is observed with the electricity mixes, material availability, and processes specific to each selected country. Figure 5.3, presents a comparison

among the countries considered across all the impact categories included in the EF method. Percentage values with respect to the highest ones (worst) are reported.

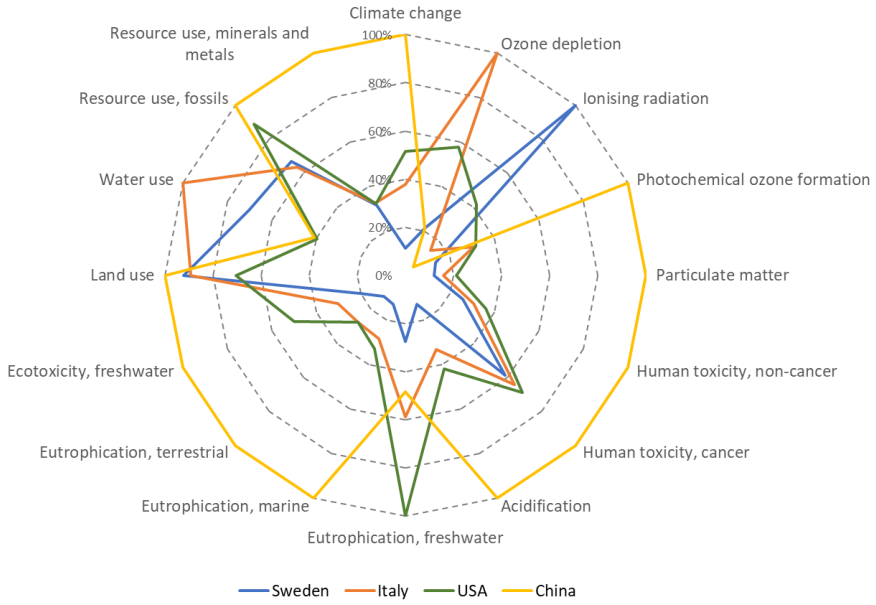

Figure 5.3 Comparison of the environmental impact for the selected countries and for all the impact categories included in the EF method

It is noticeable that China has the highest impact in almost all the categories, except for Ozone depletion, Water use, Ionising radiation and Eutrophication of the freshwater, where Italy, Sweden and the USA subcases, respectively, exhibit the highest environmental burdens. Sweden, in particular, shows an impact ranging from 10% to 30% in eleven of the categories when compared to the worst performing countries. Sweden shows the highest contribution in ionising radiation among the analysed countries, primarily due to its electricity mix, which includes a significant share of nuclear energy sources. The Italian scenario exhibits impact ranging from 15% to 30% across nine environmental categories when compared to the highest contributing country. Italy ranks lowest among the analysed countries in ozone depletion, primarily due to emissions associated with the transport of imported natural gas, which constitutes a substantial portion of its electricity mix. Additionally, Italy shows significant impact in water use, attributed to hydroelectric power generation, as highlighted in the baseline characterization. The United States exhibits impacts ranging from 30% to 50% across eleven of the assessed environmental categories and it shows the highest impact in freshwater eutrophication, primarily due to spoil generated from lignite mining processes associated with high-voltage electricity production. In the following sections, a more detailed assessment is described, focusing on the most influential impact categories contributing to the overall environmental burden. This approach aims to enhance the interpretability and relevance of the results. To identify the most significant categories, normalized and weighted results were applied in accordance with [205], following the EF method. Normalization step results in a conversion of the impact results onto

dimensionless values by comparing them to a reference unit, showing relative magnitude of each impact but not its importance.

Weighting step, on the other hand, assigns importance to each impact category using predefined percentages, enabling comparison and aggregation into a single score. The most relevant impact categories are those that, after normalization and weighting, cumulatively account for at least to 80% of the total environmental impact, starting from the highest contributors downward. This approach was used for the three LCA steps described in Chapter 4. Due to intrinsic differences in motor topology, life cycle phases, geographical scenarios, and applications, each step led to a distinct selection of relevant impact categories. For the geographical scenario, all categories are reported in Table 5.2 to support a clearer understanding of the adopted methodology. The results demonstrate that the country under consideration significantly influences the importance of each impact category. Categories are ranked by their contribution to the overall environmental impact, based on an average value derived from the order of importance assigned to each category per country. The order of importance is determined using the weighting methodology, described earlier.

Table 5.2 Impact categories selection based on the average order of importance for the selected countries of the geographical scenario

Rank	Impact Categories	Sweden	Italy	USA	China	Average
1	Climate change	4	1	1	1	1.75
2	Resource use, fossils	1	2	2	5	2.5
3	Resource use, minerals and metals	2	3	5	2	3
4	Ecotoxicity, freshwater	5	4	4	3	4
5	Eutrophication, freshwater	7	5	3	7	5.5
6	Particulate matter	6	8	7	4	6.25
7	Acidification	8	6	6	6	6.5
8	Photochemical ozone formation	10	9	9	8	9
9	Ionizing radiation	3	11	8	15	9.25
10	Water use	9	7	10	12	9.5
11	Eutrophication, terrestrial	13	10	11	9	10.75
12	Human toxicity, non-cancer	11	12	12	10	11.25
13	Eutrophication, marine	14	13	13	11	12.75
14	Human toxicity, cancer	12	14	14	13	13.25
15	Land use	15	15	15	14	14.75
16	Ozone depletion	16	16	16	16	16

To provide an immediate visual perception of the category influence across countries, a coloured map was used, varying from red (high importance) to green (low importance). The map reveals a consistent gradient from top to bottom across all countries. Notably, at least five of the top six categories identified for each country are also present among the six most impactful categories when averaged across all countries. These differences are primarily attributed to the

national energy mixes, as discussed in Chapter 4 and further analysed in this Section. Moreover, Figure 5.4 illustrates that the top six categories account for nearly 80% of the total environmental impact in three out of the four countries considered. Sweden does not reach the 80% threshold because the ionizing radiation category, where it ranks worst among the considered countries, is positioned ninth in the overall impact ranking. However, since this category and its most impactful processes have already been discussed earlier, the first six categories listed in the table are selected and analysed in the following section.

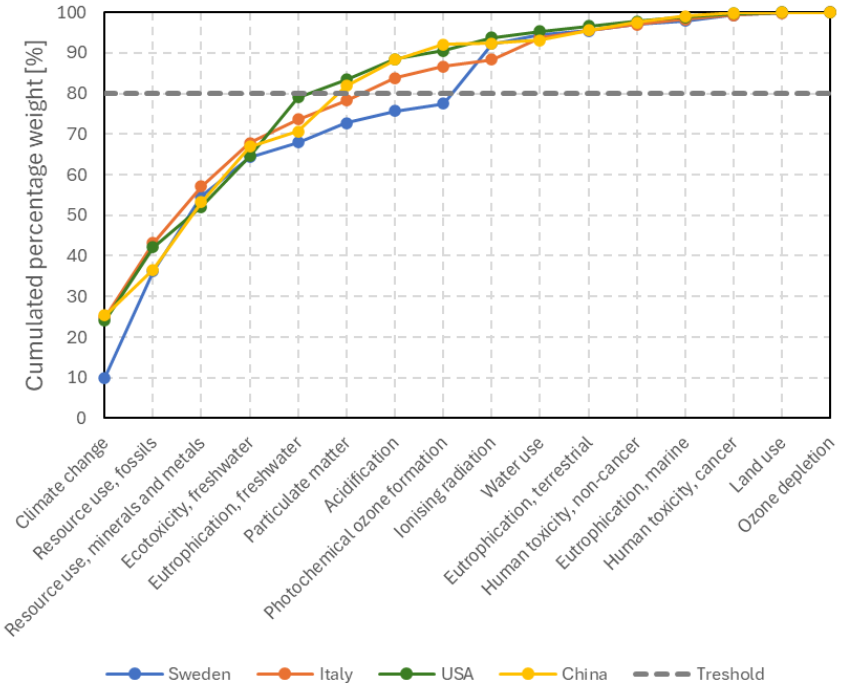

Figure 5.4 Cumulated percentage weight of the impact categories for the selected countries of the geographic scenario

Figure 5.5 shows the percentage influence of each considered life cycle phase on the overall impact for the six selected categories, displayed from left to the right in order of importance. A general dominance of the use phase is evident, consistent with the baseline subcase, which corresponds to the Italian scenario. Concerning Climate change and Resource use, fossil, the use phase contributes over 70% of the total impact across all countries, except for CO_2 equivalent emissions in Sweden. This deviation is attributed to Sweden's specific electricity mix. In this case, the most impactful process is pig iron production, used for manufacturing unalloyed steel employed in stator and rotor. Referring to the Resource use, mineral and metals category, the C2G and use phase each contribute approximately 50% across most countries. However, in China, the impact is dominated (97%) by mining and beneficiation processes for copper concentrate, primarily used in winding manufacturing. Analysing Ecotoxicity of the freshwater, the main contributor in most countries is represented by blasting operations in copper mining. In contrast, China's impact is driven by hard coal

mining and preparation for electricity production, increasing the use phase's influence.

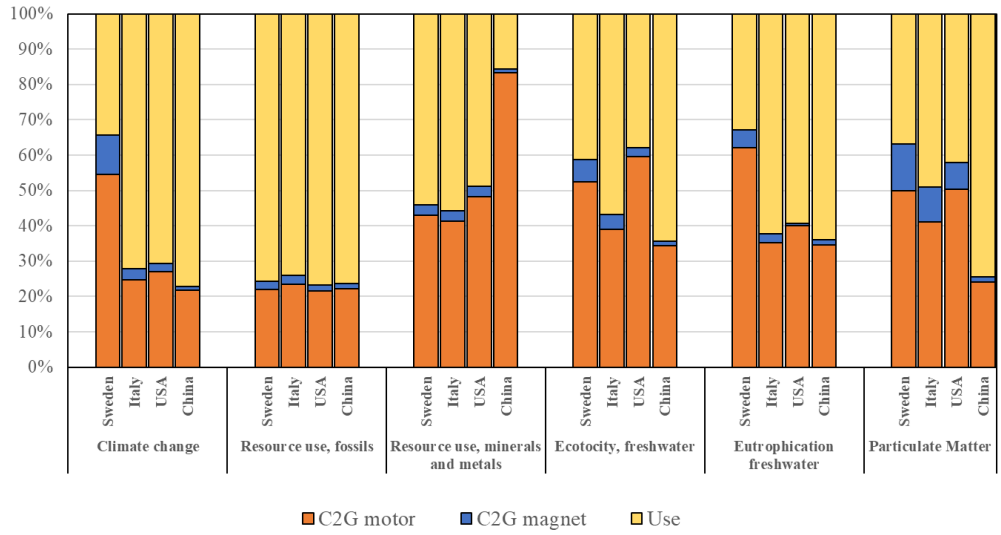

Figure 5.5 Percentage influence of the life cycle phases calculated with EF3.0 method, for the categories selected through normalization and weighting, for the geographic scenario considered in the LCA step1

Similarly, Italy shows a higher use phase impact, mainly due to anaerobic digestion treatment of sewage sludge from biogas production. In Eutrophication, Freshwater, the ranking of life cycle phases is consistent for Italy, USA, and China, with the use phase contributing around 60% of the total impact while in Sweden it accounts for only 33%. Here, the C2G phase is influenced by spoil from hard coal mining in pig iron production and sulfidic tailings from copper mining. Finally, Particulate Matter is the most variable category, with use phase contributions ranging from 37% in Sweden to 74% in China. Sweden's impact is driven by aluminium production and hard coal use in steel production, while China's is dominated by high-voltage electricity generation from hard coal. USA and Italy show a more balanced distribution between C2G and use phases. The magnet C2G phase consistently contributes less than the others, peaking at 11% for Climate Change and 13% for Particulate Matter in Sweden.

Figure 5.6 presents the results of the same analysis using absolute values to enable direct comparison between countries. Climate change differences between countries are mainly driven by national electricity mixes. In countries like Sweden, where the electricity mix is not dominated by fossil sources, the production phase, including magnet manufacturing, contributes significantly to the overall impact. The total climate change impact calculated in the Swedish scenario constitutes only 10% of the emissions observed in the Chinese scenario. Italy and USA show CO_2 emissions equal to 38% and 51% of the Chinese subcase, respectively. As mentioned, these figures are coherent with the contribution of the fossil sources to the electricity production mixes. Similarly, fossil resource use is mainly influenced by the use phase and consequently by the country electricity mix. With respect to this category, a gradual increase is visible

going from Sweden to China scenarios, where the hard coal mine operation and preparation for the high voltage electricity production is the driver.

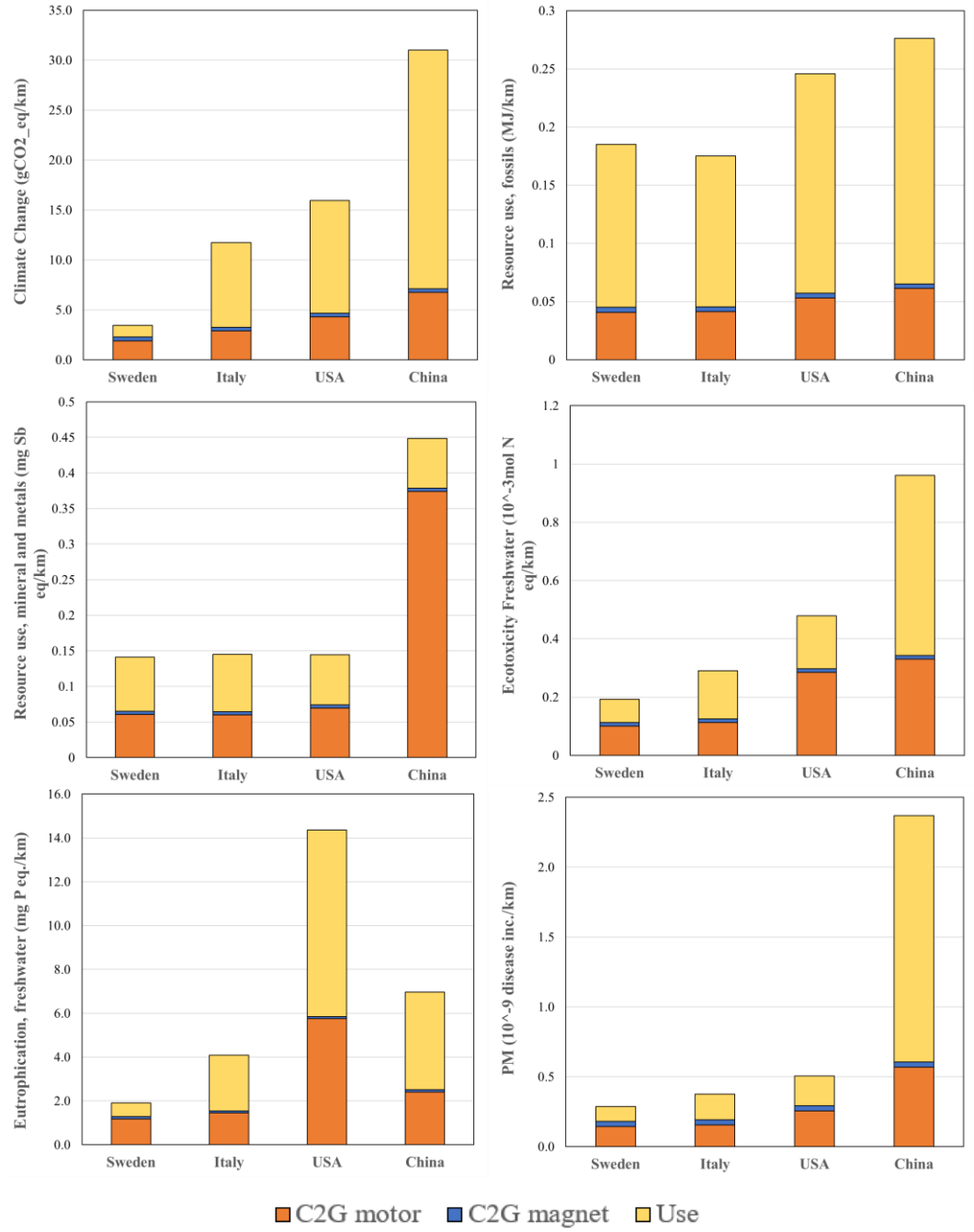

Figure 5.6 Absolute values of the life cycle phases calculated with EF3.0 method, for the categories selected through normalization and weighting, for the geographic scenario considered in the LCA step1

In this category, the Sweden scenario has a slightly higher result than in Italy scenario, that revealed to be the best because there is no nuclear share of electricity production in the Italian electricity mix. In the Italy scenario, fossil resource use is 36% lower than in the China scenario. Regarding mineral and metal resource use, the contribution of the manufacturing phase to the overall impact resulted almost constant in all countries, except for China, where a step

increase is noticeable. This is due to copper mine operations, which are more impactful on this category with respect to Europe or US, resulting in a 70% higher usage of mineral resources. Similarly, particulate matter presents a flat trend across countries, except for China where the electricity production for usage in coal mines has a huge impact with values that are between 78% and 87% higher in comparison with the other scenarios. Freshwater ecotoxicity displays an increasing trend going from Sweden to China with an 80% difference between the two scenarios. This category is driven by blasting processes in all scenarios, but the main difference noticeable in the Chinese scenario is due to the impact of the hard coal mine operation. Lastly, freshwater eutrophication is the sole category presenting a peak in the US scenario and not in China, mainly driven by the spoil from lignite mining treatment in surface landfill. In this case, the best country, Sweden, has an impact approximately 87% lower in comparison to the US scenario.

Application scenario

An assessment covering all environmental impact categories is provided using the radar chart shown in Figure 5.7 also for the application scenario. The chart illustrates that manufacturing and using the motor within the same country (Italy) leads to a more homogeneous distribution of environmental impacts across all considered categories. It is also noticeable that the impact is crescent from city car to SUV subcases for all categories. Indeed, City car, Segment B and Segment C result to have respectively around 25%, 20% and 10% to 15% lower impact than the SUV. Results are mainly driven by variations in motor size and energy requirements across vehicle applications, as detailed below.

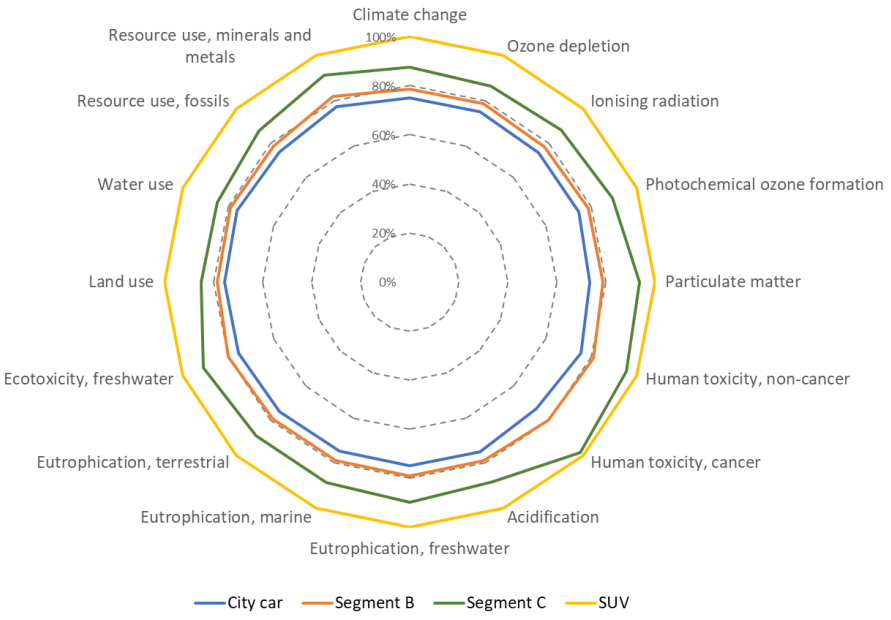

Figure 5.7 Comparison of the environmental impact for the selected applications and for all the impact categories included in the EF method

A notable deviation is observed in the Particulate Matter and Human Toxicity categories for Segment C, which shows impacts closer to the SUV than in other categories. This is mainly because the motor used in Segment C is heavier than that of the SUV, having been scaled according to power requirements, as explained in Chapter 4. The most impactful processes in these categories are indeed those related to the motor manufacturing as described in the baseline characterization. As previously mentioned, the same methodology was applied to select categories for the application scenario, with key results summarized in Table 5.3. In this case is noticeable the lower influence of the application variation on the order of the impact categories. Indeed, all the subcases share the same ranking over the sixteen categories, except for the segment C application, which aligns with the Italy subcase in the geographical scenario. Here, an inversion between the water use and acidification categories is observed. This is due to the heavier motor in Segment C, which contains more copper and aluminium than other applications, resulting in higher sulphur dioxide emissions during the manufacturing phase. In Figure 5.8 is reported also in this case the cumulated percentage weight for all the categories, showing that the first six categories, are reaching the 80% of the overall impact.

Table 5.3 Impact categories selection based on the average order of importance for the selected applications of the application scenario

Rank	Impact Categories	City car	B	C	SUV	Average
1	Climate change	1	1	1	1	1
2	Resource use, fossils	2	2	2	2	2
3	Resource use, minerals and metals	3	3	3	3	3
4	Ecotoxicity, freshwater	4	4	4	4	4
5	Eutrophication, freshwater	5	5	5	5	5
6	Water use	6	6	7	6	6.25
7	Acidification	7	7	6	7	6.75
8	Particulate matter	8	8	8	8	8
9	Photochemical ozone formation	9	9	9	9	9
10	Eutrophication, terrestrial	10	10	10	10	10
11	Ionizing radiation	11	11	11	11	11
12	Human toxicity, non-cancer	12	12	12	12	12
13	Eutrophication, marine	13	13	13	13	13
14	Human toxicity, cancer	14	14	14	14	14
15	Land use	15	15	15	15	15
16	Ozone depletion	16	16	16	16	16

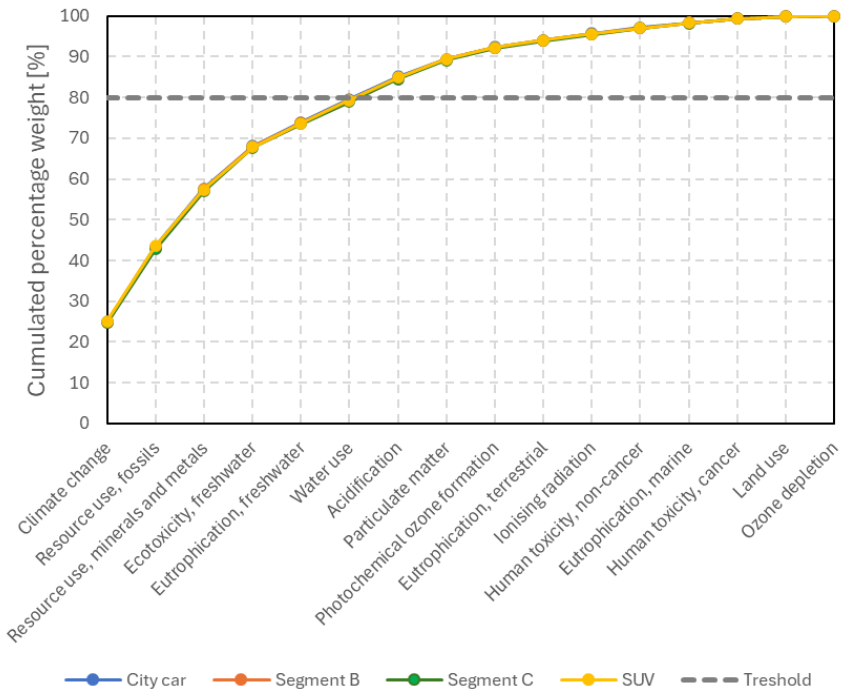

Figure 5.8 Cumulated percentage weight of the impact categories for the selected applications of the application scenario

Figure 5.9 presents the six most influential impact categories for the application scenario, selected using the methodology described above and ordered by importance.

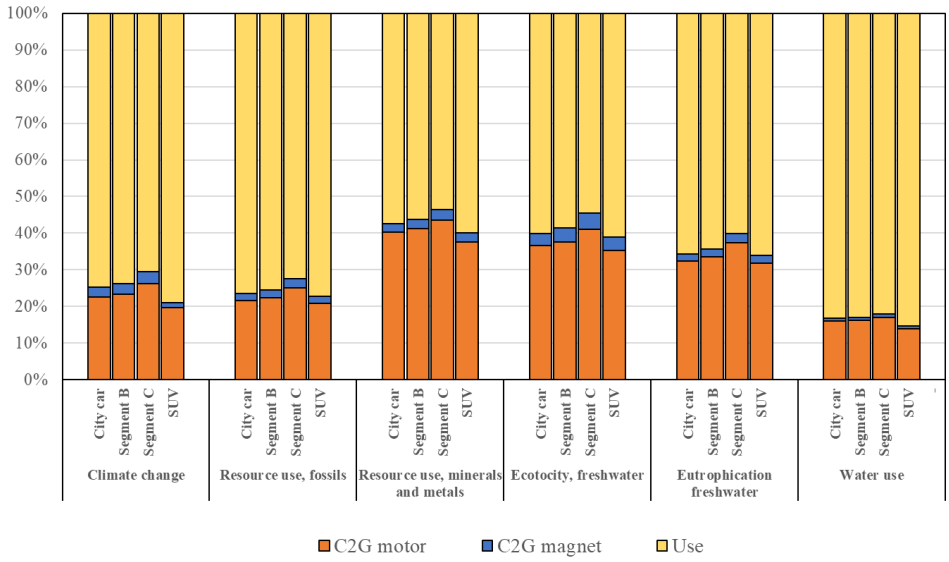

Figure 5.9 Percentage influence of the life cycle phases calculated with EF3.0 method, for the categories selected through normalization and weighting, for the application scenario considered in the LCA step1

The percentage breakdown of life cycle phases is shown for each category. This scenario is consistent with the baseline characterization in terms of phase-

related impacts, as both manufacturing and use occur in the same country (Italy). When examining the contribution of different life cycle stages, all phases show a comparable influence on the total environmental impact across the application scenarios. However, the use phase clearly dominates in categories such as Climate Change, Fossil Resource Use, and Water Use, where it accounts for 70% to 85% of the total impact. In the remaining three categories, the use phase has a lower influence, contributing approximately 53% to 65% of the overall impact.

In Figure 5.10 are reported the absolute values for all selected applications and impact categories.

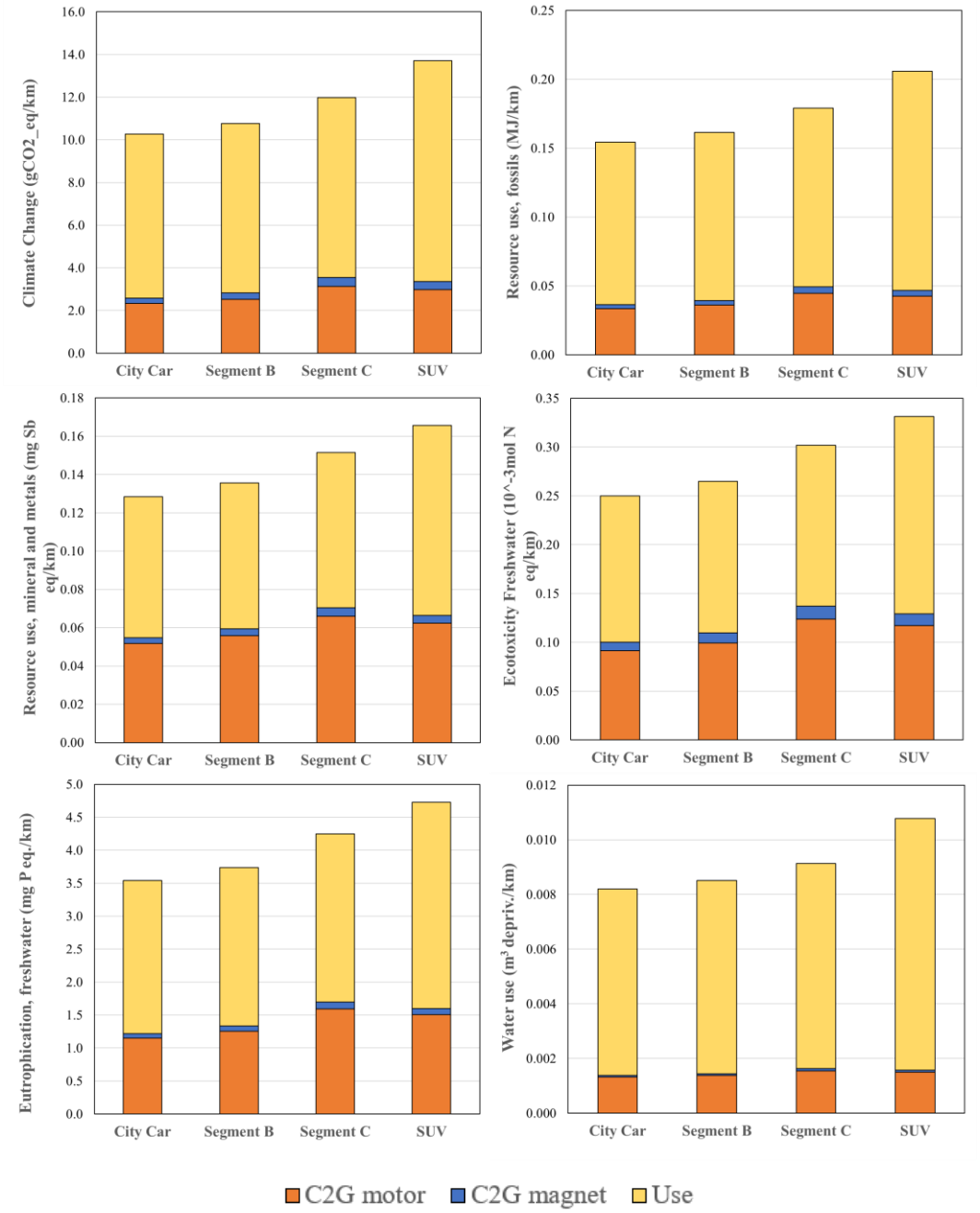

Figure 5.10 Absolute values of the life cycle phases calculated with EF3.0 method, for the categories selected through normalization and weighting, for the application scenario considered in the LCA step1

Concerning the manufacturing phase, the BOM varies on the base of the required performances. The contribution of the manufacturing stage increases linearly with the required power, as the BOMs have been scaled accordingly. All categories are characterized indeed, by an increase of the manufacturing impacts passing from the city car to segment C scenario, with a slight reduction in the SUV scenario, due to its lower power and torque compared to segment C. Instead, for the use phase, the energy required for operation is a function of the vehicle type that leads to a different efficiency map usage. The SUV scenario is characterized by an increase in all impact categories due to the higher energy absorbed over the use, given as the combination of efficiency and motor mass increase. For the other vehicles the trend is flatter because the motor mass increases from City Car to segment C is compensated by the higher efficiency of the latest, both thanks to the longer gear ratio and higher road load, that make the operating points shift towards higher iso-efficiency areas of the map. Indeed, use phase impact in all the categories is respectively 25%, 23% and 20% lower for City car to Segment C, with respect to SUV.

However, it is important to state that efficiency over the considered cycle is also due to the matching between motor and vehicle and so strongly impacted by transmission ratio. In this perspective the segment C, that is also correspondent to the considered baseline is favourite as it takes advantage of a transmission ratio and motor size, properly sized for the vehicle.

5.2.2 PMSM vs copper and aluminium winding SRM

Also in Step 2, a broader and more general results analysis is provided, as shown in Figure 5.11, which reports a comparison of all the impact categories for the selected baseline PMSM and the SRM both with copper and aluminium windings. The subcases are labelled in the following figures as PMSM baseline, CU-winding SRM and ALU-winding SRM. It is noticeable that the SRM with copper winding has the highest impact for all the categories, except for Eutrophication marine and Ecotoxicity of the freshwater in which the PMSM shows the highest impact. However, the PMSM's lower impact, ranges between 2% and 10%. The SRM with aluminium winding shows approximately 20% lower impact than the highest contributor in each category, reaching up to 50% less impact in the eutrophication marine category. This category is the only one showing a significant variation between the copper winding SRM and PMSM, primarily due to the influence of rare earth element mining and beneficiation. In step 2, the magnet manufacturing has a greater impact on Marine Eutrophication due to a different material dataset selected by the author. Specifically, the dataset used refers to RE oxide production in the Fujian region of China, whereas in Step 1, the reference was the Bayan Obo mine in Mongolia.

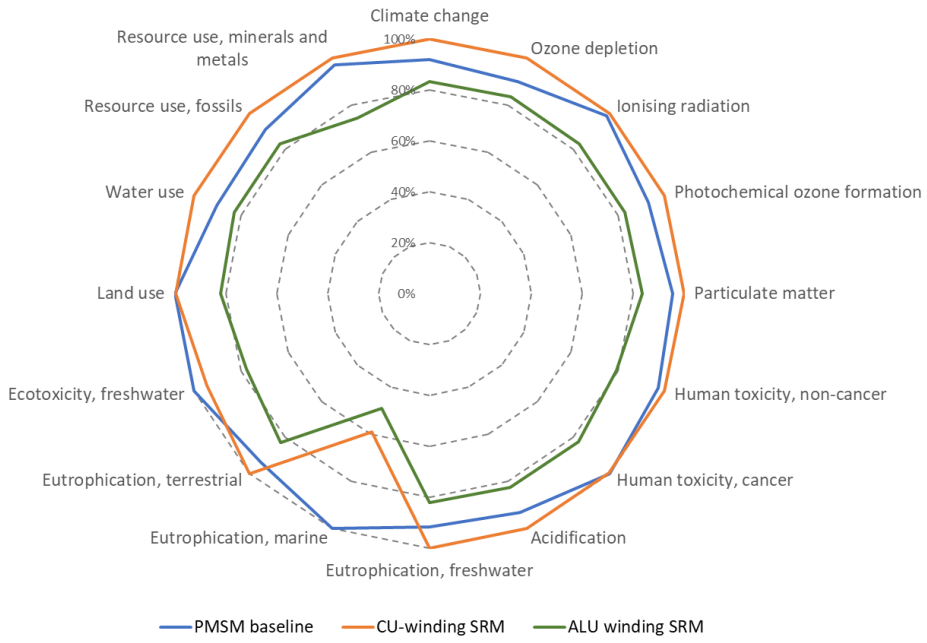

Figure 5.11 Comparison of the environmental impact for the PMSM and the SRM with copper and aluminium windings, for all the impact categories included in the EF method

As in Step 1, a selection of the most influential impact categories is performed in this case as well, using the same methodology. As shown in Table 5.4, Acidification replaces Freshwater Eutrophication among the first six categories contributing to 81% of the overall environmental impact, as illustrated in Figure 5.12.

Table 5.4 Impact categories selection based on the average order of importance for the selected motors architectures considered in Step 2

Rank	Impact Categories	PMSM	Cu-SRM	Alu-SRM	Average
1	Climate change	1	1	1	1
2	Resource use, fossils	2	2	2	2
3	Resource use, minerals and metals	3	3	3	3
4	Ecotoxicity, freshwater	4	4	4	4
5	Water use	5	5	5	5
6	Acidification	6	6	6	6
7	Eutrophication, freshwater	7	7	7	7
8	Particulate matter	8	8	8	8
9	Photochemical ozone formation	9	9	9	9
10	Eutrophication, terrestrial	10	10	11	10.3
11	Ionizing radiation	11	11	12	11.3
12	Eutrophication, marine	12	12	10	11.3
13	Human toxicity, non-cancer	13	13	13	13
14	Land use	14	14	14	14
15	Human toxicity, cancer	15	15	15	15
16	Ozone depletion	16	16	16	16

These categories have been consequently considered for the comparison in the results section. The Differences in the ranking compared to step 1 are attributed to both the increase of energy required for the use phase and the selected dataset for copper as input material. The first results in a higher weight of the water use while regarding the second, copper cathode selected for the step 2 causes higher acidification impacts than the copper primary dataset used in step 1.

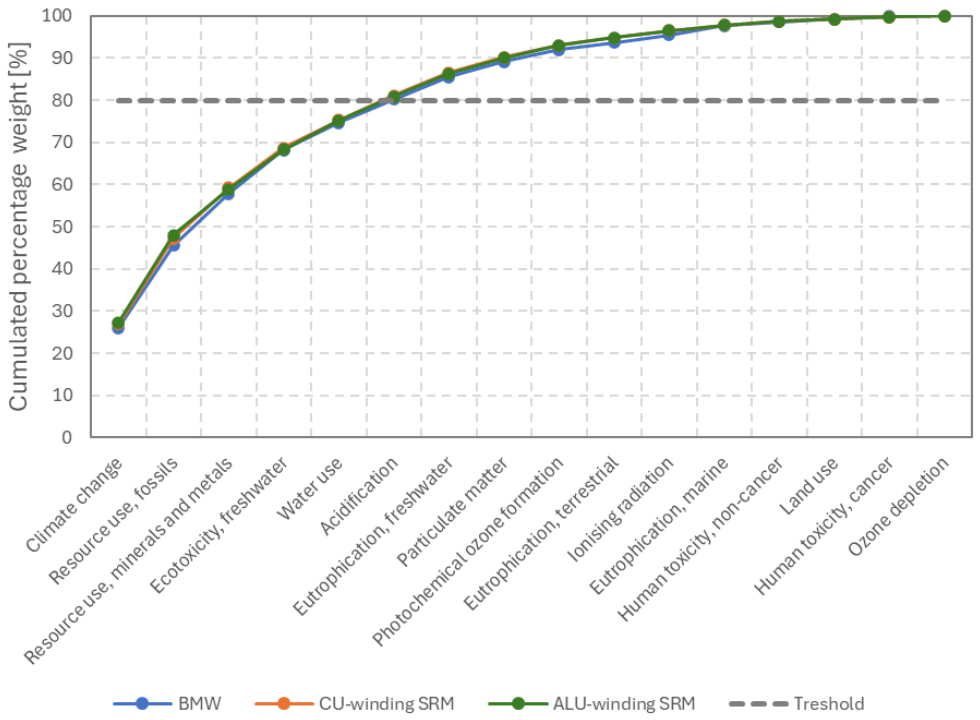

Figure 5.12 Cumulated percentage weight of the impact categories for the selected motors architectures in the Step 2

Figure 5.13 presents the percentage influence of the six most relevant impact categories on the overall life cycle environmental impact for the three motors analysed. The distribution of life cycle phase contributions is nearly identical across the three motors, particularly in the categories of Climate Change, Fossil Resource Use, Water Use, and Acidification. In all these categories the use phase is predominant, contributing between 70% to 88% of the total impact. For the above-mentioned categories C2G Magnet, has low influence, accounting for only 2% of the overall impact. For what concerns the use of mineral and metals resources and ecotoxicity freshwater, although the use phase is still the main contributor, both G2G motor and magnet have higher influence in comparison to previous cluster of categories. Transportation phase is instead negligible while EoL has a beneficial impact, estimated between 2% and 10% considering all categories, except for aluminium copper SRM in water use category, as detailly explained after. In the figure, EoL is reported with negative values according to the recommendation provided by [207]. This approach resulted in a positive (not beneficial impact) contribution that exceeds 100%. The use phase is driven by energy required over life cycle, and so it is highly dependent from the motor

efficiency itself and from the considered vehicle, which determines the cycle operating point. Another key aspect is the geographical location, as already described in the step 1. Processes and materials involved in the production of the high voltage electricity are main contributors to the use phase, and more in general to the overall impact for all the categories, as highlighted in the Geographical and Application scenarios of the step 1. Nevertheless, scope for this LCA step, is to investigate the main differences between the considered motors. The most relevant processes, contributing to the overall impact in the selected categories are those already disclosed in the baseline characterization.

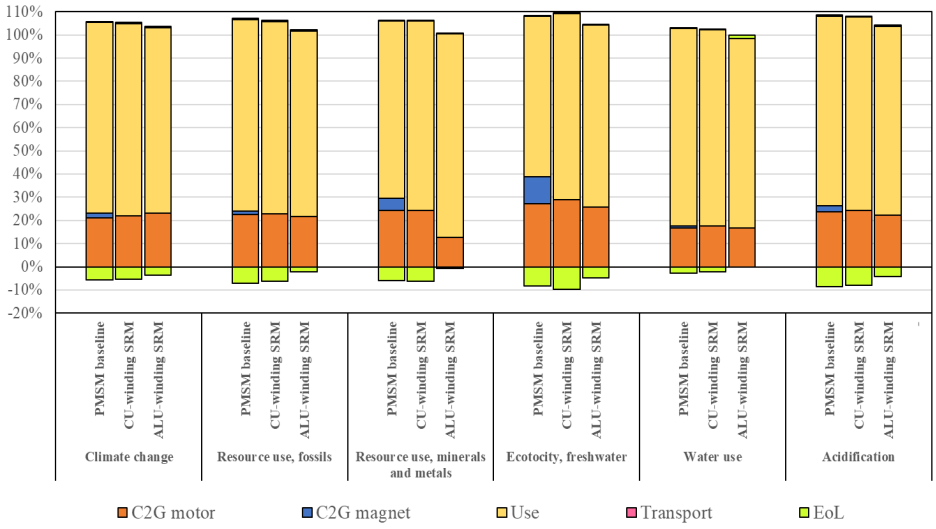

Figure 5.13 Percentage influence of the life cycle phases calculated with EF3.0 method, for the categories selected through normalization and weighting, for the motors considered in step 2

A detailed comparison of the three motors considering impact with respect to the FU is provided in

Figure 5.14 where are reported absolute values for the life cycle phases in the six selected categories. Considering the negative numbers related to EoL phase in the figure is reported also the total impact for all the categories, in order to facilitate results interpretation.

Concerning the climate change, Resource use fossil, water use and Acidification, the analysis shows a disadvantage of the copper winding SRM with respect to PMSM baseline, mainly due to the use phase, caused by lower efficiency over the considered cycle. Indeed, even if TR was adapted to ensure a fair trade-off between performance and efficiency, the copper winding SRM was not specifically sized for the selected vehicle. In addition to that, the higher copper winding SRM mass with respect to PMSM baseline, indirectly affects rolling resistance and the energy losses of the other propulsion unit components, working at higher power. SRM configurations are characterized by the absence of the C2G magnet phase, that however is compensated in terms of impact on climate change by the higher electrical steel mass, due to bigger core dimensions.

Aluminium winding SRM configuration shows reduced impact in all the relevant life cycle stages both due to the high overall efficiency over the cycle and to the lightweight design; additionally, the manufacturing phase is characterized by the adoption of a less energy intense material for the winding.

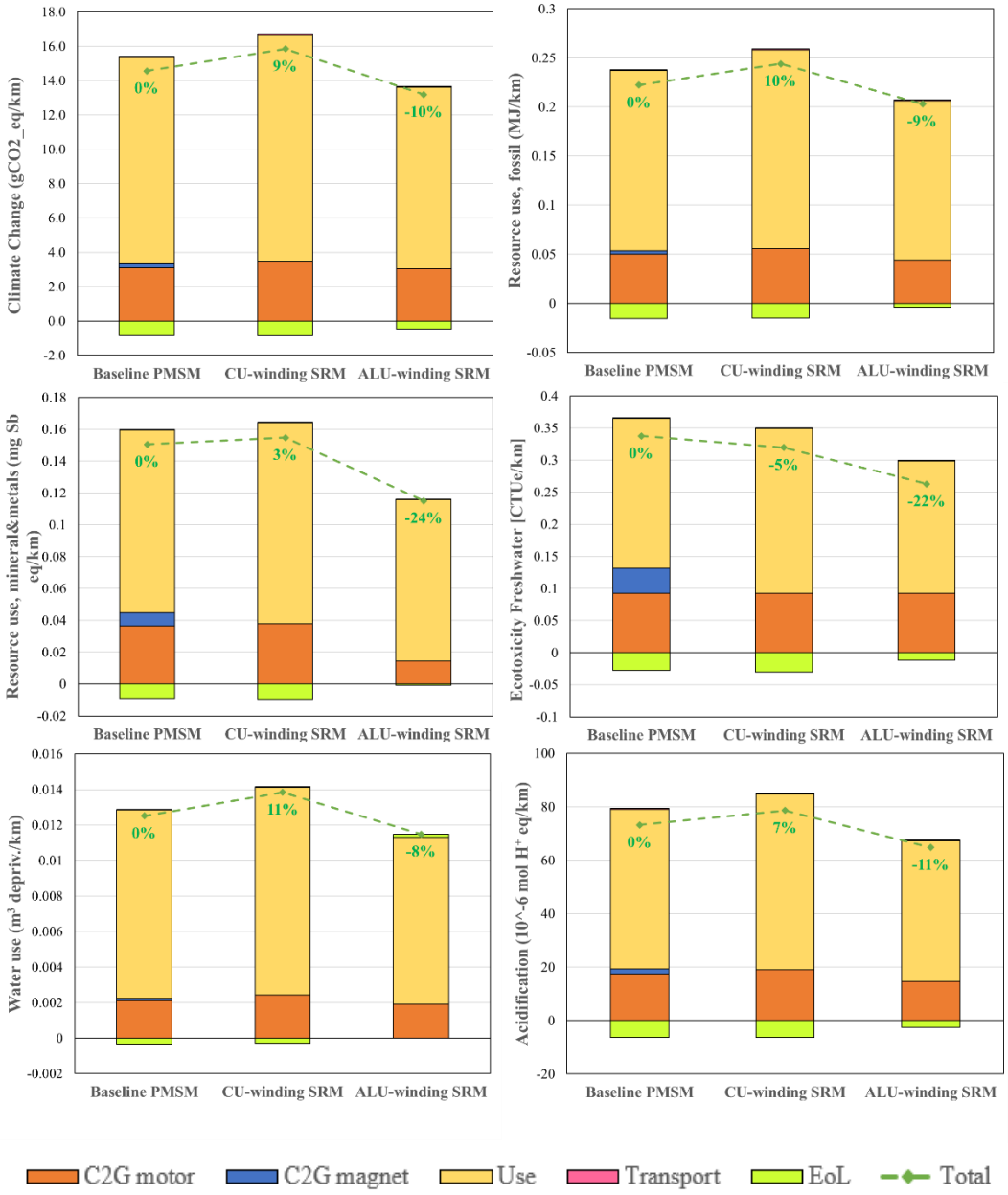

Figure 5.14 Absolute values of the life cycle phases calculated with EF3.0 method, for the categories selected through normalization and weighting, for the motors' architectures considered in the LCA step 2

Even if it is reasonable to expect a lower peak efficiency for aluminium winding SRM with respect to copper winding configuration in absolute terms, in this case the more favourable efficiency map utilization is enabled by the better matching with the selected vehicle. For what concerns mineral and metal resource use, the manufacturing phase assumes higher importance with respect to other categories, and moreover, activities for copper production are representing the

most influent processes, with reflection in a noticeable reduction of the aluminium winding SRM compared to the others. Magnet manufacturing absence in the SRM configurations is another contribution to lower resource use impact. Regarding Ecotoxicity of the freshwater the lower impact of the SRM both with copper and aluminium is primarily due to the absence of PM, being manufacturing and use phase portions almost identical for the three motors. Regarding the EoL phase the SRM with aluminium winding shows a lower benefit across all categories compared to the other motors, mainly due to the absence of copper recycling. This is particularly evident in the water use category, where the impact of the electricity production outweighs the potential benefit from recycling. Considering the overall impacts, the SRM with copper winding shows a deterioration of 7% to 11% compared to the baseline PMSM in the categories of Climate Change, Fossil Resource Use, Water Use, and Acidification. In the same categories, the SRM with aluminium winding consistently shows lower impacts, with improvements ranging from 8% to 11%. Concerning resource use, mineral and metals copper wound SRM has values comparable to the PMSM, while the aluminium wound SRM demonstrates a 24% lower impact. In the Freshwater ecotoxicity category, both SRM configurations show advantages over the PMSM with reduction ranging from 5% to 22%.

5.2.3 Circular Strategies

As in the first two steps, a broader and more general analysis is performed in Step 3, following the methodology described in Chapter 4 and applying it to the CS outlined in Chapter 3. This initial evaluation includes all the categories defined by the EF method. As shown in Figure 5.15, all CS result in a lower environmental impact compared to the Linear subcase.

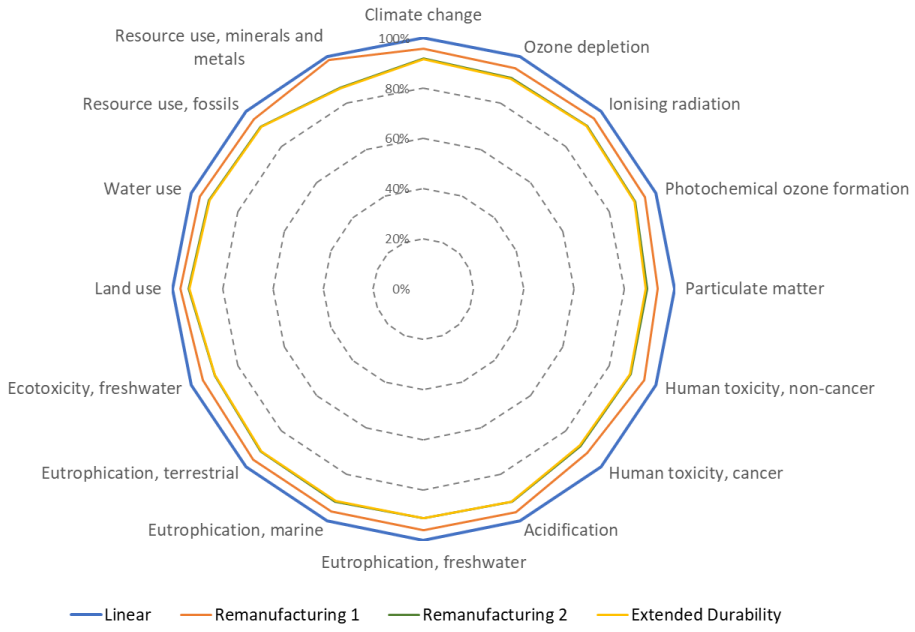

Figure 5.15 Comparison of the environmental impact for the selected Circular Strategies for all the impact categories included in the EF method for the LCA step 3

Indeed Remanufacturing 1 shows improvements ranging from 2% to 8%, while Remanufacturing 2 and Extended Durability, which are overlapped, feature advantages between 4 and 12%. In all the categories Remanufacturing 1 shows a percentage reduction that is approximately half of the other two CS, except for Resource use, mineral and metal where the percentage improvement of Remanufacturing 2 and Extended Durability is nearly nine times higher than that of the Remanufacturing 1. This is mainly due the production of two sets of winding in the latter strategy. In this step the influence of the various life cycle phases mirrors that of the SRM with copper winding subcase, which serves as the baseline linear configuration for this analysis. The environmental advantages of the Extended Durability and Remanufacturing 2 strategies, are primarily linked to the longer lifespan of the winding within the product life cycle. As a result, the influencing processes are the same as those highlighted in the previous step. Therefore, in this step, no selection of the most influential categories has been performed, and detailed information regarding the influence of life cycle phases or specific processes is not provided. Instead, detailed results are presented only for the Climate Change category, as a representative example for other impact categories, in order to illustrate the direct effect of the CS. In Figure 5.16 Climate Change results for the considered CS both including (a) and excluding (b) use phase are reported. The use phase has identical impact across all the strategies, as efficiency over lifecycle was assumed to remain constant. It is evident that without considering the use phase, the percentage advantage of the CS with respect to baseline significantly increases, reaching up to 50%. The C2G phase, which includes material acquisition, processing and component manufacturing confirms the high impact of the windings, leading to environmental advantages of the Extended Durability and Remanufacturing 2 strategies, characterized by a longer lifespan of the winding in the product lifecycle. In contrast, EoL phase has reduced beneficial effect in the CS, as only a slightly higher amount of material is recycled compared to the baseline. This modest increase does not fully compensate for the extended product lifetime. The above-mentioned percentage advantages are not negligible, taking into account the predominance of the use phase for the modelled product within the system boundaries considered. Actually, while the influence of the use phase is highly dependent by the country's electricity mix, as described in the geographic scenario, the trend over last decade has been to reduce dependency from fossil sources that however are still dominating the electricity production in certain countries. Moreover, in those countries (i.e., Sweden) where the electricity mix is not dominated by fossil sources, the production phase not only resulted in a significant contribution to the overall climate change impact, but it also gained relevance against the other life cycle phases. This underscores the relevance of introducing DfCE methodology to enhance product sustainability.

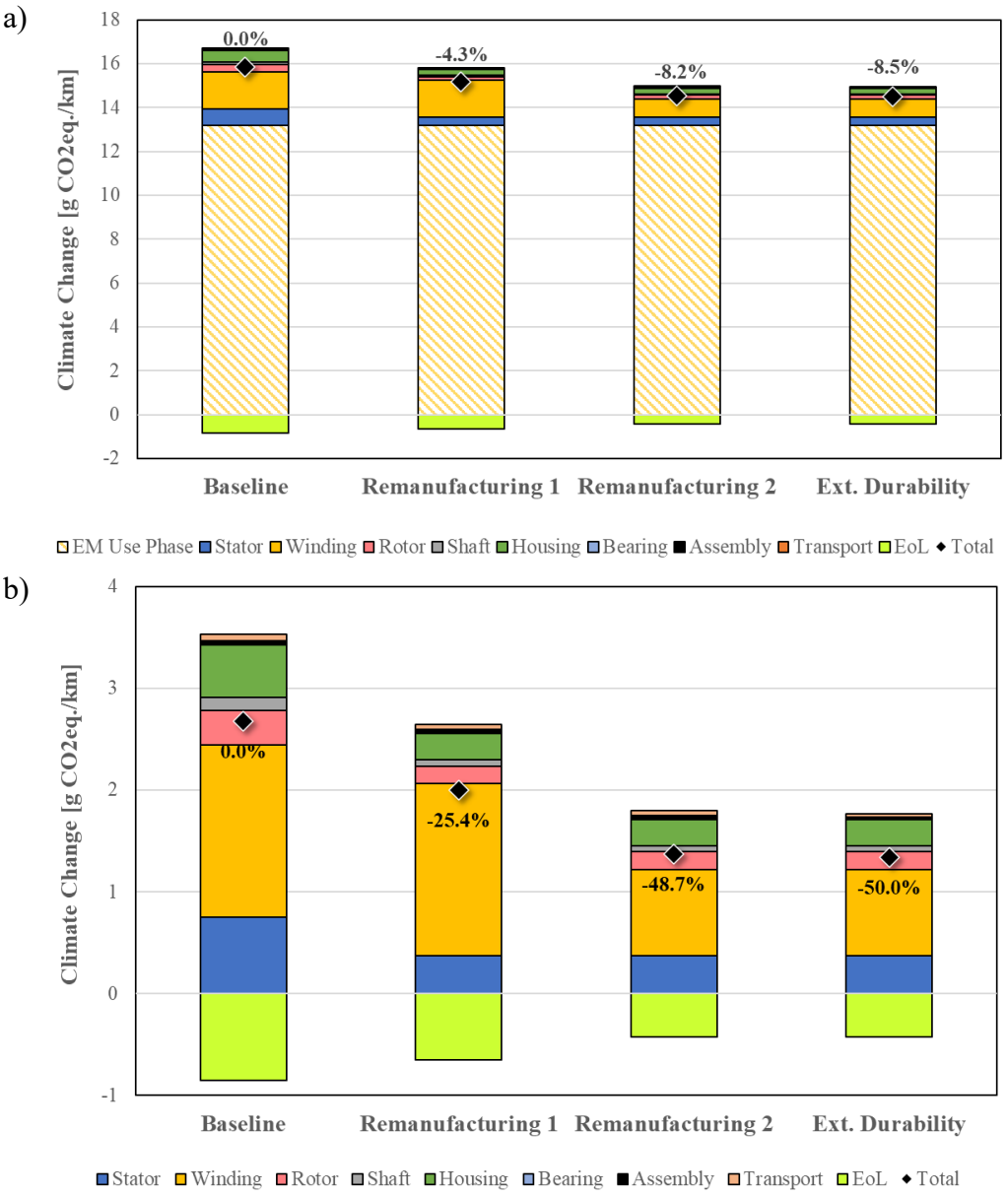

Figure 5.16 Specific CO_2 emission (gCO_2/km) calculated with EF3.0 method for the four CS broken down into life cycle phases and motor subsystems with (a) and without (b) use phase

5.3 Electric motor circularity and material flow analysis

Figure 5.17, shows PCI values for the selected CS and three recycling scenarios, calculated following the approach described in Chapter 4. All the CS are characterized, as expected, by a higher circularity of the material compared to the baseline liner model, in all the recycling scenarios. When feedstocks are constituted completely by recycled materials PCI approaches 1 even for the baseline linear model. The PCI assessment is aligned with the LCA results for what concerns the evaluation of the CS, confirming that both the design features introduced and selected CS contribute to a positive shift from linear to circular

models. This trend is even more evident in the lower rate recycling scenarios, where the benefits of CS become more pronounced.

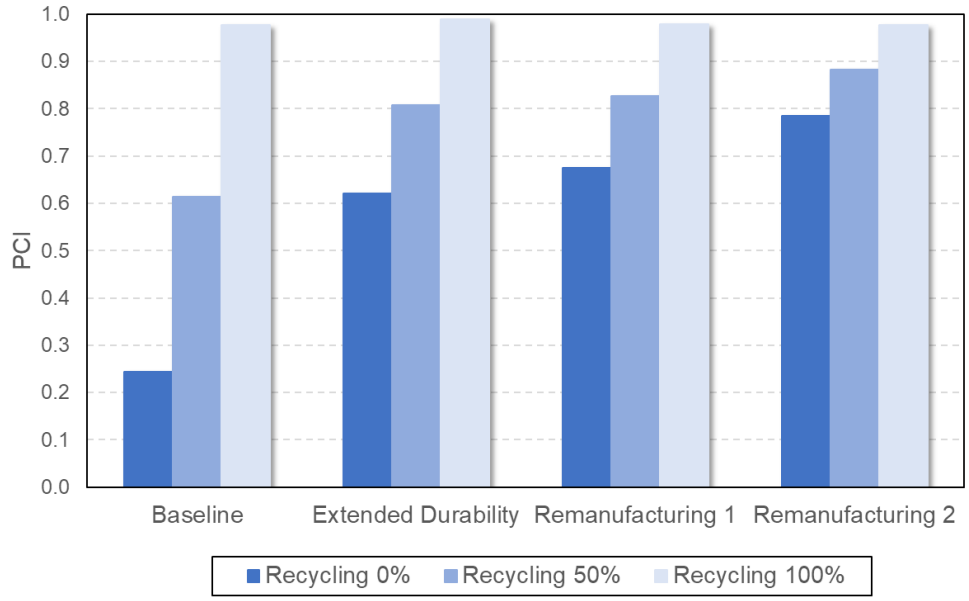

Figure 5.17 PCI calculation for the linear model and CS in the three recycling scenarios

In Figure 5.18 the same PCI results are presented, this time in relation to product utility.

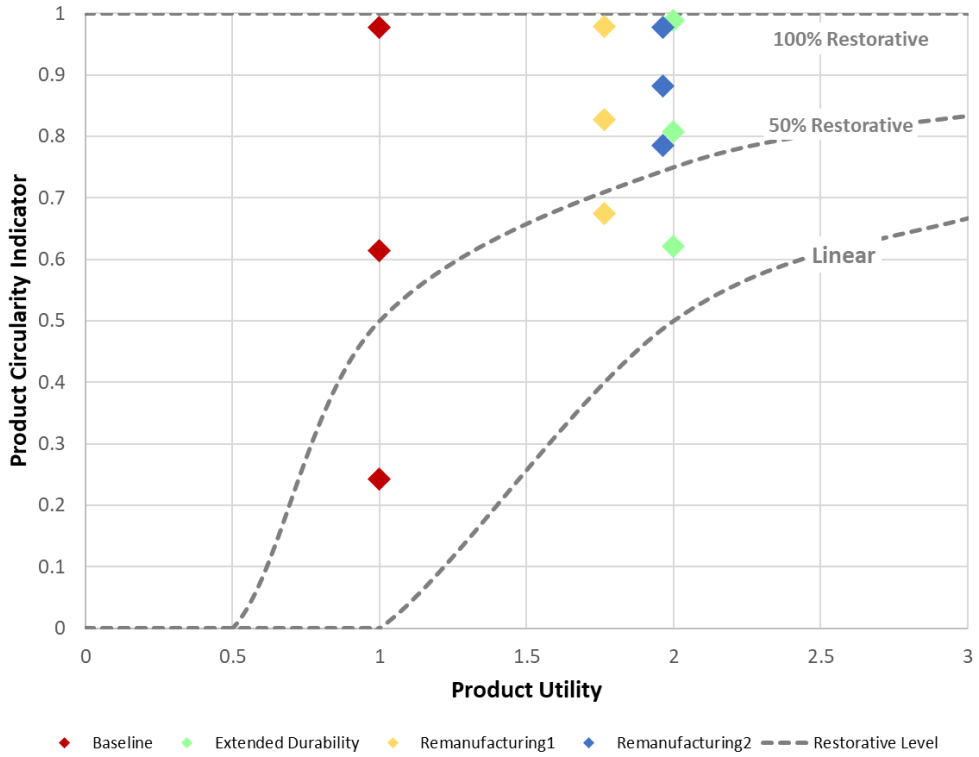

Figure 5.18 PCI calculation for the linear model and CS in the three recycling scenarios in relation to a Product Utility

A hypothetic product utility for the Remanufacturing strategies was calculated using the mass-based weighting approach, described in Chapter 4, inherently for the PCI calculation. Indeed, each component is assigned a utility factor. It is evident that both Remanufacturing strategies exhibit a higher restorative degree. These results are furtherly exploited in Figure 5.19, which presents the Material Flow Analysis (MFA) for the treated subcases. In all the Figures, material flows expressed in kg, from feedstock to component production for one or two life cycle (grey flow) are reported, taking into account the production scrap (yellow flow) and the circular path, including reuse phase (orange flow) as well as recycle phase (green flow) with associated waste (brown flow). Figure 5.19 a), illustrates the material flow for the subcases with a single life cycle (Baseline and Extended Durability), Figure 5.19 b) and c) show the two remanufacturing subcases. It is clearly visible that a second life is achievable with a small supplementary amount of material required for the motor remanufacturing, reinforcing the outcome from the PCI calculation.

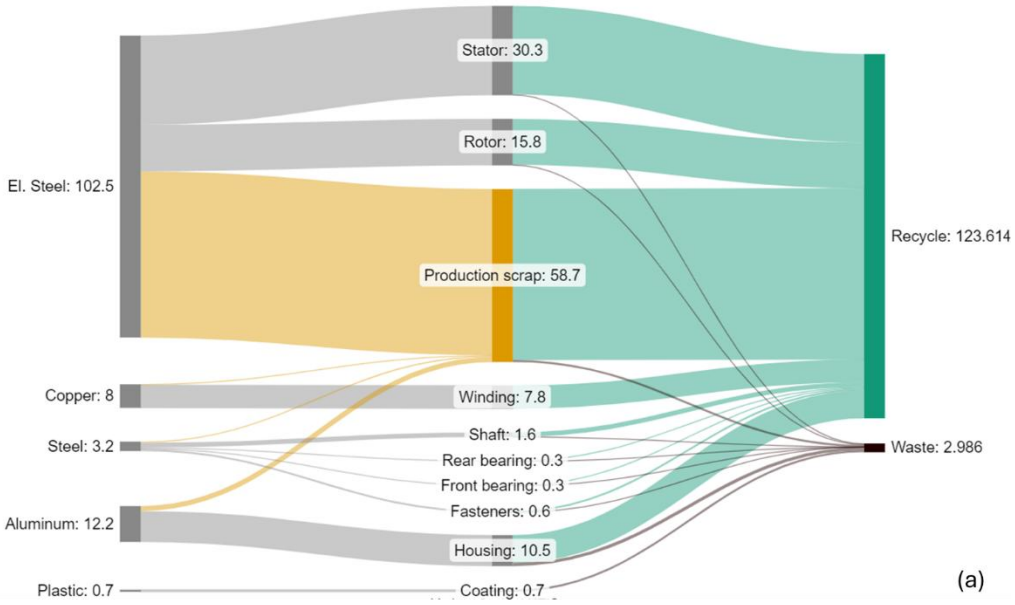

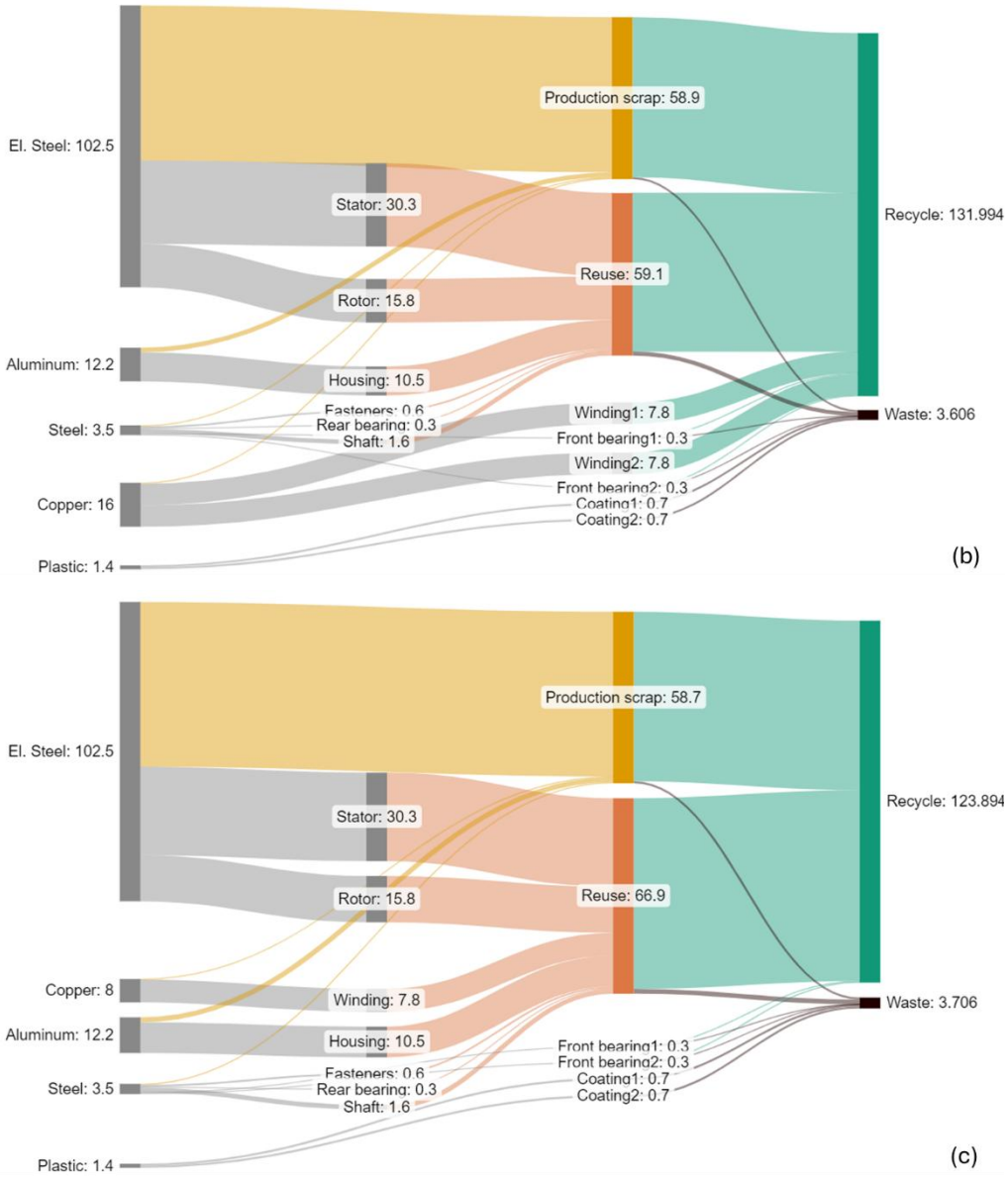

Figure 5.19 MFA for the Linear model and CS: Baseline and Extended Durability (a), Remanufacturing 1 (b), Remanufacturing 2 (c)

5.4 Electric motor economic impact

The total motor production cost has been calculated according to the methodology described in Chapter 4. To present the results, a Pareto chart is shown in Figure 5.20, illustrating cost walk of the components, and the final assembly operation. Component costs, which represent the 90% of the overall value, are broken down into subsystems and ordered in decrescent order from left to right. Cost related to aluminium structures, copper coils and ferromagnetic lamination account for the 76% of the overall motor production cost. The unusually high cost contribution of the aluminium structures is partly due to the nature of the SRM motor, being inherently less power dense than PMSMs, and largely due to the prototypal nature of the design analysed.

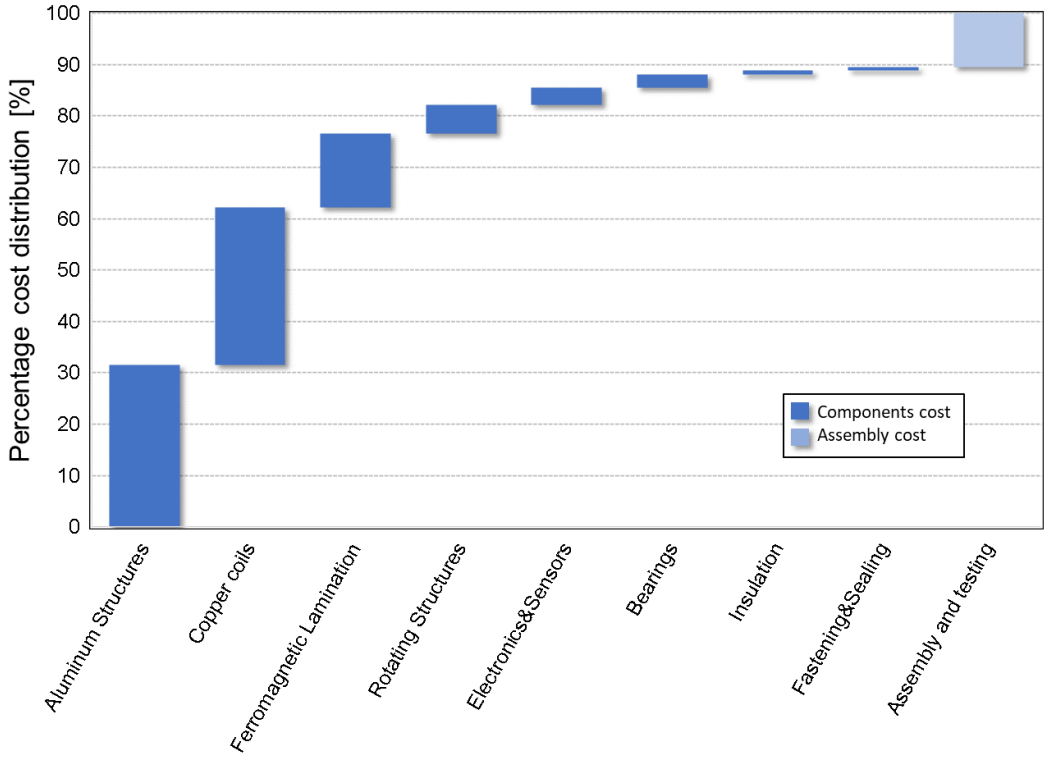

Figure 5.20 SRM total production cost breakdown

A comparison between the CS is reported in Figure 5.21. It is immediately evident that all the CS options offer significant advantages in terms of total lifecycle cost when a second life is considered. Specifically, the cost of the Remanufacturing 1 configuration results to be 0.6$ every 1000 kilometre driven cheaper than the baseline linear configuration. Remanufacturing 2 and Extended Durability exhibit a reduction of 1$ every 1000km driven when compared to the baseline. It is however extremely important to remark that, though CS 'Baseline' and 'Extreme durability' may be considered a result, the two Remanufacturing strategies fall short in terms of total cost of ownership of the inevitable charges related to the remanufacturing phase, which has to consider dismantling the apparatus from the vehicle, refurbishing and re-install. Therefore, although the total product cost presented in the chart may be considered technically correct, it does not provide a complete picture, especially from a customer-centred perspective. For the time being, these two CS simply considered within the total production cost a second motor assembly cost of identical expense to the industrial assembly cost mentioned at Section 4.4. Future research may concentrate on proper business models which shall consider a variety of factors such as in-vehicle disassembly, re-manufacturing strategy (whether workshop-based or centralized in industrial servicing/remanufacturing centres), transportation and in-vehicle reassembly.

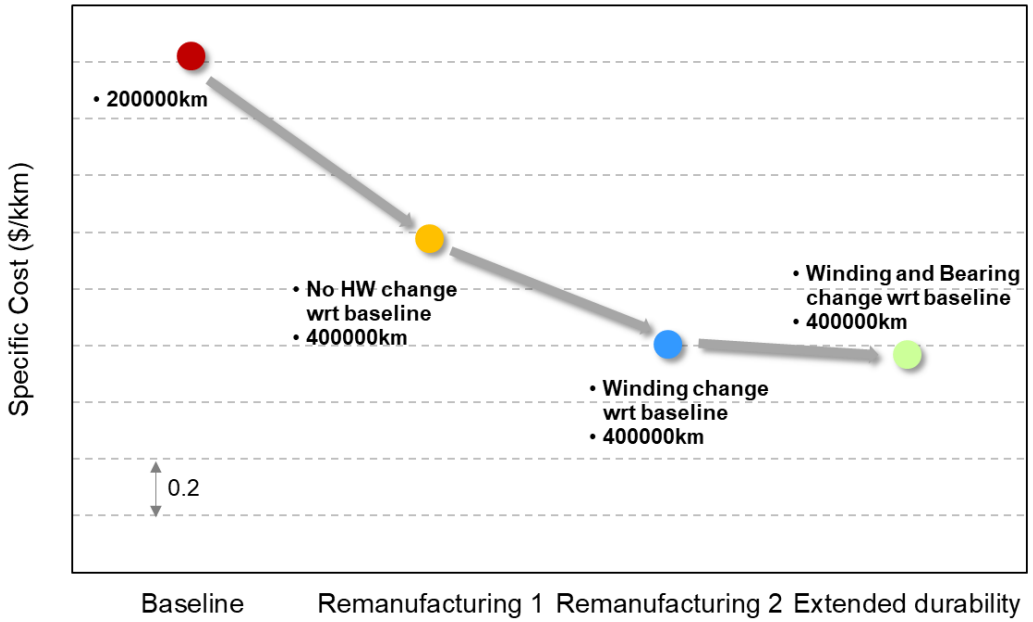

Figure 5.21 Specific cost ($/kkm) for the Linear model and for the CS indicating hardware (HW) variations with respect (wrt) to baseline and distance travelled

As described in Chapter 4, the cost figures calculated using the proposed model, have also been compared with a simplified model available in literature, enhancing the consistency of the presented normalized data. The simplified model assumes a range of values for estimating the operations related to manufacturing and testing. Figure 5.22 shows a comparison between the calculated cost values and a scatter band representing the overall manufacturing cost estimated by the simplified model. It is noticeable that the adopted cost model yields values that fall within the typical range. As mentioned in Chapter 4, certain subsystems were excluded from the original cost calculation because only cost density for metal parts is considered in the simplified model.

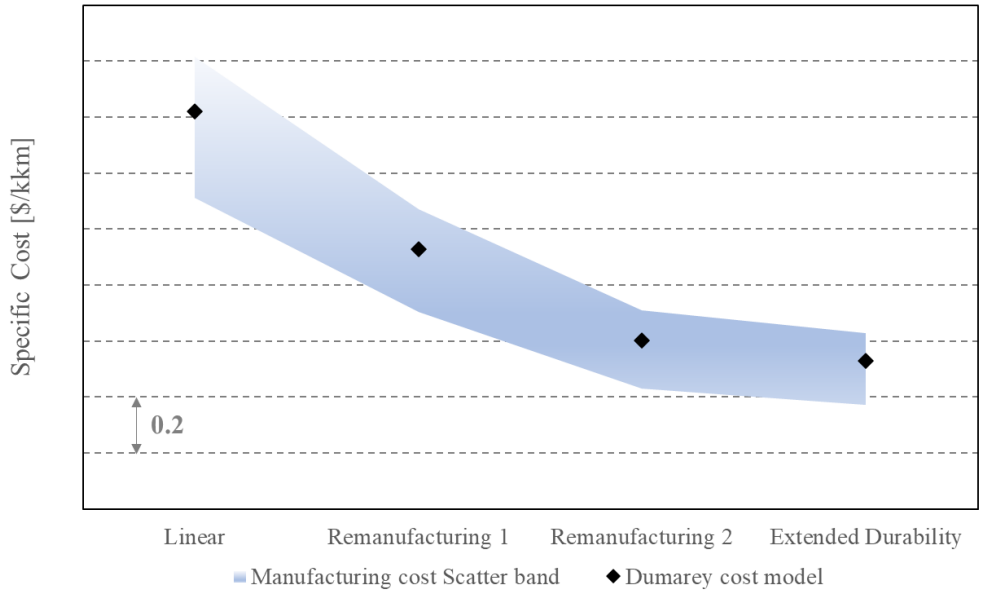

Figure 5.22 Adopted cost model comparison with simplified model available in literature

Chapter 6

Conclusions

6.1 Conclusions

Sustainability and CE concepts are increasingly integrated into industrial products development processes. The transportation sector is particularly affected by this shift, as it is one of the major contributors to global CO_2 emissions. Vehicle electrification is crucial to achieve CO_2 neutrality target set by the European commission for 2050. However, this transition implies challenges related to raw material availability, product cost and geopolitical relations. This scenario is further shaped by the introduction of the ESPR legislative package, which focuses on improving product circularity.

The present thesis aims to develop and implement a DfCE methodology within Dumarey Automotive Italia. The methodology has been applied to a magnet free SRM electric motor. The selected machine, inherently aligned with both economic and environmental sustainability goals, benefits from the novel approach, demonstrating further improvements in the targeted areas. Specifically lower cost, and performance comparability with respect to the other electric motor's topologies, and typical robustness, drove the SRM selection. Additionally, the absence of RE provide geopolitical independency to this machine. The implementation of the methodology followed the main steps below:

- Adoption of a framework for defining CS
- Introduction of design features enabling CS realization
- Development and implementation of a toolset for environmental and economic assessment

Within the framework, non-conventional design solutions were identified to improve product behaviour across its life cycle (Ecodesign), product durability and so maintenance in its life cycle, extended use and circularity, enabling the product's reintroduction into the life cycle. Subsequently, design features

supporting some of these solutions were introduced. In particular, the following features were implemented and evaluated:

- Replacement of copper windings with aluminium ones as an Ecodesign strategy impacting C2G, use and EoL phases
- Selection of bearings and windings (components considered critical for durability) to achieve an Extended Durability, doubling the motor's useful life
- Design of a motor housing that allows complete disassembly without damaging reusable parts at the end of the first life cycle. Specifically, the new component enabled two strategies named Remanufacturing 1 and 2, characterized by a different amount of component recovery after the first use. This feature to the best of author's knowledge is novel both in literature and market, and therefore, let to a patent application filing

These design strategies were developed in parallel with motor design, as sustainability requirements were integrated from the initial concept phase and the latter was embedded within the motor prototype itself. In addition to the innovative design the thesis also describes the in-house developed models for assessing environmental and economic impacts.

Regarding the toolset development, the environmental impact of the proposed solutions was evaluated through a LCA, complemented by a circularity analysis. The LCA is structured into three steps, each representing an incremental evolution of the LCA model with distinct goal and scope. Specifically, in the first step environmental impacts of a PMSM across Geographical and Application scenarios were evaluated following a cradle to use approach. In the second step, a comparative analysis of a PMSM and a SRM with both aluminium and copper windings, was executed through a cradle to grave approach. Finally, within the third step, CS applied to a SRM with copper windings were evaluated, based on the step 2 LCA model.

Despite they are more and more important, considered as relevant as performance and cost studies, LCA studies are affected by numerous assumptions. The LCA described within this thesis can be regarded as a benchmark LCA study for permanent magnet and SRM electric motors suitable for passenger cars. For each step, a preliminary analysis was conducted using all the impact categories defined by the EF method. This was followed by a selection of the most relevant categories, according to an adaptation to the investigated scenarios of the conventional normalization and weighting methodology. The analysis in step 1 highlights the relevance of consistent geographical boundary setting. Moreover, it presents a step forward with respect to the literature in terms of consistency concerning comparative LCA studies, especially when different vehicle applications are considered. The proposed scenario analysis framework focuses on crucial key aspects influencing nearly all the relevant phases of the electric motor life cycle, aiming at ensuring comparability.

A reference motor was identified as representative of the baseline. Results revealed that, the use phase is predominant, representing at least 50% of the environmental impact across all categories, except in the human toxicity carcinogenic and non-categories confirming importance of both motor efficiency and electricity mix. Considering the baseline and excluding the use phase, copper windings emerged as the highest contributor in almost all impact categories, followed by the aluminium parts comprised in the housing, electrical steel in the stator and rotor, and permanent magnets. In the geographical scenario analysis, differences are mainly due to different electricity mixes in almost all impact categories and to copper mine operations in resource use of minerals and metals.

Among selected countries, China resulted to have the highest environmental impact in almost all the categories, due to the energy mix reliance degree on fossil sources. Indeed Sweden, Italy and the USA exhibit respectively 70% to 90%, 70% to 85% and 50% to 70% lower environmental impact in comparison to the highest contributing countries.

For the Swedish scenario, where electricity mix is not dominated by fossil sources, the production phase, including magnet manufacturing, significantly contributes to the overall environmental impact in the selected influent categories. In the application scenario, the environmental impacts were investigated for four vehicle applications, selected basing on the European BEV market. It is shown that, as the vehicle varies, both use and manufacturing phases are affected. Vehicle performance requirements and characteristics, such as weight, aerodynamic and rolling resistance, influence motor design and operating points, thereby impacting both manufacturing and use phase contributions. The contribution of the manufacturing stage resulted in growing linearly with the required power. The SUV scenario resulted to be the one with the highest environmental impact across all categories. Indeed, City Car, Segment B and Segment C, exhibit respectively 25%, 20% and 10% to 15% lower impact compared to SUV. In the application scenario, the chosen case studies all fall into the passenger car category. It should be pointed out that, major differences are to be expected if the assessment is extended to 2-wheelers and/or medium- and heavy-duty vehicles.

The second step, provides a comparison in terms of environmental impact of electrical motors characterized by different technologies, designed with different targets, but intended to be used in similar applications. In particular, this portion of research shows the environmental impact of an SRM, that represents a novelty in the transportation field, compared with a baseline PMSM, representing instead the mainstream technology for the considered market. Also, to the best of author knowledge represents a first example of LCA of a SRM designed for vehicle's application. Another novel aspect characterizing this step is represented by the evaluation of the aluminium windings impact on all the life cycle phases. The LCA model in this step, was exploited adding the EoL, through the introduction of recycling scenarios. The results lead to the conclusion that the use phase is highly dependent from the efficiency over considered cycle, in this case determined mainly by matching between motor and vehicle. It is demonstrated

that copper winding SRM has comparable impacts in terms of material resource use and has a slight disadvantage for what concern climate change, fossil resource use, acidification and water use when compared to PMSM, although it is virtually installed on a vehicle for which it is oversized. However, SRM exhibits lower environmental impact compared to SRM in the freshwater ecotoxicity, due to the PM absence. In contrast, the aluminium winding SRM, shows lower environmental impact across all relevant categories selected due to both low energy requirement over use phase and employment of a less energy intense material for the winding. In addition, copper production is the main contributor to mineral and metal resource use. Apart from specific advantages related to the technology and material adopted, aluminium winding SRM configuration is demonstrating that a properly sized machine, even if intrinsically less efficient, could lead to better results coming from a favourable coupling with the application. However, this conclusion is determined by the approach followed in this study, where for the machine with aluminium winding, same core has been considered, accepting a deterioration of the performances at mid-high speed and a reduction of the overload time margin.

As the previous step, also the third, represents an advancement with respect to technical literature where LCA for CS of electric motors was not available. Within this analysis advantages of the CS up to 14% were noted, compared to the linear model. Being these results highly influenced by the use phase, and consequently electricity mix of the specific country is again relevant to highlight that when excluding the use phase, environmental impact reduction up to 50% were achieved through the CS application. The environmental benefits of the CS were further supported by a material circularity evaluation conducted at product level, confirming the increased circularity of the proposed approaches especially when components are not constituted by recycled feedstock.

CS were also assessed from an economic standpoint adopting an in-house cost model, which provided detailed cost information for each motor subsystem and for each strategy. The most impactful subsystem from a cost perspective resulted to be the aluminium structure, followed by copper winding, also due to the prototypal nature of the evaluated SRM. Additionally, the results obtained, were compared with a simplified cost model, available in the literature. It was demonstrated that cost calculated falls in the scatter band determined with the simplified model. Regarding CS, cost advantages up to 50% were achieved compared with linear model, similarly to the environmental impact.

The reduction in environmental impact, consistent with reduction in the motor production cost and increased material circularity without performance deterioration, bodes well for a successful application in the field, showing potential for a transversal methodology implementation.

Both the Ecodesign and CS evaluated lead to consistent advantages in terms of environmental and economic sustainability, even if the use phase resulted to be the most impactful in almost all the scenarios considered. However, the trend of the electricity mix, is to reduce reliance on fossil sources as already visible for the countries studied in the thesis during the 2012–2022 timeframe. All these

considerations, lead to the conclusion that the use phase will assume lower importance, justifying increasing interest in both magnet free motors as well as implementation of design strategies to improve products sustainability towards the two branches of the cost and environment.

6.2 Future Research

This work could be furtherly exploited by future methodology and product development. Additionally, will be completed through the teardown of the prototypal SRM motor after a testing campaign, to both analyse integrity of the components and effectiveness of the introduced DfCE features that were not already checked.

In future work one could consider further opportunities and performance targets to compare a design of the SRM for a baseline PMSM application and potentially to experimentally verify performance of the Ecodesign strategy with aluminium windings

In parallel, the development of tailored business models should focus on aspects that are particularly relevant to CS, such as remanufacturing operations. A critical part of these models will be the strategic setting of the selling price, which must reflect both market dynamics and the added value of circular practices.

Moreover, integrating remanufacturing operations into the LCA model could significantly enhance the comprehensiveness of the analysis. This would provide a more holistic view of the environmental impact and sustainability potential of the product lifecycle, especially considering the future trend to reduce electricity mix reliance on fossil sources and consequently the impact of the use phase. The LCA investigation could be enriched exploiting geographic and application scenarios.

Finally, the methodology developed should be extended to other propulsion unit products, with a focus on identifying and leveraging unique design features that could enable circularity. It is important to recognize that while the mindset and methodological framework may remain consistent, the specific pathways to achieve enhanced product circularity are likely to vary considerably across different applications.

References

[1] “Paris Agreement.” UNFCCC. Accessed: Oct. 28, 2025. [Online]. Available: https://unfccc.int/sites/default/files/english_paris_agreement.pdf

[2] “TRANSFORMING OUR WORLD: THE 2030 AGENDA FOR SUSTAINABLE DEVELOPMENT.” United Nations. Accessed: Oct. 29, 2025. [Online]. Available: https://sdgs.un.org/sites/default/files/publications/21252030%20Agenda%20for%20Sustainable%20Development%20web.pdf

[3] “Action on Climate and SDGs,” Unite Nations Climate Change. Accessed: Oct. 29, 2025. [Online]. Available: https://unfccc.int/topics/cooperative-activities-and-sdgs/action-on-climate-and-sdgs

[4] A. Dzebo, H. Janetschek, C. Brandi, and G. Iacobuta, “Connections between the Paris Agreement and the 2030 Agenda.” SEI - Stockholm Environment Institute, Sep. 2019. Accessed: Oct. 29, 2025. [Online]. Available: https://www.sei.org/wp-content/uploads/2019/08/connections-between-the-paris-agreement-and-the-2030-agenda.pdf

[5] “Third Global Conference on Strengthening Synergies Between the Paris Agreement and the 2030 Agenda For Sustainable Development,” Tokio, Conference report, Jul. 2022. Accessed: Oct. 29, 2025. [Online]. Available: https://sdgs.un.org/sites/default/files/2023-03/the_third_global_conference_report_11.08.2022.pdf

[6] H. Ritchie, P. Rosado, and M. Roser, “Breakdown of carbon dioxide, methane, and nitrous oxide emissions by sector,” OurWorldinData.org. Accessed: Oct. 29, 2025. [Online]. Available: https://ourworldindata.org/emissions-by-sector#article-citation

[7] “2040 climate target,” European Commision - Energy, Climate change, Environment. Accessed: Oct. 29, 2025. [Online]. Available: https://climate.ec.europa.eu/eu-action/climate-strategies-targets/2040-climate-target_en

[8] “Securing our future Europe’s 2040 climate target and path to climate neutrality by 2050 building a sustainable, just and prosperous society,” European Commission, Strasbourg, COMMISSION STAFF WORKING DOCUMENT IMPACT ASSESSMENT REPORT {COM(2024) 63 final}-{SEC(2024) 64 final}-{SWD(2024) 64 final}, Jun. 2024.

[9] M. De Santis, L. Silvestri, and A. Forcina, “Promoting electric vehicle demand in Europe: Design of innovative electricity consumption simulator and subsidy strategies based on well-to-wheel analysis,” *Energy Conversion and Management*, vol. 270, p. 116279, Oct. 2022, doi: 10.1016/j.enconman.2022.116279.

[10] IEA, “Global EV Outlook 2024 Moving towards increased affordability,” International Energy Agency (IEA). Accessed: Dec. 17, 2024. [Online]. Available: https://iea.blob.core.windows.net/assets/a9e3544b-0b12-4e15-b407-65f5c8ce1b5f/GlobalEVOutlook2024.pdf

[11] L. Wierda and A. Zanuttini, “ECODESIGN IMPACT ACCOUNTING,” Annual Overview Report 2024 2021/OP/0004/ENER/B3/FWC 2020-708/LOT 1/04/FV2022–531, Jan. 2025. Accessed: Nov. 07, 2025. [Online]. Available: https://circabc.europa.eu/ui/group/418195ae-4919-45fa-a959-3b695c9aab28/library/e2a752ef-c365-41df-8e50-98376e6ca756/details

[12] IEA, “Global EV Outlook 2025 Expanding sales in diverse markets,” International Energy Agency (IEA), Jul. 2025. Accessed: Nov. 07, 2025. [Online]. Available: https://iea.blob.core.windows.net/assets/7ea38b60-3033-42a6-9589-71134f4229f4/GlobalEVOutlook2025.pdf
[13] U.S. Department of Energy, “Rare Earth Permanent Magnets Supply Chain Deep Dive Assessment.” Accessed: Dec. 13, 2023. [Online]. Available: https://www.energy.gov/sites/default/files/2022-02/Neodymium%20Magnets%20Supply%20Chain%20Report%20-%20Final.pdf
[14] H. Jin, P. Afiuny, T. McIntyre, Y. Yih, and J. W. Sutherland, “Comparative Life Cycle Assessment of NdFeB Magnets: Virgin Production versus Magnet-to-Magnet Recycling,” *Procedia CIRP*, vol. 48, pp. 45–50, 2016, doi: 10.1016/j.procir.2016.03.013.
[15] M. Zakotnik, C. O. Tudor, L. T. Peiró, P. Afiuny, R. Skomski, and G. P. Hatch, “Analysis of energy usage in Nd–Fe–B magnet to magnet recycling,” *Environmental Technology & Innovation*, vol. 5, pp. 117–126, Apr. 2016, doi: 10.1016/j.eti.2016.01.002.
[16] European Commission. Directorate General for Climate Action., *Going climate-neutral by 2050: a strategic long term vision for a prosperous, modern, competitive and climate neutral EU economy.* LU: Publications Office, 2019. Accessed: Oct. 21, 2025. [Online]. Available: https://data.europa.eu/doi/10.2834/02074
[17] Advanced Propulsion Center UK, “Electric Machines Roadmap 2020,” Feb. 2021. Accessed: Apr. 04, 2024. [Online]. Available: https://www.apcuk.co.uk/wp-content/uploads/2021/09/https___www.apcuk_.co_.uk_app_uploads_2021_02_Exec-summary-Technology-Roadmap-Electric-Machines-final.pdf
[18] N. Tazi *et al.*, Eds., *Circularity measures on critical raw materials and e-drive motors in vehicles*. Luxembourg: Publications Office, 2025. doi: 10.2760/6053264.
[19] P. R. Shukla, J. Skea, A. R. Reisinger, and IPCC, Eds., *Climate change 2022: mitigation of climate change*. Geneva: IPCC, 2022.
[20] A. Antonacci, A. Giraldi, E. Innocenti, and M. Delogu, “A Scientific Approach for Environmental Analysis: An Asynchronous Electric Motor Case Study for Stand-By Applications,” *Machines*, vol. 11, no. 8, p. 810, Aug. 2023, doi: 10.3390/machines11080810.
[21] European Commission. Directorate General for Climate Action. and Ricardo Energy & Environment., *Determining the environmental impacts of conventional and alternatively fuelled vehicles through LCA: final report.* LU: Publications Office, 2020. Accessed: Oct. 20, 2025. [Online]. Available: https://data.europa.eu/doi/10.2834/91418
[22] European Union, “REGULATION (EU) 2024/1781 OF THE EUROPEAN PARLIAMENT AND OF THE COUNCIL - establishing a framework for the setting of ecodesign requirements for sustainable products, amending Directive (EU) 2020/1828 and Regulation (EU) 2023/1542 and repealing Directive 2009/125/EC.” Official Journal of the European Union, Jun. 28, 2024. Accessed: Oct. 20, 2025. [Online]. Available: https://eur-lex.europa.eu/legal-content/EN/TXT/PDF/?uri=OJ:L_202401781
[23] European Commission, “Ecodesign for Sustainable Products Regulation.” Accessed: Dec. 17, 2024. [Online]. Available: https://commission.europa.eu/energy-climate-change-

environment/standards-tools-and-labels/products-labelling-rules-and-requirements/ecodesign-sustainable-products-regulation_en#:~:text=The%20Ecodesign%20for%20Sustainable%20Products%20Regulation%20%28ESPR%29%2C%20which,we%20use%20them%20can%20significantly%20impact%20the%20environment.

[24] European Commission, "COMMUNICATION FROM THE COMMISSION TO THE EUROPEAN PARLIAMENT, THE COUNCIL, THE EUROPEAN ECONOMIC AND SOCIAL COMMITTEE AND THE COMMITTEE OF THE REGIONS On making sustainable products the norm." Mar. 30, 2022. Accessed: Oct. 20, 2025. [Online]. Available: https://eur-lex.europa.eu/legal-content/EN/TXT/PDF/?uri=CELEX:52022DC0140

[25] "ChangeNow 2024: Renault Group and The Future Is NEUTRAL accelerate in the circular economy," Renault Group website. Accessed: Nov. 06, 2025. [Online]. Available: https://media.renaultgroup.com/changenow-2024-renault-group-and-the-future-is-neutral-accelerate-in-the-circular-economy/?lang=eng

[26] "Stellantis Inaugurates its First Circular Economy Hub in Turin, Italy," Stellantis website. Accessed: Nov. 06, 2025. [Online]. Available: https://www.stellantis.com/en/news/press-releases/2023/november/stellantis-inaugurates-its-first-circular-economy-hub-in-turin-italy?adobe_mc_ref=

[27] "Schaeffler Vehicle Lifetime Solutions presents first repair kit for electric motor for the Hyundai Ioniq," Schaeffler website. Accessed: Nov. 06, 2025. [Online]. Available: https://www.schaeffler.com/en/media/press-releases/press-releases-detail.jsp?id=88045888

[28] N. Carey, "Volvo to issue world's first EV battery passport ahead of EU rules," Reuters. Accessed: Nov. 06, 2025. [Online]. Available: https://www.reuters.com/business/autos-transportation/volvo-issue-worlds-first-ev-battery-passport-ahead-eu-rules-2024-06-04/

[29] "Toyota Revs Up Efforts for Battery 3R to Achieve Circular Economy," Toyota website. Accessed: Nov. 06, 2025. [Online]. Available: https://global.toyota/en/newsroom/corporate/40102076.html

[30] "2024 Task Force on Climate-related Financial Disclosures (TCFD) Report," General Motors, 2024. Accessed: Nov. 06, 2025. [Online]. Available: https://www.gm.com/content/dam/company/docs/us/en/gmcom/company/2024_TCFD_Report.pdf

[31] T. Wautelet, "The Concept of Circular Economy: its Origins and its Evolution," 2018, doi: 10.13140/RG.2.2.17021.87523.

[32] K. Winans, A. Kendall, and H. Deng, "The history and current applications of the circular economy concept," *Renewable and Sustainable Energy Reviews*, vol. 68, pp. 825–833, Feb. 2017, doi: 10.1016/j.rser.2016.09.123.

[33] P. Ghisellini, C. Cialani, and S. Ulgiati, "A review on circular economy: the expected transition to a balanced interplay of environmental and economic systems," *Journal of Cleaner Production*, vol. 114, pp. 11–32, Feb. 2016, doi: 10.1016/j.jclepro.2015.09.007.

[34] F. Ceschin and I. Gaziulusoy, "Evolution of design for sustainability: From product design to design for system innovations and transitions," *Design Studies*, vol. 47, pp. 118–163, Nov. 2016, doi: 10.1016/j.destud.2016.09.002.

[35] N. M. P. Bocken, I. De Pauw, C. Bakker, and B. Van Der Grinten, "Product design and business model strategies for a circular economy," *Journal of*

Industrial and Production Engineering, vol. 33, no. 5, pp. 308–320, Jul. 2016, doi: 10.1080/21681015.2016.1172124.

[36] J. Kirchherr, D. Reike, and M. Hekkert, "Conceptualizing the circular economy: An analysis of 114 definitions," *Resources, Conservation and Recycling*, vol. 127, pp. 221–232, Dec. 2017, doi: 10.1016/j.resconrec.2017.09.005.

[37] J. Kirchherr, N.-H. N. Yang, F. Schulze-Spüntrup, M. J. Heerink, and K. Hartley, "Conceptualizing the Circular Economy (Revisited): An Analysis of 221 Definitions," *Resources, Conservation and Recycling*, vol. 194, p. 107001, Jul. 2023, doi: 10.1016/j.resconrec.2023.107001.

[38] G. C. Nobre and E. Tavares, "The quest for a circular economy final definition: A scientific perspective," *Journal of Cleaner Production*, vol. 314, p. 127973, Sep. 2021, doi: 10.1016/j.jclepro.2021.127973.

[39] *Framework for implementing the principles of the circular economy in organizations. Guide:* doi: 10.3403/30334443.

[40] M. Geissdoerfer, P. Savaget, N. M. P. Bocken, and E. J. Hultink, "The Circular Economy – A new sustainability paradigm?," *Journal of Cleaner Production*, vol. 143, pp. 757–768, Feb. 2017, doi: 10.1016/j.jclepro.2016.12.048.

[41] E. Hysa, A. Kruja, N. U. Rehman, and R. Laurenti, "Circular Economy Innovation and Environmental Sustainability Impact on Economic Growth: An Integrated Model for Sustainable Development," *Sustainability*, vol. 12, no. 12, p. 4831, Jun. 2020, doi: 10.3390/su12124831.

[42] E. S. Tan, A. W. L. Lee, Y. C. Shekar, and Y. S. Tan, "Design for Circularity: A Framework for Sustainable Product Redesign," *Procedia CIRP*, vol. 122, pp. 479–484, 2024, doi: 10.1016/j.procir.2024.01.070.

[43] S. Evans and M. Munster, "Designing for a Circular Economy," 2022. Accessed: Nov. 06, 2025. [Online]. Available: https://www.researchgate.net/publication/359992233_Designing_for_a_Circular_Economy

[44] M. Moreno, C. De Los Rios, Z. Rowe, and F. Charnley, "A Conceptual Framework for Circular Design," *Sustainability*, vol. 8, no. 9, p. 937, Sep. 2016, doi: 10.3390/su8090937.

[45] J. Jagnow, B. Stoehr, R. Bernijazov, C. Koldewey, and R. Dumitrescu, "Circular product design: a literature-based identification of challenges from the perspective of product designers," *Proc. Des. Soc.*, vol. 5, pp. 931–940, Aug. 2025, doi: 10.1017/pds.2025.10107.

[46] P. Tecchio, C. McAlister, F. Mathieux, and F. Ardente, "In search of standards to support circularity in product policies: A systematic approach," *Journal of Cleaner Production*, vol. 168, pp. 1533–1546, Dec. 2017, doi: 10.1016/j.jclepro.2017.05.198.

[47] A. Franconi, F. Ceschin, and D. Peck, "Structuring Circular Objectives and Design Strategies for the Circular Economy: A Multi-Hierarchical Theoretical Framework," *Sustainability*, vol. 14, no. 15, p. 9298, Jul. 2022, doi: 10.3390/su14159298.

[48] M. C. Den Hollander, C. A. Bakker, and E. J. Hultink, "Product Design in a Circular Economy: Development of a Typology of Key Concepts and Terms," *J of Industrial Ecology*, vol. 21, no. 3, pp. 517–525, Jun. 2017, doi: 10.1111/jiec.12610.

[49] I. C. De Los Rios and F. J. S. Charnley, "Skills and capabilities for a sustainable and circular economy: The changing role of design," *Journal of*

Cleaner Production, vol. 160, pp. 109–122, Sep. 2017, doi: 10.1016/j.jclepro.2016.10.130.
[50] M. Haines-Gadd, J. Chapman, P. Lloyd, J. Mason, and D. Aliakseyeu, "Emotional Durability Design Nine—A Tool for Product Longevity," *Sustainability*, vol. 10, no. 6, p. 1948, Jun. 2018, doi: 10.3390/su10061948.
[51] J. Chapman, *Emotionally durable design: objects, experiences and empathy*. London: Earthscan, 2006.
[52] C. Bakker, F. Wang, J. Huisman, and M. Den Hollander, "Products that go round: exploring product life extension through design," *Journal of Cleaner Production*, vol. 69, pp. 10–16, Apr. 2014, doi: 10.1016/j.jclepro.2014.01.028.
[53] S. L. Soh, S. K. Ong, and A. Y. C. Nee, "Application of Design for Disassembly from Remanufacturing Perspective," *Procedia CIRP*, vol. 26, pp. 577–582, 2015, doi: 10.1016/j.procir.2014.07.028.
[54] R. Bogue, "Design for disassembly: a critical twenty-first century discipline," *Assembly Automation*, vol. 27, no. 4, pp. 285–289, Oct. 2007, doi: 10.1108/01445150710827069.
[55] G. Johansson, "Product innovation for sustainability: on product properties for efficient disassembly," *International Journal of Sustainable Engineering*, vol. 1, no. 1, pp. 32–41, Mar. 2008, doi: 10.1080/19397030802113835.
[56] S. Gedell and H. Johannesson, "Design rationale and system description aspects in product platform design: Focusing reuse in the design lifecycle phase," *Concurrent Engineering*, vol. 21, no. 1, pp. 39–53, Mar. 2013, doi: 10.1177/1063293X12469216.
[57] J. Daae, L. Chamberlin, and C. Boks, "Dimensions of Behaviour Change in the context of Designing for a Circular Economy," *The Design Journal*, vol. 21, no. 4, pp. 521–541, Jul. 2018, doi: 10.1080/14606925.2018.1468003.
[58] S. Kunamaneni, S. Jassi, and D. Hoang, "Promoting reuse behaviour: Challenges and strategies for repeat purchase, low-involvement products," *Sustainable Production and Consumption*, vol. 20, pp. 253–272, Oct. 2019, doi: 10.1016/j.spc.2019.07.001.
[59] U. Gelbmann and B. Hammerl, "Integrative re-use systems as innovative business models for devising sustainable product–service-systems," *Journal of Cleaner Production*, vol. 97, pp. 50–60, Jun. 2015, doi: 10.1016/j.jclepro.2014.01.104.
[60] N. Boorsma, D. Peck, T. Bakker, C. Bakker, and R. Balkenende, "The strategic value of design for remanufacturing: a case study of professional imaging equipment," *Jnl Remanufactur*, vol. 12, no. 2, pp. 187–212, Jul. 2022, doi: 10.1007/s13243-021-00107-0.
[61] G. D. Hatcher, W. L. Ijomah, and J. F. C. Windmill, "Design for remanufacture: a literature review and future research needs," *Journal of Cleaner Production*, vol. 19, no. 17–18, pp. 2004–2014, Nov. 2011, doi: 10.1016/j.jclepro.2011.06.019.
[62] E. Sundin and M. Lindahl, "Rethinking product design for remanufacturing to facilitate integrated product service offerings," in *2008 IEEE International Symposium on Electronics and the Environment*, San Francisco, CA, USA: IEEE, May 2008, pp. 1–6. doi: 10.1109/ISEE.2008.4562901.
[63] L. Lindkvist Haziri and E. Sundin, "Supporting design for remanufacturing - A framework for implementing information feedback from remanufacturing to product design," *Jnl Remanufactur*, vol. 10, no. 1, pp. 57–76, Apr. 2020, doi: 10.1007/s13243-019-00074-7.

[64] R. Mugge, B. Jockin, and N. Bocken, “How to sell refurbished smartphones? An investigation of different customer groups and appropriate incentives,” *Journal of Cleaner Production*, vol. 147, pp. 284–296, Mar. 2017, doi: 10.1016/j.jclepro.2017.01.111.

[65] R. Mugge, W. De Jong, O. Person, and E. J. Hultink, “‘If It Ain’t Broke, Don’t Explain It’: The Influence of Visual and Verbal Information about Prior Use on Consumers’ Evaluations of Refurbished Electronics,” *The Design Journal*, vol. 21, no. 4, pp. 499–520, Jul. 2018, doi: 10.1080/14606925.2018.1472856.

[66] E. Worrell and M. A. Reuter, “Definitions and Terminology,” in *Handbook of Recycling*, Elsevier, 2014, pp. 9–16. doi: 10.1016/B978-0-12-396459-5.00002-7.

[67] “The Circular Design Guide,” ELLEN MACARTHUR FOUNDATION. Accessed: Oct. 30, 2025. [Online]. Available: https://www.ellenmacarthurfoundation.org/circular-design-guide/overview

[68] “The Design Process,” Sustainability Guide. Accessed: Oct. 30, 2025. [Online]. Available: https://sustainabilityguide.eu/methods/the-design-process/

[69] E. G. Andersson, “Approaches to Sustainable Design.” Accessed: Oct. 30, 2025. [Online]. Available: https://sustainabledesigncards.dk/

[70] A. Franconi, N. Terzioglu, S. Fregoni, R. Carvalho, and M. Ghoreishi, “An open-source collection of systemic design strategies to accelerate the circular economy.” Accessed: Nov. 06, 2025. [Online]. Available: https://www.circulardesign.it/?wppb_referer_url=https%3A%2F%2Fwww.circulardesign.it%2Ftool-editor%2F

[71] C. Sassanelli, A. Urbinati, P. Rosa, D. Chiaroni, and S. Terzi, “Addressing circular economy through design for X approaches: A systematic literature review,” *Computers in Industry*, vol. 120, p. 103245, Sep. 2020, doi: 10.1016/j.compind.2020.103245.

[72] A. Di Gerlando *et al.*, “Circularity potential of electric motors in e-mobility: methods, technologies, challenges,” *Jnl Remanufactur*, vol. 14, no. 2–3, pp. 315–357, Nov. 2024, doi: 10.1007/s13243-024-00143-6.

[73] D. Tiwari, J. Miscandlon, A. Tiwari, and G. W. Jewell, “A Review of Circular Economy Research for Electric Motors and the Role of Industry 4.0 Technologies,” *Sustainability*, vol. 13, no. 17, p. 9668, Aug. 2021, doi: 10.3390/su13179668.

[74] J. R. Pérez-Cardona, N. Shakelly, M. J. Triebe, and J. W. Sutherland, “Optimizing electric traction motor design: Analyzing the benefits of a circular economy,” *Journal of Cleaner Production*, vol. 486, p. 144522, Jan. 2025, doi: 10.1016/j.jclepro.2024.144522.

[75] Abimbola Oluwatoyin Adegbite *et al.*, “Modern electric motors: A review of sustainable design and maintenance principles: scrutinizing the latest trends focusing on motor efficiency, sustainability, recyclability, and reduced maintenance,” *World J. Adv. Res. Rev.*, vol. 20, no. 3, pp. 1198–1211, Dec. 2023, doi: 10.30574/wjarr.2023.20.3.2560.

[76] S. Schötz and P. Molenda, “Lean Remanufacturing Of Electric Motors: Process Steps, Challenges And Solutions,” 2024, doi: 10.15488/17707.

[77] S. Soh, S. K. Ong, and A. Y. C. Nee, “Design for assembly and disassembly for remanufacturing,” *Assembly Automation*, vol. 36, no. 1, pp. 12–24, Feb. 2016, doi: 10.1108/AA-05-2015-040.

[78] S. Prendeville, D. Peck, R. Balkenende, E. Cor, K. Jansson, and I. Karvonen, “Map of Remanufacturing Product Design Landscape,” 645984, Jan. 2016.
[79] “The technical cycle of the butterfly diagram,” ELLEN MACARTHUR FOUNDATION. Accessed: Nov. 04, 2025. [Online]. Available: https://www.ellenmacarthurfoundation.org/articles/the-technical-cycle-of-the-butterfly-diagram
[80] W. Cai, X. Wu, M. Zhou, Y. Liang, and Y. Wang, “Review and Development of Electric Motor Systems and Electric Powertrains for New Energy Vehicles,” *Automot. Innov.*, vol. 4, no. 1, pp. 3–22, Feb. 2021, doi: 10.1007/s42154-021-00139-z.
[81] Z. Cao, A. Mahmoudi, S. Kahourzade, and W. L. Soong, “An Overview of Electric Motors for Electric Vehicles,” in *2021 31st Australasian Universities Power Engineering Conference (AUPEC)*, Perth, Australia: IEEE, Sep. 2021, pp. 1–6. doi: 10.1109/AUPEC52110.2021.9597739.
[82] Yimin Gao, M. Ehsani, and J. M. Miller, “Hybrid Electric Vehicle: Overview and State of the Art,” in *Proceedings of the IEEE International Symposium on Industrial Electronics, 2005. ISIE 2005.*, Dubrovnik, Croatia: IEEE, 2005, pp. 307–316. doi: 10.1109/ISIE.2005.1528929.
[83] F. Un-Noor, S. Padmanaban, L. Mihet-Popa, M. Mollah, and E. Hossain, “A Comprehensive Study of Key Electric Vehicle (EV) Components, Technologies, Challenges, Impacts, and Future Direction of Development,” *Energies*, vol. 10, no. 8, p. 1217, Aug. 2017, doi: 10.3390/en10081217.
[84] J. De Santiago *et al.*, “Electrical Motor Drivelines in Commercial All-Electric Vehicles: A Review,” *IEEE Trans. Veh. Technol.*, vol. 61, no. 2, pp. 475–484, Feb. 2012, doi: 10.1109/TVT.2011.2177873.
[85] D. Basso *et al.*, “Improving Motor and Drive System Performance - A Sourcebook for Industry,” EERE Publication and Product Library, DOE/GO-102014-4356; 6794, 2014. Accessed: Jun. 25, 2025. [Online]. Available: https://www.energy.gov/sites/prod/files/2014/04/f15/amo_motors_sourcebook_web.pdf
[86] J. Dong, Y. Huang, L. Jin, and H. Lin, “Comparative Study of Surface-Mounted and Interior Permanent-Magnet Motors for High-Speed Applications,” *IEEE Trans. Appl. Supercond.*, vol. 26, no. 4, pp. 1–4, Jun. 2016, doi: 10.1109/TASC.2016.2514342.
[87] G. Du, N. Li, Q. Zhou, W. Gao, L. Wang, and T. Pu, “Multi-Physics Comparison of Surface-Mounted and Interior Permanent Magnet Synchronous Motor for High-Speed Applications,” *Machines*, vol. 10, no. 8, p. 700, Aug. 2022, doi: 10.3390/machines10080700.
[88] A. Vagati, G. Pellegrino, and P. Guglielmi, “Comparison between SPM and IPM motor drives for EV application,” in *The XIX International Conference on Electrical Machines - ICEM 2010*, Rome, Italy: IEEE, Sep. 2010, pp. 1–6. doi: 10.1109/ICELMACH.2010.5607911.
[89] G. Pellegrino, A. Vagati, P. Guglielmi, and B. Boazzo, “Performance Comparison Between Surface-Mounted and Interior PM Motor Drives for Electric Vehicle Application,” *IEEE Trans. Ind. Electron.*, vol. 59, no. 2, pp. 803–811, Feb. 2012, doi: 10.1109/TIE.2011.2151825.
[90] S. E. Asanov and F. Sh. Umerov, “COMPARATIVE ANALYSIS OF INTERIOR PERMANENT MAGNET MOTORS (IPM) AND SURFACE PERMANENT MAGNET MOTORS (SPM),” vol. Railway transport: topical issues and innovations, 2023 №4.

[91] M. Gobbi, A. Sattar, R. Palazzetti, and G. Mastinu, “Traction motors for electric vehicles: Maximization of mechanical efficiency – A review,” *Applied Energy*, vol. 357, p. 122496, Mar. 2024, doi: 10.1016/j.apenergy.2023.122496.
[92] X. D. Xue, K. W. E. Cheng, and N. C. Cheung, “Selection of Electric Motor Drives for Electric Vehicles,” presented at the 2008 Australasian Universities Power Engineering Conference (AUPEC’08),
[93] D. G. Dorrell, “Are wound-rotor synchronous motors suitable for use in high efficiency torque-dense automotive drives?,” in *IECON 2012 - 38th Annual Conference on IEEE Industrial Electronics Society*, Montreal, QC, Canada: IEEE, Oct. 2012, pp. 4880–4885. doi: 10.1109/IECON.2012.6389578.
[94] A. Hussain *et al.*, “Wound Rotor Synchronous Motor as Promising Solution for Traction Applications,” *Electronics*, vol. 11, no. 24, p. 4116, Dec. 2022, doi: 10.3390/electronics11244116.
[95] D. Fallows, S. Nuzzo, and M. Galea, “AN EVALUATION OF EXCITERLESS TOPOLOGIES FOR MEDIUM POWER WOUND-FIELD SYNCHRONOUS GENERATORS,” *IET Conf. Proc.*, vol. 2020, no. 7, pp. 116–121, May 2021, doi: 10.1049/icp.2021.1047.
[96] G. B. Haxel, J. B. Hedrick, and G. J. Orris, “Rare Earth Elements—Critical Resources for High Technology,” U.S. Geological Survey.
[97] S. Constantinides, “Balancing Material Supply and Demand within the Magnet Industry,” presented at the Magnetics 2015 - The International forum on Magnetic Application, Technologies & Materials, Orlando, Jan. 2015. Accessed: Jul. 03, 2025. [Online]. Available: https://www.arnoldmagnetics.com/wp-content/uploads/2017/10/Balancing-Material-Supply-and-Demand-within-the-Magnet-Industry-Constantinides-Magnetics-2015-psn-lo-res.pdf
[98] B. S. Van Gosen, P. L. Verplanck, K. R. Long, J. Gambogi, and R. R. Seal II., “The Rare-Earth Elements — Vital to Modern Technologies and Lifestyles,” U.S. Geological Survey, Fact Sheet, 2014.
[99] “Rare Earth Magnets and Motors: A European Call for Action. A report by the Rare Earth Magnets and Motors Cluster of the European Raw Materials Alliance. Berlin 2021,” Rare Earth Magnets and Motors Cluster of the European Raw Materials Alliance.
[100] J. Edmondson and M. takahashi, “Electric Motors for Electric Vehicles 2025-2035: Technologies, Materials, Markets, and Forecasts.” Accessed: Jun. 25, 2015. [Online]. Available: https://www.idtechex.com/en/research-report/electric-motors-for-electric-vehicles-2025-2035-technologies-materials-markets-and-forecasts/1031
[101] J. Edmondson, “Electric Motors for Electric Vehicles: Technologies and Market Outlook.” Accessed: Jun. 25, 2025. [Online]. Available: https://fpc-event.co.uk/wp-content/uploads/2022/03/james.edmondson.electric_machines-1.pdf
[102] J. M. D. Coey, “Perspective and Prospects for Rare Earth Permanent Magnets,” *Engineering*, vol. 6, no. 2, pp. 119–131, Feb. 2020, doi: 10.1016/j.eng.2018.11.034.
[103] “Price Development of Selected Rare Earths,” Rare Earths. Accessed: Jun. 27, 2025. [Online]. Available: https://rareearths.com/price-charts/
[104] “EU challenges China’s export restrictions on rare earths.” EU Commission - Press release, Mar. 12, 2012. Accessed: Jun. 27, 2025. [Online]. Available:

https://ec.europa.eu/commission/presscorner/api/files/document/print/en/memo_12_182/MEMO_12_182_EN.pdf
[105] Z.-Z. Li, Q. Meng, L. Zhang, O.-R. Lobont, and Y. Shen, "How do rare earth prices respond to economic and geopolitical factors?," *Resources Policy*, vol. 85, p. 103853, Aug. 2023, doi: 10.1016/j.resourpol.2023.103853.
[106] F. Giolito, A. Accardo, and E. Spessa, "Evaluation of the Environmental Benefit of an Eco-design Strategy on the Life Cycle Assessment of a Permanent Magnet Synchronous High-speed Electric Motor," *Transportation Research Procedia*, vol. 70, pp. 241–248, 2023, doi: 10.1016/j.trpro.2023.11.025.
[107] Y. Yang *et al.*, "REE Recovery from End-of-Life NdFeB Permanent Magnet Scrap: A Critical Review," *J. Sustain. Metall.*, vol. 3, no. 1, pp. 122–149, Mar. 2017, doi: 10.1007/s40831-016-0090-4.
[108] J. H. Rademaker, R. Kleijn, and Y. Yang, "Recycling as a Strategy against Rare Earth Element Criticality: A Systemic Evaluation of the Potential Yield of NdFeB Magnet Recycling," *Environ. Sci. Technol.*, vol. 47, no. 18, pp. 10129–10136, Sep. 2013, doi: 10.1021/es305007w.
[109] MAHLE, "MAHLE develops highly efficient magnet-free electric motor," Mahle Newsroom. Accessed: Jun. 20, 2025. [Online]. Available: https://newsroom.mahle.com/press/en/press-releases/mahle-develops-highly-efficient-magnet-free-electric-motor--82368#
[110] ZF, "ZF makes magnet-free electric motor uniquely compact and competitive," ZF Press center. Accessed: Jun. 20, 2025. [Online]. Available: https://press.zf.com/press/en/releases/release_60480.html
[111] Renault, "Renault ZOE," Press information. Accessed: Jun. 20, 2025. [Online]. Available: https://www.press.renault.co.uk/assets/documents/original/15365-RenaultZOEpresskit.pdf
[112] Renault, "All-new Megane E-TECH Electric: delving into the heart of innovation - episode 3 -A patent for an eco-friendlier electric motor," series. Accessed: Jun. 20, 2025. [Online]. Available: https://media.renault.com/all-new-megane-e-tech-electric-delving-into-the-heart-of-innovation-episode-3/
[113] "How the BMW iX M60 Soups Up Its Most Powerful eDrive Powertrain," *MOTORTREND*. Accessed: Jun. 20, 2025. [Online]. Available: https://www.motortrend.com/news/2023-bmw-ix-m60-xdrive50-edrive-electric-motors-explained/photos
[114] "Cyber Truck Owner's manual." Accessed: Jun. 20, 2025. [Online]. Available: https://www.tesla.com/ownersmanual/cybertruck/en_us/Owners_Manual.pdf
[115] "The 2019 Audi e-tron Introduction - eSelf-Study Program 990993." Audi of America, LLC, Feb. 2019. Accessed: Jul. 07, 2025. [Online]. Available: https://static.nhtsa.gov/odi/tsbs/2019/MC-10155750-9999.pdf
[116] R. Thomas, H. Husson, L. Garbuio, and L. Gerbaud, "Comparative study of the Tesla Model S and Audi e-Tron Induction Motors," in *2021 17th Conference on Electrical Machines, Drives and Power Systems (ELMA)*, Sofia, Bulgaria: IEEE, Jul. 2021, pp. 1–6. doi: 10.1109/ELMA52514.2021.9503055.
[117] AEM, "HDRM 300 Next-generation traction motors for commercial vehicles," AEM Advanced Electric Machines. Accessed: Jun. 22, 2025. [Online]. Available: https://advancedelectricmachines.com/hdrm-300/

[118] J. Weisheng Jiang, “THREE-PHASE 24/16 SWITCHED RELUCTANCE MACHINE FOR HYBRID ELECTRIC POWERTRAINS: DESIGN AND OPTIMIZATION,” Doctor of Philosophy, McMaster University, Hamilton, Ontario, 2015. Accessed: Jul. 03, 2025. [Online]. Available: https://macsphere.mcmaster.ca/bitstream/11375/19087/2/Jiang_Weisheng_final_submission_2016_April_PhD.pdf

[119] V. Madonna, C. M. Meano, R. Cossu, M. Pensato, and K. F. Hansen, “Investigating the Impact of Material Cost Fluctuations on the Total Manufacturing Cost of EV Traction Machines,” in *2023 IEEE Workshop on Electrical Machines Design, Control and Diagnosis (WEMDCD)*, Newcastle upon Tyne, United Kingdom: IEEE, Apr. 2023, pp. 1–6. doi: 10.1109/WEMDCD55819.2023.10110901.

[120] Institute for Power Electronics and Electrical Drives, RWTH Aachen University and B. Burkhart, “Technology, Research and Applications of Switched Reluctance Drives,” *CPSS TPEA*, vol. 2, no. 1, pp. 12–27, Apr. 2017, doi: 10.24295/CPSSTPEA.2017.00003.

[121] W. Uddin, T. Husain, Y. Sozer, and I. Husain, “Design Methodology of a Switched Reluctance Machine for Off-Road Vehicle Applications,” *January 04 2016*, vol. 52, doi: 10.1109/TIA.2015.2514283.

[122] Advanced Propulsion Center UK, “Power Electronics Roadmap 2020,” Feb. 2021. Accessed: Apr. 04, 2024. [Online]. Available: https://www.apcuk.co.uk/wp-content/uploads/2021/09/https___www.apcuk_.co_.uk_app_uploads_2021_02_Exec-summary-Technology-Roadmap-Power-Electronics-final.pdf

[123] Hummel, “Electric Car Teardown—Disruption Ahead?”

[124] Z. Q. Zhu, W. Q. Chu, and Y. Guan, “Quantitative comparison of electromagnetic performance of electrical machines for HEVs/EVs,” *Trans. Electr. Mach. Syst.*, vol. 1, no. 1, pp. 37–47, Mar. 2017, doi: 10.23919/TEMS.2017.7911107.

[125] A. V. Radun, “Design considerations for the switched reluctance motor,” *IEEE Trans. on Ind. Applicat.*, vol. 31, no. 5, pp. 1079–1087, Oct. 1995, doi: 10.1109/28.464522.

[126] P. J. Lawrenson, J. M. Stephenson, N. N. Fulton, P. T. Blenkinsop, and J. Corda, “Variable-speed switched reluctance motors,” *IEE Proc. B Electr. Power Appl. UK*, vol. 127, no. 4, p. 253, 1980, doi: 10.1049/ip-b.1980.0034.

[127] K. M. Rahman, B. Fahimi, G. Suresh, A. V. Rajarathnam, and M. Ehsani, “Advantages of switched reluctance motor applications to EV and HEV: design and control issues,” *IEEE Trans. on Ind. Applicat.*, vol. 36, no. 1, pp. 111–121, Feb. 2000, doi: 10.1109/28.821805.

[128] T. J. E. Miller, “Optimal Design of Switched Reluctance Motors,” *IEEE TRANSACTIONS ON INDUSTRIAL ELECTRONICS*, vol. 49, no. 1, pp. 15–27, 2002.

[129] R. Krishnan, *Switched Reluctance Motor Drives: Modeling, Simulation, Analysis, Design, and Applications*, 1st ed. CRC Press, 2017. doi: 10.1201/9781420041644.

[130] D. Meeker, “Finite Element Method Magnetics Version 4.2.” 2019.

[131] V. Madonna, C. M. Meano, S. Mafrici, and K. F. Hansen, “Copper vs. aluminium winding SRMs: a multidisciplinary performance assessment,” in *12th International Conference on Power Electronics, Machines and Drives (PEMD 2023)*, Brussels, Belgium: Institution of Engineering and Technology, 2023, pp. 49–56. doi: 10.1049/icp.2023.1978.

[132] A. Dorneles Callegaro, J. Liang, J. W. Jiang, B. Bilgin, and A. Emadi, “Radial Force Density Analysis of Switched Reluctance Machines: The Source of Acoustic Noise,” *IEEE Trans. Transp. Electrific.*, vol. 5, no. 1, pp. 93–106, Mar. 2019, doi: 10.1109/TTE.2018.2887338.

[133] D. E. Cameron, J. H. Lang, and S. D. Umans, “The origin and reduction of acoustic noise in doubly salient variablereluctance motors,” *IEEE TRANSACTIONS ON INDUSTRY APPLICATIONS*, vol. 28, no. 6, pp. 1250–1255, Dec. 1992.

[134] “RENAULT KANGOO AND KANGOO E-TECH 100% electric,” Renault web page. Accessed: Jun. 28, 2025. [Online]. Available: https://cdn.group.renault.com/ren/gb/transversal-assets/brochures/van-ebrochures/KANGOO-eBrochure.pdf.asset.pdf/57c4a55762.pdf

[135] E. A. Grunditz and T. Thiringer, “Performance Analysis of Current BEVs Based on a Comprehensive Review of Specifications,” *IEEE Trans. Transp. Electrific.*, vol. 2, no. 3, pp. 270–289, Sep. 2016, doi: 10.1109/TTE.2016.2571783.

[136] austin H. bonnet and C. Yung, “A CONSTRUCTION, PERFORMANCE AND RELIABILITY COMPARISON FOR PRE-EPACT, EPACT AND PREMIUM-EFFICIENT MOTORS,” in *2006 Record of Conference Papers*, IEEE, p. 7.

[137] ABB, “Motors don’t just fail..do they? A guide to preventing failure,” ABB. Accessed: Dec. 17, 2024. [Online]. Available: https://new.abb.com/docs/librariesprovider53/about-downloads/motors-ebook.pdf

[138] A. Selema, M. N. Ibrahim, and P. Sergeant, “Metal Additive Manufacturing for Electrical Machines: Technology Review and Latest Advancements,” *Energies*, vol. 15, no. 3, p. 1076, Jan. 2022, doi: 10.3390/en15031076.

[139] L. Gargalis *et al.*, “Additive Manufacturing and Testing of a Soft Magnetic Rotor for a Switched Reluctance Motor,” *IEEE Access*, vol. 8, pp. 206982–206991, 2020, doi: 10.1109/ACCESS.2020.3037190.

[140] G.-M. Tseng, K. Jhong, M.-C. Tsai, P.-W. Huang, and W.-H. Lee, “Application of Additive Manufacturing for Low Torque Ripple of 6/4 Switched Reluctance Motor,” in *2016 19th International Conference on Electrical Machines and Systems (ICEMS)*, Chiba, Japan: IEEE, Feb. 2017.

[141] H. Zhao *et al.*, “State-of-the-Art Shaped Profile Windings and Their Integrated Cooling Configurations Enabled by Additive Manufacturing Technology,” *IEEE Trans. Transp. Electrific.*, pp. 1–1, 2025, doi: 10.1109/TTE.2025.3569591.

[142] N. Simpson, G. Yiannakou, H. Felton, J. Robinson, A. Arjunan, and P. H. Mellor, “Direct Thermal Management of Windings Enabled by Additive Manufacturing,” *IEEE Trans. on Ind. Applicat.*, vol. 59, no. 2, pp. 1319–1327, Mar. 2023, doi: 10.1109/TIA.2022.3209171.

[143] Equipmake, “AMPERE-220 The Additive Manufactured Motor.” Accessed: Dec. 17, 2024. [Online]. Available: https://equipmake.co.uk/products/ampere-220/

[144] J. Auer and A. Meincke, “Comparative life cycle assessment of electric motors with different efficiency classes: a deep dive into the trade-offs between the life cycle stages in ecodesign context,” *Int J Life Cycle Assess*, vol. 23, no. 8, pp. 1590–1608, Aug. 2018, doi: 10.1007/s11367-017-1378-8.

[145] advancedelectricmachines, “SSRD Next-generation passenger car motor delivering ultra-high performance and sustainability,” AEM Advanced Electric Machines. Accessed: Oct. 05, 2025. [Online]. Available: SSRD – ultra-high performance for passenger cars | AEM

[146] Ricardo, “Alumotor: the environmentally efficient e-motor solution,” Ricardo. Accessed: Oct. 05, 2025. [Online]. Available: https://www.ricardo.com/en/news-and-insights/industry-insights/alumotor-the-environmentally-efficient-e-motor-solution

[147] P. H. Mellor, D. Salt, N. Simpson, and R. Wrobel, “Comparative Study of Copper and Aluminium Conductors - Future Cost Effective PM Machines,” in *7th IET International Conference on Power Electronics, Machines and Drives (PEMD 2014)*, Manchester, UK: Institution of Engineering and Technology, 2014, p. 2.1.02-2.1.02. doi: 10.1049/cp.2014.0292.

[148] R. Wrobel, N. Simpson, P. H. Mellor, J. Goss, and D. A. Staton, “Design of a Brushless PM Starter Generator for Low-Cost Manufacture and a High-Aspect-Ratio Mechanical Space Envelope,” *IEEE Trans. on Ind. Applicat.*, vol. 53, no. 2, pp. 1038–1048, Mar. 2017, doi: 10.1109/TIA.2016.2633944.

[149] S. Ayat, R. Wrobel, J. Baker, and D. Drury, “A comparative study between aluminium and copper windings for a modular-wound IPM electric machine,” in *2017 IEEE International Electric Machines and Drives Conference (IEMDC)*, Miami, FL, USA: IEEE, May 2017, pp. 1–8. doi: 10.1109/IEMDC.2017.8002010.

[150] G. Petrelli *et al.*, “Comparison of Aluminium and Copper Conductors in Hairpin Winding Design for High Power Density Traction Motors,” in *2022 International Conference on Electrical Machines (ICEM)*, Valencia, Spain: IEEE, Sep. 2022, pp. 1635–1641. doi: 10.1109/ICEM51905.2022.9910796.

[151] T. A. Burress *et al.*, “EVALUATION OF THE 2010 TOYOTA PRIUS HYBRID SYNERGY DRIVE SYSTEM.” Accessed: Apr. 04, 2024. [Online]. Available: https://info.ornl.gov/sites/publications/files/Pub26762.pdf

[152] Stevens Tim, “The 2025 Hyundai Ioniq 5 N Is So Good It’ll Make Enthusiasts Like EVs.” Accessed: Apr. 04, 2024. [Online]. Available: https://www.motor1.com/reviews/697151/2025-hyundai-ioniq-5-n-review/

[153] A. Walker, M. Galea, D. Gerada, C. Gerada, A. Mebarki, and N. Brown, “Development and Design of a High Performance Traction Machine for the FreedomCar 2020 Traction Machine Targets.”

[154] A. W. Leissa, *Vibration of shells*, vol. 288. Washington, Scientific and Technical Information Office, National Aeronautics and Space Administration, 1973. Accessed: Mar. 23, 2026. [Online]. Available: https://archive.org/details/vibrationofshell0000leis

[155] SKF, “Rolling bearings.” SKF, Oct. 2018.

[156] P. Giangrande, V. Madonna, S. Nuzzo, and M. Galea, “Moving Toward a Reliability-Oriented Design Approach of Low-Voltage Electrical Machines by Including Insulation Thermal Aging Considerations,” *IEEE Trans. Transp. Electrific.*, vol. 6, no. 1, pp. 16–27, Mar. 2020, doi: 10.1109/TTE.2020.2971191.

[157] V. Madonna, P. Giangrande, and M. Galea, “Weibull Distribution and Geometrical Size Factor for Evaluating the Thermal Life of Electrical Machines’ Insulation,” in *IECON 2020 The 46th Annual Conference of the IEEE Industrial Electronics Society*, Singapore, Singapore: IEEE, Oct. 2020, pp. 1114–1119. doi: 10.1109/IECON43393.2020.9255227.

[158] N. G. Author, “FY2016 Electric Drive Technologies Annual Progress Report,” DOE/EE--1532, 1413876, Jul. 2017. doi: 10.2172/1413876.
[159] J. M. Miller, “2013 U.S. DOE Hydrogen and Fuel Cells Program and Vehicle Technologies Program Annual Merit Review and Peer Evaluation Meeting,” Project ID: APE051, May 2013.
[160] G. Lonca, R. Muggéo, H. Imbeault-Tétreault, S. Bernard, and M. Margni, “Does material circularity rhyme with environmental efficiency? Case studies on used tires,” *Journal of Cleaner Production*, vol. 183, pp. 424–435, May 2018, doi: 10.1016/j.jclepro.2018.02.108.
[161] S. Mafrici, A. Accardo, E. Spessa, and A. Tenconi, “A Novel Scenario Analysis Framework for the Life Cycle Assessment of Permanent Magnet Synchronous Motors for Electric Vehicles,” *IEEE Access*, vol. 12, pp. 156837–156848, 2024, doi: 10.1109/ACCESS.2024.3486380.
[162] S. Mafrici, V. Madonna, C. Maria Meano, K. Friis Hansen, and A. Tenconi, “Switched Reluctance Machine for Transportation and Eco-Design: A Life Cycle Assessment,” *IEEE Access*, vol. 12, pp. 68334–68344, 2024, doi: 10.1109/ACCESS.2024.3400324.
[163] S. Mafrici, C. M. Meano, V. Madonna, F. Magni, and A. Tenconi, “Electric Motor Design for Circular Economy / Elektromotorendesign für die Kreislaufwirtschaft,” in *46th International Vienna Motor Symposium 14 - 16 May 2025*, Österreichischer Verein für Kraftfahrzeugtechnik (ÖVK), 2025. doi: 10.62626/61u7-sqmf.
[164] E. a Westberg, “Environmental Impact of an Electric Motor and Drive - Life Cycle Assessment and a study of a Circular Business Model,” 2021. Accessed: Dec. 13, 2023. [Online]. Available: http://www.diva-portal.se/smash/get/diva2:1658729/FULLTEXT01.pdf
[165] A. Rassõlkin *et al.*, “Life cycle analysis of electrical motor-drive system based on electrical machine type,” *Proc. Estonian Acad. Sci.*, vol. 69, no. 2, p. 162, 2020, doi: 10.3176/proc.2020.2.07.
[166] S. Orlova, A. Rassõlkin, A. Kallaste, T. Vaimann, and A. Belahcen, “Lifecycle Analysis of Different Motors from the Standpoint of Environmental Impact,” *Latvian Journal of Physics and Technical Sciences*, vol. 53, no. 6, pp. 37–46, Dec. 2016, doi: 10.1515/lpts-2016-0042.
[167] M. Torrent, E. Martínez, and P. Andrada, “Life cycle analysis on the design of induction motors,” *Int J Life Cycle Assess*, vol. 17, no. 1, pp. 1–8, Jan. 2012, doi: 10.1007/s11367-011-0332-4.
[168] P. Andrada, B. Blanqué, E. Martínez, J. I. Perat, J. A. Sánchez, and M. Torrent, “Comparison of environmental and life cycle impact of switched reluctance motor drive and inverter-fed induction motor drives,” *REPQJ*, vol. 1, no. 07, pp. 260–264, Apr. 2009, doi: 10.24084/repqj07.319.
[169] A. Rassolkin, S. Orlova, T. Vaimann, A. Belahcen, and A. Kallaste, “Environmental and life cycle cost analysis of a synchronous reluctance machine,” in *2016 57th International Scientific Conference on Power and Electrical Engineering of Riga Technical University (RTUCON)*, Riga: IEEE, Oct. 2016, pp. 1–5. doi: 10.1109/RTUCON.2016.7763127.
[170] W. Boughanmi, J. P. Manata, and D. Roger, “Contribution of LCA approach to the choice of rotating electrical machines for environmental impact minimization,” in *2012 XXth International Conference on Electrical Machines*, Marseille, France: IEEE, Sep. 2012, pp. 122–128. doi: 10.1109/ICElMach.2012.6349851.

[171] R. Orbay *et al.*, “Sustainable Design and LCA of non-RE PMSynRM with Bioplastic Rotor Shroud,” in *2022 12th International Conference on Power, Energy and Electrical Engineering (CPEEE)*, Shiga, Japan: IEEE, Feb. 2022, pp. 34–40. doi: 10.1109/CPEEE54404.2022.9738657.

[172] A. Nordelöf, E. Grunditz, S. Lundmark, A.-M. Tillman, M. Alatalo, and T. Thiringer, “Life cycle assessment of permanent magnet electric traction motors,” *Transportation Research Part D: Transport and Environment*, vol. 67, pp. 263–274, Feb. 2019, doi: 10.1016/j.trd.2018.11.004.

[173] H. Schillingmann, S. Gehler, and M. Henke, “Life cycle assessment of electrical machine production considering resource requirements and sustainability,” in *2021 11th International Electric Drives Production Conference (EDPC)*, Erlangen, Germany: IEEE, Dec. 2021, pp. 1–7. doi: 10.1109/EDPC53547.2021.9684195.

[174] A. Nordelöf, E. Grunditz, A.-M. Tillman, T. Thiringer, and M. Alatalo, “A scalable life cycle inventory of an electrical automotive traction machine—Part I: design and composition,” *Int J Life Cycle Assess*, vol. 23, no. 1, pp. 55–69, Jan. 2018, doi: 10.1007/s11367-017-1308-9.

[175] A. Nordelöf and A.-M. Tillman, “A scalable life cycle inventory of an electrical automotive traction machine—Part II: manufacturing processes,” *Int J Life Cycle Assess*, vol. 23, no. 2, pp. 295–313, Feb. 2018, doi: 10.1007/s11367-017-1309-8.

[176] S. Jain and B. N. Singh, “Environmental Impacts of Reclaiming, Recycling, and Reusing (R^3) Parts of Electric Vehicles’ Powertrain,” in *2022 IEEE International Conference on Power Electronics, Drives and Energy Systems (PEDES)*, Jaipur, India: IEEE, Dec. 2022, pp. 1–6. doi: 10.1109/PEDES56012.2022.10080569.

[177] A. Tintelecan, A. C.- Dobra, and C. Martis, “Life Cycle Assessment Comparison of Synchronous Motor and Permanent Magnet Synchronous Motor,” in *2020 International Conference and Exposition on Electrical And Power Engineering (EPE)*, Iasi, Romania: IEEE, Oct. 2020, pp. 205–210. doi: 10.1109/EPE50722.2020.9305636.

[178] A. Tintelecan, A. C. Dobra, and C. Martis, “LCA Indicators in Electric Vehicles Environmental Impact Assessment,” in *2019 Electric Vehicles International Conference (EV)*, Bucharest, Romania: IEEE, Oct. 2019, pp. 1–5. doi: 10.1109/EV.2019.8892893.

[179] *ISO 14044:2006. Environmental management. Life cycle assessment. Requirements and guidelines,*.

[180] *ISO 14040:2006. Environmental management. Life cycle assessment. Principles and framework.*, Place of Publication Not Identified.

[181] “Ecoivent Version 3.8.” Accessed: Apr. 04, 2024. [Online]. Available: https://support.ecoinvent.org/ecoinvent-version-3.8

[182] *SimaPro*. Accessed: Apr. 04, 2024. [Online]. Available: https://simapro.com/

[183] J. B. Guinee, “Handbook on life cycle assessment operational guide to the ISO standards,” *Int J LCA*, vol. 7, no. 5, pp. 311, BF02978897, Sep. 2002, doi: 10.1007/BF02978897.

[184] T. Yanni and P. J. Th. Venhovens, “Impact and Sensitivity of Vehicle Design Parameters on Fuel Economy Estimates,” presented at the SAE 2010 World Congress & Exhibition, Apr. 2010, pp. 2010-01–0734. doi: 10.4271/2010-01-0734.

[185] Bureau of International Recycling, S. Grimes, J. Donaldson, and J. Grimes, “Report on the Environmental Benefits of Recycling – 2016 edition,” 2016. Accessed: Dec. 13, 2023. [Online]. Available: https://www.bir.org/publications/facts-figures/download/172/174/36?method=view
[186] European Commission. Joint Research Centre. Institute for Environment and Sustainability., *International Reference Life Cycle Data System (ILCD) Handbook :general guide for life cycle assessment : detailed guidance.* LU: Publications Office, 2010. Accessed: Jul. 03, 2025. [Online]. Available: https://data.europa.eu/doi/10.2788/38479
[187] tim burress, “2013 U.S. DOE Hydrogen and Fuel Cells Program and Vehicle Technologies Program Annual Merit Review and Peer Evaluation Meeting,” Oak Ridge National Laboratory, Project ID: APE006, May 2013.
[188] “Quattroruote.” Accessed: Dec. 13, 2023. [Online]. Available: https://www.quattroruote.it/listino/
[189] “EVSpecifications - Specification, news and comparison.” Accessed: Dec. 13, 2023. [Online]. Available: https://www.evspecifications.com/
[190] “Automobile Catalog.” Accessed: Dec. 13, 2023. [Online]. Available: https://www.automobile-catalog.com/#gsc.tab=0
[191] IEA, “Global EV Outlook 2023 Catching up with climate ambitions.” Accessed: Dec. 13, 2023. [Online]. Available: https://iea.blob.core.windows.net/assets/dacf14d2-eabc-498a-8263-9f97fd5dc327/GEVO2023.pdf
[192] European Council, “Net electricity generation by type of fuel - monthly data.” Accessed: Jan. 26, 2024. [Online]. Available: https://www.consilium.europa.eu/en/infographics/how-is-eu-electricity-produced-and-sold/
[193] IEA, “World Energy Balances (2022).” Accessed: Mar. 08, 2025. [Online]. Available: https://www.iea.org/data-and-statistics/data-product/world-energy-balances-highlights
[194] “Sea-distances.org,” Sea-distances.org. Accessed: Mar. 08, 2025. [Online]. Available: https://sea-distances.org/
[195] EPA, “2021 Test Car List Data.” Accessed: Dec. 13, 2023. [Online]. Available: https://view.officeapps.live.com/op/view.aspx?src=https%3A%2F%2Fwww.epa.gov%2Fsystem%2Ffiles%2Fdocuments%2F2022-04%2F21-tstcar-2022-04-15.xlsx&wdOrigin=BROWSELINK
[196] Argonne National Laboratory, “D3 2014 BMW i3BEV.” Accessed: Dec. 13, 2023. [Online]. Available: https://www.anl.gov/taps/d3-2014-bmw-i3bev
[197] Ellen Macarthur foundation and Granta MAterial Intelligence, “Circularity Indicators - An approach to Measuring Circularity,” 2019. Accessed: Dec. 18, 2024. [Online]. Available: https://emf.thirdlight.com/link/3jtevhlkbukz-9of4s4/@/preview/1?o
[198] V. Elia, M. G. Gnoni, and F. Tornese, “Measuring circular economy strategies through index methods: A critical analysis,” *Journal of Cleaner Production*, vol. 142, pp. 2741–2751, Jan. 2017, doi: 10.1016/j.jclepro.2016.10.196.
[199] M. Niero and P. P. Kalbar, “Coupling material circularity indicators and life cycle based indicators: A proposal to advance the assessment of circular economy strategies at the product level,” *Resources, Conservation and*

Recycling, vol. 140, pp. 305–312, Jan. 2019, doi: 10.1016/j.resconrec.2018.10.002.

[200] K. Mantalovas and G. Di Mino, "Integrating Circularity in the Sustainability Assessment of Asphalt Mixtures," *Sustainability*, vol. 12, no. 2, p. 594, Jan. 2020, doi: 10.3390/su12020594.

[201] E. Bracquené, W. Dewulf, and J. R. Duflou, "Measuring the performance of more circular complex product supply chains," *Resources, Conservation and Recycling*, vol. 154, p. 104608, Mar. 2020, doi: 10.1016/j.resconrec.2019.104608.

[202] K. Vadoudi, P. Deckers, C. Demuytere, H. Askanian, and V. Verney, "Comparing a material circularity indicator to life cycle assessment: The case of a three-layer plastic packaging," *Sustainable Production and Consumption*, vol. 33, pp. 820–830, Sep. 2022, doi: 10.1016/j.spc.2022.08.004.

[203] L. Rigamonti and E. Mancini, "Life cycle assessment and circularity indicators," *Int J Life Cycle Assess*, vol. 26, no. 10, pp. 1937–1942, Oct. 2021, doi: 10.1007/s11367-021-01966-2.

[204] S. Manfredi, K. Allacker, N. Pelletier, and D. M. de Souza, *Product Environmental Footprint (PEF) Guide*.

[205] European Commission. Joint Research Centre., *Suggestions for updating the Organisation Environmental Footprint (OEF) method.* LU: Publications Office, 2019. Accessed: Dec. 13, 2023. [Online]. Available: https://data.europa.eu/doi/10.2760/424613

[206] Database & Support team at PRé Sustainability, "SimaPro database manual Methods library." Mar. 2023. Accessed: Sep. 05, 2025. [Online]. Available: https://simapro.com/wp-content/uploads/2020/10/DatabaseManualMethods.pdf

[207] L. zampori and R. Plant, "Suggestions for updating the Product Environmental Footprint (PEF) method," European Commission - JRC, 2019.

Appendix

A.1 Circular Design Validation: Rotor assembly

This section describes the validation of some features introduced in the SRM design. Specifically, a partial teardown of the motor has been executed to substitute bearings, shaft and sealing damaged by a malfunctioning of the test rig during experimental activities. Indeed, the motor's shaft bent at the location of the sealing ring seat as shown in Figure A.1, where is noticeable the inclination of the shaft itself in the externally to the housing. In order to analyse and replace the damaged parts, was not necessary to fully disassembly the motor, but the sole rotor assembly was extracted from the housing.

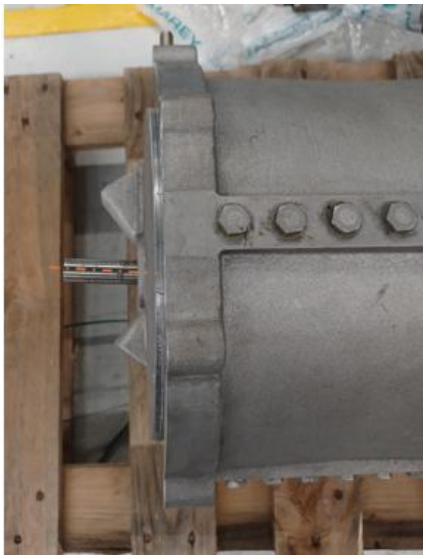

Figure A.1 Detail of the motor (front-top view) and final part of the bent shaft after testing activities

However, the teardown execution followed the path described in Chapter 3, through the unscrewing of the rear aluminium cover and the removal of shaft, rotor and bearings pushed away from screws into the front side of the cover. The steps are displayed in Figure A.2. In particular, Figure a) shows the unscrewed rear cover, while in Figure b) and c) are noticeable both externally and internally to the motor housing, the screws purposely mounted into the front side of the housing to push away the rotor assembly towards the rear side as visible from Figure d)

Figure A.2 Rotor assembly teardown steps: a) unscrewing of the rear cover, b) and c) external and inner view of the housing and stator with the three screws used to push away the rotor assembly d) extraction of the components on rear side

Specifically, the screws have been used to push on front bearings surface and are necessary because the extraction of these parts, without damaging recoverable components, would have been not possible as the bearing after usage could have interference, or very small clearances with the housing. with the housing. The teardown was instead easily executed in few minutes and shaft and bearings, damaged during testing, have been substituted, recovering all the other parts. It is possible to apply same approach to remove stator assembly at the end of the first lifecycle as described in the remanufacturing strategies. The features useful to implement such a strategy will be validated in future.

A.2 Step1 Baseline Inventory

A complete inventory related to Baseline case study is reported in Table A.1 allowing to LCA practitioners to reproduce the same study, described in the paper. The table is reporting all data divided in sub tables related to each component and by cycle phases, facilitating comprehension of the breakdown results illustrated in the thesis.

For each flow is reported if is an input or output of the model, its general description and the selected voice within the Ecoinvent database. Furthermore, there's a column related to the manufacturing process, that connects the data to the literature reference model (cited in the thesis). To avoid repetitions the detailed LCI is reported just for the Baseline as the other scenarios and steps followed the same approach, with the exception of the EoL phase that is however explained in detail in Chapter 4.

Table A.1 Inventory of the baseline for the LCA step1

Stator					
Direction	**Flow description**	**Manufacturing Process**	**Unit**	**Value**	**Selected process in database**
Inflow	Unalloyed steel	Hot rolling silicon Steel	kg	32.7	Steel, unalloyed {RER}| steel production, converter, unalloyed | APOS, U
Inflow	Ferrosilicon		g	700.7	Ferrosilicon {RoW}| production | APOS, U
Inflow	Aluminium		g	133.5	Aluminium, primary, ingot {IAI Area, EU27 & EFTA}| production | APOS, U
Inflow	Hot rolling of silicon steel alloy		kg	33.4	Hot rolling, steel {RER}| processing | APOS, U
Inflow	Phenolic resin	electrical steel manufacturing	g	29.3	Phenolic resin {RER}| market for phenolic resin | APOS, U
Inflow	Electricity		kWh	18.4	Electricity, medium voltage {IT}| market for | APOS, U
Inflow	Propane/LPG		g	351.2	Liquefied petroleum gas {Europe without Switzerland}| market for liquefied petroleum gas | APOS, U
Inflow	Sulfuric acid		g	556.1	Sulfuric acid {RER}| production | APOS, U
Inflow	Rolling/lubricating oil		g	11.7	Lubricating oil {RER}| production | APOS, U
Inflow	Quicklime powder		g	23.4	Quicklime, milled, packed {RER}| market for quicklime, milled, packed | APOS, U
Inflow	Electricity	Punching of stator laminations	Wh	198.2	Electricity, medium voltage {IT}| market for | APOS, U
Inflow	Electricity	Stackling&welding of stator laminations	Wh	30.2	Electricity, medium voltage {IT}| market for | APOS, U
Inflow	Argon shielding gas		g	30.2	Argon, liquid {RER}| market for argon, liquid | APOS, U
Inflow	Extrusion of plastic film for the slot insulation	PET foil manufacturing	kg	0.2	Extrusion, plastic film {RER}| extrusion, plastic film | APOS, U

Inflow	PET granulates for PET foil manufacturing		g	166.0	Polyethylene terephthalate, granulate, bottle grade {RER}| production | APOS, U
Outflow	Steel scrap, Punching process	Punching	kg	13.7	Scrap steel {Europe without Switzerland}| market for scrap steel | APOS, U
Outflow	Steel scrap, stackling and welding process	Stackling&welding	g	152.4	Scrap steel {Europe without Switzerland}| market for scrap steel | APOS, U
Outflow	Carbon dioxide to air,	electrical steel manufacturing	g	1053.7	Carbon dioxide
Outflow	Nitrogen oxides to air		g	2.9	Nitrogen oxides
Outflow	Sulfur oxides to air		g	1.8	Sulfur oxides
Outflow	Steel scrap		kg	3.3	Scrap steel {Europe without Switzerland}| market for scrap steel | APOS, U
Outflow	Sludge, dry content		g	96.6	Refinery sludge {Europe without Switzerland}| treatment of refinery sludge, hazardous waste incineration | APOS, U
Winding					
Direction	**Flow description**	**Manufacturing Process**	**Unit**	**Value**	**Selected process in database**
Inflow	drawing of pure copper wire	Copper wire drawing	kg	5.7	Wire drawing, copper {RER}| processing | APOS, U
Inflow	copper ingot		kg	5.7	Copper {RER}| production, primary | APOS, U
Inflow	Liquid enamel, polyester share	Copper wire enamaling	g	245.2	Polyester resin, unsaturated {RER}| market for polyester resin, unsaturated | APOS, U
Inflow	Liquid enamel, xylene solvent share		g	131.1	Xylene {RER}| market for xylene | APOS, U
Inflow	Electricity		kWh	2.9	Electricity, medium voltage {IT}| market for | APOS, U
Inflow	Silicone granulates	Silicone cable manufacturing	g	28.0	Silicone product {RER}| market for silicone product | APOS, U
Inflow	Extrusion of silicone rubber tubing		g	28.1	Extrusion, plastic pipes {RER}| extrusion, plastic pipes | APOS, U
Inflow	Nylon lacing cord	Bandaging and pressing	g	6.0	Nylon 6-6 {RER}| market for nylon 6-6 | APOS, U
Inflow	Electricity		Wh	24.0	Electricity, medium voltage {IT}| market for | APOS, U
Inflow	Electricity	Impregnation and curing	Wh	456.0	Electricity, medium voltage {IT}| market for | APOS, U
Inflow	Silica filler in epoxy resin		g	102.0	Silica sand {DE}| production | APOS, U
Inflow	Liquid epoxy resin		g	321.0	Epoxy resin, liquid {RER}| market for epoxy resin, liquid | APOS, U
Inflow	copper ingot for lugs	Copper sheet rolling	g	51.0	Copper {RER}| production, primary | APOS, U
Inflow	Sheet rolling of copper		g	51.0	Sheet rolling, copper {RER}| processing | APOS, U
Inflow	Machine working of copper	Copper lugs manufacturing	g	51.0	Metal working, average for copper product manufacturing {RER}| processing | APOS, U

Inflow	Tin plated copper lugs	Lugs plating	dm^2	0.4	Tin plating, pieces {RER}| processing | APOS, U
Inflow	Electricity	Wire termination	Wh	24.0	Electricity, medium voltage {IT}| market for | APOS, U
Outflow	Xylene to air	Copper wire enamaling	g	131.1	Xylene
Outflow	Copper scrap	Winding and phase isolation installation	g	55.9	Scrap copper {Europe without Switzerland}| market for scrap copper | APOS, U
Outflow	Hydrocarbons to air	Impregnation and curing	g	16.0	Hydrocarbons, aliphatic, unsaturated
Outflow	Copper scrap	Wire termination	g	36.0	Scrap copper {Europe without Switzerland}| market for scrap copper | APOS, U

Shaft

Direction	Flow description	Manufacturing Process	Unit	Value	Selected process in database
Inflow		Hot rolling of low-alloy carbon steel	kg	4.9	Hot rolling, steel {RER}| processing | APOS, U
Inflow			kg	4.9	Steel, low-alloyed {RER}| steel production, converter, low-alloyed | APOS, U
Inflow		Section bar rolling of steel coil	kg	4.9	Section bar rolling, steel {RER}| processing | APOS, U
Inflow		Machining working of steel	kg	4.9	Metal working, average for steel product manufacturing {RER}| processing | APOS, U
Inflow	Cutting fluid, concentrated	Shaft turning	g	31.3	Naphtha {RER}| market for | APOS, U
Inflow	Cutting fluid, water		g	606.1	Tap water {Europe without Switzerland}| market for | APOS, U
Inflow	Electricity		Wh	422.3	Electricity, medium voltage {IT}| market for | APOS, U
Inflow	Cutting fluid, concentrated	Shaft end spline milling	g	40.1	Naphtha {RER}| market for | APOS, U
Inflow	Cutting fluid, water		g	712.0	Tap water {Europe without Switzerland}| market for | APOS, U
Inflow	Electricity		Wh	249.0	Electricity, medium voltage {IT}| market for | APOS, U
Inflow	Quenching fluid, concentrated	Shaft induction hardening	kg	2.8	Propylene glycol, liquid {RER}| market for propylene glycol, liquid | APOS, U
Inflow	Quenching fluid, water		kg	15.1	Tap water {Europe without Switzerland}| market for | APOS, U
Inflow	Electricity		Wh	62.3	Electricity, medium voltage {IT}| market for | APOS, U
Outflow	Steel scrap	Shaft turning	kg	1.0	Scrap steel {Europe without Switzerland}| market for scrap steel | APOS, U
Outflow	Waste oil, conc. share in dilution		g	31.3	Waste mineral oil {Europe without Switzerland}| market for waste mineral oil | APOS, U
Outflow	Waste oil, conc. share in dilution	Shaft end milling	g	40.1	Waste mineral oil {Europe without Switzerland}| market for waste mineral oil | APOS, U
Outflow	Waste quenching fluid, conc. share	Shaft induction hardening	kg	2.8	Spent antifreezer liquid {GLO}| market for | APOS, U

Rotor and Magnet Assembly					
Direction	**Flow description**	**Manufacturing Process**	**Unit**	**Value**	**Selected process in database**
Inflow	Unalloyed steel	Hot rolling silicon Steel	kg	21.4	Steel, unalloyed {RER}| steel production, converter, unalloyed | APOS, U
Inflow	Ferrosilicon		g	457.7	Ferrosilicon {RoW}| production | APOS, U
Inflow	Aluminum		g	87.2	Aluminium, primary, ingot {IAI Area, EU27 & EFTA}| production | APOS, U
Inflow	Hot rolling of silicon steel alloy		kg	21.8	Hot rolling, steel {RER}| processing | APOS, U
Inflow	Phenolic resin	electrical steel manufacturing	g	19.1	Phenolic resin {RER}| market for phenolic resin | APOS, U
Inflow	Electricity		kWh	12.0	Electricity, medium voltage {IT}| market for | APOS, U
Inflow	Propane/LPG		g	229.4	Liquefied petroleum gas {Europe without Switzerland}| market for liquefied petroleum gas | APOS, U
Inflow	Sulfuric acid		g	363.2	Sulfuric acid {RER}| production | APOS, U
Inflow	Rolling/lubricating oil		g	7.6	Lubricating oil {RER}| production | APOS, U
Inflow	Quicklime powder		g	15.3	Quicklime, milled, packed {RER}| market for quicklime, milled, packed | APOS, U
Inflow	Electricity	Punching of rotor lamination	Wh	131.1	Electricity, medium voltage {IT}| market for | APOS, U
Inflow	Electricity	Stackling of rotor laminations	Wh	2267.5	Electricity, medium voltage {IT}| market for | APOS, U
Inflow	Magn. fix. resin, methacrylate ester		g	70.8	Methyl methacrylate {RER}| market for methyl methacrylate | APOS, U
Inflow	Nd(Dy)FeB nickel coated magnet		kg	1.7	Described in the dedicated Table Magnet Production
Outflow	Carbon dioxide	electrical steel manufacturing	g	688.2	Carbon dioxide
Outflow	Nitrogen oxides		g	1.9	Nitrogen oxides
Outflow	Sulfur oxides		g	1.1	Sulfur oxides
Outflow	Steel scrap		kg	2.2	Scrap steel {Europe without Switzerland}| market for scrap steel | APOS, U
Outflow	Sludge, dry content		g	63.1	Refinery sludge {Europe without Switzerland}| treatment of refinery sludge, hazardous waste incineration | APOS, U
Outflow	Steel scrap, Punching process	Punching of rotor lamination	kg	9.1	Scrap steel {Europe without Switzerland}| market for scrap steel | APOS, U
Magnet Production					
Direction	**Flow description**	**Manufacturing Process**	**Unit**	**Value**	**Selected process in database**
Inflow	Neodymium oxide	Production of neodymium metal through fused-salt electrolysis	kg	0.7	Neodymium oxide {CN-NM}| rare earth oxides production, from rare earth oxide concentrate, 50% REO | APOS, U
Inflow	Electricity		kWh	5.5	Electricity, medium voltage {CN}| market group for | APOS, U

Inflow	Lithium fluoride		g	5.2	Lithium fluoride {CN}| production | APOS, U
Inflow	Lime		g	23.4	Quicklime, milled, packed {RoW}| market for quicklime, milled, packed | APOS, U
Inflow	Graphite (anode)		kg	0.2	Anode, graphite, for Li-ion battery {CN}| market for anode, graphite, for Li-ion battery | APOS, U
Inflow	Unalloyed steel	Production of electrolytic iron	kg	1.5	Steel, unalloyed {RoW}| steel production, converter, unalloyed | APOS, U
Inflow	Electricity		kWh	2.8	Electricity, medium voltage {CN}| market group for | APOS, U
Inflow	Boron carbide	Production of Nd(Dy)FeB nickel coated magnet	g	25.2	Boron carbide {GLO}| market for | APOS, U
Inflow	Nickel		g	17.8	Nickel concentrate, 7% Ni {CN}| market for nickel concentrate, 7% Ni | APOS, U
Inflow	Dysprosium oxide		g	77.1	Dysprosium oxide {CN-FJ}| rare earth oxides production, from rare earth carbonate concentrate | APOS, U
Inflow	Electricity, for heating		kWh	14.1	Electricity, medium voltage {CN}| market group for | APOS, U
Inflow	Electricity, other		kWh	9.4	Electricity, medium voltage {CN}| market group for | APOS, U
Inflow	Hydrogen		kg	1.0	Hydrogen, liquid {RoW}| market for | APOS, U
Inflow	Caustic soda		g	1.7	Sodium hydroxide, without water, in 50% solution state {RoW}| chlor-alkali electrolysis, mercury cell | APOS, U
Inflow	Sulfuric acid		g	2.3	Sulfuric acid {CN}| smelting of copper concentrate, sulfide ore | APOS, U
Inflow	Water		kg	10.1	Tap water {RoW}| market for | APOS, U
Outflow	Carbon dioxide	Production of neodymium metal through fused-salt electrolysis Production of electrolytic iron	kg	0.6	Carbon dioxide
Outflow	Hydrogen fluoride		g	3.6	Hydrogen fluoride
Outflow	Dust (neodymium oxide)		g	2.6	Particulates, > 2.5 um, and < 10um
Outflow	Sludge, dry content		g	49.9	Sludge, NaCl electrolysis {GLO}| market for | Cut-off, U
Outflow	Sludge, dry content		kg	0.3	Refinery sludge {RoW}| treatment of, hazardous waste incineration | APOS, U
Outflow	Nickel to air	Production of Nd(Dy)FeB nickel coated magnet	mg	7.0	Nickel
Outflow	Nickel sulfamate to water		mg	8.6	Nickel subsulfide
Outflow	Neodymium-iron-boron scrap		g	335.4	Scrap steel {Europe without Switzerland}| market for scrap steel | APOS, U
Outflow	Sludge, dry content		g	3.5	Refinery sludge {RoW}| treatment of, hazardous waste incineration | APOS, U
Rotor Assembly with Shaft, Magnet, End Plate and Balancing					
Inflow	Stainless steel, 18/8 grade, ingot	Hot rolling Stainless steel	kg	1.0	Steel, chromium steel 18/8 {RER}| steel production, electric, chromium steel 18/8 | APOS, U
Inflow	Hot rolling of		kg	1.0	Hot rolling, steel {RER}| processing |

	stainless steel alloy				APOS, U
Inflow	Sheet rolling of stainless steel	Sheet rolling Stainless steel	kg	1.0	Sheet rolling, chromium steel {RER}| processing | APOS, U
Inflow	Electricity	End plate manufacturing	Wh	5.2	Electricity, medium voltage {IT}| market for | APOS, U
Outflow	Steel scrap		kg	0.4	Steel and iron (waste treatment) {GLO}| recycling of steel and iron | APOS, U
Inflow	Electricity	Assembly rotor package	Wh	42.0	Electricity, medium voltage {IT}| market for | APOS, U
Inflow	Electricity	Balancing rotor package	Wh	8.0	Electricity, medium voltage {IT}| market for | APOS, U
Housing					
Direction	**Flow description**	**Manufacturing Process**	**Unit**	**Value**	**Selected process in database**
Inflow	Aluminium	Die Casting aluminium	kg	21.2	Aluminium, primary, ingot {IAI Area, EU27 & EFTA}| production | APOS, U
Inflow	Heat, from natural gas		MJ	216.4	Heat, central or small-scale, natural gas {RER}| market group for | APOS, U
Inflow	Electricity		kWh	52.1	Electricity, medium voltage {IT}| market for | APOS, U
Inflow	Lubricating oil		g	400.8	Lubricating oil {RER}| market for lubricating oil | APOS, U
Inflow	Cutting fluid, concentrated	Machining housing	g	374.0	Naphtha {RER}| market for | APOS, U
Inflow	Cutting fluid, water		kg	7.0	Tap water {Europe without Switzerland}| market for | APOS, U
Inflow	Electricity		kWh	1.5	Electricity, medium voltage {IT}| market for | APOS, U
Inflow	Cutting fluid, concentrated	Machining 2 housing	g	85.0	Naphtha {RER}| market for | APOS, U
Inflow	Cutting fluid, water		kg	1.6	Tap water {Europe without Switzerland}| market for | APOS, U
Inflow	Electricity		kWh	0.3	Electricity, medium voltage {IT}| market for | APOS, U
Inflow	Cutting fluid, concentrated	Machining end bells	g	70.0	Naphtha {RER}| market for | APOS, U
Inflow	Cutting fluid, water		kg	1.4	Tap water {Europe without Switzerland}| market for | APOS, U
Inflow	Electricity		Wh	280.0	Electricity, medium voltage {IT}| market for | APOS, U
Inflow	Electricity	Cleaning	kWh	0.9	Electricity, medium voltage {IT}| market for | APOS, U
Inflow	PBT granulates	PBT mounting	g	130.0	Polyethylene terephthalate, granulate, bottle grade {RER}| production | APOS, U
Inflow	Injection molding of PBT		kg	0.1	Injection moulding {RER}| processing | APOS, U
Outflow	Aluminium	Die Casting aluminium	g	8.0	Aluminium, unspecified
Outflow	VOC		g	20.0	NMVOC, non-methane volatile organic compounds, IT
Outflow	Waste aluminium		kg	1.2	Waste aluminium {GLO}| market for | APOS, U
Outflow	Aluminium scrap	Machining housing	kg	0.5	Waste aluminium {GLO}| market for | APOS, U
Outflow	Waste oil, conc. share in dilution		g	374.0	Waste mineral oil {Europe without Switzerland}| market for waste mineral oil | APOS, U

Outflow	Aluminium scrap	Machining 2 housing	kg	0.5	Aluminium (waste treatment) {GLO}| recycling of aluminium | APOS, U
Outflow	Waste oil, conc. share in dilution		g	85.0	Waste mineral oil {Europe without Switzerland}| market for waste mineral oil | APOS, U
Outflow	Aluminium scrap	Machining end bells	g	140.0	Aluminium (waste treatment) {GLO}| recycling of aluminium | APOS, U
Outflow	Waste oil, conc. share in dilution		g	70.0	Waste mineral oil {Europe without Switzerland}| market for waste mineral oil | APOS, U
Final Assembly Painting, building service					
Direction	**Flow description**	**Manufacturing Process**	**Unit**	**Value**	**Selected process in database**
Inflow	Hot rolling of low-alloy carbon steel	Hot rolling low alloy steel	kg	0.6	Hot rolling, steel {RER}| processing | APOS, U
Inflow	Low-alloy carbon steel, ingot		kg	0.6	Steel, low-alloyed {RER}| steel production, converter, low-alloyed | APOS, U
Inflow	Section bar rolling of steel coil	Section bar rolling	kg	0.6	Section bar rolling, steel {RER}| processing | APOS, U
Inflow	Machining working of steel	Bearing manufacturing	kg	0.6	Metal working, average for steel product manufacturing {RER}| processing | APOS, U
Inflow	Hot rolling of low-alloy carbon steel	Hot rolling low alloy steel	kg	0.2	Hot rolling, steel {RER}| processing | APOS, U
Inflow	Low-alloy carbon steel, ingot		kg	0.2	Steel, low-alloyed {RER}| steel production, converter, low-alloyed | APOS, U
Inflow	Section bar rolling of steel coil	Section bar rolling	kg	0.2	Section bar rolling, steel {RER}| processing | APOS, U
Inflow	Machining working of steel	Plates, nuts manufacturing	kg	0.2	Metal working, average for steel product manufacturing {RER}| processing | APOS, U
Inflow	Galvanization	Plates, nuts zinc coating	m2	0.0	Zinc coat, coils {RER}| zinc coating, coils | APOS, U
Inflow	Electricity	Assembly	Wh	170	Electricity, medium voltage {IT}| market for | APOS, U
Inflow	Liquid varnish, solid share	Painting	g	205.0	Alkyd resin, long oil, without solvent, in 70% white spirit solution state {RER}| market for alkyd resin, long oil, without solvent, in 70% white spirit solution state | APOS, U
Inflow	Liquid varnish, solvent share		g	189.0	Naphtha {RER}| market for | APOS, U
Inflow	Electricity		kWh	1.2	Electricity, medium voltage {IT}| market for | APOS, U
Inflow	Electricity for heating	Technical building service	kWh	3.6	Electricity, medium voltage {IT}| market for | APOS, U
Inflow	Electricity for basic functions		kWh	2.9	Electricity, medium voltage {IT}| market for | APOS, U
Inflow	Electricity for general work		kWh	1.7	Electricity, medium voltage {IT}| market for | APOS, U
Inflow	Electricity for compressed air		kWh	0.7	Electricity, medium voltage {IT}| market for | APOS, U
Outflow	VOC	Painting	g	189.0	NMVOC, non-methane volatile organic compounds, IT

Transport				
Direction	**Flow description**	**Unit**	**Value**	**Selected process in database**
Inflow	Transport in Italy of the material to motor factory	tkm	90.4	Transport, freight, lorry >32 metric ton, EURO6 {RER}| transport, freight, lorry >32 metric ton, EURO6 | APOS, U
Inflow	Transport from China to Italy	tkm	29	Transport, freight, sea, ferry {GLO}| transport, freight, sea, ferry | APOS, U
Inflow	Transport in China from mine to magnet factory	tkm	2.3	Transport, freight train {CN}| market for | APOS, U
Use				
Direction	**Flow description**	**Unit**	**Value**	**Selected process in database**
Inflow	WLTP Energy calculated on 200000km	kWh	4332.0	Electricity, low voltage {IT}| market for | APOS, U